GENERATION AND NONLINEAR PROPAGATION OF ULTRASHORT NEAR INFRARED LASER PULSES

Peter N. Kean

A Thesis Submitted for the Degree of PhD
at the
University of St Andrews

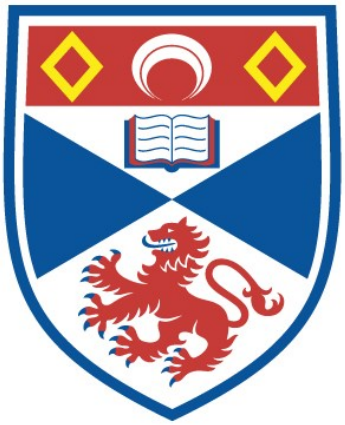

1990

Generation and Nonlinear Propagation of Ultrashort Near Infrared Laser Pulses.

Thesis submitted for the degree of Doctor of Philosophy to the University of St. Andrews

by

Peter N. Kean, B.Sc.

Department of Physics and Astronomy

University of St. Andrews

North Haugh

St. Andrews, Fife

Scotland. KY16 9SS

June 1989.

Declaration.

I hereby certify that this thesis has been composed by myself, that it is a record of my own work and that it has not been accepted in partial or complete fulfilment of any other degree of professional qualification.

I was admitted to the Faculty of Science of the University of St. Andrews as a candidate for the degree of Ph.D under ordinance general no.12 on 1st October 1985.

Signed Date 6/9/89

Certificate.

I hereby certify that the candidate has fulfilled the conditions of the Resolution and Regulations appropriate to the degree of Ph.D.

Signature of Supervisor Date 6/9/89

Copyright.

In submitting this thesis to the University of St. Andrews I understand that I am giving permission for it to be made available for use in accordance with the regulations of the University Library for the time being in force, subject to any copyright vested in the work not being affected thereby. I also understand that the title and abstract will be published, and that a copy of the work may be made and supplied to any bona fide library or research worker.

To my Parents.

(Even though they may not understand it !)

Abstract.

By utilising a CW mode-locked Nd:YAG pump laser an experimental study of self-phase modulation (SPM) and stimulated Raman scattering (SRS) in single mode optical fibres has been conducted. The dependence of the spectral broadening due to SPM upon the launched optical power was observed to obey a linear relationship in agreement with a simple theory. A deviation from this occurred for high input powers due to the onset of stimulated Raman scattering which caused a preferential depletion of the leading edge of the pump pulse and an increased spectral broadening to the long wavelength side of the spectrum. The pulses exiting the fibre were then compressed using a pair of holographic diffraction gratings, which were able to compensate for the linear part of the frequency chirp imposed on the pulse by SPM and the 1.06 μm pulses were reduced in duration from ~ 100 ps to approximately 4 ps by this method.

By making use of Raman generation in the fibre, a synchronously pumped fibre Raman oscillator was constructed. This enabled the generation of frequency tunable (1.07 - 1.12 μm) near infrared pulses by the method of time dispersion tuning. By incorporating two fibre grating reflectors onto the ends of the optical fibre, an all-fibre device was constructed having the potential advantages of compactness and stability.

The generation of mode-locked pulses around the 1.5 μm wavelength region was accomplished with the use of a colour centre laser based upon a stabilised F_2^+ centre in NaCl or a thallium centre in KCl. Both of these lasers were examined, although to date the poor quality of our NaCl laser crystals has meant that most of the work reported here was performed with KCl:Tl. This laser produced pulses of ≈ 20 ps duration, tunable over 1.45 - 1.55 μm with average powers ≈ 200 mW. A simple experiment to observe soliton propagation of these pulses in an optical fibre was conducted and this compressed the pulses to ≈ 0.8 ps, although this does not represent the optimum compression that could be achieved.

Using nonlinear pulse propagation in an optical fibre, the mode-locked characteristics of the colour centre laser were dramatically improved with the duration of the pulses from

the laser being reduced to ≈ 200 fs. This enhancement was achieved by the use of a nonlinear external cavity containing the optical fibre, which reinjected the pulses back into the main laser cavity, with an increased spectral bandwidth due to SPM. It was initially thought that the explanation to this effect was due to soliton formation within the control cavity, however experimental evidence is presented here which shows that the mode-locking enhancement phenomena is in fact quite general and does not rely on dispersion in the control cavity.

Contents.

Abstract.

Chapter 1. General Introduction **Page.**

1.1 Historical Background and Introduction 1

1.2 Introduction to Mode-Locking 3

1.2.1 Active Mode-Locking 6

1.2.2 Passive Mode-Locking 8

1.3 Ultrashort Pulse Measurement Techniques 9

1.3.1 The Electron-Optical Streak Camera 9

1.3.2 The Second Harmonic Generation Autocorrelator 12

1.4 A Brief Review of the Guiding Properties of Optical Fibres 17

1.5 Conclusions 21

References 23

Chapter 2. The Acousto-Optically Mode-locked Nd:YAG Laser

2.1 Introduction 26

2.2 The Spectra-Physics Series 3000 Laser System 27

2.2.1 The Acousto-Optic Mode-Locker 29

2.3 Laser Performance and Characterisation 32

2.4 Conclusions 40

References 42

Chapter 3. Nonlinear Pulse Propagation in Optical Fibres

3.1 Introduction 43

3.2 Self-Phase Modulation (SPM) 45

3.2.1 Theory of SPM 45

3.2.2 Experimental Observation of SPM 53

3.3 Optical Pulse Compression 62

3.4 Stimulated Raman Scattering (SRS) 72

3.4.1 Effect of SRS on SPM and Pulse Compression 75

3.4.2 The Fibre Raman Oscillator 80

3.4.3 Fibre Raman Oscillator with Fibre Grating Reflectors 87

3.5 Conclusions 98

References 100

Chapter 4. The KCl:Tl and NaCl:OH^- Colour Centre Lasers

4.1 Introduction 103

4.2 Some Basic Physics of Laser-Active Colour Centres 105

4.3 The F_2^+ and $(F_2^+)_A$ Centres 110

4.4 The Stabilised F_2^+ Centre in NaCl 113

4.5 The $Tl^0(1)$ Centre in KCl 115

4.6 Colour Centre Laser Resonators 118

4.6.1 The Burleigh Colour Centre Laser 122

4.7 The Mode-Locked KCl:Tl Colour Centre Laser 127

4.8 The NaCl:OH^- Colour Centre Laser 134

4.9 Conclusions 137

References 138

Chapter 5. Optical Solitons and the Soliton Laser

5.1 Introduction 140

5.2 A Derivation of the NLS for Nonlinear Pulse Propagation 143

5.3 Soliton Solutions to the NLS 146

5.4 Observation of Optical Solitons 151

5.5 The Soliton Laser 154

5.6 Conclusions 160

References 162

Chapter 6. Coupled-Cavity Mode-Locking

6.1 Introduction 164

6.2 The Experimental System 164

6.3 The CCM Laser with Normally Dispersive Fibre 169

6.3.1 The LiF:F_2^+ Coupled-Cavity Laser 178

6.4 The CCM Laser with a Semiconductor Diode Amplifier 179

6.5 A Discussion of the CCM Process 181

6.6 Conclusions 189

References 191

Chapter 7. General Conclusions 192

References 197

Appendix. 198

Acknowledgements. 199

Publications. 200

Chapter 1.

General Introduction.

1.1 Historical Background and Introduction.

In the 1960's, soon after the development of the laser, much consideration was given to the production of short, intense pulses of light. It was realised that the large bandwidth of lasers gave them the potential to produce extremely short light pulses in the region of picoseconds (10^{-12} s) or femtoseconds (10^{-15} s). The technique of mode-locking for producing such pulses was first described in papers by DiDomenico [1], Hargrove et al [2] and Yariv [3] and several experiments were performed on mode-locking the He-Ne laser [4,5]. As early as 1966 the Nd:YAG laser was mode-locked, producing ultrashort pulses in the infrared at 1.06 μm [6]. An early review paper on the theory of mode-locking by intracavity loss modulation was published by Harris [7]. It was demonstrated by Mocker and Collins [8] that a saturable dye in the laser cavity could also be used to mode-lock a laser. This important method of mode-locking has led to some of the shortest pulses ever produced in the colliding pulse mode-locked ring dye laser [9]. Mode-locking by intracavity loss or gain modulation, has become known as active mode-locking, while the use of saturable elements (dyes or multiple quantum wells) is known as passive mode-locking.

Theory showed that the minimum duration of these mode-locked pulses was of the order of the reciprocal of the oscillation bandwidth of the laser and measurements of laser bandwidths indicated pulses as short as a few picoseconds could be produced. It soon became clear that there were no suitable detectors to measure the duration of these mode-locked pulses, the fastest detectors had rise times a good fraction of a nanosecond (10^{-9} s). Early methods of estimating pulse durations involved comparing the level of second harmonic generation in a nonlinear crystal. If the laser output consists of short mode-locked pulses, the amount of second harmonic light is enhanced from that where the laser

is of a continuous wave (CW) nature. This lead to DiDomenico et al [6] estimating ≈ 80 ps for the pulse duration from the mode-locked Nd:YAG laser. Development of the second harmonic autocorrelator [10,11], described later in this chapter, now enables pulse durations of only a few femtoseconds to be measured. Unfortunately, because this measurement technique is a nonlinear autocorrelation of the pulses, information on the temporal profile of the pulse is lost and one has to assume a pulse shape. Linear measurement techniques such as fast photodiodes [12] and the electron-optical streak camera [13] overcome this disadvantage, although to-date their temporal resolution is not much better than 1 ps.

Ultrashort pulses in the near infrared (NIR) spectral region (roughly 800 nm to 5 μm) have become of major importance in many areas of physics, chemistry and biology. Such pulses are used in the study of ultrafast chemical dynamics, vibration dephasing times in excited molecules and in spectroscopy for the measurement of fluorescence rise and decay times [14,15]. Relaxation, diffusion and nonlinear processes may be studied in narrow band gap semiconductors and multiple quantum wells [16,17]. A developing field is that of electro-optic sampling, where short light pulses are used to characterise and measure the response of electrical circuits [18]. Ultrashort pulses enable the direct measurement of processes in the time domain, shorter pulses enabling higher temporal resolution and is a complementary approach to measuring slow events in the frequency domain with narrow linewidth lasers. Perhaps one of the most exciting applications of ultrashort NIR pulses, is towards optical communications [19]. Communication via optical fibres enables much higher data rates to be achieved and all optical switches have the potential to be much faster than electrical methods. In this regard, much experimental and theoretical work has been conducted on the propagation of pulses in optical fibres and in chapter 3, a study of two major nonlinear effects of pulse propagation in optical fibres is presented.

Mode-locked dye lasers have been standard sources of tunable NIR pulses for a number of years [20-22]. Until recently however, their production of pulses in the wavelength region > 1 μm has been very limited. New dyes such as styrl 14 [23] and dye no. 5 and 26 [24,25] have permitted the generation of stable, subpicosecond pulses around

1.3 and 1.5 μm. Colour centre lasers have proved to be extremely useful sources of tunable NIR radiation. These solid state lasers, with similar optical properties to dyes, can provide infrared radiation over the 0.8 - 4 μm spectral range with average powers of hundreds of milliwatts [26]. Mode-locked colour centre lasers have produced subpicosecond pulses by synchronous and passive mode-locking at around 950 nm [27] and 870 nm [28] respectively, and the recent development of the 'soliton' laser, to be described in chapter 5, has enabled the production of 60 fs pulses at 1.5 μm [29].

My work for this thesis, has concentrated on the generation of frequency tunable, ultrashort optical pulses in the near infrared. The nonlinear propagation of pulses in optical fibres is one method by which this may be achieved through the process of stimulated Raman scattering (chapter 3), and a more direct approach using colour centre lasers is described in chapter 4. The marriage of these two (nonlinear pulse propagation and ultrashort pulse generation) is hopefully further demonstrated in chapters 5 and 6, with the introduction of the soliton laser and the discovery of the more general technique which we have termed coupled-cavity mode-locking. The remainder of this chapter is devoted to an introduction of ultrashort pulse generation via mode-locking, pulse measurement techniques and a brief overview of the guiding properties of optical fibres.

1.2 Introduction to Mode-locking.

A laser usually consists of a gain, or amplifying, medium enclosed within an optical resonator, as indicated in figure 1. The optical radiation circulating inside the resonator is confined to well defined modes, characterised by the field distribution transverse to the laser beam direction of propagation. Insertion of a simple aperture or careful alignment of the resonator, confines the laser to operate in the most fundamental transverse mode, the TEM_{00} mode, which has a gaussian intensity profile. Since the resonator shown in figure 1 is a closed optical loop, a standing wave is established where an integral number of half wavelengths fit into the cavity, ensuring a node at each end mirror. Considering the cavity by itself for the moment, an infinite number of discrete longitudinal modes may exist for this single TEM_{00} transverse mode, separated in frequency by

$$\Delta f = c/2L \qquad (1.1)$$

where L is the optical path length of the resonator. Superimposed on top of this is the gain profile of the amplifying medium, which serves to both define the central operating wavelength of the laser and limit the number of longitudinal modes allowed to reach threshold. This situation is shown in figure 1b.

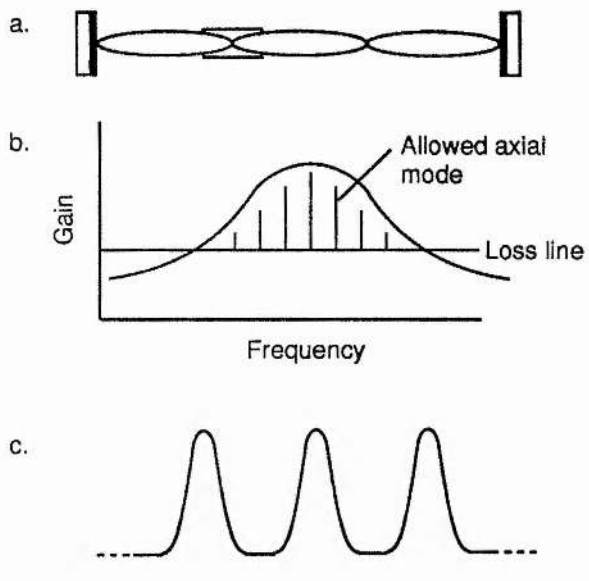

Figure 1.
(a) A laser resonator containing the gain medium and showing a single longitudinal mode. (b) Gain profile imposed on the longitudinal modes of the resonator, allowing a limited number to reach laser threshold. (c) Temporal output of a mode-locked laser.

In this situation each oscillating mode will be independent of any other and the laser output will fluctuate in time as the modes interfere in a random manner due to perturbations within the gain medium. By inserting frequency selecting elements into the cavity (e.g etalons), a single longitudinal mode may be made to oscillate, the output is then of a very high spectral quality (narrow linewidth) and long coherence length. Alternatively, by forcing the modes to maintain a fixed phase relationship, the output becomes periodically modulated as a train of short pulses, each separated by the round trip time of the cavity - 2L/c. The laser is then said to be phase locked or more commonly, mode-locked [30,31]. Mode-locking may be accomplished by periodically modulating the cavity losses or the

gain, which creates sidebands on each of the cavity modes. If the modulation period coincides with the cavity roundtrip time, the sidebands will overlap with an adjacent cavity mode and injection locking effects lead to strong mode coupling and cause phase-locking of the longitudinal modes. The greater the number of modes that are phase locked, the shorter the duration of each pulse and the peak intensity of each pulse is a factor of N^2 greater than that of any single mode, where N is the number of oscillating, phase locked, modes. An inhomogeneously broadened laser, such as many gas or ion lasers, will spontaneously oscillate on many longitudinal modes and mode-locking is easily achieved by applying sufficient modulation, enabling phase-locking to occur. In contrast, a homogeneously broadened laser, will normally oscillate on only one or at most, a few, longitudinal modes (due to spatial hole-burning effects) near the peak of the gain. In this case the mode-locker acts to transfer energy from the central axial modes to those further out in the spectrum. Competing with this, is the tendency of the homogeneous laser to narrow the spectrum and therefore broaden the mode-locked pulse.

From simple Fourier theory, the duration of the mode-locked pulses, τ_p, is inversely proportional to the oscillating bandwidth, $\delta\nu$:

$$\tau_p \, \delta\nu = \alpha \qquad (1.2)$$

where α is a constant and depends on the exact shape of the pulse (a list of values of α for some typical pulse shapes is given later in table 1). If equation 1.2 is satisfied, the pulse duration produced represents the fundamental minimum attainable for the particular $\delta\nu$ and the pulses are said to be bandwidth or transform limited. However, it is quite often the case that 1.2 may not be exactly satisfied and there exists some oscillating modes which are not phase-locked. These modes will be out at the edge of the lasing bandwidth (and therefore of low intensity) and generally cause the output to fluctuate in time and the pulse to have some substructure. This incomplete mode-locking results from cavity fluctuations, dispersive elements within the cavity, insufficient gain or loss modulation and from fluctuations in the pump source.

1.2.1 Active Mode-locking.

Mode-locking by intracavity loss or gain modulation or by frequency modulation, is known as active mode-locking. Several review papers [30,32-34] describe mode-locking techniques and it is the purpose of this section to briefly describe these methods.

Acousto-optic loss modulation.

The most widely used intracavity loss modulator is an acousto-optic (AO) modulator based on the diffraction of light by ultrasound [35]. Figure 2 shows a schematic diagram of the arrangement. A radio frequency (r.f) signal is applied to a transducer attached to a crystal of quartz. An ultrasonic standing wave is set up in the crystal modulator which acts as phase grating (due to refractive index variations)

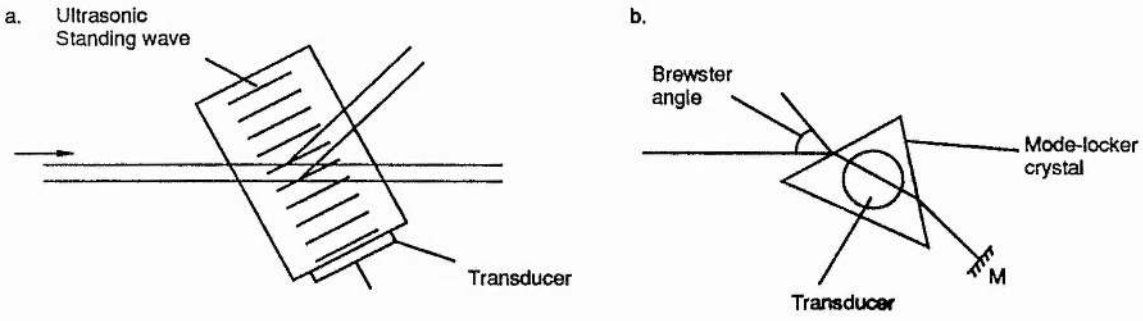

Figure 2.
Arrangement for mode-locking by intracavity loss modulation (a) Bragg angle modulator (b) Raman-Nath regime.

to incident light and causes diffraction. Twice every r.f period the standing wave collapses and the modulator then appears as a low loss element within the cavity. Thus the AO modulator acts as an optical shutter, being closed when diffraction occurs and transparent or open, at twice the r.f frequency. With the r.f frequency set to half the intermode spacing (Δf) of the resonator, mode-locking of the laser can be thought to arise due this shuttering action (in the time domain) or, as described above, due to the generation of sidebands at the cavity mode spacing (in the frequency domain). The diffraction efficiency and hence degree of mode-locking, is enhanced by greater r.f powers and also

higher frequencies. This type of modulator may be operated in one of two ways. With the light incident to the acoustic standing wave at the Bragg angle, the device is said to be operated in the Bragg regime and if the light is incident normally, the Raman-Nath regime. Generally speaking the Bragg regime produces a greater diffraction of the light and therefore better mode-locking for a given r.f power.

Mode-locking by synchronous pumping.

Active mode-locking by modulating the gain of a laser is more commonly known as synchronous pumping. This method is commonly used for dye and colour centre lasers, where the gain medium is optically pumped by another laser. The pump laser is mode-locked and excites a laser (the slave) whose cavity length is closely matched to that of the pump (or a multiple or sub-multiple of the pump laser). Thus the slave laser is very strongly gain modulated and mode-locking results. The tolerance on the slave laser cavity length is typically only a few microns and several studies on the length detuning effects of synchronously pumped lasers have been reported [36,37]. Pulse shortening effects on both the leading and trailing edges occur in the slave laser, the cavity length is adjusted to give preferential amplification to the peak of the pulse and the large stimulated emission caused by the high intensity pulse, causes strong gain saturation which tends to sharpen the trailing edge [38]. The effects of synchronously pumping a laser with a low stimulated emission cross section (long upper state lifetime) such as the KCl:Tl laser, are discussed in chapter 4, but we may note here that this reduces the effectiveness of gain saturation and leads to less efficient mode-locking and broader mode-locked pulses.

FM Mode-locking.

Frequency modulation (FM) of a laser may also be used to produce mode-locked pulses [33,39]. The situation for FM mode-locking is shown in figure 3. An FM modulator, such as an electro-optic phase modulator, will generally cause the circulating radiation to receive a Doppler shift proportional to $d\phi/dt$ where $\phi(t)$ is the intracavity phase modulation. Successive passes through the modulator eventually push the energy outside of the gain

bandwidth. If, as in figure 3, the laser pulse passes through the modulator at a stationary point in phase, then no Doppler shift is imparted and the

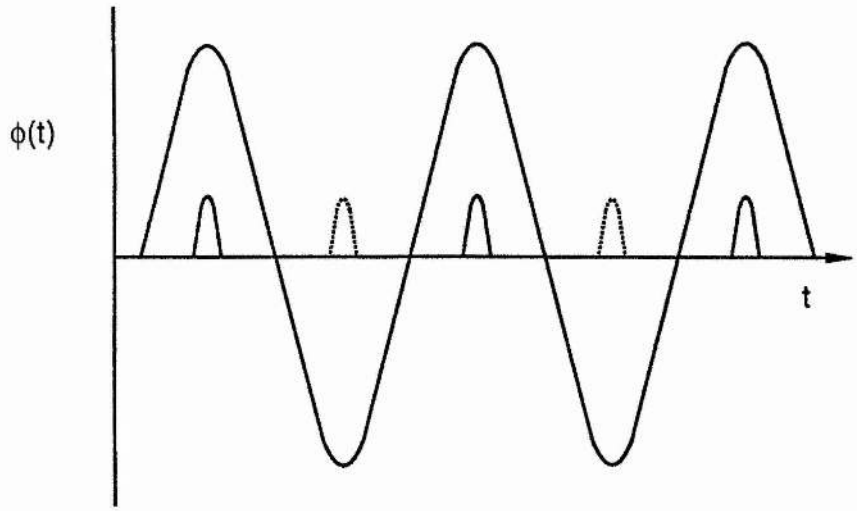

Figure 3.
Representation of FM mode-locking, achieved by the use of an electro-optic phase modulator or, equivalently, vibrating one end mirror.

modulator appears transparent. Note there are two stationary points, which cause an uncertainty in the mode-locked pulse position and may result in double pulsing and instability. Also the quadratic variation of $\phi(t)$ over the pulse arrival at the modulator, causes the mode-locked pulses to contain a frequency sweep or 'chirp'.

Since the mode-locking is achieved by external means, the above methods enable the central wavelength of the laser output to be tuned over most of the gain bandwidth whilst still retaining mode-locking. However, a laser actively mode-locked by either of these techniques, is very sensitive to cavity length fluctuations.

1.2.2 Passive Mode-locking.

Including a saturable absorber in a laser resonator, enables mode-locking by passive means where there is no externally applied modulation [40,41]. With sufficient pumping, a relatively intense burst of spontaneous emission from the CW pumped gain medium causes the absorber to saturate or bleach and so is able to experience a net gain. This noise burst

rapidly becomes shorter in duration and higher in intensity, forming a well defined shape and becomes a mode-locked pulse. Pulse shortening effects in both the gain medium and the saturable absorber are responsible for the mode-locking process. Many dye lasers are mode-locked very successfully by this method and the colliding pulse mode-locked dye laser has directly produced some of the shortest optical pulses ≈ 19 fs [42,43]. The cavity length of a laser mode-locked in this way is of relatively minor importance (mode-locking is independent of the cavity period) and so length fluctuations are much less critical. A disadvantage with this mode-locking method is that the output wavelength is fixed, being determined by the absorption peak of the saturable absorber.

1.3 Ultrashort Pulse Measurement Techniques.

The dramatic drop in pulse durations attainable from continuous wave mode-locked lasers has led to a lack of measurement devices of sufficient temporal resolution made available. The most direct and simplest way of measuring ultrashort pulses is to use a photodiode and sampling oscilloscope. This method is generally limited by the rise time of the detector head, which is about 4.5 ps at the present [44]. (In the near infrared, ~ 1.5 μm, the resolution limit is approximately 10ps). The electron optical streak camera, described below, has a resolution of around 1 ps in syncroscan operation [45], and was used for many of the experiments described in this work. By far the best temporal resolution to-date is achieved with the nonlinear second harmonic autocorrelator, which has enabled the measurement of compressed pulses ≈6 fs in duration [46]. This was also employed in much of the work here, and while these measurement techniques are described in detail elsewhere [31,47], a brief review will be given here for familiarity.

1.3.1 The Electron - Optical Streak Camera.

Originally pioneered by Zavoisky and Franchenko [48], the streak camera has been developed to be a standard method of ultrashort pulse measurement in the picosecond regime. With reference to figure 4, the device operates in the following way. A CW mode-locked pulse train is incident on a Michelson type interferometer which divides each pulse into two at the beamsplitter and forms a calibrated delay line, simply by moving mirror M_1

a known distance with respect to M_2. Each pulse is then directed onto the slit of the streak camera and imaged onto the photocathode. The number of photoelectrons produced is proportional to the input signal intensity, and so the temporal profile of the pulse is recorded. An anode at high potential accelerates the liberated electrons down the tube where they are deflected by a voltage ramp applied to a pair of deflection plates. The temporal distribution of photoelectrons is converted to a spatial distribution and a 'streaked' image of the pulses appears on the phosphor screen at the rear of the tube. Although the streak camera may be operated in a single shot mode, enabling sub-picosecond resolution [49], it is of great advantage to operate in synchronisation with the mode-locked laser [50], giving a real time display of the pulses. In this case a small fraction of the beam is directed onto a photodiode/tunnel diode oscillator. The tunnel diode is biased so that a pulse incident on the optical diode causes oscillation, and the output is then a sine wave at the exact repetition frequency of the optical pulse train. This sine wave is frequency doubled (in this case to

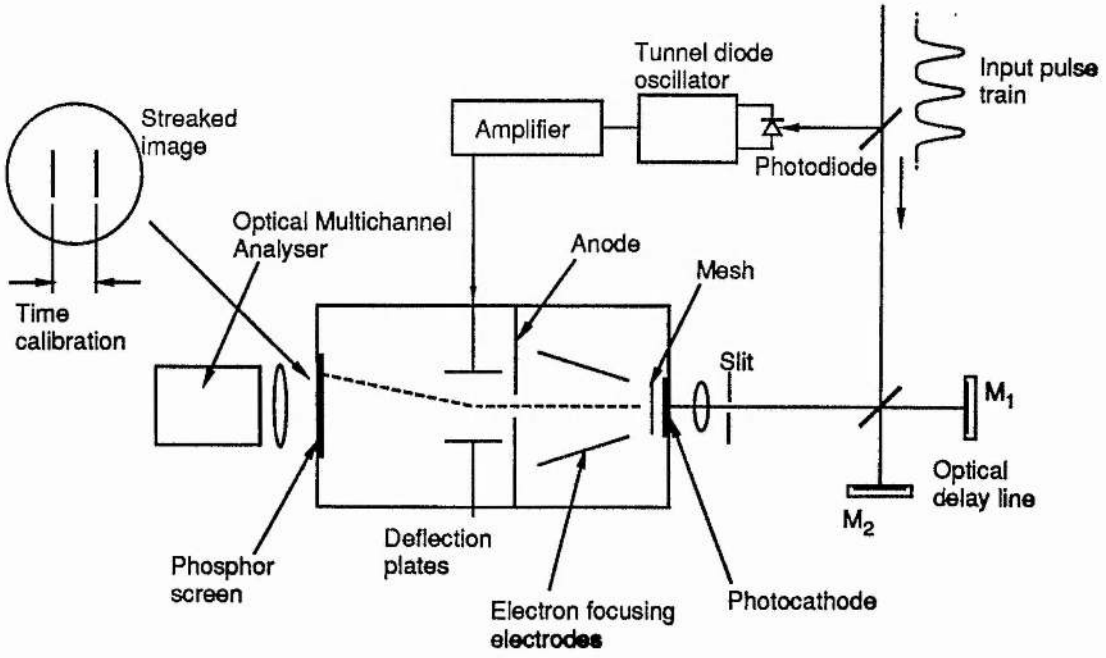

Figure 4.
Arrangement for the syncronously operating streak camera.

give ~ 164 MHz) to achieve a higher writing speed, and amplified to approximately 10 - 15 W before being applied to the deflection plates. An adjustable electrical delay line ensures that the electrons produced by the light pulses are incident at the deflection plates during the linear section of the deflecting voltage ramp. This ramp is linear to within 5% for approximately one sixth of the period. Streaked images of the pulses are repetitively superimposed on the phosphor screen with picosecond accuracy and the image is directly read using an optical multi-channel analyser (O.M.A). In the work here this was a 500 channel silicon intensified vidicon, having a read out time of ≈ 30 ms, giving an image integrated over ~ 10^6 pulses. Both a real time display and plotting a captured image facility were available.

The temporal resolution of the streak camera is limited by the photoelectron transit time dispersion and the technical time resolution. In synchroscan mode, phase jitter between the deflecting voltage ramp and the arrival of the mode-locked pulses also tends to decrease the resolution. Transit time dispersion arises due to an energy spread in the liberated photoelectrons, mainly caused by lattice scattering and pair production within the photocathode. The time dispersion can be expressed in terms of the energy distribution, $\Delta\varepsilon$, and the extraction field at the cathode, E, as [51]:

$$\Delta t = \frac{2.34 \times 10^{-8} \sqrt{\Delta\varepsilon}}{E} \qquad (1.3)$$

Operating the photocathode near its long wavelength cutoff, reduces $\Delta\varepsilon$ and by inserting a high potential mesh just behind the photocathode, E may be made very large so minimising Δt. With a cathode-mesh distance of 0.5 mm, extraction fields of ≈ 20 KV/cm are possible enabling subpicosecond transit time dispersions to be obtained. The technical time resolution is dependant on the streak speed and the dynamic spatial resolution (a function of the electron focusing elements). Space charge effects also reduce the resolution as the traveling packet of electrons mutually repel each other.

The streak camera used in the work here was a photochron IIA [52], with an S1 type response photocathode; in synchroscan mode this type of tube has successfully demonstrated a resolution of ≈ 1 ps.

1.3.2 The Second Harmonic Autocorrelator.

This technique for ultrashort pulse measurement is based upon the process of second harmonic generation (SHG) in a nonlinear crystal [10]. Briefly, the pulse train (of central frequency ω) is again incident to an optical delay line, the pulses are divided equally into two and made to overlap in a nonlinear crystal where SHG takes place. A slow, square law detector (photomultiplier tube) detects the light produced at 2ω (a filter blocks the residual fundamental light), the level of signal produced being dependent on the temporal overlap of the two sub-pulses. Translating one mirror through the matching point, produces a trace which represents the pulse autocorrelation.

There are essentially two types of SHG autocorrelation corresponding to the two types of phase matching. In type I, the two sub-pulses incident on the crystal are polarised in the same manner whilst for type II, the pulses are orthogonally polarised. Type II phase matching requires that both pulses be present in the crystal for any SHG to occur and is thus a background free measurement technique. Type I on the other hand, allows second harmonic generation for either pulse, resulting in a pulse on top of a background signal. However, a noncolinear method is also widely used [47], whereby the two pulses are laterally displaced slightly and then combined in the crystal. This also gives a background free detection method. Observation of the peak to background contrast ratio enables a clear indication of the pulse coherence and the Type I colinear method was used throughout this work. A schematic diagram of the SHG autocorrelator is shown in figure 5. Because the detector is relatively slow and responds to the intensity of the signal at 2ω, the (normalised) detector output current, I_d, represents the correlation of the sub-pulses [53]:

$$I_d(\tau) = 1 + 2G^2(\tau) + S(\tau) \qquad (1.4)$$

where $G^2(\tau)$ is the second order correlation function of the intensity of the pulse and is defined by

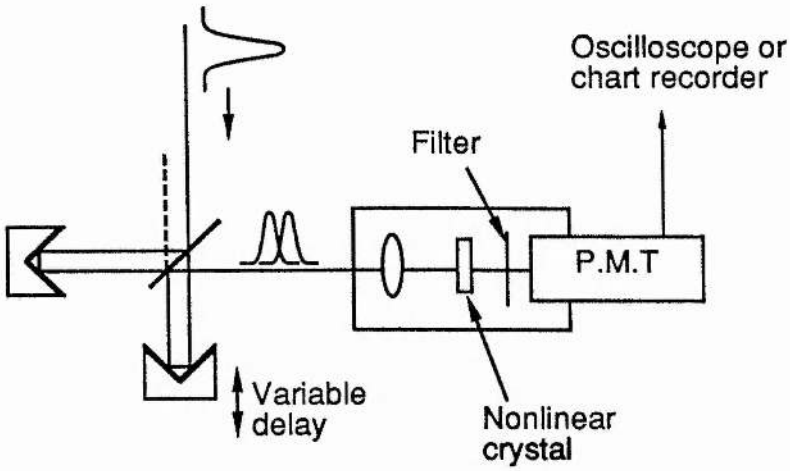

Figure 5.
A schematic diagram of the arrangement for second harmonic autocorrelation.

$$G^2(\tau) = \frac{\int_{-\infty}^{\infty} I(t)I(t-\tau)\,dt}{\int_{-\infty}^{\infty} I^2(t)\,dt} \qquad (1.5)$$

where τ is the delay between the two pulses. The $S(\tau)$ term is a rapidly varying interference term which averages to zero. For a coherent ultrashort pulse of duration τ_p (FWHM) we have

$$I_d(0) = 3 \text{ and } I_d(\tau >> \tau_p) = 1$$

since $G^2(0) = 1$ and $G^2(\tau >> \tau_p) = 0$. Thus the resulting autocorrelation consists of a pulse of (normalised) amplitude 3 on top of a background of unity, as shown in figure 6a. For the case of a free-running laser, with modes oscillating independently, it is still true that $I_d(0) = 3$, since incoherent light is correlated with itself at zero delay. When $\tau > 0$ or when τ is longer than the coherence time of the light, then

$$G^2(\tau) = \frac{\langle I(t)\rangle^2}{\langle I^2(t)\rangle} \qquad (1.6)$$

where the brackets indicate time averaging. For incoherent light, $\langle I(t)\rangle = 1/\sqrt{2}\sqrt{\langle I^2(t)\rangle}$, and so $I_d(\tau>0) = 2$. This trace is shown in figure 6b. A pulse of incoherent light, or a noise burst, will consist of a narrow coherence spike on top of a broader pedestal, with peak to pedestal to background heights in the ratio 3:2:1 as in figure 6c. Note also that a pulse consisting of N peaks, will give an autocorrelation with 2N-1 peaks. Relating the width of the autocorrelation trace to the FWHM, τ_p, of the pulse requires an assumption of the pulse shape since it is seen that the correlation function, G^2, is symmetrical and information on the pulse intensity profile is lost. The relation between the

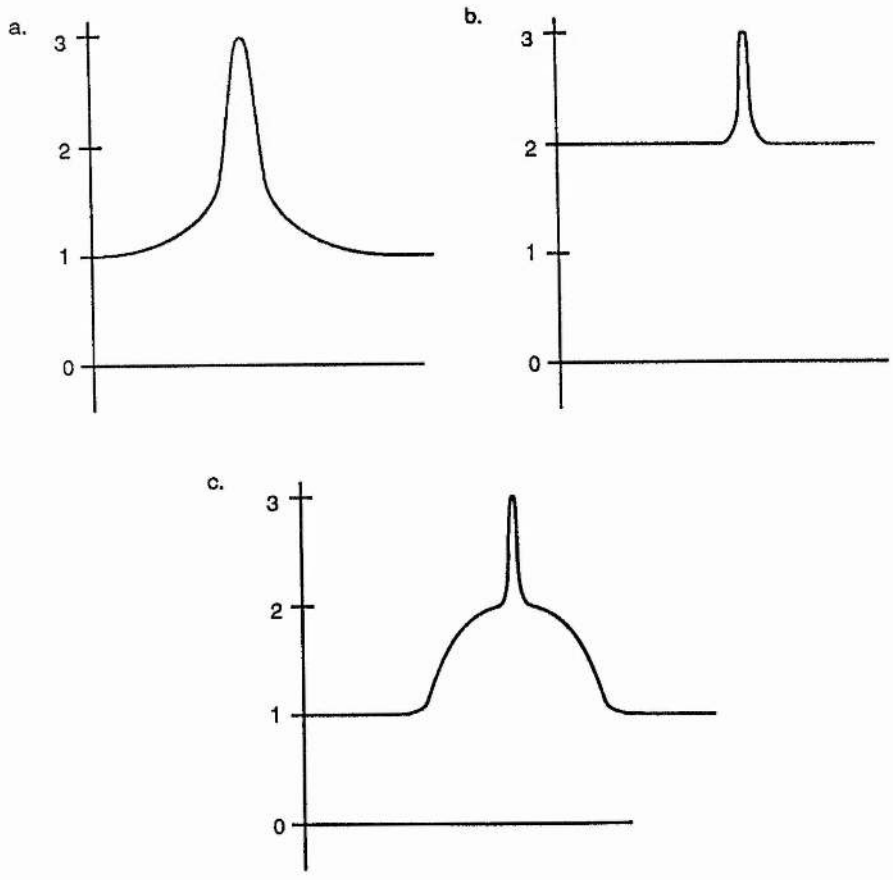

Figure 6.
Intensity autocorrelations for (a) a mode-locked pulse (b) a CW laser - randomly phased modes (c) a noise burst.

correlation width, Δt, and the FWHM of the pulse is

$$\tau_p = \frac{\Delta t}{k} \qquad (1.7)$$

where k is a constant depending on the actual shape of the pulse. Table 1 gives values of k for some standard pulse shapes along with the time-bandwidth product, α. Selection of an appropriate pulse shape is some what arbitrary but by measuring the pulse spectrum simultaneously, the time-bandwidth product for each shape may be deduced and the one closest to the particular α selected. A more precise method is to use higher order correlation functions which enable the direct determination of pulse shape.

Table 1.

Pulse Shape	Intensity profile	k	α
Square	1 $\lvert t \rvert \leq \tau_p/2$ 0 $\lvert t \rvert > \tau_p/2$	1	0.886
Gaussian	$\exp-\left(\frac{4\ln 2\ t^2}{\tau_p^2}\right)$	$\sqrt{2}$	0.441
Hyperbolic Sech^2	sech^2 (1.76 t/τ_p)	1.55	0.315

List of autocorrelation correction factors and time-bandwidth products for some typical pulse shapes. τ_p is the pulse FWHM.

Unfortunately however, these require even higher powers and signal detection becomes a major problem.

Interferometric autocorrelations.

In this case the scanning mirror is scanned slowly or, equivalently, the response time of the square law detector is increased. The interference term in equation (1.4) is then resolvable and the autocorrelation trace shows the fringes associated with the interference of the two pulses overlapping in the crystal. A typical interferometric autocorrelation trace is shown in figure 7. The peak to background contrast ratio increases to 8:1, while at the centre of the pulse the minimum signal level is zero. The autocorrelation is now self calibrating since the separation between the interference peaks is equal to one wavelength.

However, it is somewhat more difficult to infer a pulse duration from this type of autocorrelation since the shape of the envelope is extremely sensitive to frequency chirp on the pulse. By fitting a computer generated envelope to the interferometric autocorrelation, the discrepancy from a standard pulse shape may be determined and an indication of the amount of frequency chirp obtained. It has been shown [54], that a linear chirp such as that produced by dispersion alone, leads to rising wings in the autocorrelation, while nonlinear chirp (from say SPM) causes excessive fringing in the wings.

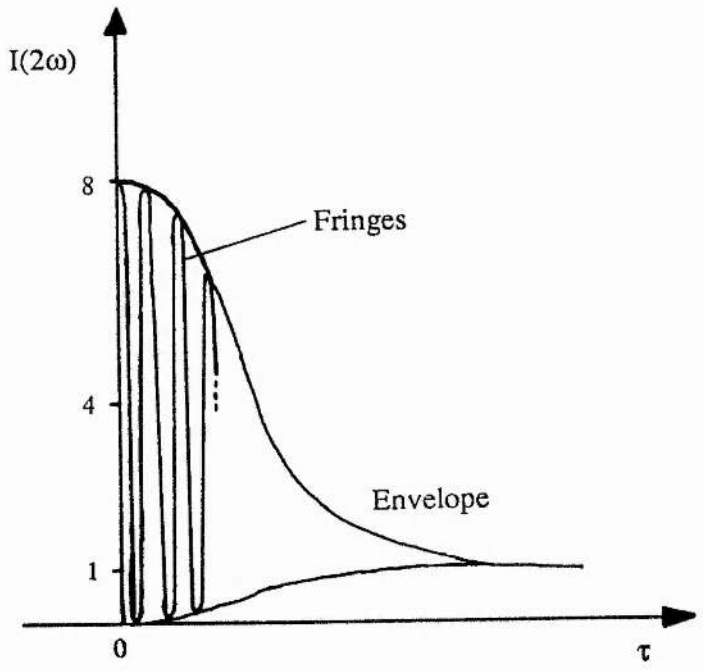

Figure 7.
Appearance of a typical interferometric autocorrelation.

The temporal resolution of the SHG autocorrelation method is determined by the bandwidth over which phase matching may occur in the crystal - the phase matching bandwidth of the crystal [55]. This is determined by the dispersion of the crystal and for a 0.6mm piece of lithium niobate ($LiNbO_3$) the temporal resolution is ≈ 400 fs at 1.06 μm [56]. By strongly focusing into the nonlinear crystal, not only is the signal level increased

but also the resolution is improved, since the interaction length or the effective crystal thickness, is reduced. At 1.5 μm a 2mm crystal was seen to have a resolution of approximately 200 fs. A 2mm thick piece of $LiNbO_3$ was used for most pulse width measurements down to approximately 0.5 ps and for pulse durations less than this, a 100 μm piece of KDP was used. It has also been shown that pulse to pulse duration fluctuations affect the measured autocorrelation width. Since the SHG efficiency is increased for higher peak powers (shorter pulses) the autocorrelation tends to weight shorter pulses more favourably and therefore probably gives a pulse width measurement less than the true average [57].

For autocorrelations at 1.5 μm, the PM tube, nonlinear crystal and focusing lens were all enclosed within a light tight box and optical access was through an AR coated silicon filter. This had a transmission cut on at ≈1.32 μm allowing only fundamental 1.5 μm light through, enabling autocorrelations to be taken in normal room light. By mounting one mirror (actually corner cubes were used so as to enable a sideways displacement of both beams) on a motor driven translation stage, a hard copy trace of the autocorrelation could be taken over a period of ≈ 30s. Also one mirror was mounted on a loud speaker and vibrated at about 25 Hz, enabling a real time monitor of the pulse duration to be displayed on a simple oscilloscope [58] greatly facilitating optimisation of the mode-locked laser.

It is worth pointing out that the straight forward linear autocorrelation (i.e no second harmonic crystal) records no more information than the spectrum of the pulse, it is simply presented in a different form than usually encountered. If the first order correlation were to be measured, information on the coherence length of the pulse is obtained which is only related to the actual pulse duration in the bandwidth limited case.

1.4 A Brief Review of the Guiding Properties of Optical Fibres.

It had long been realised that communications by light, that is visible or near visible radiation, held great potential, but until the manufacture of low loss optical fibres, only line of sight communication was a possibility. Today low loss (< 1 dB/km) single-mode optical fibres are readily available and are being installed as transmission lines in domestic

telecommunications networks. Much of the work here has involved the propagation of pulses in single-mode fibres and while chapter 3 is devoted to a study of nonlinear pulse propagation, a brief review of the general guiding properties of optical fibres is appropriate here.

An optical fibre is a cylinder made from transparent dielectric materials, usually based on fused silica (SiO_2). A central region, the core, is surrounded by a cladding region of lower refractive index and the whole structure is normally coated in a protective jacket. The optical characteristics of a fibre are determined by its refractive index profile which is usually circularly symmetric, depending only on the radial coordinate. Many types of fibre with different refractive index profiles exist [59], that of a 'step index' circular optical fibre is given by

$$n(r) = \begin{matrix} n_1 & r < a \\ n_2 & r > a \end{matrix}$$

where a is the core radius. As in figure 8 the basic guiding principle is that light incident to the cladding layer from the core, at an angle greater than the critical angle, will be reflected. Successive reflections guide the radiation down the fibre.

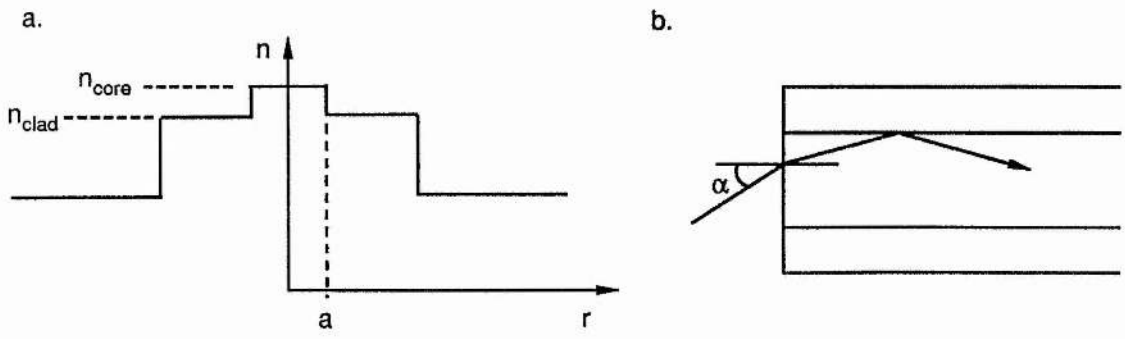

Figure 8.
(a) Refractive index profile of a step index fibre. (b) Guiding nature of a circular optical fibre.

For such a fibre the maximum acceptance angle, α_{max}, to the fibre axis within which the light will be guided is easily shown to be given by

$$n_0 \sin \alpha_{max} = n_1(1 - \sin^2\theta_c)^{1/2} = (n_1^2 - n_2^2)^{1/2} \qquad (1.8)$$

where n_0 is the index of the medium surrounding the fibre (usually air), n_1 and n_2 are core and cladding refractive indices respectively. The quantity $(n_1^2 - n_2^2)^{1/2}$ is known as the numerical aperture of the fibre. If the fibre is bent to severely, then radiation may leak from the fibre and losses are incurred. These are known as bending losses.

The ray picture of light propagating in a fibre is somewhat simplistic and the full solution is obtained by solving Maxwells equations in the core and cladding regions. Since the fibre is of circular geometry, the equations are written in spherical coordinates and the boundary conditions of (i) matching fields at the interface and (ii) a decaying (non-radiative) field in the cladding, are applied. The solutions are derived in many standard texts [59,60] and are in the form of Bessel functions. For the guided mode, there exists a discrete set of solutions and the mode propagation constant may not take on any arbitrary value. TE and TM mode solutions exist as well as hybrid modes, labeled HE and EH, which have longitudinal electric and magnetic field components. In terms of a ray analogy, the TE and TM modes correspond to meridional rays and the hybrid modes to skew rays. The finite number of discrete modes leads to a finite number of possible propagation constants within the guide. These fall within the range

$$n_2 k < |\beta_g| < n_1 k$$

where β_g is the guided mode propagation constant and k ($=2\pi/\lambda$) the free space propagation constant. A constant Δ is known as the average core/cladding index difference and defined as

$$\Delta = \frac{n_1 - n_2}{n_1} . \qquad (1.9)$$

It is usually the case that $\Delta << 1$ and a fibre with this property is known as a weakly guiding fibre [61]. In this case it can be shown that the guided modes are very nearly linearly polarised and are designated LP modes [61].

It also turns out that a parameter known as the fibre 'V' number [59-61], determines the number of modes which may propagate down the fibre without radiating energy into the cladding. This V number is defined by

$$V = 2\pi/\lambda \, a \, (n_1^2 - n_2^2)^{1/2}$$

$$\approx k \, a \, n_1 \, (2\Delta)^{1/2} \qquad (1.10)$$

for the case of $\Delta << 1$. The number of modes is given approximately by $N \approx V^2/2$. As V becomes close to the cutoff value for a particular mode, progressively more radiation is carried in the cladding region. When $V \leq 2.405$ only the single LP_{01} mode may exist in the fibre and all others are radiation modes. The fibre is then said to be single-mode. (There are actually two modes possible with orthogonal polarisations, the term single-mode refers to the case of a single input polarisation). It is possible therefore to construct a fibre to be single-mode at a given wavelength by choosing appropriate values of Δ and core radius a.

Polarisation maintaining fibres.

Single-mode fibres do not normally preserve the polarisation state of the input signal. An ideal fibre can support two independent modes of arbitrarily orthogonal polarisations, both as fundamental HE_{11} modes. These modes would have the same phase velocity and the polarisation would be a linear superposition of these two polarisation eigenmodes. In a real fibre however, imperfections such as stresses and a noncircular core, lift the degeneracy of the two modes causing a difference in the effective refractive index for each mode and they propagate with different phase velocities. This index difference is known as the fibre birefringence. Normal single-mode fibres have a low birefringence which is sensitive to external influences such as bending, twisting, temperature, applied pressure and stray electric and magnetic fields. These effects cause scattering between the two polarisation states and the output polarisation becomes pseudorandom and unpredictable. Some control over the output polarisation may be achieved by bending or stressing the fibre [62], and provided the surrounding conditions are constant, the polarisation will then remain steady. In fact low birefringent fibres are useful in sensing applications where a change in external conditions causes a measurable change in the polarisation state [63]. In many instances, however, it is useful for a fibre to preserve the input polarisation state. It is therefore necessary to construct a fibre with a high internal birefringence so that external perturbations have an insignificant effect on the total fibre birefringence. This may be

achieved by geometrical or stress induced methods. A fibre with a highly elliptical core and large index difference between the core and cladding, enables high internal birefringence and polarisation maintaining properties to be obtained but the core then needs to of small dimensions in order to preserve the single-mode nature [64]. Other methods of obtaining a high birefringence involve surrounding the core with an elliptical or nonsymmetrical region in the cladding. More detailed reviews of high birefringent fibres may be found in references [65,66].

Fibre dispersion.

Dispersion in a single-mode fibre is composed of two effects, material and waveguide dispersion. The first of these simply arises from the well known variation in refractive index with wavelength in a dielectric material. The second derivative of this with respect to wavelength, $d^2n/d\lambda^2$, gives rise to group velocity dispersion (GVD), causing a spreading or broadening of an optical pulse propagating along a fibre. As will be described in chapter 5, the GVD of fused silica passes through zero at $\approx$ 1.3 μm, becoming anomalous for wavelengths greater than this, i.e the group velocity decreases with increasing wavelength [67]. Waveguide dispersion also causes GVD but is due to the variation of the guided mode velocity with the fibre V parameter [59]. If the mode is not close to cutoff then material dispersion usually dominates. For the case of a small core however (such as that encountered in elliptical core fibres), waveguide dispersion can become important and significantly alter the dispersion characteristics of the fibre [68].

1.5 Conclusions.

In this introductory chapter a brief description of the process of mode-locking has been presented along with two techniques for the measurement of ultrashort pulses which were extensively used in the work for this thesis. An introduction to the guiding properties of optical fibres has also been given.

In the following chapter a description and characterisation of the Nd:YAG laser, employed as the pump source for all further experiments here, is presented. Chapter 3 concentrates upon the nonlinear propagation of pulses in optical fibres, specifically self-

phase modulation and stimulated Raman scattering and their applications to optical pulse compression and fibre Raman oscillators. The direct generation of tunable NIR optical pulses around the important wavelength region of 1.5 μm using colour centre lasers, is described in chapter 4 and the nonlinear propagation of such pulses in optical fibres, leading to the phenomena of optical solitons is presented in chapter 5. By combining a length of optical fibre into the feedback loop of a KCl:Tl colour centre laser, it is shown in both chapters 5 and 6, that subpicosecond NIR pulses may be produced, enabling this broad bandwidth laser medium to be used to its full potential.

References.

1. M DiDomenico; J Appl. Phys. **35**, 2870 (1964)
2. L E Hargrove, R L Fork, M A Pollack; Appl. Phys. Lett. **5**, 4 (1964)
3. A Yariv; J Appl. Phys. **36**, 388 (1965)
4. H Statz, C L Tang; Quant. Electronics III, P Grivet, N Bloembergen Eds. Columbia University Press p.469 (1964)
5. E O Ammann, B J McMurtry, M K Oshman; IEEE J Quant. Electron. **QE-1**, 263 (1965)
6. M DiDomenico, H M Marcos, J E Geusic, R E Smith; Appl. Phys. Lett. **8**, 180 (1966)
7. S E Harris; Proc. IEEE **54**, 1401 (1966)
8. H W Mocker, R J Collins; Appl. Phys. Lett. **7**, 270 (1965)
9. R L Fork, C V Shank, R Yen, C A Hirlimann; IEEE J Quant. Electron. **QE-19**, 500 (1983)
10. J A Armstrong; Appl. Phys. Lett. **10**, 16 (1967)
11. H P Webber; J Appl. Phys. **38**, 2231 (1967)
12. S Y Wang, D M Bloom, D M Collins; Appl. Phys. Lett. **42**, 190 (1983)
13. W Sibbett; SPIE **348**, Conference on High Speed Photography, San Diego (1982)
14. C V Shank, R L Fork, R F Leheny, J Shah; Phys. Rev. Lett. **42**, 112 (1977)
15. L Reekie, I Ruddock, R Illingworth; in 'Picosecond Chemistry and Biology' T Doust, M West Eds. Sience Reviews Limited (1983)
16. D S Chemla, D A B Miller; J Opt. Soc. Am. B **2**, 1155 (1985)
17. R J Manning, D W Crust, D W Craig, A Miller, K Woodbridges; J Mod. Optics **35**, 541 (1988)
18. D H Auston, M C Nuss; IEEE J Quant. Electron. **QE-24**, 184 (1988)
    also in same issue; K J Weigarten, M J W Rodwell, D M Bloom; p.198
19. P Kaiser, W T Anderson; J Lightwave Tech. **LT-4**, 1157 (1986)
20. J P Ryan, L S Goldberg, D J Bradley; Opt. Comm. **27**, 127 (1978)
21. K Smith, W Sibbett, J R Taylor; Opt. Comm. **49**, 359 (1984)

22. C V Shank, R L Fork, F Beisser; Laser Focus p.59 June 1983

23. M D Dawson, T F Boggess, A L Smirl; Opt. Lett. **12**, 590 (1987)

24. P Beaud, B Zysset, A P Schwarzenbach, H P Webber; Opt. Lett. **11**, 24 (1986)

25. H Lobentanzer, H J Polland; OPt. Comm. **62**, 35 (1987)

26. C R Pollack, J F Pinto, E Georgiou; Appl. Phys. B **48**, 287 (1989)

27. N Langford, K Smith, W Sibbett; Opt. Lett. **12**, 817 (1987)

28. N Langford, K Smith, W Sibbett; Opt. Lett. **12**, 903 (1987)

29. F M Mitschke, L F Mollenauer; Opt. Lett. **12**, 407 (1987)

30. A E Siegman, D J Kuizenga; Opto-Electronics **6**, 43 (1974)

31. D J Bradley, G C H New; Proc. IEEE **62**, 313 (1974)

32. P W Smith; Proc. IEEE **58**, 1342 (1970)

33. D J Kuizenga, A E Siegman; IEEE J Quant. Electron. **QE-6**, 694 (1970)

34. G H C New, L A Zenteno; Opt. Comm. **48**, 149 (1983)

35. A J De Maria; J Appl. Phys. **34**, 2984 (1963)

36. C P Ausschnitt, R K Jain, J P Heritage; IEEE J Quant. Electron. **QE-15**, 912 (1979)

37. M D Dawson, D Maxson, T F Boggess, A L Smirl; Opt. Lett. **13**, 126 (1988)

38. U Stamm, F Weidner; Appl. Phys. B **48**, 149 (1989)

39. D J Kuizenga, A E Siegman; J Quant. Electron. **QE-6**, 709 (1970)

40. E P Ippen, C V Shank, A Dienes; Appl. Phys. Lett. **21**, 348 (1972)

41. H A Haus; J Appl. Phys. **46**, 3049 (1975)

42. J A Valdmanis, R L Fork, J P Gordon; Opt. Lett. **10**, 131 (1985)

43. A Finch, G Chen, W Sleat, W Sibbett; J Mod. Optics **35**, 345 (1988)

44. D J Parker, P J Say, A M Hanson, W Sibbett; Electron. Lett. **23**, 527 (1987)

45. A Finch, W E Sleat, W Sibbett; Rev. Sci. Instrum. To be published (1989)

46. R L Fork, C H Brito Cruz, P C Becker, C V Shank; Opt. Lett. **12**, 483 (1987)

47. E P Ippen, C V Shank; Chapter 2 in 'Ultrashort Light Pulses' Ed. S L Shapiro, Springer Verlag (1977)

48. E K Zavoisky, S D Franchenko; Sov Phys Doklady **1**, 285 (1956)

49a D J Bradley, W Sibbett; Appl. Phys. Lett. **27**, 382 (1975)

49b A Finch, Y Lui, H Niu, W Sibbett, W E Sleat, D R Walker, H Yang, R Zang; Ultrafast Phenomena VI Springer series in chemical physics **48**, 159 (1988)

50. M C Adams, W Sibbett, D J Bradley; Advances in Electronics and Electron Physics **52**, 265 (1979)
51. W Sibbett; PhD Thesis, Queens University of Belfast (1973)
52. J P Willson, W Sibbett, W E Sleat; Opt. Comm. **42**, 208 (1982)
53. A Yariv; 'Optical Electronics' chapter 6 Holt & Saunders 3rd ed. (1985)
54. J M Diels, J J Fontaine, I C McMichael, F Simoni; Appl. Opt. **24**, 1270 (1985)
55. A M Weiner, IEEE J Quant. Electron. **QE-19**, 1276 (1983)
56. J Comly, E Garmire; Appl. Phys. Lett. **12**, 7 (1968)
57. E W Van Stryland; Opt. Comm. **31**, 93 (1979)
58. R L Fork, F A Beisser; Appl. Opt. **17**, 3534 (1978)
59. 'Optical Fibre Telecommunications' S E Miller, A G Chynoweth Eds. Academic (1979)
60. A H Cherin, 'An Introduction to Optical Fibres' McGraw-Hill (1983)
61. D Gloge; Appl. Opt. **10**, 2252 (1971)
62. H C Lefevre; Electron. Lett. **16**, 778 (1980)
63. See papers in J Lightwave Tech. **LT-5** (1987)
64. R B Dyott, J R Cozens, D G Morris; Electron. Lett. **15**, 380 (1979)
65. M P Varnham, D N Payne, A J Barlow, R D Birch; IEEE J Lightwave Tech. **LT-1**, 332 (1983)
66. J Noda, K Okamoto, Y Sasaki; IEEE J Lightwave Tech. **LT-4**, 1071 (1986)
67. D N Payne, W A Gambling; Electron. Lett. **11**, 178 (1975)
68. H Tsuchiya, N Imoto; Electron. Lett. **15**, 476 (1979)

Chapter 2.

The Acousto-Optically Mode-Locked Nd:YAG Laser.

2.1 Introduction.

The Nd:YAG laser was first developed in 1964 [1] and is now well established as a pump source for dye lasers [2,3] and colour centre lasers [4]. Both the fundamental emission (1.064 μm) and the second harmonic (532 nm) are extensively used for optical pumping and other applications such as Raman generation and pulse propagation studies in optical fibres [5-7]. Mode-locking of this laser was first demonstrated by DiDomenico et al [8], producing pulses of ≈ 80 ps duration with intracavity acousto-optic (AO) loss modulation. Later Osternik and Foster [9] obtained 30 ps pulses using an electro-optic phase modulator.

Due to homogeneous line broadening within the gain medium, Nd:YAG lasers are almost exclusively actively mode-locked. This method of mode-locking does not generally produce pulses as short as passively mode-locked systems and it is also more difficult to control the stability of the output pulse train. While passively mode-locked YAG lasers operating in a pulsed mode have generated pulses as short as 28 ps [10], it is generally more convenient to have a continuous train of pulses as provided by AO mode-locking. In common with other solid state lasers, the CW pumped Nd:YAG laser is susceptible to relaxation oscillations [11,12] causing output fluctuations in both pulse width and amplitude. Careful design of the laser resonator and the use of active feedback systems for mode-locking, have enabled the Nd:YAG laser to become a reliable source of ultrashort pulses in the near infrared with average powers of tens of Watts. A CW mode-locked YAG laser was used as the pump source for all the experiments described in later chapters of this thesis and so a detailed characterisation of the laser is presented in this chapter.

2.2 The Spectra Physics Series 3000 Laser System.

Neodymium doped Yttrium Aluminum Garnet is the gain medium of the so called 'YAG' laser and possesses properties which are highly favourable for laser operation. About 1% of Y^{3+} ions are substituted by Nd^{3+} ions and the energy level of these ions in YAG are shown in figure 1. The medium constitutes a four level system and together with a narrow fluorescent line width, results in a low threshold for laser operation. Although several laser transitions exist, giving operation at 940nm and 1.36 μm, the well known 1.064 μm line is the strongest. This transition occurs from the upper component of the $^4F_{3/2}$ level to the $^4I_{11/2}$ level which is 2111 cm^{-1} above the ground state. Hence the population of this level at room temperature is only a factor of $\exp(\Delta E/KT) \sim \exp(-10)$ of the ground state density. The fast relaxation of the nonradiative transition $^4I_{11/2} \rightarrow {}^4I_{9/2}$ and the fact that the

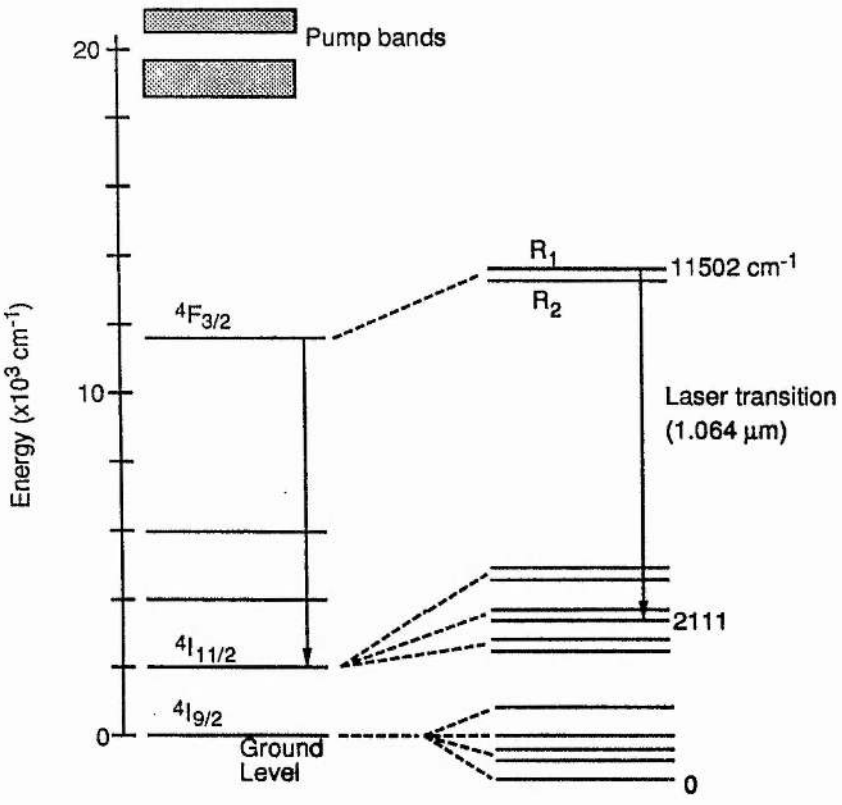

Figure 1.
Energy level diagram for Nd ions within YAG.

lower level is not thermally populated, both ensure that the threshold condition is easily reached. A number of broad pump bands exist, those at 810 nm and 750 nm being the strongest. Thus the Nd:YAG medium is well suited to optical pumping by a high pressure Krypton arc lamp [13]. The fluorescent efficiency of the upper laser level is ~ 99.5% which means that almost all the ions excited from the ground state end up in the upper laser level. The spontaneous fluorescent lifetime of this level (which includes all possible decays) is ~ 230 μs. This value is long indeed compared to that for ion lasers and dye lasers. Some physical and optical properties are summarised in table 1.

Table 1.

Chemical formula	$Nd:Y_3Al_5O_{12}$
Nd atoms / cm^3	1.38×10^{20}
Thermal conductivity	0.13 $Wcm^{-1}K^{-1}$
Line width	4.5 Å (120 GHz)
main lasing transition	1.064 μm
σ	8.8×10^{-19} cm^2
τ	230 μs
n	1.82 (at 1.06 μm)

Some physical and optical properties of Nd:YAG. σ stimulated emission cross section; τ spontaneous fluorescent lifetime; n refractive index. (After reference [12])

The laser used in these experiments was a Spectra Physics series 3000 Nd:YAG. The active medium was in the form of a 4 mm diameter cylinder, with a length of approximately 80 mm. This was located at one focus of a gold coated elliptical reflector chamber and pumped with a high pressure Krypton arc lamp, located at the other focus. The lamp was typically run at a current of 17 A but this needed to be increased as the lamp aged. Lamps were changed after approximately every 400 hours of use. Two pyrex flow tubes placed over the lamp and rod prevented UV light being incident on the rod which would otherwise cause a decrease in the output power due to the formation of colour centres. The total power dissipated in the lamp was approximately 2 - 3 kW, causing considerable heating of both the lamp and Nd:YAG rod and so a closed loop water cooling system is provided. This must contain deionized water to prevent arcing between the electrical contacts of the lamp.

A major problem in the design of high power Nd:YAG lasers occurs due to the heating of the rod by optical pumping. The low thermal conductivity of Nd:YAG leads to a radial temperature gradient being set up, which causes the rod to behave as a thick lens for light propagating along its axis. The effective focal length depends on the output power from the lamp and therefore on the lamp current, higher currents giving shorter focal lengths. The laser resonator was designed to stay within the stability condition over the widest possible range of currents. If the current is too large, the cavity becomes unstable due to the strong focusing of the rod. In some lasers a concave - convex mirror arrangement is implemented, the focusing effect of the rod being used to compensate for the diverging effect of the convex mirror [14]. However, in the Spectra laser two concave mirrors of radius 60 cm were used, separated by approximately 1.8 m. The Nd:YAG rod was positioned in the centre, giving an overall optical path length of ≈ 1.86m. The beam diameter changes within the cavity, being largest at the rod allowing maximum extraction of energy from the gain medium - see figure 2.

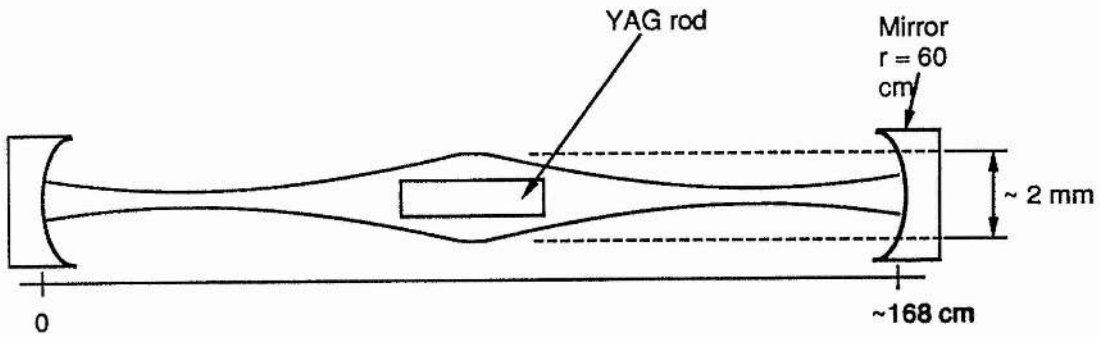

Figure 2.
Typical beam profile within the Nd:YAG laser cavity.

The output mirror had a reflectivity of 85% and the laser gave typically 7 to 8 W time averaged output power (mode-locked) in a vertically polarised TEM_{00} beam.

2.2.1 The Acousto-Optic Mode-Locker.

Mode-locking of the laser was achieved by using an intracavity acousto-optic loss modulator, the basic principles of which have been described in the previous chapter. The Spectra Physics mode-locker was in the form of a small triangular quartz prism mounted at

the rear of the laser, such that reflection losses from the prism were minimised. Figure 3 shows a schematic diagram of the device and the optical beam is incident normally to the ultrasonic standing wave (known as the Raman-Nath regime). The mode-locker had 20 to 30 resonances separated by 400 kHz and centred on 41 MHz. The separation of these resonances is obtained from the usual formula, c/2L, where here L is the width of the prism and c is the velocity of sound in the crystal. When the frequency of an r.f driver signal matches one of the resonances, the modulator appears as a 50 Ω load and maximum power transfer to the crystal takes place. This results in maximum diffraction efficiency and optimum mode-locked performance.

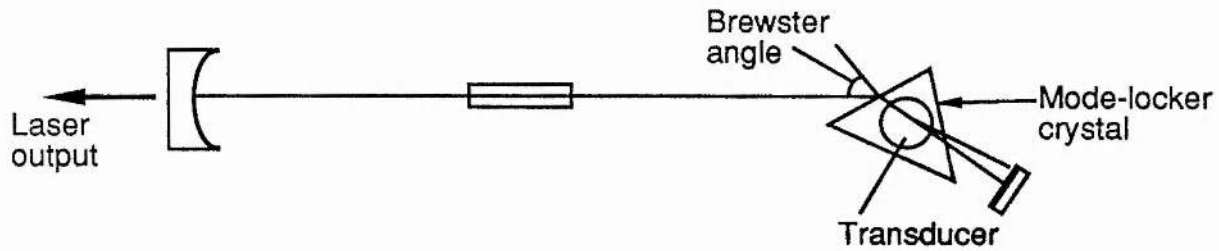

Figure 3.
A schematic diagram of the AO mode-locker.

However, the frequency of the resonance is extremely temperature dependent and so any fluctuations of the modulator temperature will cause changes in the diffraction efficiency and fluctuations in the mode-locked output. An oven around the modulator keeps its temperature constant and held a few degrees above ambient, prevents room temperature fluctuations disrupting the mode-locking. Heating of the mode-locker crystal still occurs from the laser beam itself and the applied r.f signal, which was typically 1 - 2 W. As the crystal is heated, the resonance frequency of the crystal rises and as it does so the coupling of r.f power into the crystal falls, allowing the crystal to cool. The resonance frequency then falls again, until it coincides with the driver frequency. Many AO mode-lockers operate in this metastable condition, with the diffraction efficiency being less than maximum. If for some reason the crystal cools (for instance, the laser is turned off) and the

driver frequency exceeds that of the resonance, the coupling efficiency is again reduced and the crystal will cool further, increasing the difference between the driver and resonant frequencies. This effect is known as thermal runaway and mode-locking will be lost. To over come this, the Spectra Physics mode-locker used an active feedback loop controlling the r.f power applied and hence the temperature of the crystal. The system was developed by Klann et al [15] and is shown diagrammatically in figure 4.

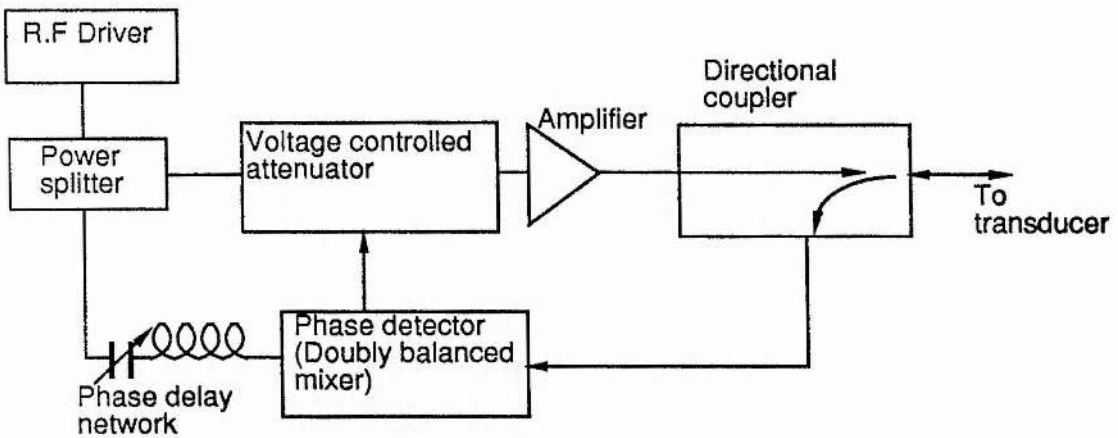

Figure 4.
Schematic diagram of the active feedback loop employed with the mode-locker.

The phase of the reflected signal from the mode-locker transducer is compared with the input signal by a doubly balanced mixer. This generates a voltage proportional to the difference between the phases of the two signals. This is applied to a voltage controlled attenuator (VCA) which allows the r.f power applied to the transducer to be varied. As the driver signal is tuned from below an acoustic resonance to above, the phase of the reflected signal shifts by 180° relative to the input. If the resonance frequency drops due to the crystal cooling, the output of the phase detector causes the VCA to increase the power applied to the transducer, heating the crystal and bringing the resonance back to the frequency of the driver signal. Similarly, if the crystal heats up, the power applied is decreased causing the modulator to cool. The acoustic resonance thus remains locked at the

driver frequency and there is no danger of thermal runaway. Also higher r.f powers may be used enabling greater diffraction efficiencies.

The mode-locker electronics provided a step wise variation of the drive frequency as well as a fine frequency control, giving ~ ± 300 Hz adjustment. Also the modulator position could be varied via a screw thread, enabling the cavity length to be matched to that corresponding to twice the acoustic frequency. Once the laser was mode-locked, occasional adjustments of the frequency were required for optimum stability but it was very seldom that mode-locked operation was lost.

Another useful advantage obtained with this type of active stabilisation, is that is possible to increase the modulation applied to the laser field. A higher modulation depth in the AO modulator essentially means that the mode-locker appears transparent to the optical field for a shorter time period, thus giving rise to the production of shorter pulses. This was achieved in the following way. Once the laser had been initially mode-locked onto a crystal resonance, the r.f drive frequency was gradually stepped up. As the feedback loop detected a frequency mismatch, the servo system increased the r.f power applied to the modulator thereby also pushing up the crystal resonance. Hence a higher power is applied to the transducer increasing the acoustic modulation and by following the increased frequency with a decrease in cavity length, improved mode-locked operation is obtained.

2.3 Laser Performance and characterisation.

The laser is specified to produce time average powers > 7 W with a mode-locked pulse duration of 120ps. For the majority of the work reported in this thesis, the laser did meet these specifications although over the last few months a gradual decline in output power occurred. A schematic diagram of the experimental arrangement for the laser characterisation is shown in figure 5. The photodiode was an AEG Telefunken BPW 28 which provided a trigger for the streak camera system (see chapter 1) and also enabled monitoring of the pulse train on a Tektronix 7834 storage oscilloscope and a Hewlett-Packard 8558B spectrum analyser.

Initially the output power as a function of lamp current was recorded and the results are shown in figure 6a. The cavity clearly begins to become unstable at a current of ≈ 17.6 A. Note that the absolute values of current indicated here only apply to this particular lamp, alignment etc., and will vary with different lamps and time. It was predicted that increasing the mode-locker drive frequency and thereby the modulation depth, should enable the production of shorter pulses. This was evaluated experimentally by gradually increasing

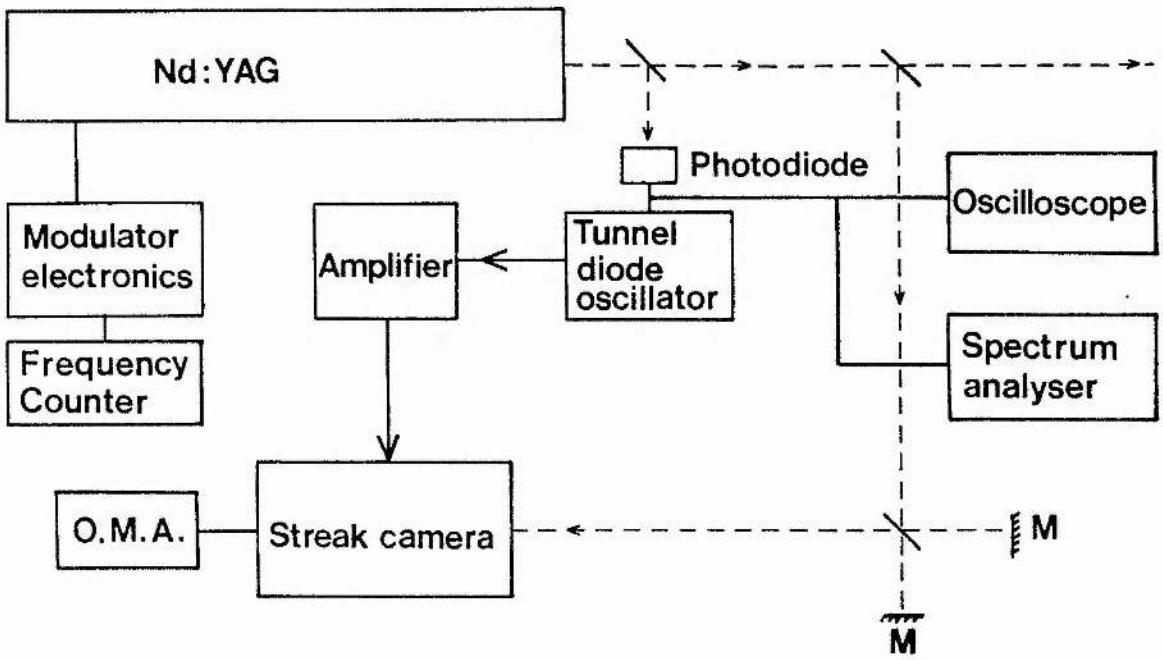

Figure 5.
The experimental arrangement for a laser characterisation.

the r.f frequency and optimising for the best pulses at each step by shortening the cavity length. The plots in figure 6b show the increase in applied r.f power and corresponding decrease in pulse duration as the frequency was incremented. The average laser power remained approximately constant. In figure 7 the recorded streak camera traces of the shortest pulses obtained are shown, along with a photograph of a typical pulse train.

With the laser adjusted to give pulses of shortest duration (the shortest recorded were ≈ 74 ps) it was often noted that a small 'foot' was present to the rear of the pulse as in figure 7a. In some cases this became of

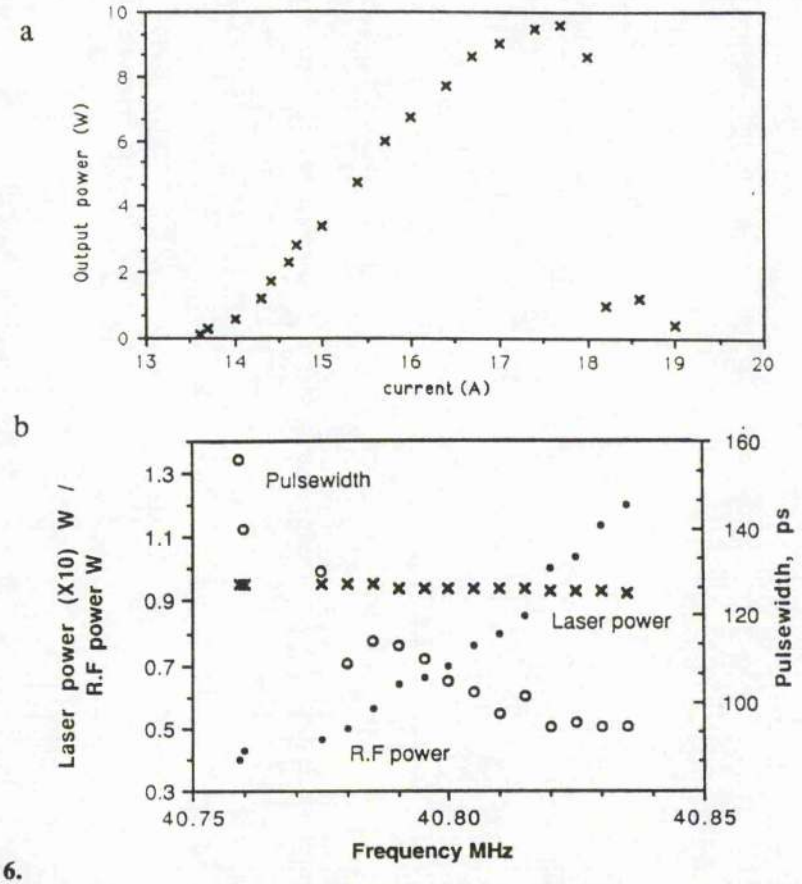

Figure 6.
(a) Laser output power as a function of lamp current (b) the r.f power, average laser power and pulse width plotted as a function of modulator drive frequency.

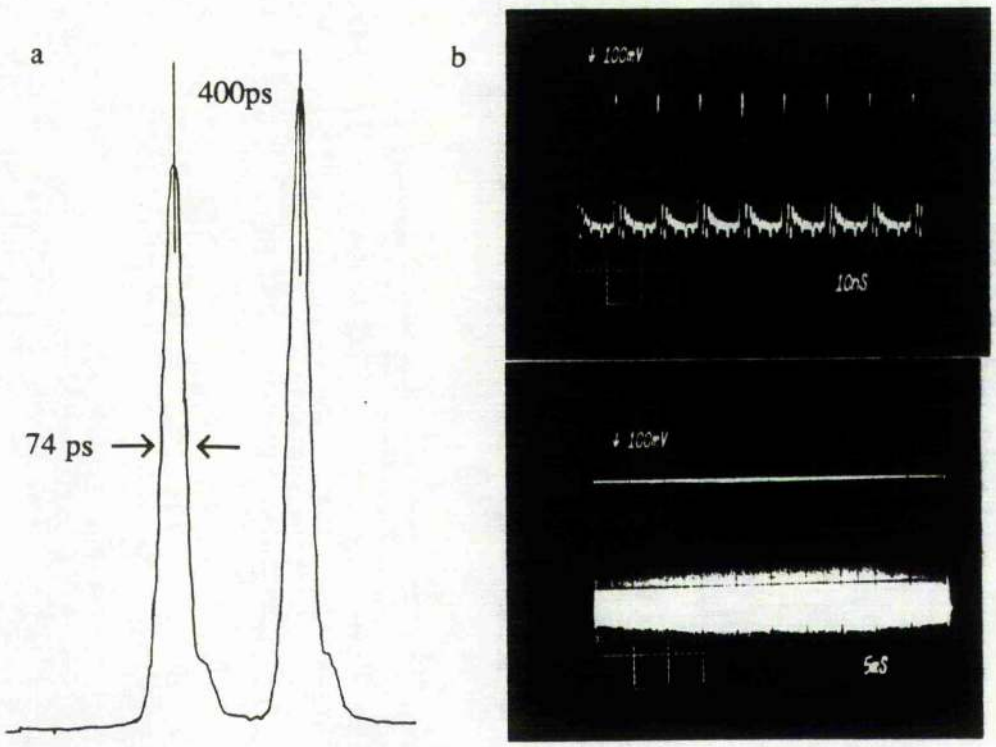

Figure 7.
(a) Streak camera trace of the shortest pulses recorded from the laser (b) typical pulse train as observed on the photodiode.

sufficient intensity to constitute a second pulse. However, by correct alignment of the cavity short pulses could be produced with only slight pulse asymmetry. It was noted that the laser pulse duration and stability were very sensitive to the mode-locker frequency and so an investigation into frequency detuning effects was conducted. It was found easier and more reliable to alter the modulator frequency, leaving the cavity length unchanged. This was because fine frequency adjustments could be made without affecting the resonator alignment as might easily be the case by trying to adjust the resonator on the length control. In any case, the two adjustments have the same effect, decreasing the frequency would be the same as decreasing the cavity length.

Pulse amplitude fluctuations for the optimally mode-locked Nd:YAG were found to have two major components. (Optimal mode-locking is taken here to mean minimum pulse duration). The first component was a regular ripple (~ 3% peak-to-peak) on a millisecond timescale attributed to the Krypton arc lamp power supply. The second was manifest as a pair of sidebands separated from the central ~ 82 MHz spectral peak by ~ 60 KHz on the spectrum analyser, and also as a 4% ripple with period ~ 15 μs on the oscilloscope. This is seen in figure 8a. The second component may be attributed to relaxation oscillations in the gain medium [11,16]. Relaxation oscillations and spiking are common in lasers where the recovery time of the excited state population inversion is substantially longer than the cavity decay time. In other words, if the gain medium has a long upper state lifetime compared to the cavity decay time. Solid state lasers are particularly prone to this type of oscillation and is a major cause of instability. The relaxation period is a characteristic of the cavity and gain medium, resulting from an interplay between the optical field and population inversion. An increasing optical field intensity depletes the inversion, lowering the optical gain available until at some point the optical field begins to decrease. This means that less stimulated emission occurs allowing the inversion to build up again and the cycle is repeated. Generally the oscillations result from some perturbation of the laser and exponentially decay away. However if some driving force is present, the oscillations may be sustained

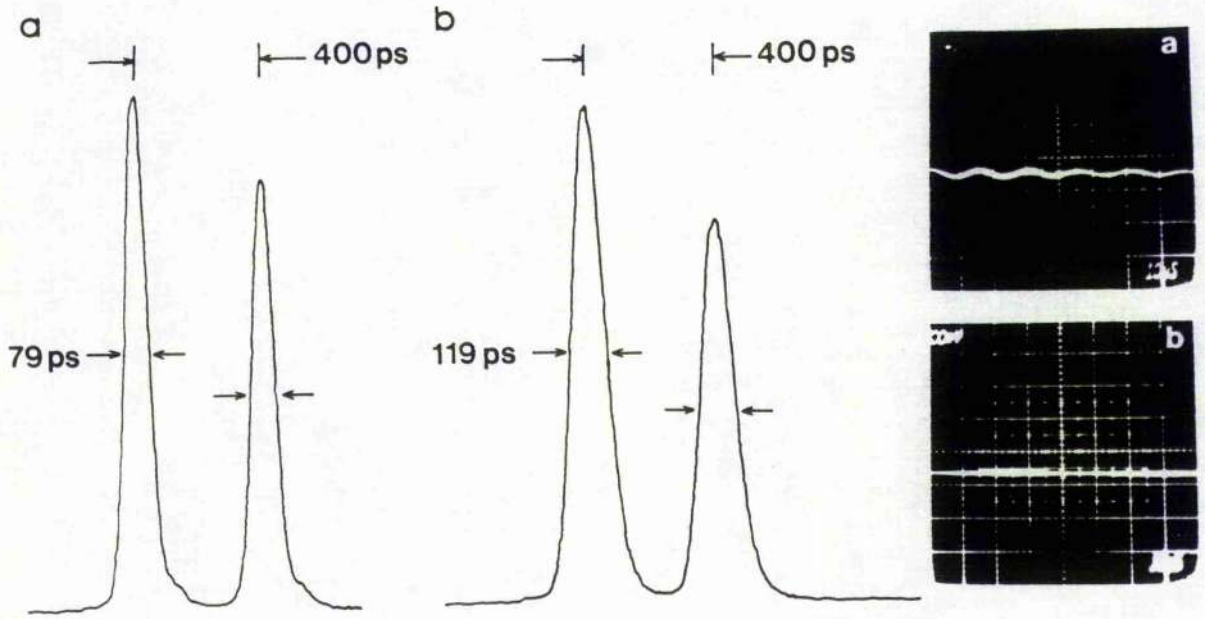

Figure 8.
Synchroscan streak camera intensity profiles of (a) short pulses (f = 40.800272 MHz) and (b) pulses corresponding to minimum 60 kHz modulation ($\Delta f \approx -181$ Hz). The photographs show pulse amplitude fluctuations for each case. (200 mV/div; 10 μs/div).

and become of such magnitude that the laser self Q-switches, as described below. From a simple theoretical treatment of these relaxation oscillations [16,17], a period of ~ 20 μs is predicted for the parameters applying to our laser, in good agreement with the our observations. Detuning the frequency from this 'optimum' led to increased mode-locked pulse widths and a plot of pulse duration verses drive frequency detuning is presented in figure 9. Of particular interest was the laser behaviour for slight negative detuning. For a small frequency range ($\Delta f \sim -100$ to -250 Hz) a significant reduction in relaxation oscillation amplitude modulation and corresponding sideband intensity was observed. This region is shown shaded in figure 9. The synchroscan streak camera intensity profile in figure 8b was obtained for a detuning of -181 Hz where the 60 KHz sidebands were no longer apparent. Pulses of 119 ps duration were recorded and the output power showed no reduction from that measured for the shortest pulses. At further negative frequency

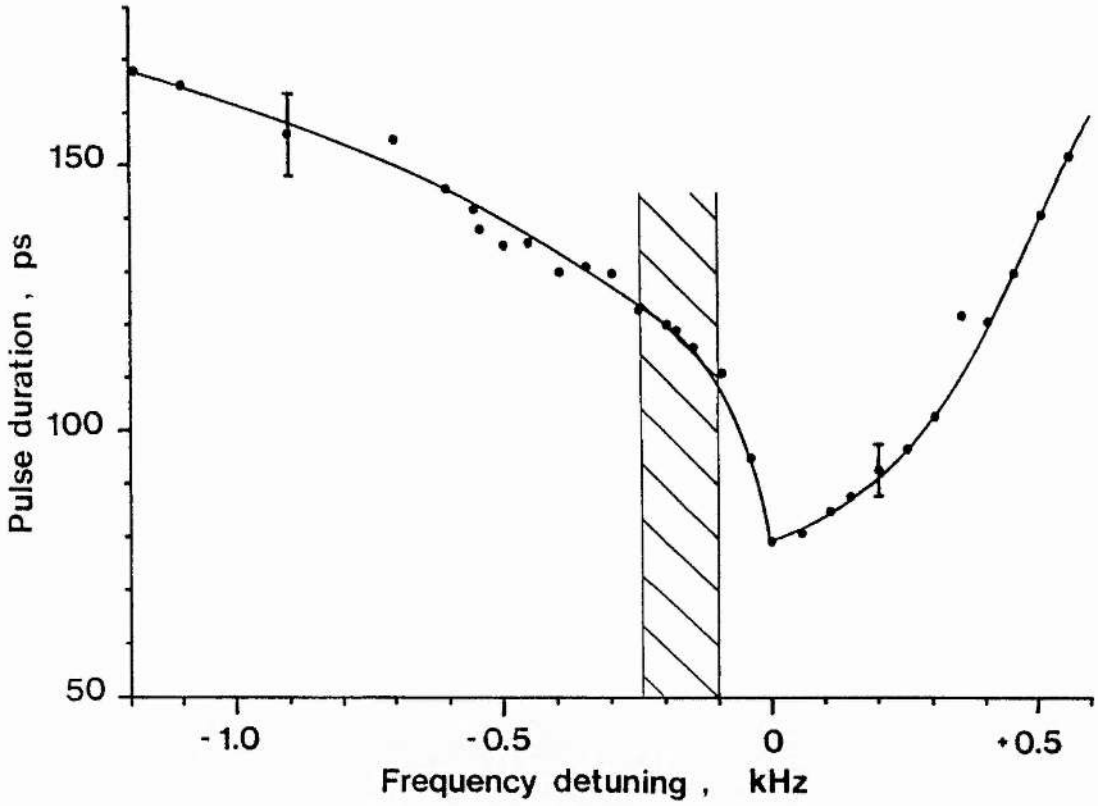

Figure 9.
The dependence of mode-locked pulse duration on frequency detuning from the optimum modulator frequency (f = 40.800272 MHz). The shaded area indicates the region of minimum sideband intensity.

detunings, greater pulse durations with an increased presence of the 60 kHz modulation were observed. However even at the largest negative detuning (~ -1 kHz) shown in figure 9, the 60 kHz modulation depth (or sideband intensity) did not approach the magnitude experienced at only 500 Hz positive detuning where similar pulse durations were recorded. A positive frequency detuning of only 50 Hz caused a marked increase in the amplitude modulations and instabilities due to relaxation oscillations.

In reference [18] it was reported that for particular frequency detunings (both positive and negative) undamped oscillations were obtained so that the laser emitted a regular series of spikes as the envelope of the pulse train. This 'self Q-switching' behaviour was also observed in our laser for frequency detuning over the approximate ranges -2 kHz to -4 kHz and +1 kHz to +3 kHz. Operation in the positive range however was undesirable since the

stability in terms of amplitude fluctuations, Q-switched oscillation period and envelope duration was very poor. On the negative detuning side the stability of the Q-switched output was excellent with peak-to-peak amplitude fluctuations as low as 5% on a millisecond timescale. Figure 10 shows the onset of the Q-switched operation. During self Q-switching operation the spectrum analyser revealed a series of stable sidebands (typically 5-10 pairs) separated by 50 - 100 kHz. Time average output powers of ≈ 7.5 W were typical during this behaviour. Figure 11 shows how both the oscillation period and the envelope duration varied as a function of frequency detuning. It can be seen that as the frequency was decreased, the oscillation period decreased and the envelope broadened. In addition it was noted that the magnitude of the Q-switched envelope increased for smaller frequency detunings, in accordance with the observation that the average power remained essentially constant. This overall behaviour was also

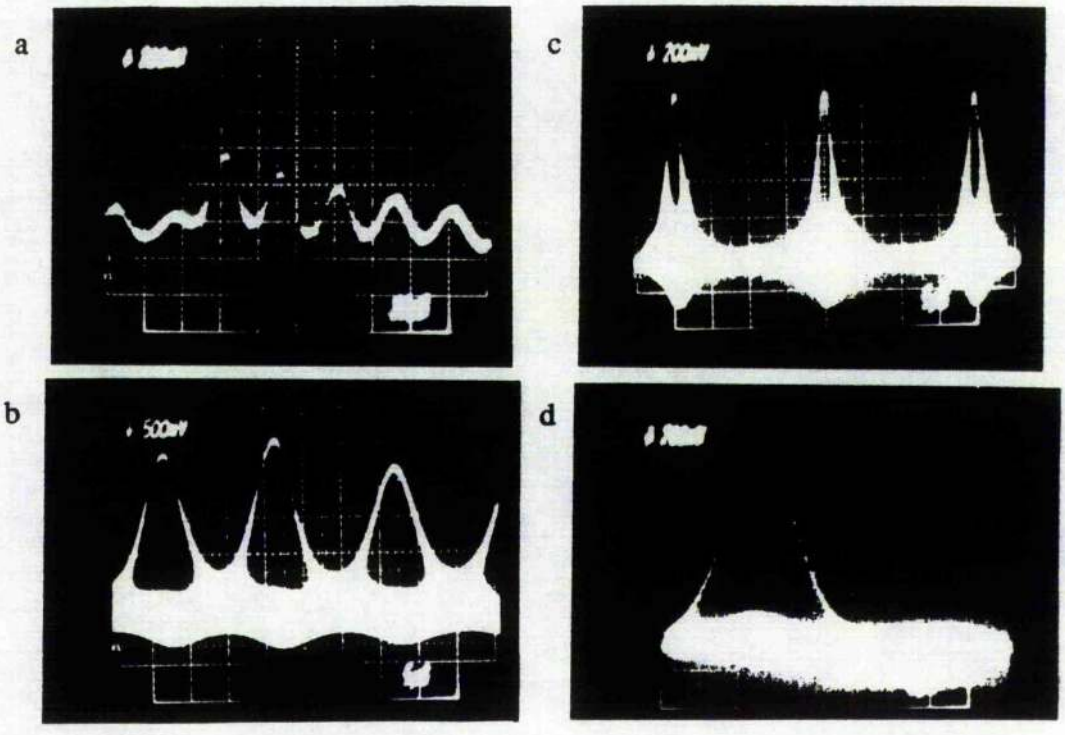

Figure 10.
(a) Onset of damped relaxation oscillations due to small positive or negative detuning $\Delta f \approx 1$ kHz (b) laser beginning to self Q-switch, $\Delta f \approx -2$ kHz (c) Output train of stable self Q-switched pulse envelopes (5 μs/div) (d) Single Q-switched envelope (1 μs/div). ($\Delta f \approx -2.1$ kHz)

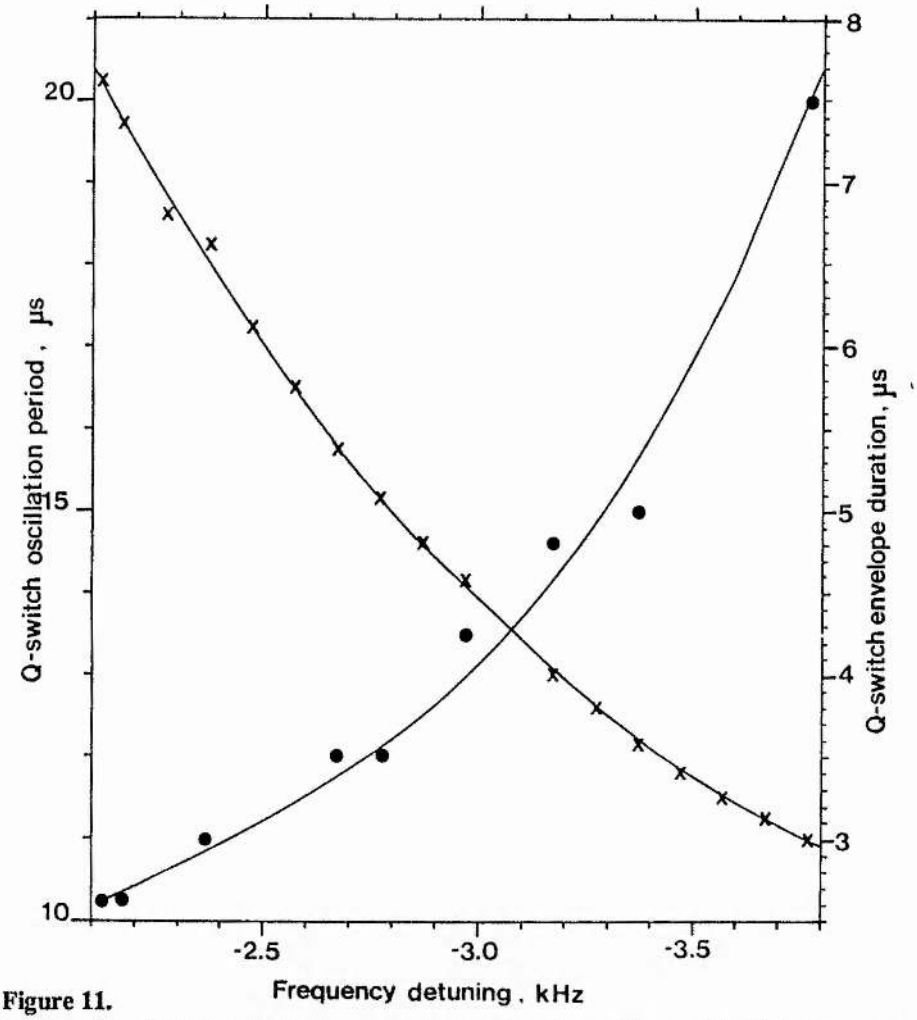

Figure 11.
Plot of Q-switched oscillation period (crosses) and envelope width (dots) as a function of frequency detuning.

observed for positive frequency detuning. The Q-switched envelope was composed of many mode-locked pulses and in order to obtain an estimate of the Q-switched mode-locked pulse duration, the syncroscan streak camera was employed. In this case the driving signal for the deflection plates was derived from an r.f reference output of the mode-locker electronics. This signal was amplified and frequency doubled twice to obtain the required sweep frequency of ≈ 164 MHz. Typical pulse intensity profiles are shown in figure 12, again for a detuning of $\Delta f \approx -2.1$ kHz. The pulse measurement of 237 ps (FWHM) is in good agreement with the photodetector and sampling oscilloscope measurement (~ 200 ps) reported in reference [18]. These Q-switched mode-locked pulses typically had pulse energies ~ 4 - 5 times greater than the CW mode-locked pulses at $\Delta f = 0$.

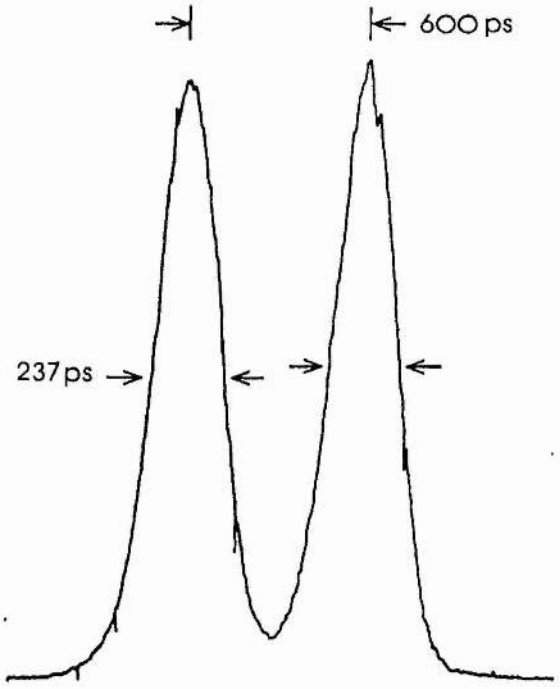

Figure 12.
Synchroscan streak camera intensity profiles of the Q-switched mode-locked pulses. ($\Delta f \approx -2.1$ kHz)

Investigation of the background radiation between the Q-switched envelopes, using the 7834 oscilloscope, revealed mode-locked pulses whose energy content was about 10^3 smaller than those at the peak of the envelope, however the picosecond nature of the pulses did not decay between the Q-switched spikes.

2.4 Conclusions.

A description of the Nd:YAG laser used as a pump source and the results of a characterisation have been presented. Typical pulse durations of approximately 90 ps were routinely obtained with time average output powers ≈ 7.5 W. However, it has been observed that reduced pulse amplitude fluctuations can be obtained for a slight negative frequency detuning of the mode-locker drive frequency, giving rise to pulses ≈ 120 ps in duration. As will be seen in the following chapters, this effect may be used to advantage in the observation of self-phase modulation in optical fibres and the optical pumping of the

KCl:Tl colour centre laser. In particular, the operation of the 'Soliton' laser (chapters 5,6) was found to be dependant upon a stable pump source. The drawback of a slight increase in pump pulse duration, was more than offset by greater laser stability.

For the work in the following chapter, an AO modulator as described above was used. However, for the optical pumping of the KCl:Tl colour centre laser described in chapter 4, a new mode-locker was used which operated in the Bragg regime and was situated just before the output coupler. The laser exhibited a similar behaviour with this new mode-locker and was usually operated in the region of minimum noise. Under these conditions the pulse duration was typically 100 ps with ~ 3% peak-to-peak amplitude modulations due to the Krypton arc lamp power supply.

There have recently been other servo systems developed and reported in the literature which monitor the actual laser pulse train and use active feedback to the AO modulator to greatly reduce both the amplitude and phase noise of the laser [19,20].

References.

1. J E Geusic, H M Marcos, L G Van Hitert; Appl. Phys. Lett. **4**, 182 (1964)
2. A Seilmeier, W Kaiser, B Sens, K H Drexhage; Opt. Lett. **8**, 205 (1983)
3. P Beaud, B Zysset, A P Schwartzenbach, H P Weber; Opt. Lett. **11**, 24 (1986)
4. L F Mollenauer, N D Vieira, L Szeto; Opt. Lett. **7**, 414 (1982)
5. B P Nelson, D Cotter, K J Blow, N J Doran; Opt. Comm. **48**, 292 (1983)
6. A S L Gomes, W Sibbett, J R Taylor; Appl. Phys. B **39**, 43 (1986)
7. A S Gouveia-Neto, M E Faldon, A S B Sombra, P G J Wigley, J R Taylor; Opt. Lett. **13**, 901 (1988)
8. M DiDomenico, J E Geusic, H M Marcos, R G Smith; Appl. Phys. Lett. **8**, 180 (1966)
9. L M Osternik, J D Foster; J Appl. Phys. **39**, 4163 (1968)
10. A R Clobes, M J Brienza; Appl. Phys. Lett. **14**, 287 (1969)
11. W Koechner; IEEE J Quant. Electron. **QE-8**, 656 (1972)
12. W Koechner; 'Solid State Laser Engineering' Springer Verlag (1988)
13. T B Read; Appl. Phys. Lett. **9**, 342 (1966)
14. R B Chesler, D Maydan; J Appl. Phys. **43**, 2254 (1972)
15. H Klann, J Kuhl, D Von der Linde; Opt. Comm. **38**, 390 (1981)
16. A Yariv; 'Optical Electronics' 3rd ed. Holt and Saunders (1985)
17. A Siegman; 'Lasers' University Science Books (1986)
18. H J Eichler; Opt. Comm. **56**, 351 (1986)
19. M J W Rodwell, K J Weingarten, D M Bloom; Opt. Lett. **11**, 638 (1986)
20. M J W Rodwell, D M Bloom, K J Weingarten; IEEE J Quant. Electron. **QE-25**, 817 (1989)

Chapter 3.

Nonlinear Pulse Propagation in Optical Fibres.

3.1 Introduction.

Since the development of the laser in 1960, a revolution has taken place in the field of nonlinear optics. Our knowledge and understanding of the behaviour of matter under the influence of intense optical fields has been dramatically increased and a whole range of new phenomena have been discovered [1,2]. The availability of low loss, single-mode optical fibres has recently opened up a new era in nonlinear optics, due mainly to the following reasons: (1) the small core sizes (typically ~ 2-8 μm in diameter) enable high power densities to be achieved with relatively low input powers; (2) these high power densities can be maintained over long distances due to the guiding nature of optical fibres and so greatly increased interaction lengths are obtained compared to bulk materials; and (3) the transverse profile of the beam is well characterised and virtually all of the beam experiences the same nonlinearity [32]. These factors can considerably lower the threshold powers required for the nonlinear processes. While it is considered that nonlinear effects in optical fibres will be the main optical power limitation to an optical communications network, some of these same effects have potentially useful applications as optical amplifiers and oscillators and the nonlinear propagation of pulses in fibres has been extensively studied over the last few years. The main nonlinear processes in optical fibres are: stimulated Brillouin scattering (SBS), stimulated Raman scattering (SRS), the optical Kerr effect, self-phase modulation (SPM), four-photon mixing, nonlinear absorption and most recently second harmonic generation.

Stimulated Brillouin scattering [3] has potentially the lowest threshold in glass fibres. SBS results from the interaction of the incident light with a generated acoustic wave and the scattered light or Stokes wave. In a classical picture the incident pump light creates a

pressure (acoustic) wave due to electrostriction, which then scatters some of the pump creating a Stokes wave. The frequency shift of the Stokes from the pump light depends on the scattering angle and is a maximum for 180° and zero for 0°. Thus in optical fibres SBS only creates a backward traveling wave. The Brillouin gain coefficient, G_B ($\approx 4.3\times10^{-11}$m/W) is dependent upon the ratio of the Brillouin linewidth, $\Delta\upsilon_B$, to the pump linewidth, $\Delta\upsilon_p$. For the case were $\Delta\upsilon_p << \Delta\upsilon_B$, the gain coefficient is independent of $\Delta\upsilon_p$, but for $\Delta\upsilon_p > \Delta\upsilon_B$ it is proportional to $\Delta\upsilon_B/\Delta\upsilon_p$ [4]. In fused silica $\Delta\upsilon_B \sim$ 38 MHz at λ= 1.0 μm and it varies as λ^{-2}. The threshold (or critical power, since there is no actual 'threshold' value) for SBS is [4]

$$P_c = \frac{21A}{G_B L}\frac{\Delta\upsilon_p}{\Delta\upsilon_B}\times 2 \qquad (3.1)$$

where A is the effective core area and L is the effective fibre length which is different from the actual length, l, due to fibre loss (see section 3.2.1). The factor of two is included for fibres that do not preserve the input polarisation. Typically, in our experiments $L \approx l \approx$ 200 m (since the fibre loss is small ~0.9 dB/km), $A \approx 4\times 10^{-11}$ and using a CW mode-locked Nd:YAG laser, $\Delta\lambda_p \approx$ 0.04 nm thus $\Delta\upsilon_p \approx$ 10 GHz. Putting these into equation (3.1) gives $P_c \approx$ 50 W. The maximum available pump power from the laser was ~ 8 W, so we did not expect any significant SBS to occur and this was indeed the case. Note that since SBS is a backward wave interaction, the Brillouin wave sees the average power of a train of pulses rather than the peak power.

The work in this chapter has been mainly concerned with SPM and SRS in optical fibres. These two processes will be described in detail and experimental data presented, along with their relevance to the temporal compression of optical pulses and fibre Raman oscillators respectively. Many articles describe the other nonlinear processes [4-7] which are not of a major relevance here and it suffices to say that relatively short interaction lengths and\or the lack of phase matching, prevented their observation.

3.2 Self-Phase Modulation (SPM).

The nonlinear response of almost any transparent material to a high intensity optical field gives rise to the optical Kerr effect. It is essentially manifest as an intensity dependent change in the refractive index of the material which can then cause self-phase modulation (SPM) and self-focusing. A beam propagating in a bulk material with a transverse gaussian intensity profile, will experience a higher refractive index at the centre of the beam than in the wings and so it creates its own positive lens in the medium, causing a self-focusing effect [8]. The already high intensity beam after self-focusing has an even greater power density and this often leads to physical damage of the material. Frequency broadening due to SPM was first observed in such a self-focused beam by Shimizu in CS_2 [9]. In (single-mode) optical fibres, however, the beam is already well confined, so that appreciable SPM may occur in the absence of any self-focusing effects. As was pointed out earlier, long lengths of fibre reduce the power required to observe self-phase modulation, and since the effect is accumulative over length, optical fibres are an ideal medium in which to study SPM.

Due to the combined action of SPM and group velocity dispersion, pulses propagating along a fibre develop a frequency sweep or 'chirp' across the pulse which, in conjunction with a suitable dispersive delay line, gives rise to the powerful technique of optical pulse compression and this will be described later. We first develop a simple theory of SPM for a gaussian input pulse and then compare this to an experimental study of the peak power and pulsewidth dependencies of SPM in three samples of single-mode optical fibre.

3.2.1 Theory of SPM.

An electric field E applied to a dielectric induces a polarisation P in the medium due to a distortion of the electron charge clouds. For small applied fields, the polarisation is linear with E i.e. $P \propto E$ or $P = \varepsilon_o \chi_1 E$, where ε_o is the permittivity of free space and χ_1 is the susceptibility of the material. If the field strength is increased, P may vary nonlinearly with E and is more generally expressed as

$$P = \varepsilon_o \chi_1 E + \chi_2 E^2 + \chi_3 E^3 + \ldots \qquad (3.2)$$

with χ_2, χ_3 etc. being the (weaker) nonlinear susceptibility terms. (Strictly speaking, P is a vector and the susceptibility constants are tensor quantities). Since E is an optical wave, the second term in (3.2) can give rise to second harmonic generation. This will not occur in isotropic crystals however, were reversing the direction of E, simply reverses the direction of P i.e. P(E) = -P(-E). In this case all the terms with even powers of E must be identically equal to zero. Such is the case in glasses and specifically in fused silica from which the majority of optical fibres are fabricated. The total electric displacement induced in the medium is defined as:

$$D = \varepsilon_o E + P \, .$$

Substituting (3.2) into the above with $\chi_2 = 0$ and neglecting terms higher than χ_3,

$$\begin{aligned} D &= \{ \varepsilon_o(1+\chi_1)+\chi_3 E^2 \}E \qquad (3.3) \\ &= (\varepsilon_1 + \chi_3 E^2)E \end{aligned}$$

for an isotropic medium, where $\chi_3 E^2$ is the nonlinear dielectric constant. The refractive index of the medium is related to ε by $n = \sqrt{\varepsilon/\varepsilon_o}$ and so

$$n = \frac{1}{\sqrt{\varepsilon_o}} (\varepsilon_1+\chi_3 E^2)^{1/2} \, .$$

By expanding this as a Taylor series about E=0, we obtain

$$n = \frac{1}{\sqrt{\varepsilon_o}} (\varepsilon_1^{1/2} + \frac{\chi_3}{2\,\varepsilon_1^{1/2}} E^2 + \ldots)$$

and neglecting terms involving E^3 and greater, this then gives us the following expression for a nonlinear index of refraction:

$$n = n_o + n_{2E} E^2$$

where n_o is the linear or low intensity refractive index and n_{2E} the nonlinear index. From the above, it can be seen that an optical signal of angular frequency ω, will generate the third harmonic at 3ω due to the χ_3 term. However this is weak and in most cases is not phase-matched. There will also be a time averaged change in the index which can be written as

$$n = n_o + n_{2E}\langle E^2 \rangle$$
$$= n_o + \delta n$$
$$= n_o + n_2 I \qquad (3.4)$$

where $\langle E^2 \rangle$ is the time average of the square of the field and I the optical field intensity. This then is the optical Kerr effect and n_2 is called the Kerr coefficient or self-focusing coefficient. The value of $n_2 \sim 3.2 \times 10^{-20}$ m²/W for fused silica. The nonlinearity described above is assumed to have an instantaneous response time, this would not seem to be an unreasonable assumption due to the electronic nature of the effect, and a response time ~ 10^{-15} s has been confirmed [10,11].

We now consider an optical pulse with a gaussian temporal profile propagating along a length of fibre. It is clear that each part of the pulse, having a different intensity, will experience a different refractive index and hence a change in phase occurs across the pulse given by

$$\Delta\Phi(t) = - kn_2 I(t) L \qquad (3.5)$$

where k is the wavenumber of the pulse and L is the *effective* fibre length. Since an optical fibre has a finite absorption, the actual length l, of the fibre is replaced by the effective length defined as [12]

$$L = \int_0^l \exp(-\alpha x)\, dx$$

$$\therefore \quad L = \frac{1-e^{-\alpha l}}{\alpha} \qquad (3.6)$$

where α is the fibre attenuation coefficient with dimensions of length^{-1}.

Since the intensity and hence the phase shift, is a function of time, the pulse develops a frequency shift, $\Delta\omega$, from the carrier, ω_o, which is proportional to the time derivative of the intensity:

$$\Delta\omega(t) \approx \frac{d\Delta\Phi(t)}{dt} = - kn_2 L \frac{dI(t)}{dt} \; . \qquad (3.7)$$

From this it can be seen that the instantaneous frequency of the carrier in the leading part of the pulse ($t<0$) will be down-shifted, while in the trailing part ($t>0$) it will be up-

shifted. A gaussian input pulse of duration T_p full width at half maximum (FWHM) has the form

$$I = I_o \exp-(t/\tau)^2 \qquad (3.8)$$

$$\text{where} \quad T_p = 2\sqrt{\ln 2}\,\tau\,.$$

The instantaneous frequency shift as a function of time, for such a pulse is shown in figure 1b. The maximum phase shift occurs at the peak of the pulse, $\Delta\Phi_{max} = -kLn_2I_o$, and the maximum frequency shift at the points of inflection, where dI/dt is a maximum. Setting $d^2I/dt^2 = 0$ we obtain:

$$t = \tau/\sqrt{2}$$

and

$$\Delta\omega_{max} \approx \pm\sqrt{2/e}\; kLn_2I_o\,\frac{2\sqrt{\ln 2}}{T_p}\,. \qquad (3.9)$$

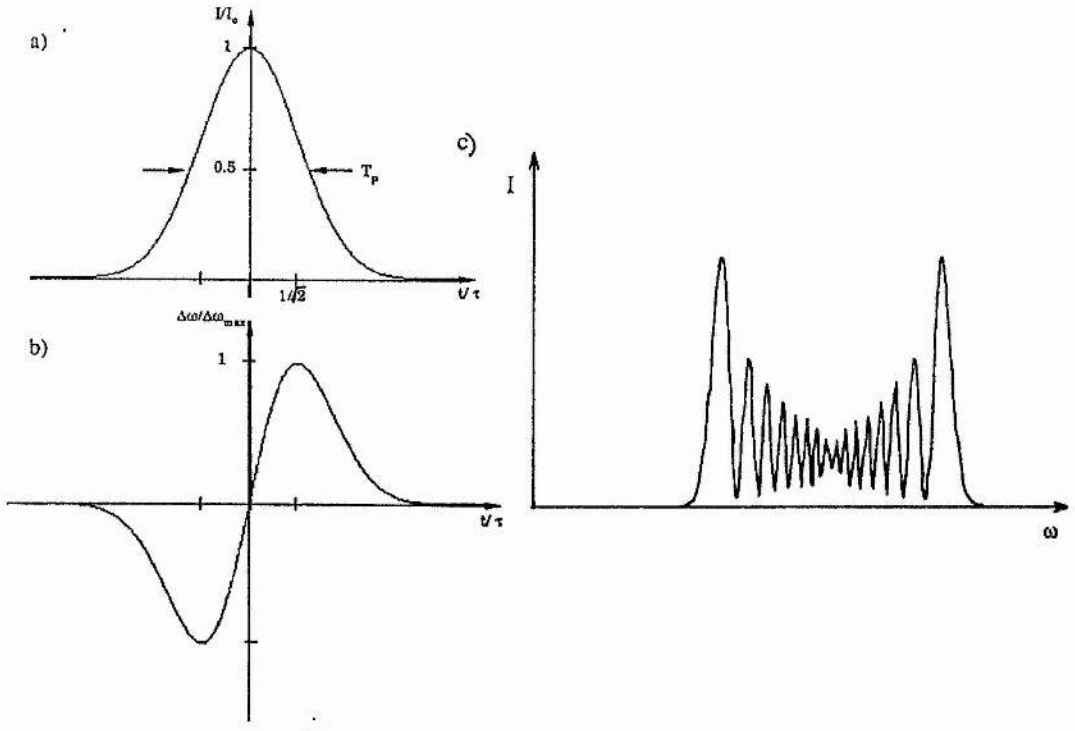

Figure 1.
(a) Input gaussian pulse (b) Instantaneous frequency shift due to SPM and (c) Frequency spectrum of pulse after propagating through a length of fibre.

The linear portion of the curve in figure 1b, extending over approximately $-0.5 \leq t \leq +0.5$, is termed the linear frequency chirp of the pulse, and it is this part which is

successfully utilised in pulse compression. The chirp is also referred to as an up-chirp, since the frequency increases with time. It should be noted that the time-dependent phase modulation does not affect the temporal intensity distribution of the pulse and in the absence of any group velocity dispersion, the pulse envelope after propagating through a length of fibre should be exactly the same as the input pulse.The actual frequency spectrum is obtained from the Fourier transform of the electric field of the pulse. For the gaussian pulse of (3.8), the electric field amplitude is

$$E(t) = \sqrt{I_o}\ \exp -1/2(t/\tau)^2\ \exp j\omega_o t\ . \qquad (3.10)$$

After passing through a length of fibre, SPM transforms this to

$$E_{out}(t) = \sqrt{I_o}\ \exp -1/2(t/\tau)^2\ \exp j(\omega_o t - \Delta\Phi(t))$$

so the frequency spectrum will then be given by $|E(\omega)|^2$ where

$$E(\omega) = \sqrt{I_o} \int_{-\infty}^{\infty} \exp -1/2(t/\tau)^2 \exp -j\Delta\Phi(t) \exp -j(\omega-\omega_o)t\ dt\ . \qquad (3.11)$$

This function can be evaluated numerically and a typical example is plotted in figure 1c. From figures 1a,b it can be seen that there are in general two points in time which give the same frequency shift. The characteristic interference structure of the SPM spectrum can be thought to arise from the constructive and destructive interference of the pairs of frequency components generated from the two points in time.

For experimental measurements on SPM, we normally measured the total bandwidth in terms of wavelength and so (3.9) can be converted to give the maximum spectral width of the pulse:

$$\Delta\lambda = \Delta\lambda_i + \frac{\lambda L n_2 P_o}{cAT_p}\ 4\sqrt{2\ln 2/e}\ . \qquad (3.12)$$

Here $\Delta\lambda_i$ is the initial bandwidth of the pulse, P_o the pulse peak power and A the effective core area.A significant fraction of the pulse energy may propagate in the cladding of the fibre, although the intensity will be low enough to prevent any significant SPM and so the area used in the above is an effective area, not the actual core area A_{core}. This fraction depends on the V number (the normalised frequency) for the propagating mode and for

smaller V values, more of the pulse energy will be in the cladding. The ratio A/A_{core} is approximately 1 for V = 2.55 and larger for smaller V values. The table below gives some values of A/A_{core} for different V numbers.

Table 1.

V	A/A_{core}
1.5	2.43
2.0	1.47
2.5	1.1
2.53	1.09
3.0	0.93
4.0	0.77

So far, it has been assumed that linear polarisation is maintained within the fibre but for non-polarisation preserving fibres, the polarisation is completely scrambled which effectively reduces δn. This is accounted for by averaging the values of δn for linear and circular polarisations, giving a correction factor of 6/5 [12]. Hence

$$n_2 \text{ (linear)} = \frac{6}{5} n_2 \text{ (average)} .$$

Effect of Group Velocity Dispersion (GVD).

In all of the above analysis, the refractive index of the medium has been assumed to be independent of the optical frequency. In a real medium, n is generally a function of ω and this gives rise to chromatic or group velocity dispersion (GVD). If $k = 2\pi / \lambda_o$ is the free space propagation constant of an optical pulse, the propagation constant in the medium, β, will be

$$\beta(\omega) = n(\omega)\, k .$$

The effect of dispersion can then be accounted for by expanding β as a Taylor series about the centre frequency ω_o ,

$$\beta(\omega) = \beta_o + \beta`(\omega - \omega_o) + 1/2\, \beta``(\omega - \omega_o)^2 + ... \qquad (3.13)$$

where the primed terms refer to derivatives with respect to ω. Now the pulse group velocity $v_g = d\omega/d\beta$ or $\beta' = 1/v_g$ and thus

$$\beta'' = \frac{d}{d\omega} 1/v_g = -\frac{1}{v_g^2} \frac{dv_g}{d\omega}$$

which is a measure of the group velocity dispersion. An initially unchirped, bandwidth limited pulse of arbitrarily low intensity, after propagating through a length L of fibre, will suffer temporal broadening and develop a linear frequency chirp due to GVD. By considering the phase shift, $\beta(\omega)L$, acquired by the pulse and using (3.13), it can be shown (see Appendix) that the broadening of a low intensity gaussian pulse is given by:

$$T_{out} = \left(T_{in}^2 + \left[\frac{4\ln 2\ \beta''\ L}{T_{in}} \right]^2 \right)^{1/2} \qquad (3.14)$$

where the pulse durations are FWHM. The dispersion, D, of a fibre is defined as $D = 1/L\ dT/d\lambda$ where T is the transit time of the fibre i.e. $T = L/v_g$ and D is normally measured in units of ps/nm/km. Thus D is related to β'' by

$$\beta'' = \frac{\lambda^2}{2\pi\ c} D \qquad (3.15)$$

enabling (3.14) to be expressed in a practical form.

For the case where SPM is significant, the input pulse will develop extra frequency components and so the broadening of such a pulse will tend to be greater than that given by (3.14). The full treatment of a pulse experiencing both SPM and GVD in a fibre, involves the derivation and solution of the nonlinear Schrödinger equation [13,14]. However we can qualitatively see that a pulse chirped by SPM and influenced by normal GVD, will broaden into a 'square topped' shape pulse. It can be seen in figure 1b, that the edges of the pulse ($-1/\sqrt{2} > t/\tau > +1/\sqrt{2}$) show a down-chirp (frequency decreasing with time) and so will actually be compressed within the fibre. Thus the sides of the pulse become steeper while the main central part is broadened and more of the pulse is then described by a linear frequency chirp. These features are illustrated in figures 2a,b which should be compared to figures 1a,b. It should perhaps be pointed out that a pulse chirped in this way will broaden if $\lambda_o < 1.3\ \mu m$ where the dispersion in fused silica is positive and 'red' component

frequencies travel faster than 'blue' components. For $\lambda_o > 1.3$ μm the dispersion is of opposite sign and temporal compression within the fibre takes place, leading to the possibility of optical solitons [15] (see chapter 5).

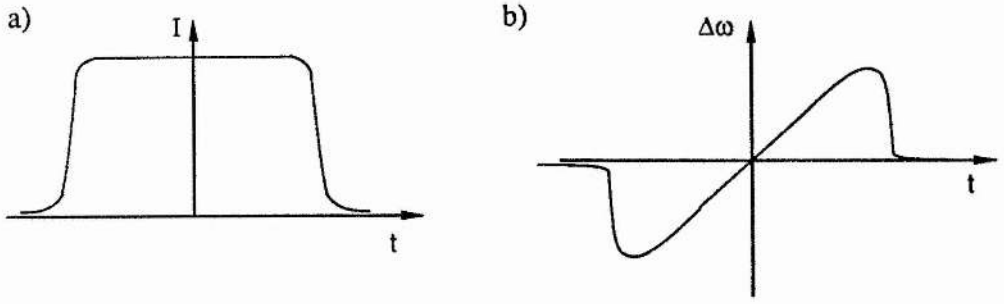

Figure 2.
(a) Pulse shape and (b) instantaneous frequency shift of a gaussian input pulse after experiencing SPM and significant GVD due to propagation through a length of dispersive fibre.

In our experiments described in the next section, where the effects of SPM on optical pulses is examined, the maximum fibre length used was approximately 150 m. The fibre dispersion at 1.06 μm, D ≈ 30 ps/nm/km and the input pulse durations were about 100 ps. Using (3.14) and (3.15) with these values, T_{out} is calculated to be 100 ps and so no observable pulse broadening would be expected for the case of GVD alone. However, we have to consider whether the presence of GVD *and* SPM will cause a significant broadening to occur over this length.

We follow the approach of Fisher and Bischel [16] where a pulse is considered to propagate through a purely nonlinear section and then a purely dispersive section of fibre. Suppose that due to SPM and GVD, the pulse doubles in duration after a critical length L_c, it is assumed that over the first half of L_c, only SPM acts and only GVD over the second half. Then the pulse will develop a bandwidth,$\Delta\lambda$ given by (3.12)

$$\Delta\lambda = \frac{\lambda\, n_2\, I_o}{c\, T_p}\,\frac{L_c}{2}\,4\sqrt{2\ln 2/e}\ .$$

For the second half of L_c, GVD acts to broaden the pulse by one pulse width, T_p. So

$$T_p = D\,\Delta\lambda\,L_c/2$$

combining these two equations we obtain an expression for the critical length :

$$L_c = (2\ln 2/e)^{-1/4}\,(cT_p^2/D\lambda n_2 I_o)^{-1/2}$$

$$\approx T_p\,c\,(D\lambda\,c\,n_2 I_o)^{-1/2}\,.$$

Taking the usual values with $I_o \approx 5\times 10^{-1/2}$ W/m^2, we get $L_c \approx 1$ km which is much greater than the lengths used here. So it was not expected that any significant pulse broadening would occur due to the combined action of GVD and SPM.

3.2.2 Experimental observation of SPM.

The experimental arrangement used in our experiments to observe SPM is shown in figure 3. The CW mode-locked Nd:YAG laser described in chapter 2 was used as the pump source and typically generated pulses of 120-140 ps duration with time averaged powers ~ 7 W. A small fraction of the laser output was taken via the beamsplitter BS_1 in order to trigger the sweep electronics of the Synchroscan streak camera (chapter 1). Beamsplitter BS_2 enabled the input pulses to the fibre to be monitored continuously throughout the series of experiments. The optical-delay arrangement formed by mirrors M_1 and M_2 provided a time calibration for the streak camera and the pulses were monitored in real time using an optical multichannel analyser (O.M.A). The remainder of the beam was then coupled into a length of single-mode optical fibre.

In order to achieve good coupling of the pump beam into the fibre, it was necessary for the fibre ends to be cleaved. The fibre is surrounded by a protective coating which was first removed by simply scraping gently with finger nails. A better method is to soak the length of fibre to be stripped in methylene chloride for ~ 1-2 minutes. This attacks the coating which is then removed by wiping, leaving the glass fibre untouched. This exposed the bare fibre which was cleaved using a Fujikura hand held optical fibre cleaver. Coupling into and out of the optical fibre was achieved by × 10 and × 20 antireflection (AR) coated microscope objectives respectively, with a maximum overall efficiency of typically 50%. It was found initially that the 4% reflection from the cleaved face of the fibre gave severe

feedback problems, causing the laser to suffer relaxation oscillations [17]. This was almost completely eliminated by positioning the input objective at just over half a cavity length from the output coupler of the Nd:YAG laser so that a reflected pulse would pass through the gain medium behind the intracavity pulse and thus be attenuated.

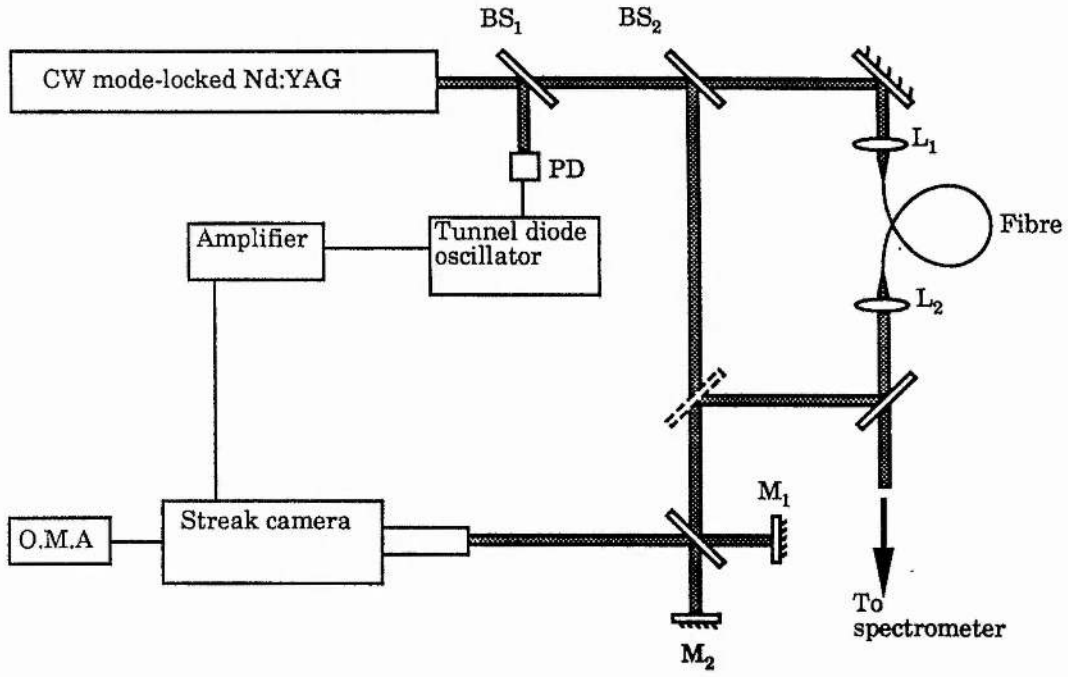

Figure 3.
Schematic diagram of the experimental arrangement.BS; beamsplitters, PD: Photodiode, L_1, L_2 microscope objectives.

The spectrum of the pulses exiting the fibre was monitored by a Monospek 1000 monochromator with the output slit of the spectrometer removed and a linear charged coupled device (CCD) positioned in the focal plane. Home built electronics driving the CCD, enabled us to monitor the spectrum in real-time using a standard oscilloscope. Some of the output from the fibre could also be directed onto the streak camera for temporal measurements.

Two types of fibre were used in the measurements here, firstly two lengths of single-mode, non-polarisation preserving fibre and secondly, a single-mode fibre with a high

birefringence giving it polarisation maintaining properties [18]. The fibre characteristics are summarised below in Table 2.

Table 2.

Fibre no.	Type	Length	Fibre parameters
#1.	non-pol. preserving	150 m	a = 3.5 μm, Δ = 0.004, α = 0.9 dB/km = 0.21 km^{-1}
#2.	non-pol. preserving	82 m	" " "
#3.	polarisation preserving	154 m	a = 3.0 μm, Δ = 0.005, α = 1.1 dB/km = 0.25 km^{-1}

a = core radius, Δ = average core\cladding index difference, α = attenuation.

With the polarisation preserving fibre, a half-wave plate inserted just before the input microscope objective was used to insure that the linearly polarised 1.064 μm radiation was launched into the fibre along one of its axes, so as to maintain a state of linear polarisation throughout the fibre length.

Results and discussion.

By altering the focus position of the microscope objective L_1, it was possible to adjust the coupling efficiency and thereby the average (peak) power in the fibre (measured after L_2). Figure 4 shows the observed spectral character of the pulses emerging from the 150 m length of fibre (fibre #1) for various peak powers and a constant input pulse duration (T_p = 140 ps). For the lowest power (figure 4a) no significant SPM was seen which is consistent with the theoretically calculated critical power, P_c, of 2.8 Watts given by [19]

$$P_c = \frac{1}{\pi n_2} \frac{\lambda A}{L} . \qquad (3.16)$$

Equation (3.16) is obtained by assuming that a significant amount of SPM is just obtained when $\Delta\Phi_{max} = 2$.

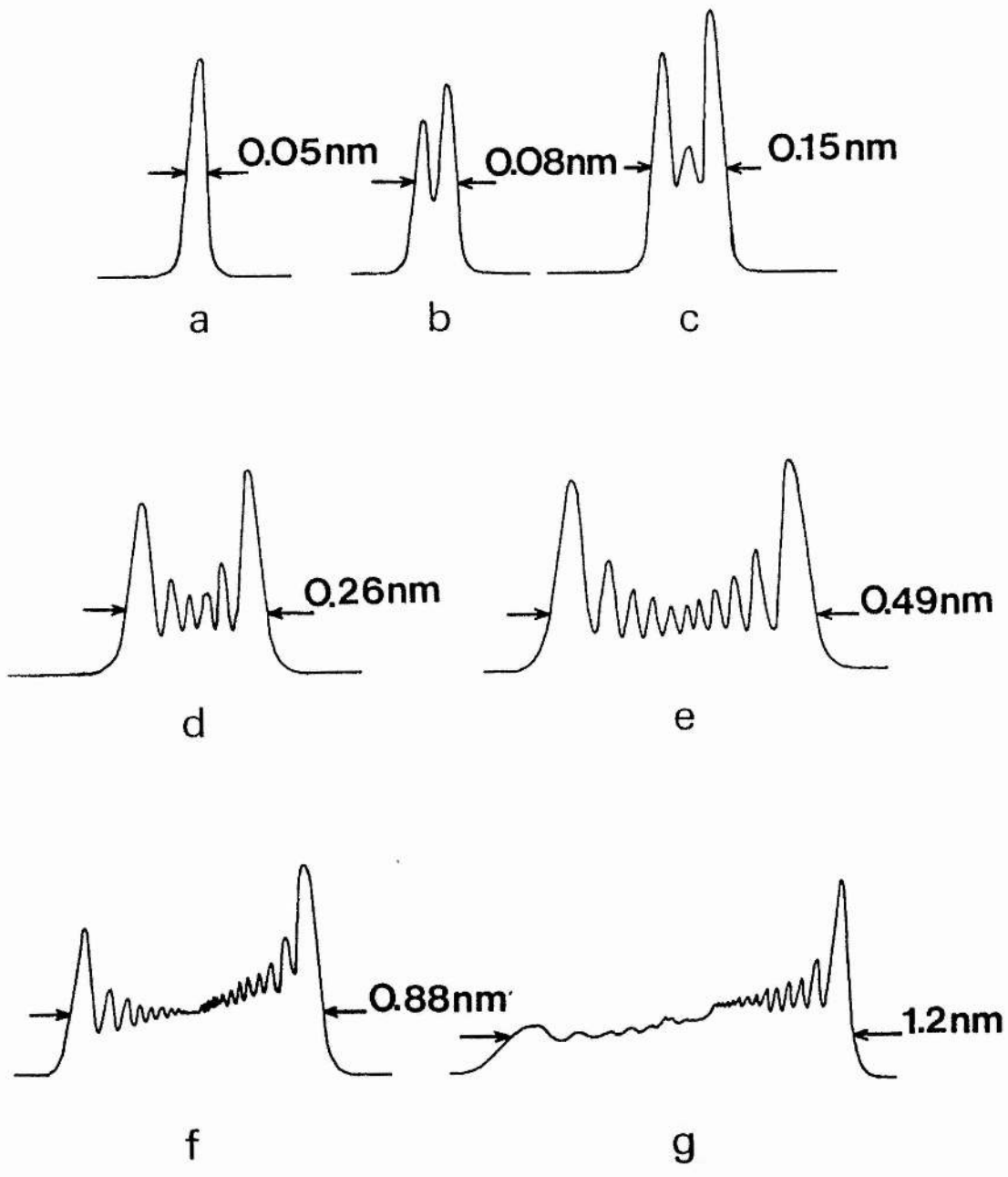

Figure 4.
Observed self-phase modulated spectra of the output pulses from fibre #1 for peak powers of (a) 3 W (b) 8 W (c) 12 W (d) 25 W (e) 53 W (f) 106 W (g) 148 W (wavelength increases from right to left).

As the peak power in the fibre was increased the spectrum broadened significantly and the classical SPM spectral shapes were clearly seen (figures 4 b-e). The good visibility of

the fringes is indicative of stable pump pulses since only slight variations in pulse duration or peak power, would cause the spectral broadening to fluctuate and the fringes to wash out. Indeed, by observing the SPM spectrum, we were able to slightly adjust the frequency of the mode-locker and 'peak up' the stability of the Nd:YAG laser through optimising the fringe visibility. It was found that the maximum fringe visibility was obtained for modulator frequencies slightly detuned from that which gave the shortest pulses and this is consistent with the greater stability of the laser discussed previously (chapter 2).The spectrum was observed to broaden symmetrically up to a peak power ~ 98 W. Beyond this a depletion of the down-shifted frequency components was evident (fig.4 f,g) which is due to the onset of stimulated Raman scattering and this will be discussed further in section 3.4.1.

Equation (3.12) implies that the total bandwidth of the self-phase-modulated pulse will be directly proportional to the peak power and in figure 5, the spectral width of the pulses as a function of peak power for fibres #1 and #2 is shown. A linear relationship is seen to hold for powers up to ~ 100 W for fibre #1 while for #2 there is no observable deviation even at the highest powers. In the following analysis, we only consider points that obey the linear relationship, above this stimulated Raman scattering is the cause of the deviation and will be explained in section 3.4.1. The solid lines in figure 5 are a least squares fit to the data and we obtain values for the gradients and intercepts of $8.1 \pm 0.3 \times 10^{-12}$ m/W, 0.04 ± 0.01 nm and $4.6 \pm 0.2 \times 10^{-12}$ m/W, 0.02 ± 0.01 for fibres #1 and #2 respectively. The latter value, according to our simple theory, represents the Nd:YAG laser bandwidth and is in agreement with accepted values [20,21].

From equation (3.12) we would also expect a linear relationship between the maximum bandwidth and the reciprocal of the input pulse duration. In order to confirm this, the duration of the pump pulses were altered by frequency detuning the Nd:YAG mode-locker drive unit and then the average power in the fibre (#1) was adjusted (via focusing of L_1') so that the peak power remained constant. The results are shown in figure 6 where the peak power is ~ 70 W. A least squares fit to the data gives gradient and intercept values of $7.3 \pm 0.6 \times 10^{-20}$ ms and 0.06 ± 0.03 nm respectively.

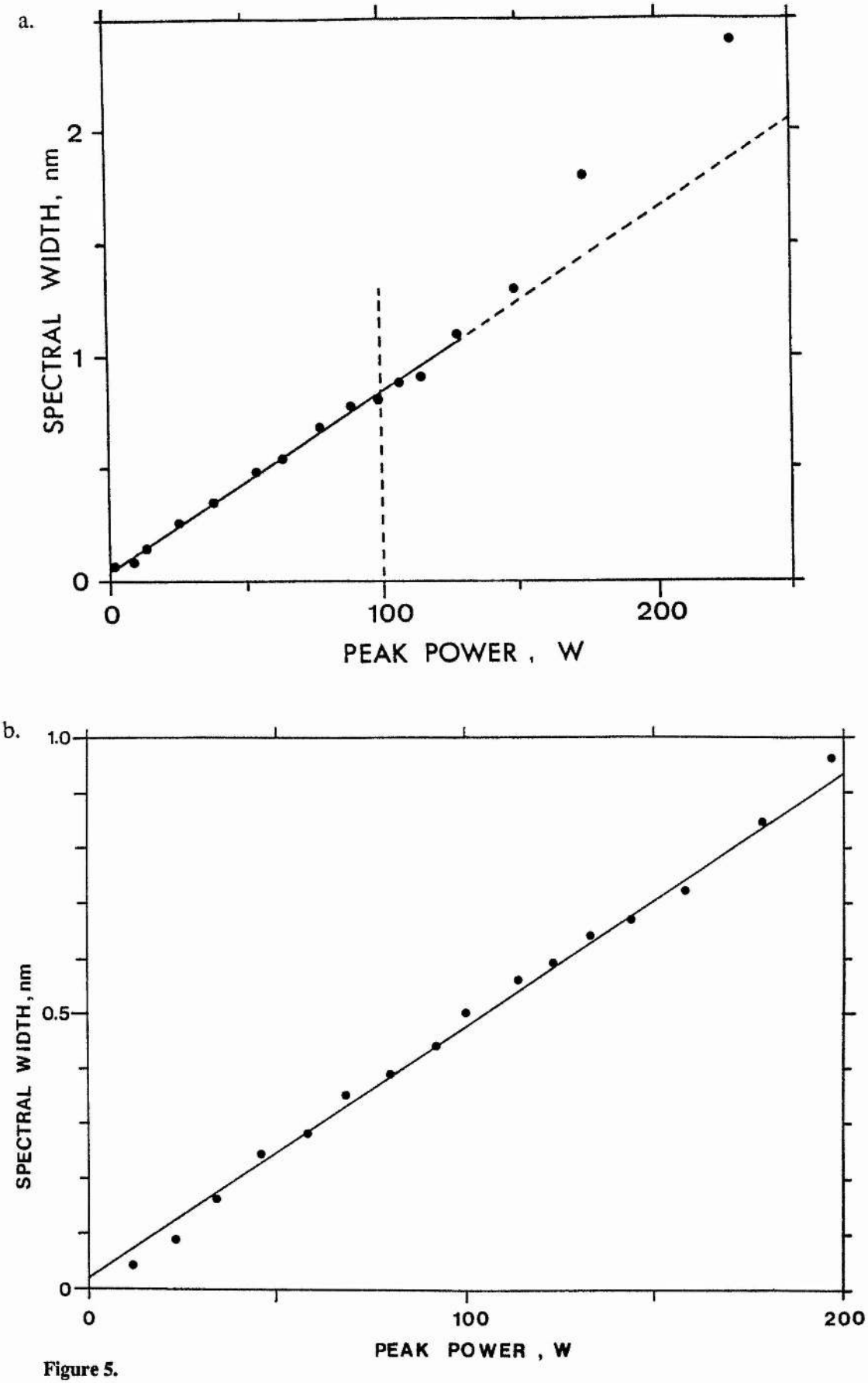

Figure 5.
SPM bandwidth as a function of peak power for fibres #1 (a), & #2 (b). The input pulse durations were ~ 140 ps for fibre #1 and ~ 127 ps for fibre #2.

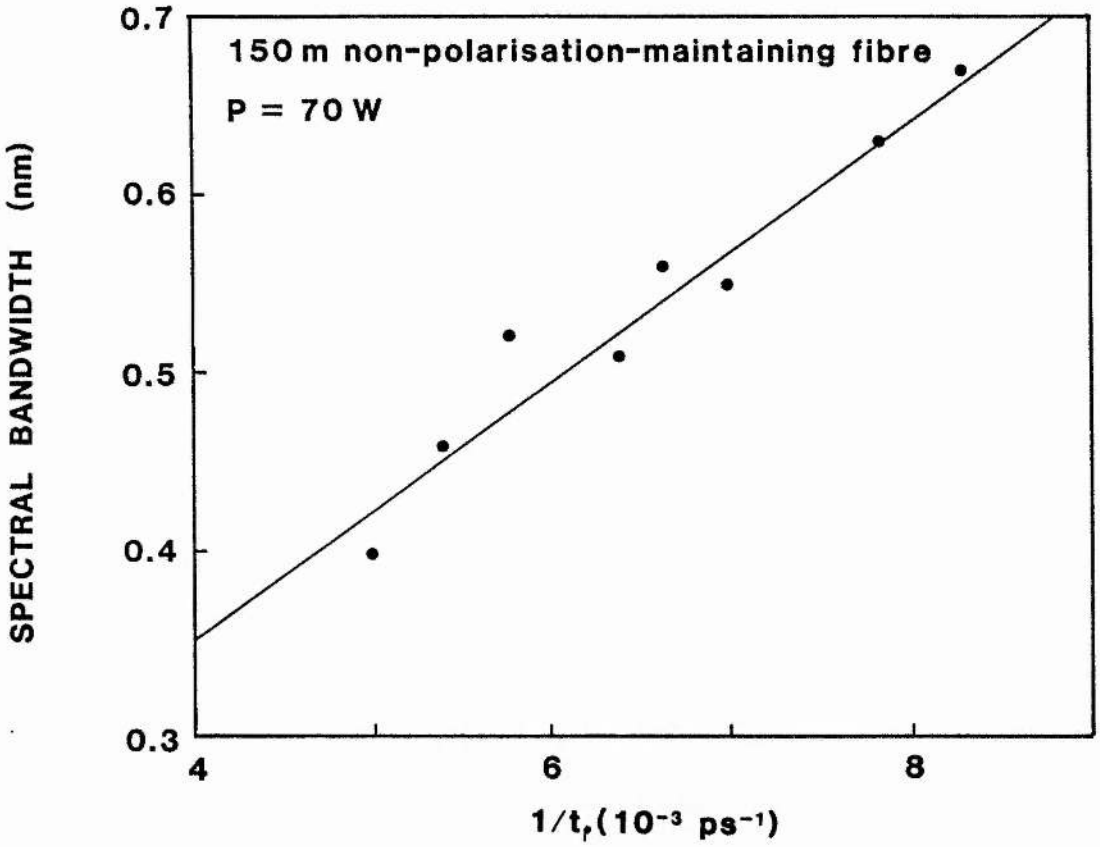

Figure 6.
A plot of the maximum SPM bandwidth as a function of the reciprocal of the input pulse width with constant peak power of ~ 70 W. (Fibre length = 150 m).

The increased error in this estimate is due to (i) the SPM spectral instability associated with the larger amplitude fluctuations in the frequency detuned Nd:YAG laser, and (ii) the difficulty in maintaining a constant peak power in the fibre by simply adjusting the L_1 focus position. Since in this experiment, the peak power was to be kept constant, the maximum phase shift experienced by the pulse should also be constant. It is this latter factor that determines the number of oscillation peaks within the SPM spectrum and we would therefore expect that the number of such oscillations should remain fixed throughout the set

of readings in figure 6. By monitoring the number of oscillation peaks we were able to make a check that the peak power was in fact remaining constant.

The gradients of the lines in figures 5 and 6 with equation (3.12) enable us to obtain values for the nonlinear self-focusing coefficient, n_2 , for germania doped fused silica. Using an effective core area, A , of 4.0×10^{-11} m^2 , and an effective fibre length of 148 m (81 m for the 82 m length), the respective values of n_2 from figures 5 and 6 are calculated to be $3.6 \pm 0.3 \times 10^{-20}$ m^2/W (fibre #1), $3.4 \pm 0.3 \times 10^{-20}$ m^2/W (fibre #2) and from figure 6, $3.4 \pm 0.5 \times 10^{-20}$ m^2/W including the correction factor of 6/5 since these two fibres are non-polarisation preserving.

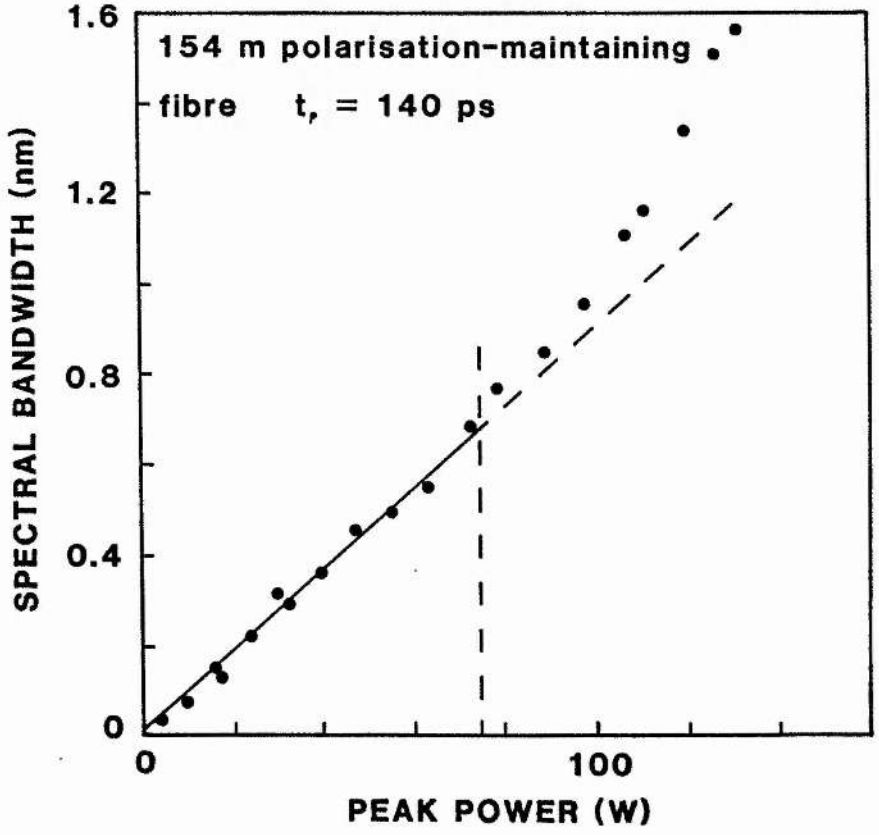

Figure 7.
Maximum SPM bandwidth as a function of peak power for the length of polarisation preserving fibre.

In order to verify the correction factor, a length of polarisation preserving fibre (#3) was used and a similar set of SPM spectra to those in figure 4 were observed. The onset of SRS, however, occurred at a lower peak power ~ 75 W (dashed ordinate fig.7) which is attributed to the lower threshold due to the polarisation preserving nature of the fibre. A plot of $\Delta\lambda$ against P_o is shown in figure 7 with a least squares fit for the powers below 75 W giving a gradient of 9.0×10^{-12} m/W. From this n_2 is calculated to be $3.4 \pm 0.3 \times 10^{-20}$ m^2/W (without the correction factor) which agrees well with those values obtained with the non-polarisation preserving fibre. These values are close to that determined by Stolen and Lin [12] of 3.3×10^{-20} m^2/W (1.14×10^{-13} e.s.u), with a 15% error for a silica-core, borosilicate clad fibre.

In figure 8 the duration of the pulses exiting the fibre is plotted as a function of peak power. It is seen that contrary to the earlier assumption that the pulse duration should be unchanged by passage through the fibre, a small deviation by ~ 30% was observed. For powers above 100 W the decrease in pulse width is accounted for by stimulated Raman scattering (section 3.4.1). The change in pulse duration for the lower powers may be due to the interaction of GVD with an initial frequency down-chirp present on the input pulses, causing the initial pulse narrowing. However, the magnitude of this chirp would not be significant compared to the SPM induced chirp within the fibre once the SPM threshold had been exceeded. It was also noted that the pulse duration as recorded on the streak camera, appeared to be a function of the spatial position of the beam on the input slit of the camera. It was not properly understood why this should be so, although it may have been due to the presence of a weak second mode in the fibre. Despite these changes in the output pulse duration, the theory described here seems able to predict the peak power and pulse width dependence of SPM in an optical fibre for the range powers and pulse durations used here.

A major advantage of this method in measuring n_2 , is that no secondary standards are involved. Other methods measure one or more components of the nonlinear susceptibility, χ_3, which then have to be related to n_2 using certain approximations [11,22,23]. Some

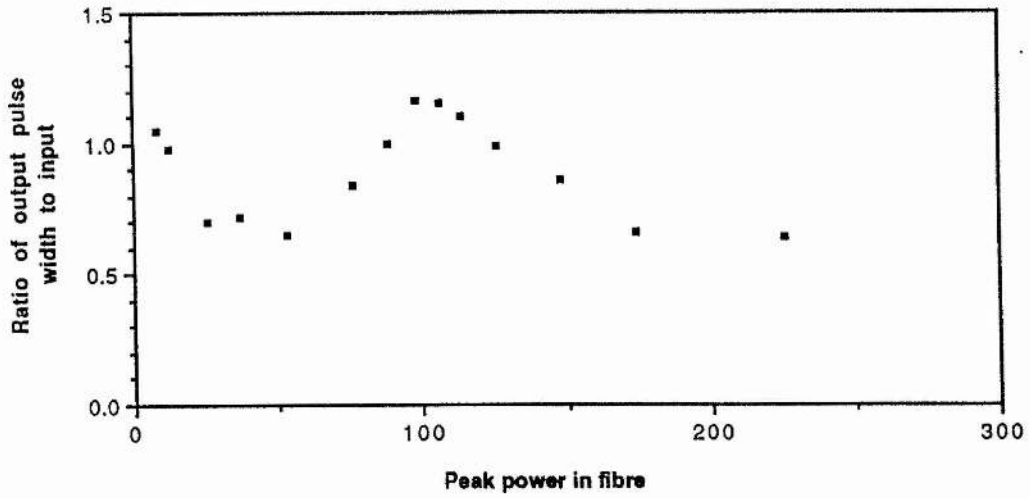

Figure 8.
Variation of output pulse width as a function of peak power for the 150 m fibre (#1).

assumptions are required here in the calculation of the 6/5 correction factor, but these are seen to be valid due to the good agreement between the values of n_2 with the polarisation preserving and non-polarisation preserving optical fibres.

The equipment described above was then used as the first stage of an optical pulse compressor which is detailed in the next section.

3.3 Optical pulse compression.

Optical pulse compression has been used very successfully over the last few years for the production of pulses only tens of femtoseconds in duration [24,25]. Most recently, by using a two stage compressor and compressing the pulses from a colliding pulse mode-locked (CPM) dye laser and amplifier, pulses of only 8 fs have been reported [26]. Gires and Tournois [27] proposed the possibility of compressing optical pulses by using a technique similar to that used at microwave frequencies but the method of using diffraction gratings which is predominantly used today, was first suggested by Treacy [28]. After the pulses pass through a nonlinear medium (such as an optical fibre) they develop a positive frequency chirp (see figure 1) with the front edge down shifted in frequency and the rear

edge up shifted. A negatively dispersive delay line can then be used to temporally compress the pulses by allowing the low frequency components of the pulse to be retarded with respect to the high frequency components by approximately the width of the uncompressed pulse, enabling most of the pulse energy to arrive at a point in space over a very short time interval. The most common delay line consists of a pair of reflection diffraction gratings operated in the near-Littrow configuration. Other methods have been used, such as sodium vapour cells and prism arrangements [29,30], but the grating pair offers the greatest flexibility and a wide range of pulse widths may be compressed simply by varying the distance between the two gratings.

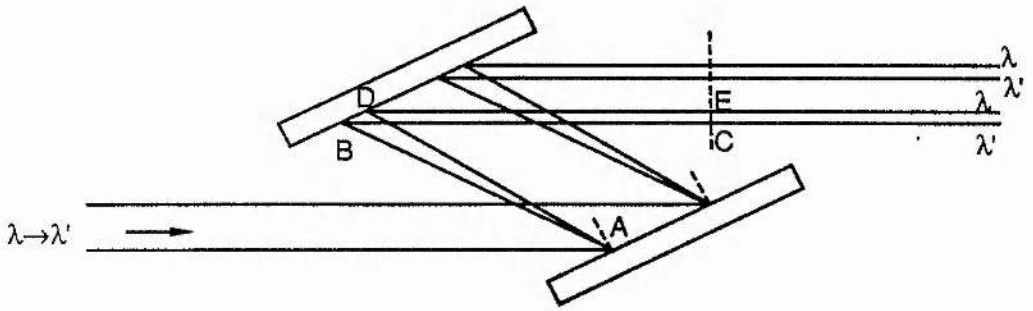

Figure 9.
Arrangement of diffraction gratings in the near Littrow configuration for pulse compression ($\lambda` > \lambda$).

The diffraction gratings are arranged as shown in figure 9. A pulse is diffracted by the gratings, the longer wavelength components, $\lambda`$, traveling a greater distance (ABC) than the shorter components, λ, which travel along ADE. Pulse compression is thus attained for pulses whose leading edge is red shifted with respect to the trailing edge. In order to see that the grating pair compensates for a linear chirp, it is necessary to find how the group delay (i.e the delay experienced by one frequency component after passage through the gratings) varies as a function of frequency. If τ is the group delay, it has been shown by Treacy [28] that for a pulse of centre frequency ω_o,

$$\frac{\partial \tau}{\partial \omega} = \frac{-\,4\pi^2\, c\, b}{\omega_o^3\, d^2 \cos^2\gamma} = \mu \qquad (3.17)$$

where b is the centre to centre distance between the gratings, d is the groove spacing and γ is the angle between the diffracted beam and the normal to the grating surface. Hence the delay through the gratings can be written as:

$$\tau = \tau_o + \frac{\partial \tau}{\partial \omega}(\omega - \omega_o) + 1/2\frac{\partial^2 \tau}{\partial \omega^2}(\omega - \omega_o)^2 + \ldots$$

$$\approx \tau_o - \mu\,(\omega - \omega_o) \qquad (3.18)$$

τ_o is the delay for the centre frequency and μ is the expression in (3.17) (with the minus sign given explicitly). The delay is linear in frequency, equation (3.18), and so (to first order) the grating pair will compensate for a linear frequency sweep imposed upon an optical pulse. The phase delay or phase function, $\phi(\omega)$, of the grating pair is obtained by integrating τ with respect to ω,

$$\phi(\omega) = \phi_o + \tau_o(\omega - \omega_o) - 1/2\mu(\omega - \omega_o)^2$$

$$\text{where the coefficient, } 1/2\mu = a_o = \frac{b\lambda^3}{4\pi c^2 d^2 \cos^2\gamma}\ , \qquad (3.19)$$

is the compressor constant. A linearly chirped pulse has a phase function which is quadratic in frequency, so the ideal delay line is one with a negative quadratic phase function. As shown above, the grating pair is a reasonable approximation to a quadratic compressor and so is well suited for the compression of SPM chirped optical pulses. The delay τ, has only been expanded to first order in ω and so the theory is valid provided the pulse has a small fractional bandwidth. If group velocity dispersion is the single influence on a pulse of initially minimum bandwidth, the pulse will broaden and develop a linear frequency chirp over the full extent of the pulse. The grating pair will then be able to compress the pulse back to its original width. For pulses experiencing SPM in an optical fibre there are two regimes of importance: the case were GVD acts upon the pulse to linearise the chirp and the case for which GVD is negligible and SPM is the only chirp producing factor. The first case is the most desirable and an optimum fibre length exists for which GVD linearises most of the chirp enabling a pulse to be most effectively compressed by a grating pair. However, an excessively long length of fibre will cause optical wave

breaking to occur whereby some of the up-shifted frequency components catch up with the down-shifted components and mixing occurs producing new frequency components that bear no fixed phase relationship and hinder pulse compression [31]. Numerous studies of optical pulse compression can be found in the literature e.g. [32,33], one of the most comprehensive being by Tomlinson et al [34]. Using numerical methods they studied the propagation of pulses in an optical fibre using the nonlinear Schrödinger (NLS) equation and deduced an optimum fibre length, Z_{opt}, such that a pulse may be optimally compressed by a grating pair. Their expression for this optimum length is given as:

$$Z_{opt} = \frac{1.6}{\alpha} Z_o$$

$$\text{where} \quad \alpha = \sqrt{P/P_1} \quad , \quad Z_o = \frac{0.322\,\pi^2\,c}{D\,\lambda^2}\,T_p^2 \qquad (3.20)$$

$$\text{and} \quad P_1 = \frac{\lambda\,A}{4\,n_2\,Z_o} \ .$$

Here T_p and P are the input pulse duration (FWHM) and peak power respectively. The normalised parameters P_1, Z_o, and α result from the use of the NLS equation for solitons in optical fibres. Although in this context (positive GVD), solitons are unable to form, it turns out that Z_o represents the length of fibre for the input pulse to approximately double in duration due to GVD (in the absence of any SPM) and P_1 is the peak power required for SPM to double the spectral width of the pulse in a fibre of length Z_o (in the absence of any GVD). If we consider a wavelength of λ = 1.06 μm, D = 30 ps/nm/km and T_p = 100 ps we can calculate a value of Z_o = 280 km. In our experiments the maximum average power coupled into the fibre was about 2 W i.e a peak power P ≈ 250 W and (using $n_2 = 3.4\times10^{-20}$ m^2/W, $A = 4\times10^{-11}$ m^2) hence $Z_{opt} \approx$ 1 km. This is much greater than the maximum fibre length used of about 150 m, which confirms again that we may neglect the effects of GVD. Because of this, the quality of the compressed pulses was not expected to be very good and one would at best expect a short compressed pulse on top of a broad pedestal, resulting from the uncompressed wings of the pulse. In figure 10 the input pulse and optimally compressed pulse are illustrated, using a grating pair when the influence of GVD is negligible and for the case of optimum compression when $Z \sim Z_{opt}$.

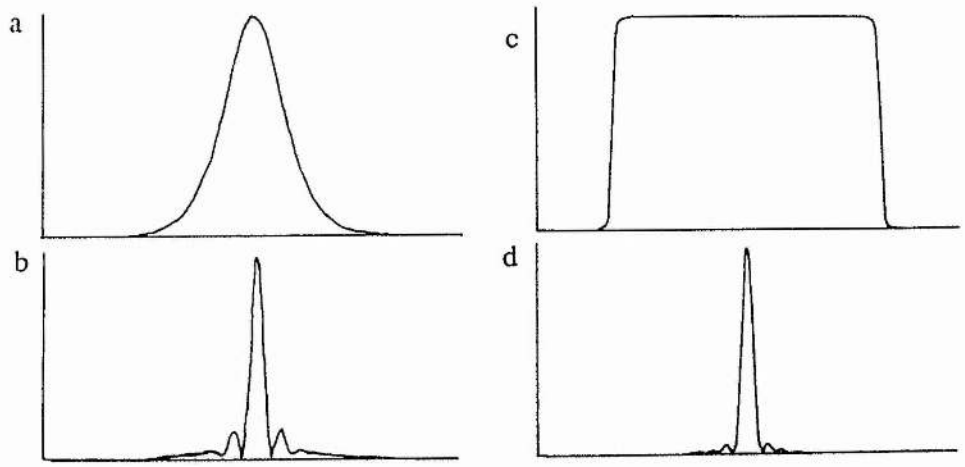

Figure 10.
(a) Input pulse to a grating pair when $Z \ll Z_{opt}$ (b) optimally compressed pulse with a quadratic compressor (c) pulse exiting a length of fibre where $Z \sim Z_{opt}$ (d) optimally compressed pulse .

The broad pedestal in (b) arises from the wings of the pulse where as can be seen from figure 1, a *negative* frequency chirp exists and so the grating pair will broaden the extreme leading and trailing edges of the pulse. A pulse whose chirp is linearised by GVD has a much smaller fraction of the pulse containing a negative chirp and the pedestal is almost completely eliminated (fig.10d).

Our pulse compression setup is shown schematically in figure 11. The pulses emerge from the fibre, are collimated by the objective L_2 and are then incident on the first diffraction grating. Both holographic gratings were blazed at 1.06 μm and had a diffraction efficiency of about 90% into the first order when in the near-Littrow configuration. After diffraction from the second grating (G_2) a retroreflector (corner cube) was positioned to reflect the pulses back through the gratings slightly displaced downwards in the vertical plane. This enabled the distance between the two gratings to be halved and a greater effective separation was achievable. The returning pulses were directed into the monitoring streak camera or second harmonic generation autocorrelator systems.

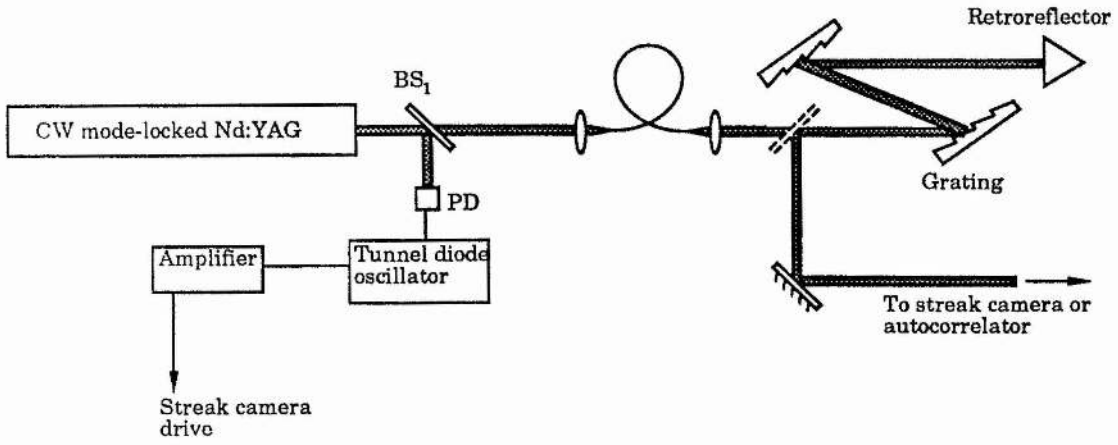

Figure 11.
Schematic diagram of the arrangement for optical pulse compression.

At first, a 50 m length of fibre having a cutoff wavelength of 1.2 μm was used which was therefore weakly multimode at 1.06 μm.From reference [34] the optimum compression factor for the case of $Z \ll Z_{opt}$ is given by

$$a_o = 0.25 \frac{Z_o}{A^2 Z} T_p^2 / 4\ln 2 \qquad (3.21)$$

for a gaussian pulse. Using the value of $Z_o \sim 280$ km calculated previously and (3.19) combined with (3.21) we obtain a value for the grating separation of b ~ 100 cm. The optimum compressed pulse width is given by

$$T_{comp} = \frac{T_p}{1 + 0.9A^2 Z/Z_o} \qquad (3.22)$$

and this gives a value of $T_{comp} \sim 4$ ps. The compressed pulses were optimised by monitoring the real-time autocorrelation trace and adjusting the power in the fibre for differing values of the grating separation. The shortest pulses obtained were ~ 4 ps in duration (see figure 12a) for a grating separation of about 50 cm i.e b ~ 100 cm and an average (peak) power of 1.7 W (210 W) in the fibre, which is in excellent agreement with the theoretical values. For values of b slightly larger

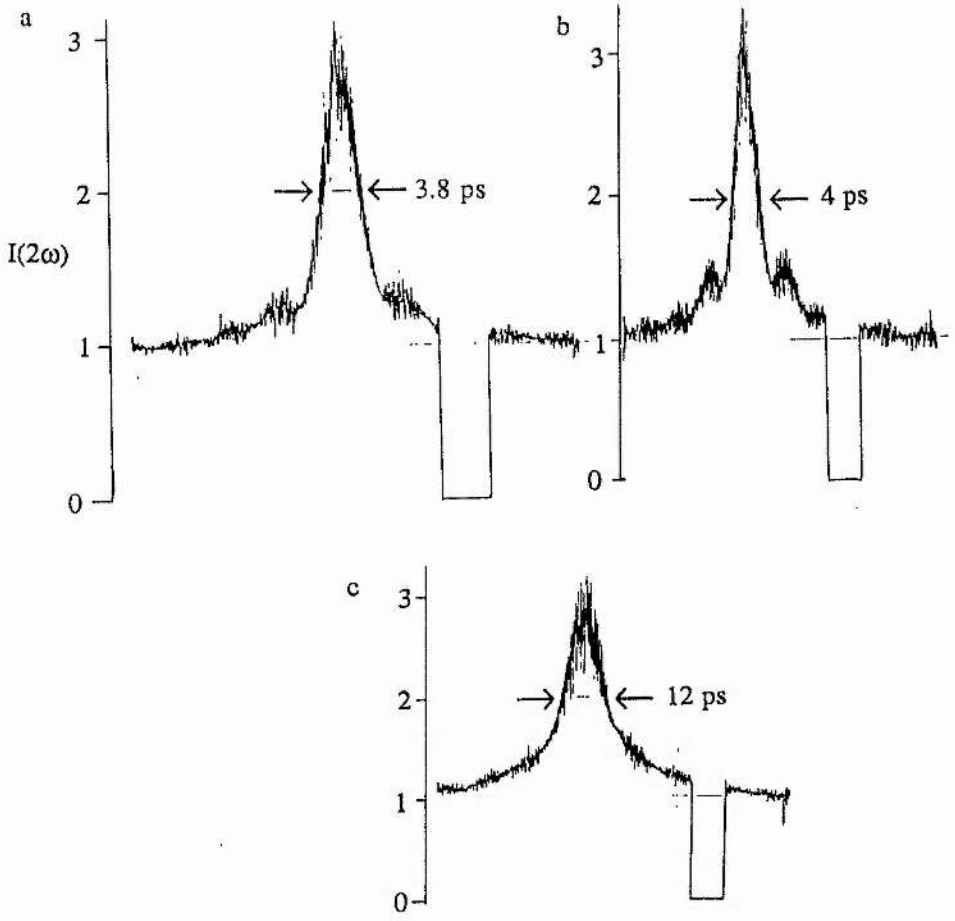

Figure 12.
Autocorrelation traces of (a) the shortest pulse (b) the compressed pulse for a grating separation slightly larger than optimum (c) compressed pulse for slightly lower peak power than optimum. Fibre length = 50 m.

than optimum, the compressed pulse developed very noticeable side lobes, which can be seen in figure 12b. With lower peak powers in the fibre, these features disappeared and a broad pulse sitting on top of a large pedestal developed (figure 12c). Figure 13 is a plot of the compressed pulse durations as a function of the grating separation, b, and clearly shows the existence of an optimum grating separation.

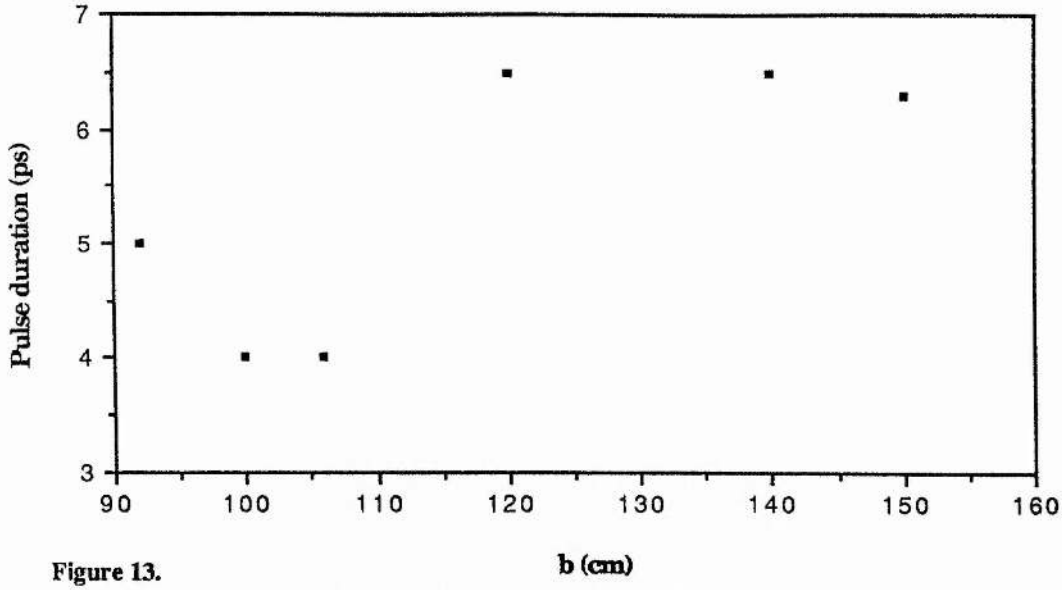

Figure 13.
Duration of compressed pulses as a function of grating separation for a 50 m length of fibre. The power in the fibre was constant for all measurements.

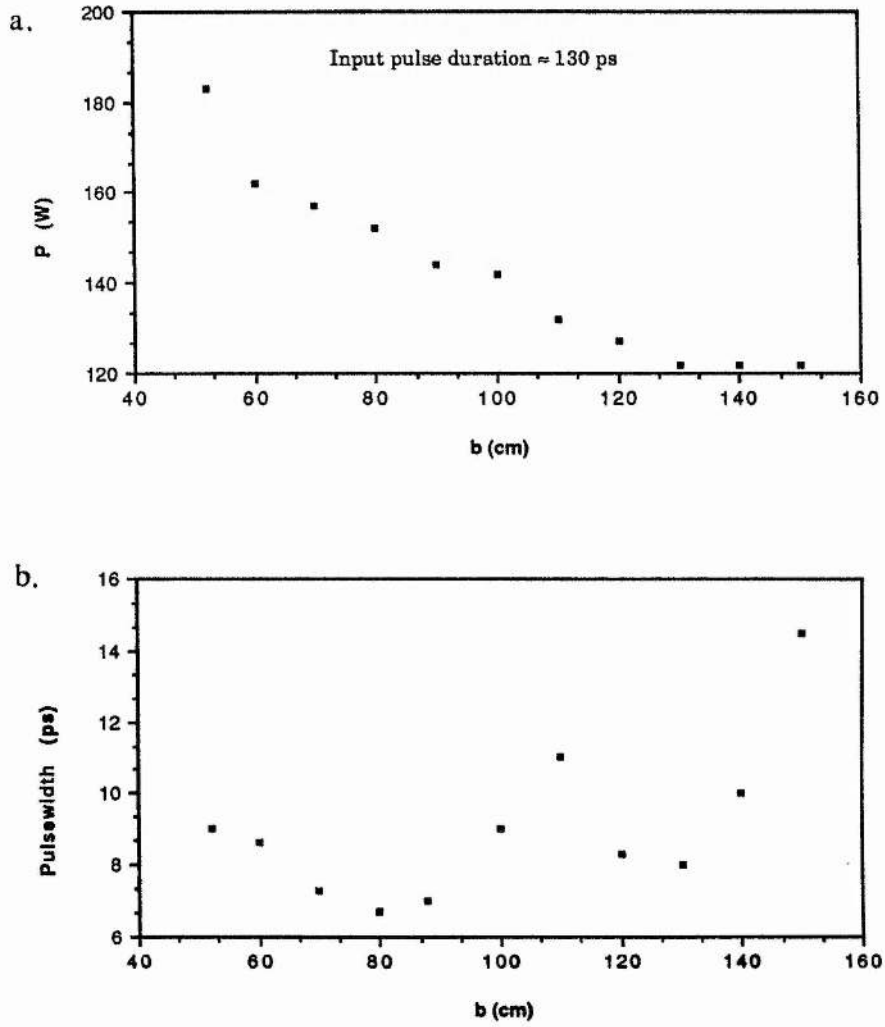

Figure 14.
(a) The optimum peak power and (b) the compressed pulse duration plotted against the grating separation for a 70 m length of fibre.

A 70 m length of non-polarising preserving fibre was then used to induce a frequency chirp on the optical pulses. Very similar results were recorded to those observed with the previous length in terms of the pulse shape and the presence of side lobes. Optimally compressed pulses were obtained for a grating separation of roughly 40 cm (b = 80 cm) and the minimum pulse duration was ~ 6.5 ps. Plots 14a,b show the optimum peak power and pulse duration verses grating separation respectively.

For an ideal compressor, the duration of the compressed pulses should be a continuously decreasing function of peak power in the fibre, i.e. higher peak powers generate pulses with a greater bandwidth and hence a temporally shorter pulse once the grating separation has been optimised. Figure 15 is the experimentally determined curve of the optimum compressed pulse width as a function of input peak power (three curves are shown for fixed values of the effective grating separation of 60, 70 and 80 cm). The curves show a definite minimum indicating that the grating pair is not the 'ideal' compressor. The

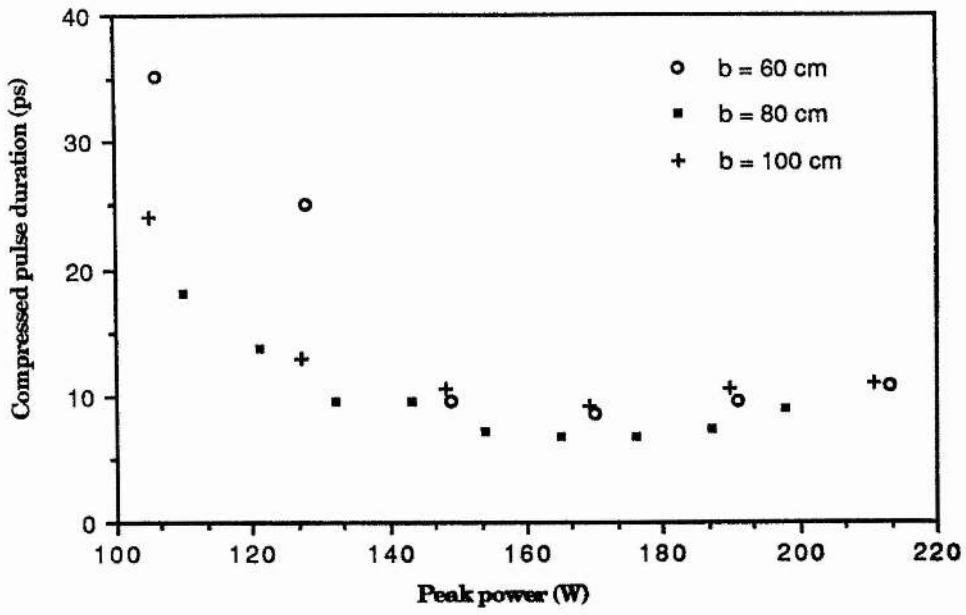

Figure 15.
Optimum compressed pulse width as a function of peak power in the fibre (l = 70 m) for three different values of the grating parameter.

error results from taking the expansion for τ (equation 3.18) only to first order and therefore obtaining the phase function only to second order. This limitation to the theory was pointed out by Treacy [28] and can be accounted for by including the cubic phase term in $\phi(\omega)$. This term becomes important for the case when the pulse bandwidth is a significant fraction of the frequency and when included in the theoretical considerations, an optimum peak power of the input pulse is predicted [35].

Finally, a 150 m fibre length was used and the compressed pulses monitored on a streak camera. Pulses of approximately 6 ps were recorded although at this time no autocorrelation traces could be taken and the actual duration would almost certainly have been less than 5 ps. The S1 streak camera was operating close to its limit of resolution, the shortest pulse recorded being 5.8 ps.

A brief study of the temporal compression provided by a grating pair on a pulse chirped by SPM in an optical fibre has been described for the case of negligible GVD. The peak power of the compressed pulse will be $P_c = \Gamma\ P_{in}T_p\ /T_{comp}$, where Γ is the overall transmission of the gratings. The transmission for the gratings used here should be $\sim 0.9^4$ (four diffractions) i.e 65%. However, the measured transmission of our grating compressor was much less than this. This was due to the fact that the gratings were polarisation sensitive and the fibre used was nonpolarisation preserving. In order to maximise the output, a polarisation rotator similar to that described in reference [36] was inserted in the fibre. Using this we were able to roughly optimise the polarisation of the light exiting the fibre and obtain a grating transmission of ~ 15%. Peak power enhancements of approximately 3.5 times were then obtained. From (3.20) and (3.22) we can see that the compressed pulse width is inversely proportional to the peak power times the fibre length and thus $P_c \propto \Gamma\ Z\ P_{in}^2$. Notice the compressed pulse peak power is proportional to the input power squared and so in order to achieve short compressed pulses with high peak powers, one should choose the combination of high input powers and short fibre lengths. Stimulated Raman scattering may put an upper limit on the input power since this will cause a depletion of the pulse leading edge and asymmetric spectral broadening.

If a fibre length that is close to the optimum length (Z_{opt}) can be used, both the pulse quality and duration will be significantly improved. Recent work by Fork et al [37], has shown that a combination of prisms can provide a cubic phase compensation and, in conjunction with a standard grating pair, pulses of 6 fs, the shortest reported to date, have been produced.

3.4 Stimulated Raman Scattering (SRS).

The process of Raman scattering is basically a scattering of the incident light from optical phonons (optical vibrational modes) in a material. The scattered light has a characteristic frequency shift determined by the molecular vibrations of the medium and is termed the Stokes wave. The process may be regarded as a three level system, were the pump excites an atom to a higher level which then radiatively decays to a lower level with the creation of a vibrational mode (creation of optical phonons). The scattered light is thus frequency down-shifted. If the medium is initially in an excited state, due say to high energy phonon modes, then the scattered radiation may be up-shifted and this is termed anti-Stokes radiation. At high enough optical intensities the scattered Raman light may experience gain from the pump and stimulated emission occurs, giving rise to stimulated Raman scattering (SRS) [38-40]. In an initially unexcited medium, however, the anti-Stokes radiation experiences a net absorption rather than gain. The amorphous nature of glasses such as silicon dioxide, gives rise to the production of a broad band Raman spectrum (due to the breakdown of wavevector selection rules) rather than discrete lines and the characteristic spontaneous Raman gain curve of SiO_2 is shown in figure 16. The peak of the gain has a frequency shift ~ 490 cm^{-1}, so for pump light at 1.064 μm the Stokes-shifted light will peak at 1.1 μm. Although the peak gain coefficient is relatively small, $G_R = 1 \times 10^{-11}$ cm/W, significant SRS can occur in long lengths of optical fibre and dopants such as GeO_2, can significantly increase the gain coefficient which is useful for obtaining SRS at low pump powers or in short fibre lengths [41]. Larger Raman shifts may be obtained by doping with PO_2 or by molecular diffusion of gasses into the fibre. Deuterium gives a shift of $\Delta\nu_R$ ~ 3000 cm^{-1}, taking the Stokes wavelength to ~ 1.56 μm for

λ_p = 1.06 μm [42]. The problem here is that extremely high pressures are needed for the actual diffusion process and the fibre then has to be held at low temperatures to prevent outgassing from the fibre. Any impurity in the SiO_2 generally increase the fibre loss and fibres with low concentrations of impurities have a Raman spectrum determined mainly by that of SiO_2. The Raman gain is inhomogeneously broadened due to each Stokes band being associated with a particular mode of vibration. This makes it more difficult to produce a narrow line width source but aids the production of ultrashort pulses using Raman generation.

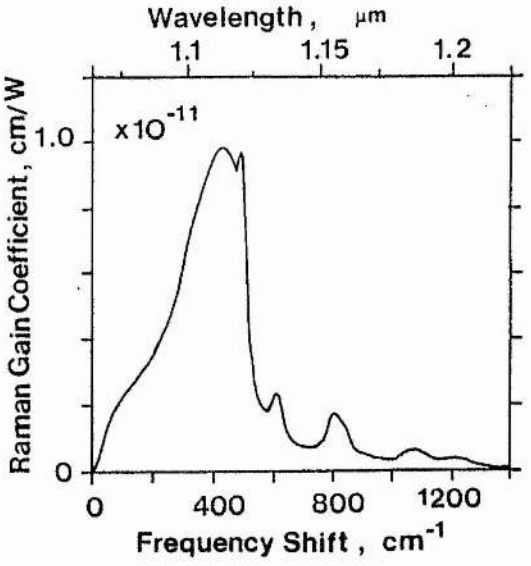

Figure 16.
Raman gain curve for SiO_2.

As for SBS and SPM, there exists no actual threshold value for Raman generation but since the Raman gain is exponential, there is only a small difference in pump power between negligible SRS and near total conversion. Smith has defined a critical value of the pump power, P_c, from which SRS builds up to equal the pump power [43]:

$$P_c = 32\, A / G_R L \qquad (3.23)$$

which represents the case for 50% conversion.Equation (3.23) assumes that the fibre does not maintain linear polarisation. Raman gain is zero for orthogonally polarised pump

and Stokes beams and a maximum for parallel polarisations, thus in a polarisation preserving fibre, the expression for P_c is reduced by a factor of two as for SBS. Again L is the effective fibre length and A is the effective area of the fibre core as determined by the overlap integral of the pump and stokes modal fields - see Table 1 for a list of some ratios of A/A_{core} for various V numbers. Absorption in the fibre limits the length over which the Raman light will experience gain and this is taken into account by using the effective fibre length as defined by equation (3.6). For ultrashort pulses, another limit to this length arises due to group velocity dispersion. Material dispersion in the fibre causes the longer wavelength Raman pulse to propagate with a slightly greater group velocity than the pump, so it will tend to walk through and then move ahead of the pump pulse. Since material dispersion is the dominant dispersion mechanism in single-mode fibres, the time separation of the pulses after traveling a length l in a fibre of dispersion D is:

$$\delta t = l\, D\, \delta\lambda \qquad (3.24)$$

for a wavelength separation of $\delta\lambda$. Equation (3.24) can then be used to calculate an interaction length for SRS, defined by the length of fibre over which the Raman pulse 'walks through' the pump pulse. The interaction length will be limited to about 80 m for pump and Raman pulses separated by ~ 40 nm and a pulse duration of 100 ps.

In order to obtain long interaction lengths the group velocities of the pump and Raman pulses should be matched and this can be achieved by two methods. The first is to use a fibre with core dimensions such that the pump pulse propagates in the fundamental mode while the Stokes pulse travels in a slower higher order mode of the fibre [44]. The second technique is to use the minimum dispersion point in the fibre [45]. The idea is to have the pump and Stokes wavelengths equispaced either side of the minimum dispersion point and hence both have the same group velocity. This can only apply over a small wavelength region whereas the former technique can be used for any λ_p.

The dependence of the group velocity on wavelength is utilised in the tunable fibre Raman oscillator, where the actual wavelength of operation is determined by the Raman

gain profile and the cavity length, since the interaction length seen by wavelengths other than at the gain peak can be increased by adjusting the cavity length (section 3.4.2).

3.4.1 Effect of SRS on SPM and Pulse Compression.

By considering the combined effects of SRS and SPM in an optical fibre, it is possible to explain the observed departure from theory of the results in section 3.3. In the first instance

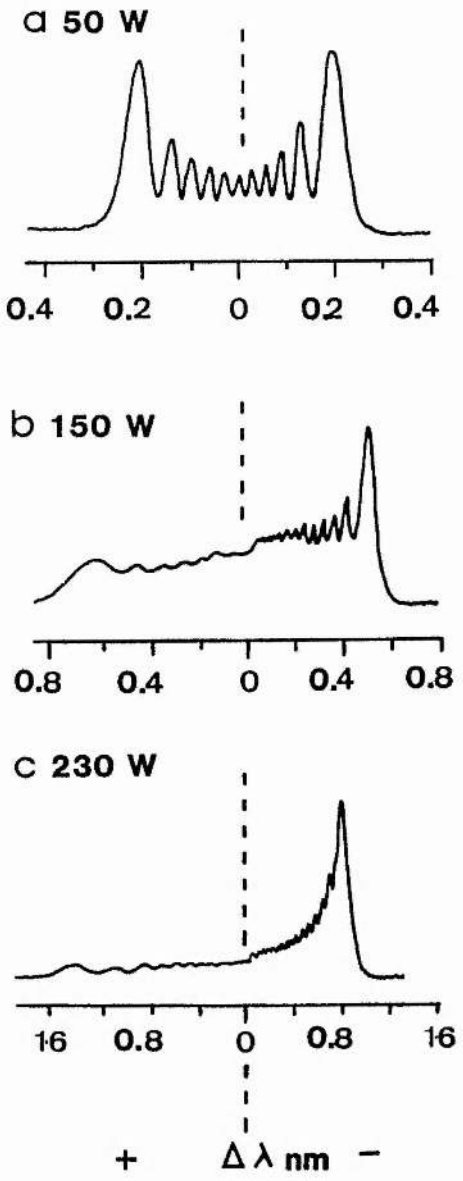

Figure 17.
SPM spectra of the pulses exiting 150 m of fibre for average powers of (a) 50 W (b) 150 W and (c) 230 W showing the depletion of the long wavelength components due to SRS.

we calculate the critical power for SRS using equation 3.23 and obtain $P_c \approx 110$ W for the 150 m length (the interaction length of 116 m is used, calculated from equation 3.24 with $\delta t = 140$ ps). We see in figure 5 that for this fibre length, a significant deviation from linearity occurs for powers exceeding 140 W, i.e. when the power is significantly in excess of P_c. For the 82 m fibre the interaction length from equation 3.24 is ≈ 100 m, so we must use the actual fibre length in equation 3.23 and thus in this case P_c is ≈ 156 W. The maximum peak power used was 200 W which is not greatly in excess of P_c and actually no significant deviation was observed in this case.

We noticed that for high peak powers with the 150 m length, the SPM spectrum became severely depleted on the longer wavelength side. This was evident in figure 4 and is demonstrated more clearly in figure 17. This depletion of the longer wavelength components can be explained as follows. The SRS pulse will initially receive its maximum gain at the centre of the pump pulse. Due to GVD it will then travel with a greater velocity than the pump and so take gain from the leading edge. Thus the leading edge of the pump pulse becomes depleted, which is of course the part of the pulse experiencing a downshift in frequency due to SPM. It is also noticed in figure 17, especially for the highest peak power (c), that the SPM spectrum extends further on this depleted side than on the shorter wavelength side. An explanation of this effect can be offered by referring to figure 18. Here the temporal profiles of the input pulse and pump and Raman pulses exiting the fibre as recorded on the streak camera are reproduced. The Raman pulse is ahead of the pump as expected, but also the duration of the pump pulse has reduced from the ~ 100 ps input duration. Again this is due to a depletion of the pump pulse leading edge by SRS and it can be seen in the figure that the risetime of the pump pulse has decreased on exiting the fibre i.e. it has a sharper leading edge. Since the maximum frequency shift due to SPM is proportional to dI/dt (equation (3.7)), it follows that the steeper leading edge will give rise to a greater maximum wavelength shift as in figures 17 b,c. Since in our measurements on the SPM bandwidth the total spectral width was measured, the reason for the departure of the experimental points from a straight line in figures 5,7 is now clear, being due to the

development of an asymmetric pump pulse due to the onset of Raman generation, which in turn gives rise to a greater maximum frequency shift than would be obtained from SPM alone.

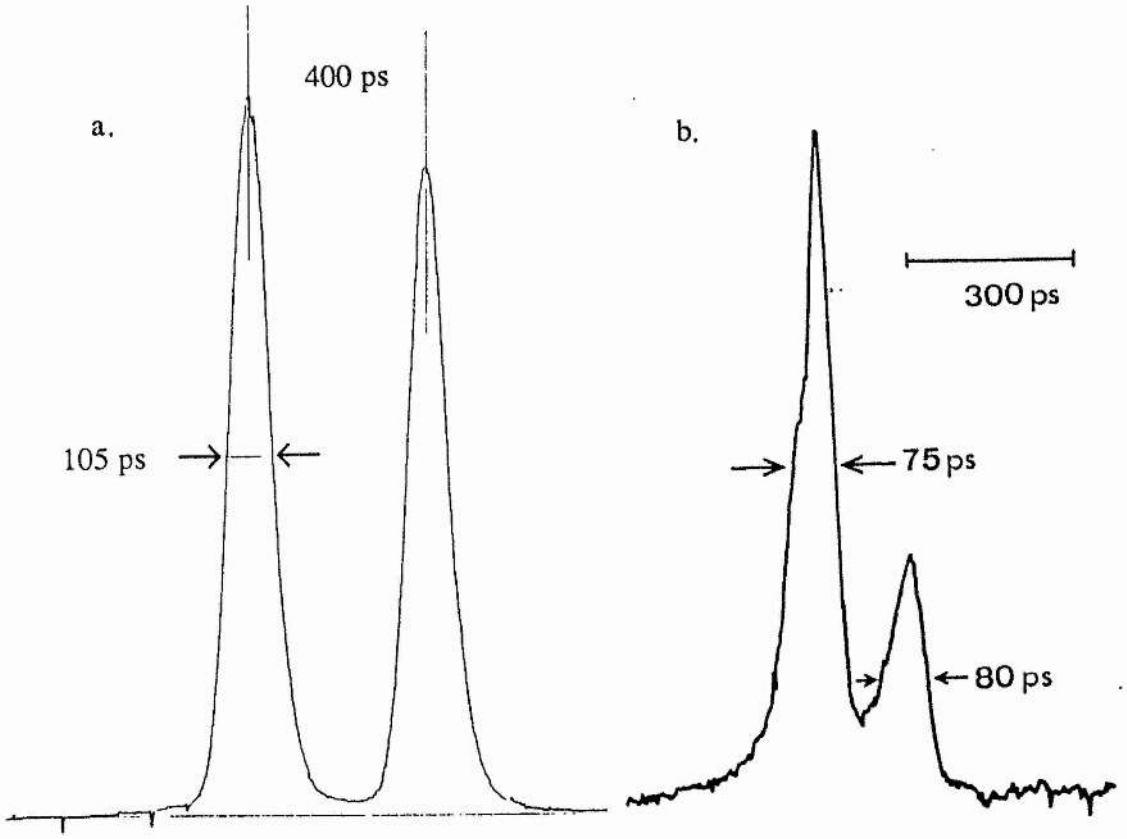

Figure 18
Temporal profiles of (a) the input pulses and (b) the pump and Raman pulses exiting the fibre (one arm of the delay line being blocked).

The effect of SRS on optical pulse compression was not experimentally investigated during this project but there have been some studies reported in the literature. Stimulated Raman scattering limits the maximum input power in the fibre since in the presence of SRS pump depletion occurs generating an asymmetric spectrum. This will then have a serious effect on the quality of the compressed pulses since the chirp will no longer be linear. However, recent studies of pulse compression in the presence of SRS [46-49], have shown that the stability of the compressed pulse can be much improved if some SRS occurs in the fibre and spectral windowing of the SPM spectrum is implemented. Because

of the critical dependence of the compressed pulse width on the input peak power, slight fluctuations in this can cause quite severe instabilities in the compressed pulses. Raman generation serves to clamp the peak power of the pulse in the fibre and thus stabilise the ouput pulses from the compressor.

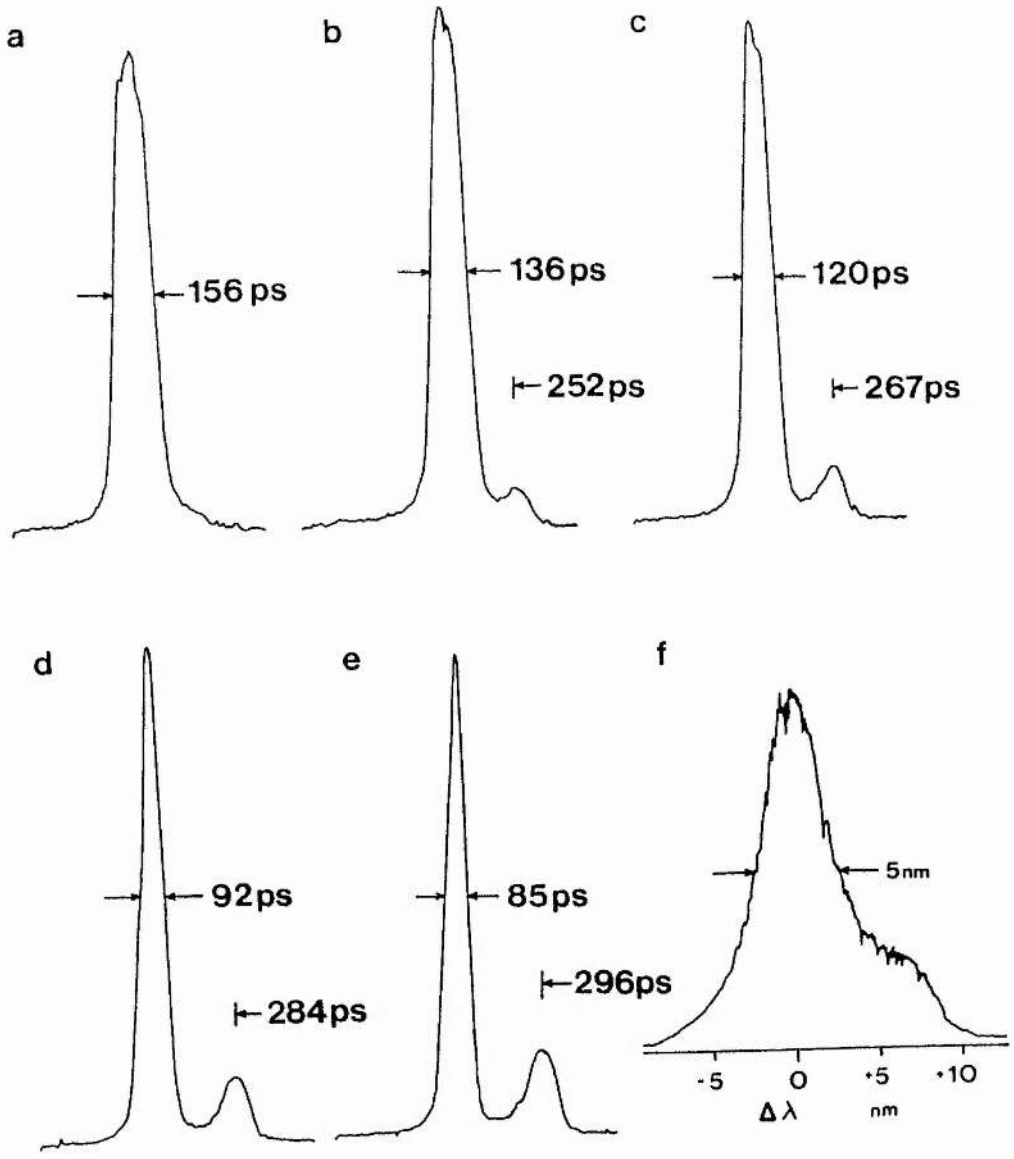

Figure 19.
Syncroscan streak camera intensity profiles of pump and Raman pulses for peak pump powers of (a) 113 W (b) 126 W (c) 148 W (d) 174 W (e) 226 W and (f) first Stokes Raman spectrum recorded for a peak power of 148 W.

The sequence of figures 19 a-f show the temporal profiles of the pump and first order Stokes pulses for different power levels in the 150 m length of fibre (time increases from right to left). The effect of positive GVD can be seen in that the Raman pulse arrives before the pump. Figure 19a was taken just above the Raman threshold and reveals a weak SRS pulse just ahead of the pump. As the power was increased, the pump pulse was observed to narrow significantly to ~ 85 ps at a peak power of 226 W. The Raman pulse grew in amplitude and the time delay between the pulses increased. Throughout this set of data the peak wavelength of the Raman pulse (1.116 μm) remained constant (spectrum reproduced in fig.19f). The decrease in duration of the pump pulse is again attributed to the depletion of the pump leading edge by the Raman pulse. For low peak powers in the fibre (just above the SRS threshold) it would be expected that the Raman pulse would require a finite length of fibre in order to develop and so the length of fibre over which GVD acts to separate the pulses is reduced, resulting in only a small time delay at the fibre end. As the peak power increased, the Raman pulse was generated at an earlier stage in the fibre, giving rise to a greater separation of the pump and Raman pulses at the fibre output.

An investigation of the time delay between pump and Raman pulses was undertaken for different fibre lengths with a constant peak power ~ 230 W. Figure 20 shows a plot of the results for lengths ranging from 150 m to 70 m (at shorter lengths the peaks were not sufficiently resolved for accurate measurements to be taken). A least squares fit to the data points (solid line) gives a gradient of 2.2 ps/m giving a value for the fibre dispersion of approximately 42 ps/nm/km. Using this value of the dispersion and equation (3.24) we can calculate the time separation expected between the pump and Raman pulses for the highest peak power. Assuming Raman generation occurs very close to the beginning of the fibre (i.e l = 150 m) and $\delta\lambda = 52$ nm, the time delay δt is deduced to be 328 ps which is slightly greater than that observed experimentally (fig.19e). The discrepancy is due to the fact that the Raman pulse will not properly form immediately at the beginning of the fibre but the length required to form the pulse will decrease for higher pump powers. If we take the observed value of the time delay from fig.19e, the length of fibre needed to generate the

Raman pulse is approximately 20 m. This is in agreement with the intercept shown in figure 20.

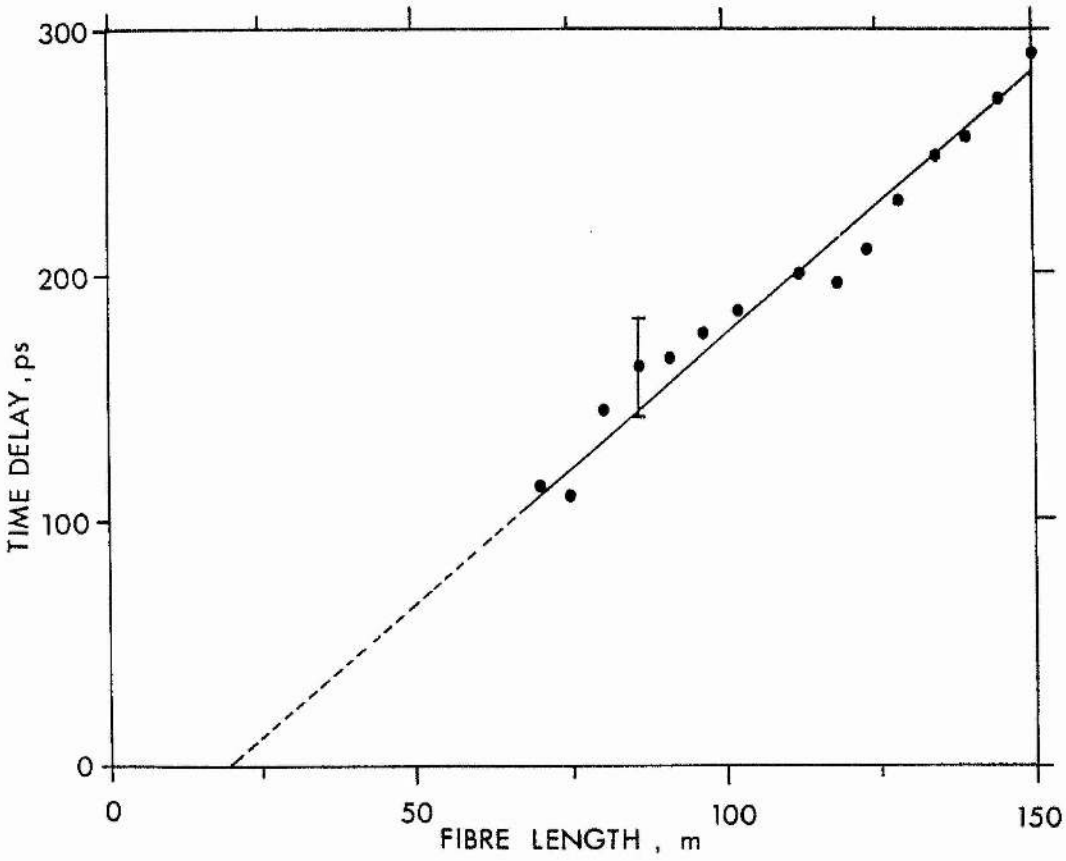

Figure 20.
Plot of the time delay between the pump and Raman pulse peaks versus the fibre length for a peak power of 230 W.

3.4.2 The Fibre Raman Oscillator (FRO)

In the preceding section, the observation of SRS in an optical fibre has been described with the generation of a first order Stokes pulse at 1.12 μm. As an extension of this work we constructed an optical resonator incorporating a length of fibre as the Raman-active gain medium. Long lengths of fibre (many metres) used in a fibre Raman oscillator (FRO) enable low threshold powers to be attained and a CW pump may be used with only about 1W of pump power [50]. The broadband Raman spectra of glass fibres also enables FRO's to be tuned over ~ 500 cm^{-1} for a single Stokes band. If the pump-to Stokes conversion is

high, higher order Stokes lines may oscillate extending the tuning range even further [51]. The large gain bandwidth of the FRO makes possible the generation of tunable ultrashort pulses in the near-infrared by using the technique of synchronous mode-locking [52]. In the work described here, the mode-locked Nd:YAG laser was used to synchronously pump a FRO and a spectral and temporal characterisation was performed.

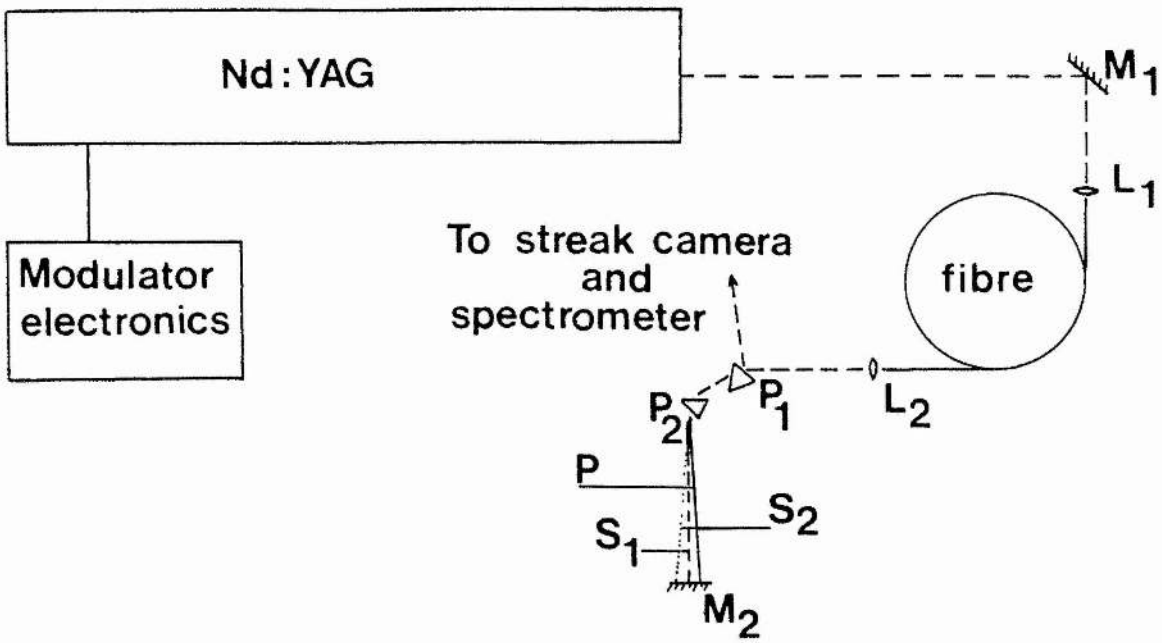

Figure 21.
Experimental arrangement for the fibre Raman oscillator.

Figure 21 is a schematic diagram of the fibre Raman oscillator. The arrangement is similar to that for the experiments on SPM and SRS with the addition of the two prisms, P_1 & P_2 and the end mirror M_2. A 150 m length of fibre, similar to that described previously (#1), was used as the gain medium. The fused silica, Brewster-angled prisms were incorporated within the FRO cavity to provide spatial separation of the pump (P) and Stokes (S_1, S_2) wavelengths and thereby prevent feedback of the pump light which could cause a degradation of the pump laser mode-locking. Mirror M_2 constituted one end reflector of the FRO and was adjusted to feedback the first Stokes Raman light through the

fibre. In addition, the position of M_2 was adjustable on an optical rail so that the FRO cavity length could be matched to a large integral multiple of the pump laser cavity length, thus satisfying the requirement for synchronous pumping. The second end mirror of the FRO was the output coupler of the Nd:YAG pump laser. As is seen in the figure, the output of the FRO was taken as a reflection off one of the prism surfaces and monitored by both a 1m scanning monochromator (resolution $\approx$ 0.05 nm) coupled to an S1 response photomultiplier and temporal measurements were taken with a streak camera. The trigger for the sweep electronics of the streak camera was normally taken from a portion of the optical beam exiting the YAG laser and an appropriate photodetector (chapter 2). In this case, however, the glass slide taking this fraction of the beam would be inside the FRO cavity and cause excessive loss. We therefore chose the alternative of triggering the sweep electronics from the r.f modulator drive electronics as when studying the Q-switching behaviour of the pump laser (see chapter 2).

The variation of the peak oscillating wavelength of the FRO as a function relative cavity length and corresponding relative time delay, is plotted in figure 22. This tunability of the synchronously pumped FRO simply by varying the cavity length, is a consequence of the time synchronisation between the pump and Raman pulses and is known as time dispersion tuning. The particular oscillating Stokes wavelength must have a round-trip time equal to that of the pump laser in order to achieve synchronous pumping. Since pulses with different central wavelengths travel at slightly different group velocities, adjusting the cavity length causes a pulse with a different Stokes wavelength to be time synchronised with the pump pulses. Consequently, by translating one mirror of the FRO cavity, we can vary the wavelength of operation. A tuning range of almost 50 nm (1.0725 - 1.1220 μm) was obtained by translating the mirror by 10 cm, equivalent to a relative time delay of 330 ps. Longer Stokes wavelengths were obtained for longer cavity lengths, which would be expected since these travel with the largest velocity and so the cavity needs to be longer than the pump cavity length in order to match the round-trip times. The dispersion of the fibre in the region of 1.1 μm

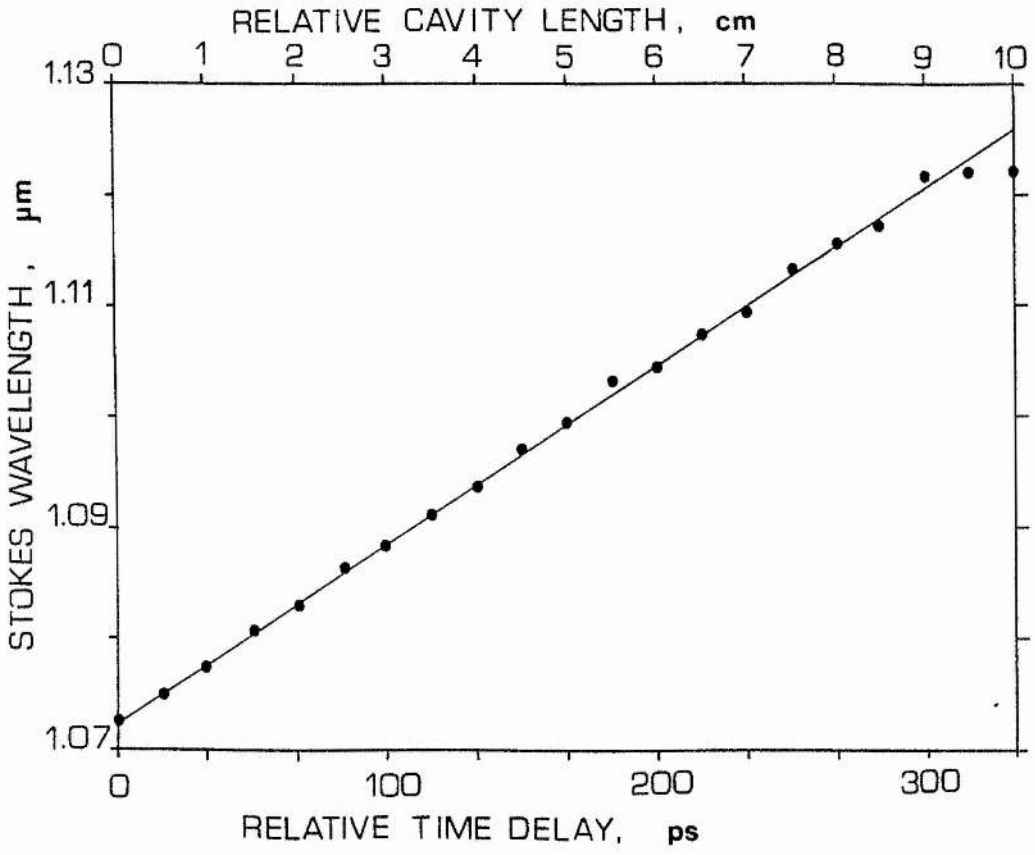

Figure 22.
Dependence of the oscillating Stokes wavelength on the relative cavity length (ΔL) and also depicted in terms of the relative time delay, $\Delta T = \Delta L / c$.

may be determined from the gradient of the line in figure 22. The gradient is $\delta\lambda/\delta t$ = 0.1613 nm ps^{-1}, the fibre length l = 150 m and together with equation (3.24) the fibre dispersion can be calculated to be D = 41 ps/nm/km which is in good agreement with that deduced from figure 20.

The spectral characteristics of the FRO output are presented in figures 23 and 24. The cavity length dependence of the various spectral components are shown in figure 23. The curve (b) is the relative intensity of a second Stokes band produced when the oscillating first Stokes was of high enough intensity. Note that this second-order Stokes was not oscillating in the cavity but merely 'spontaneous noise'. Curve (c) represents the

'nonlasing' first-order Stokes emission. This arises when the cavity length is short and so favouring the shorter Raman spectral bands. Here the low Raman gain cross-section is offset by a long interaction length but the instantaneous energy depletion of the pump pulse is small. Consequently the pump pulse has sufficient intensity to generate a Raman component at the gain peak early in the fibre, which will not oscillate because of the incorrect cavity length. These features are also illustrated in figure 24. The solid line (a) is for a long cavity length and shows the oscillating first Stokes and a small second Stokes component at about 1.18 μm. The dashed line (b) shows a small nonlasing first-order Stokes line and also a second Stokes emission generated from the oscillating ('lasing') first Stokes. For the shortest length (c), a relatively large nonlasing first order Stokes

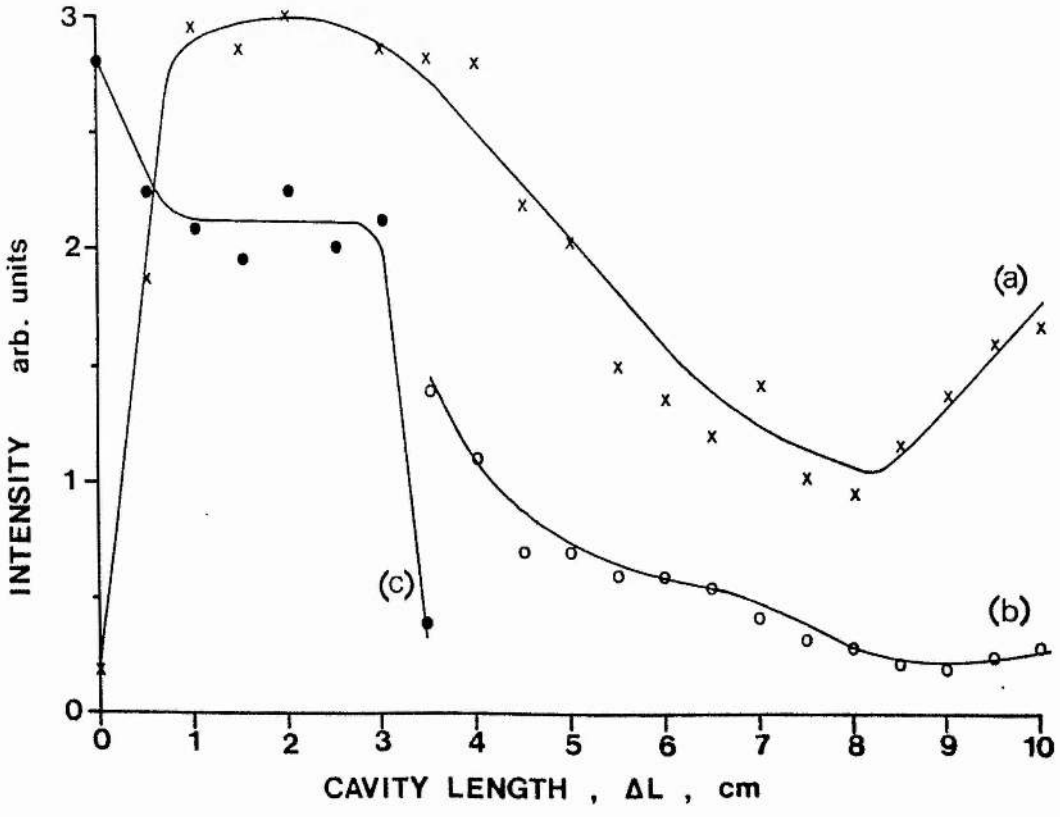

Figure 23.
Intensity of (a) the oscillating first Stokes, (b) the second-order Stokes and (c) the 'nonlasing' first-order Stokes as a function of relative cavity length.

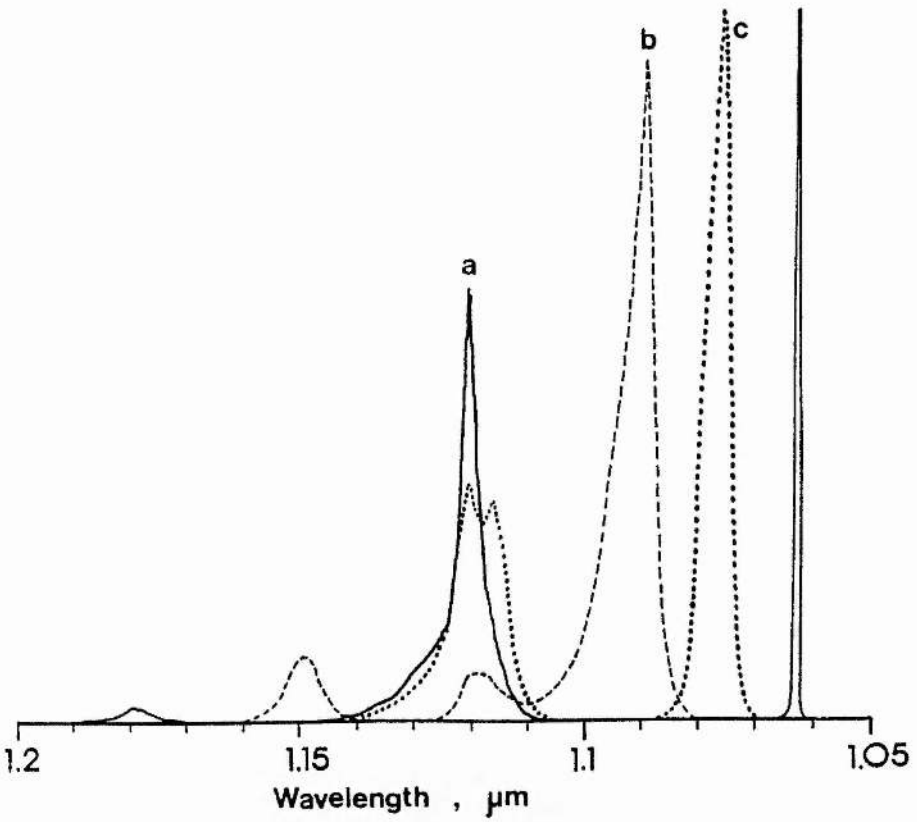

Figure 24.
Spectral output of the FRO for a cavity length mismatch ΔL of (a) +10 cm (b) +3.5 cm and (c) +1 cm.

component was produced which shows two peaks corresponding to the two peaks in the Raman gain curve (see figure 16). (In all cases the sharp peak on the extreme right of figure 24 corresponds to the pump pulses at 1.064 μm).

The reflectivity of the Nd:YAG output coupler is a maximum at 1.06 μm and falls off slightly over the wavelength region of the FRO. This would contribute to the overall output characteristics of the FRO, but it is the interplay between the Raman gain cross-section and the interaction length which predominantly determine the wavelength of operation.

Figure 25a shows the temporal behaviour of the FRO for a relative cavity length of +4.0 cm. With the cavity frustrated, the single pass behaviour was observed (solid line) the SRS pulse leading the pump by ~ 300 ps and peaking at approximately 1.12 μm (fig.25b). Plotted with the same vertical scale, the dashed line shows the ouput of the FRO. The

pump pulse (P) is severely depleted by the strong oscillating first Stokes (S_1), which is able to generate a second Stokes component (S_2). It is also noticed that the oscillating first Stokes leads the pump by a shorter time interval (~ 200 ps) than the single pass Raman pulse. This is due to the wavelength shift of the first Stokes component to approximately 1.095 μm when the cavity was unblocked. The difference in group velocities between the pump and Raman pulses is then not so great resulting in a smaller time separation.

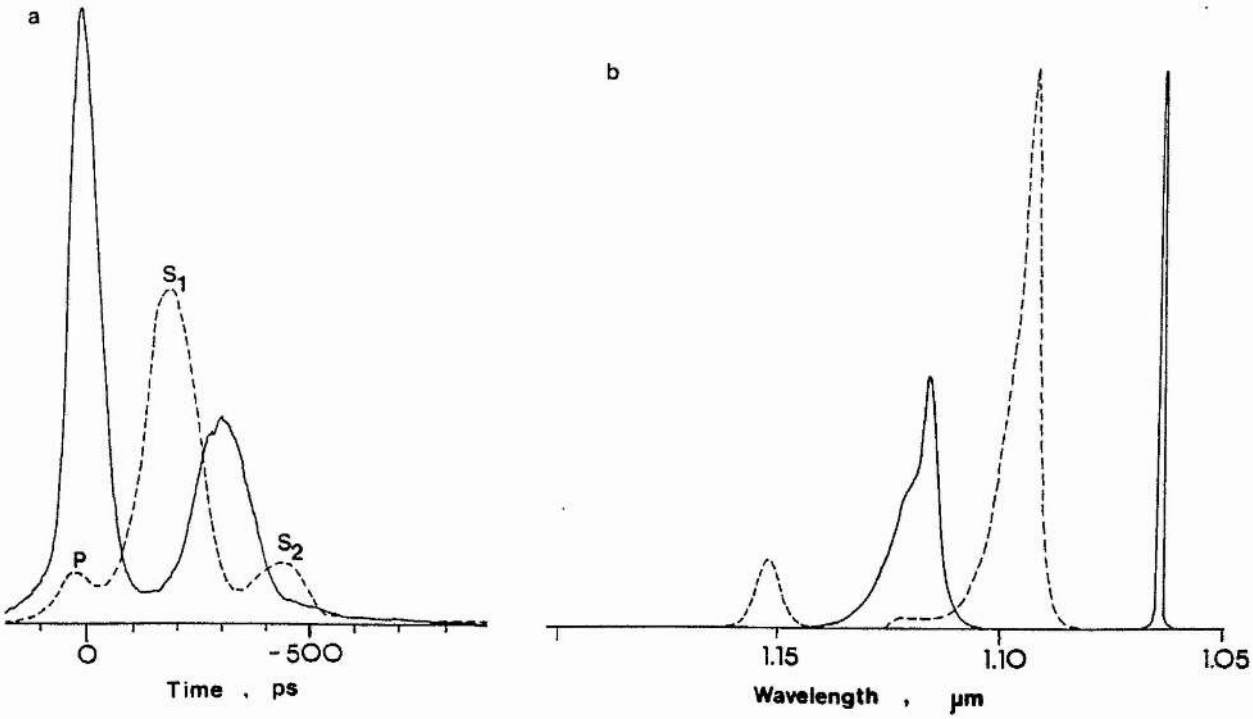

Figure 25.
Temporal (a) and spectral (b) output of the FRO for a relative cavity length of +4 cm. The solid line is for the single pass case (cavity blocked) and the dashed line for the case of laser operation.

By taking the output from the first reflection of P_2, the different spectral components were spatially resolved and we were able to monitor each separately. For this cavity length the durations of the depleted pump (P), first Stokes (S_1) and second Stokes (S_2) pulses were 91ps, 111ps and 116ps respectively and an output power of approximately 40 mW was recorded for S_1 and 9 mW for S_2. No output coupler was available to us at this time

but a mirror with the correct reflectivity would improve the performance of the FRO and enable the best output power to be extracted.

3.4.3 Fibre Raman Oscillator with fibre Grating reflectors (FROG).

The fibre Raman oscillator described in the previous section has been used as a source of tunable, near-infrared pulses for many applications, especially for studies with optical fibres [53]. Although in this case only the gain medium was an optical fibre, there are many potential applications for all-fibre lasers were no bulk external optics are involved. This section describes the construction and charaterisation of an all-fibre FRO, where the conventional external mirrors are replaced by fibre grating reflectors.

Fibre grating reflectors.

The basic construction of a fibre grating is shown in figure 26. A piece of fibre is cemented into a curved groove cut in a glass substrate and the fibre cladding is polished to within ~ 1 μm of the fibre core. A layer of photoresist is then applied to the surface and exposed to an interference pattern produced by two laser beams. Following development of the photoresist, the resulting pattern is transferred to the fibre by reactive ion etching, forming a grating in the fibre with a period determined by the interference fringe spacing. The groove depth is typically 100 nm and the grating length approximately 1-2 mm. A thin layer of aluminium oxide is deposited on top of the grating and a small drop of index matching oil (the superstrate) on top of this, enables the structure to act as a first-order Bragg reflector.

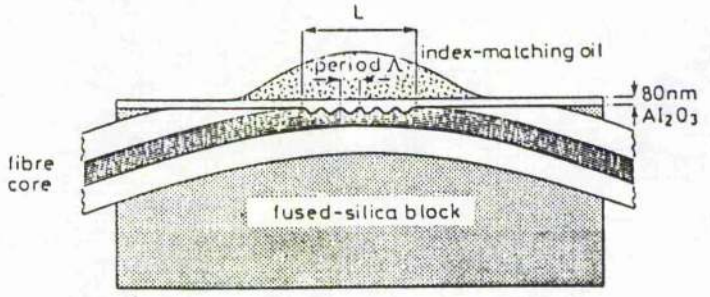

Figure 26.
Schematic diagram showing the construction of a fibre grating reflector.

The operation of the device as a Bragg reflector is most easily described in terms of wave-vector space diagrams - see figure 27. In fig.27a the propagation constant of the guided fibre mode is β and K is the grating constant where $K = 2\pi/\Lambda$ for the grating period of Λ. Coupling into lossy radiation modes occurs for the phase matching condition of

$$\beta - K = k_{s,c} \sin\theta_{s,c}$$

where $k_{s,c} = n_{s,c}\, k_o$ and $k_o = 2\pi/\lambda_o$, the free space wavenumber. The subscripts s,c refer to the substrate and cladding respectively. The first-order Bragg condition is satisfied when $K = 2\beta$ as in figure 27b. Since $\beta = n_e\, k_o$ where n_e is the effective fibre mode index, the Bragg condition can also be expressed as :

$$\lambda_o = 2n_e \Lambda \ . \qquad (3.25)$$

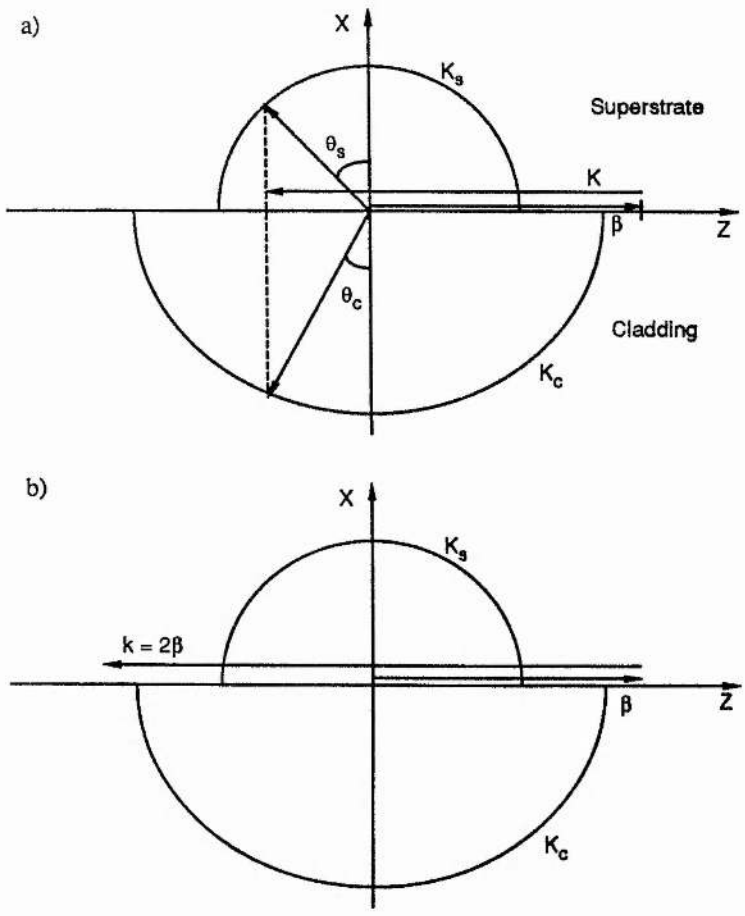

Figure 27.
k-space diagrams to show the phase-matching conditions for coupling of the guided mode to radiation modes (a) and for first-order Bragg reflection (b).

The fibre mode can therefore be efficiently scattered in the backward direction, i.e. reflected. Note that β is always greater than $k_{s,c}$ in order for the *guided* mode to exist in the fibre. For wavelengths shorter than that given by equation 3.25, we can have $K < 2k_c$ and the grating may couple radiation into the cladding. No phase matching is possible for longer wavelengths than that given by equation 3.25 (smaller β and k_c) and the propagating mode is unaffected by the grating. Normally the guided mode field has a small value at the core boundaries which would cause only a small interaction with the grating and very little reflection. To overcome this, a layer of Al_2O_3 is deposited on the grating surface and index matching fluid on top of this. The high index layer of Al_2O_3 ($n \sim 1.68$) 'pulls' the mode field towards the surface and yet is thin enough to prevent the propagation of higher order modes. The oil superstrate further pulls the mode to the core boundary and greatly increases the reflectivity. A more detailed description of the fabrication and operation of fibre gratings is given in references 54, 55.

The two gratings used in our experiments were supplied by Plessey Research Ltd and their characteristics are shown in figure 28. The peak reflectivity was centred at 1.089 μm with one grating nominally 100% reflecting (G_1) and the other ~ 70% (G_2). The high reflector had a transmission of 80% at 1.064 μm, allowing efficient coupling of the pump light into the main fibre. With no index matching fluid on the gratings they behaved as low loss elements with little reflection, whereas with an oil having a refractive index of 1.454 on top, the above reflectivities were obtained. There were two minima in the transmission curve of the output grating (fig.28c), the longer wavelength band corresponding to Bragg reflection while the other is associated with loss to a leaky higher-order mode of the grating.

The FROG1.

The first stage in the construction of the all-fibre device was to insert the highly reflecting grating just before the main length of fibre of the standard FRO of figure 21, the rest of the cavity remaining unchanged. The grating was supplied with fibre pigtails about

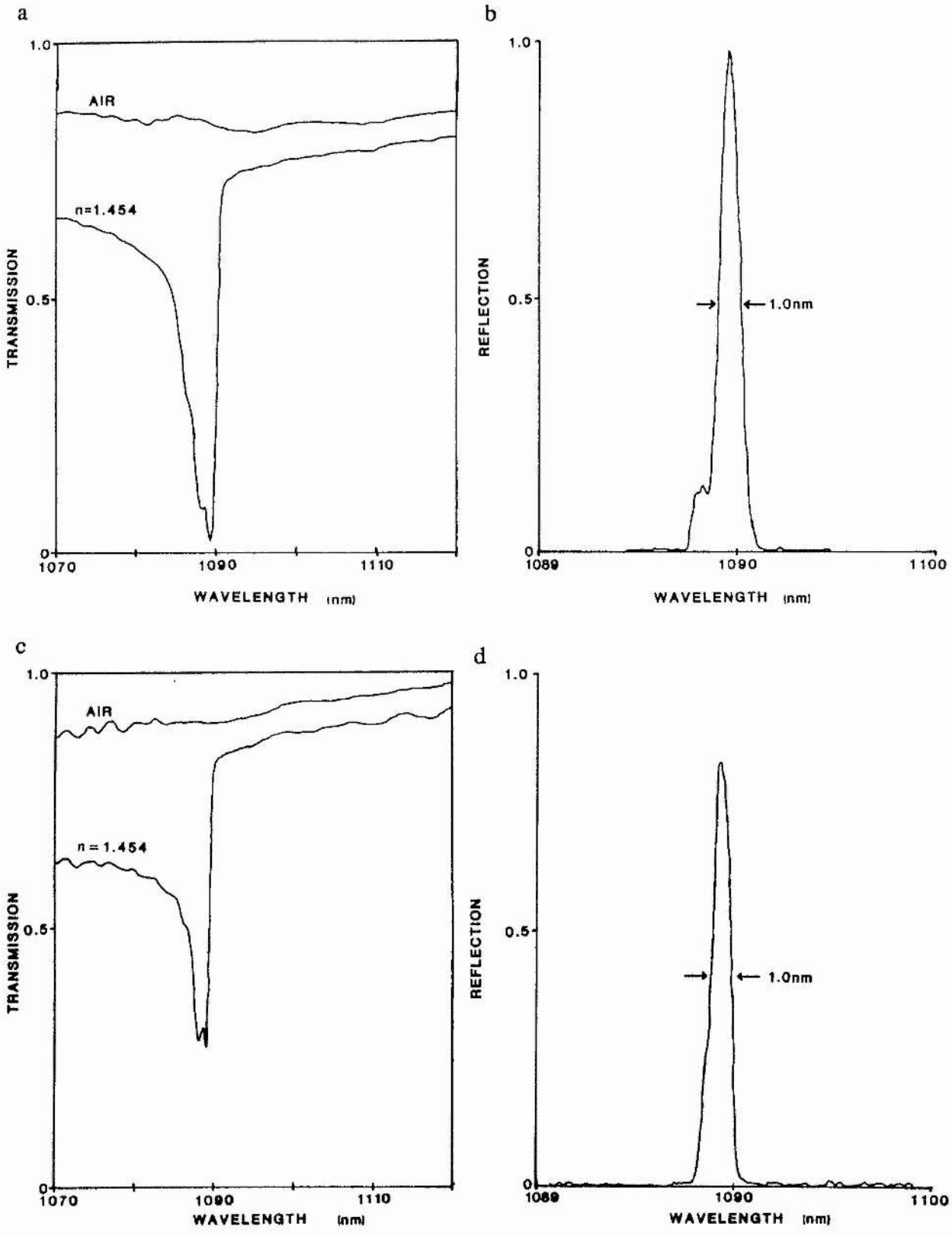

Figure 28.
Transmission and reflection characteristics for the high reflectivity grating, G_1, (a,b) and output coupler grating, G_2, (c,d).

50 cm in length on either side, one was butted up to the main fibre length and the pump light was coupled into the other end. A small drop of index matching fluid was placed at the butt between the two fibres and with this a coupling efficiency of ~ 70% across the butt was achieved. We designated this as the FROG1 configuration and it is illustrated in figure 29. The characteristics of the FROG1 are presented in figure 30 as a function of relative cavity length. Depending on the position of M_2 from the end of the fibre, the laser behaved as a normal tunable FRO or a fixed wavelength FROG. FRO operation was obtained for relative cavity lengths of 5 - 32 cm where the cavity length between the grating and M_2 was incorrectly matched for synchronous pumping of the FROG1. Instead, the grating acted as a lossy element within the cavity of the standard FRO, formed by M_2 and the Nd:YAG output coupler. From fig.30a,b we can see that as the cavity length approached that at which the FRO would oscillate at 1.089 μm, the output dropped sharply. This was due to the grating having a very high loss at this wavelength but oscillation did not occur between M_2

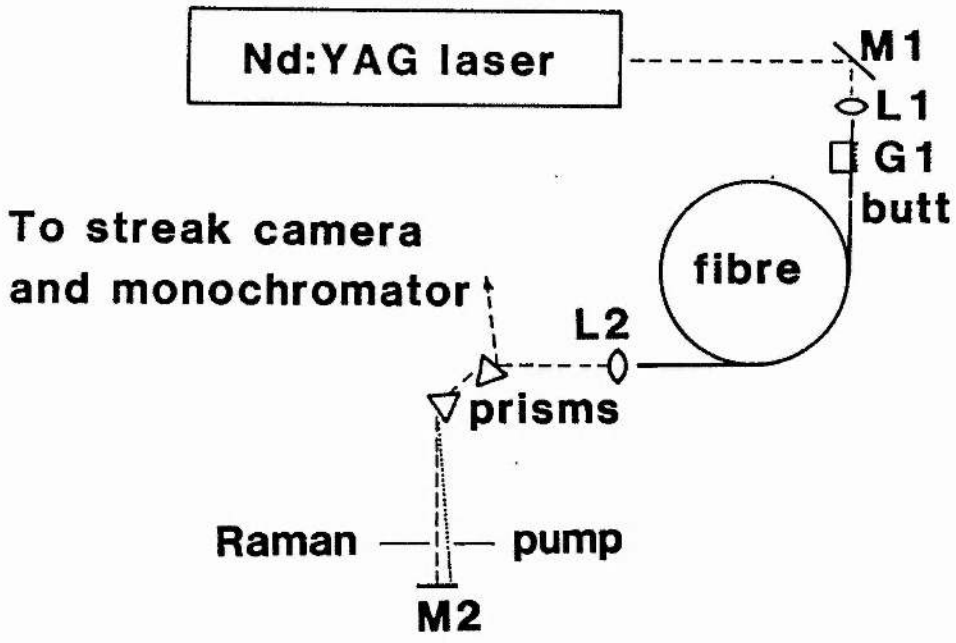

Figure 29.
Experimental arrangement for the FROG1. All components are as for the FRO with the addition of the high reflectivity grating G_1.

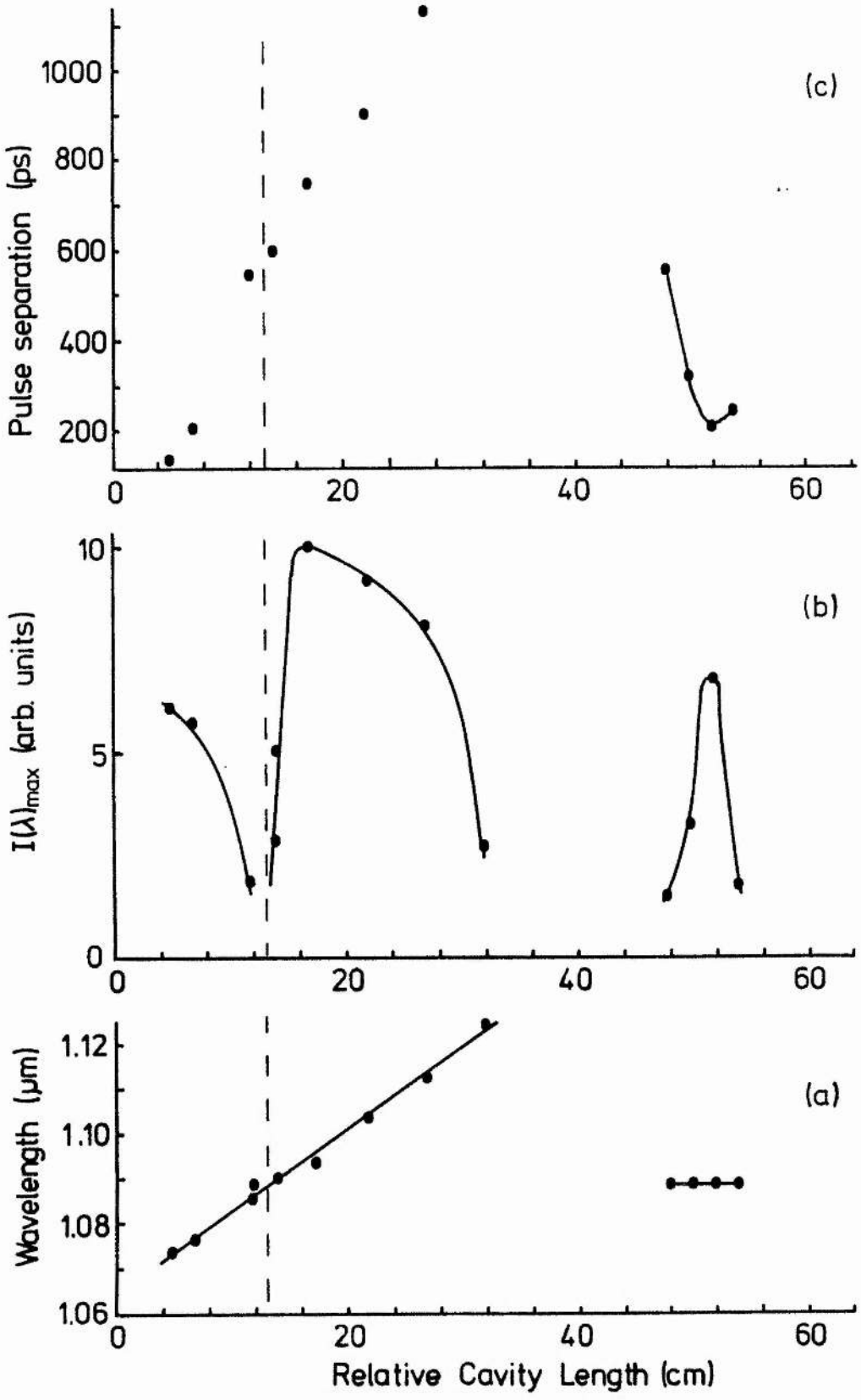

Figure 30.
Characteristics of the FROG1. (a) Wavelength (b) intensity and (c) pump and Raman pulse separation as a function of relative cavity length.

and the grating G_1, since the length was not correct for time synchronisation with the pump pulses. The output power of the FRO was greater for wavelengths longer than 1.089 μm, which was due to the higher transmission of the grating for wavelengths exceeding the Bragg reflection wavelength (see figure 28a).

To obtain laser oscillation between M_2 and the grating, G_1, the mirror was positioned at the point where the FRO would oscillate at 1.089 μm and then pulled back from the fibre by a distance equivalent to the optical path between the Nd:YAG output coupler and G_1. The pump cavity period was then matched to that of the FROG1 (G_1 - M_2) and a signal was observed at 1.089 μm. It was found that Raman oscillation could be maintained over a range of ± 25 mm about the optimum position, the wavelength being defined by the grating reflectivity and so remaining fixed at 1.089 μm. This is indicated by the horizontal line in

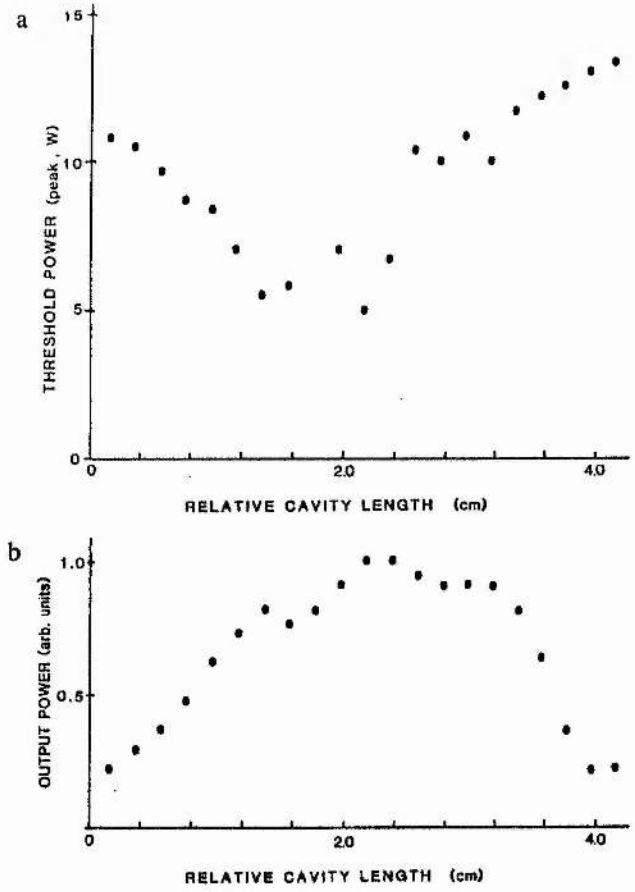

Figure 31
Dependence of (a) oscillation threshold and (b) output power on relative cavity length for the FROG1.

fig.30a and the sharply peaked power curve of fig.30b. Figure 31 shows experimental data for the output power and threshold power of the FROG1 as a function of cavity length. The decrease in output power and increase in threshold as the mirror was taken away from the optimum position is due to the decrease in the overlap of the pump and Raman pulses in the fibre, although small deviations about the optimum matching condition could be tolerated by a slight 'velocity modification' of the Raman pulse. This velocity modification is manifest as a change in the time delay observed between the pump and Raman pulse exiting the fibre as seen in fig.30c and in more detail in figure 32. There is a large change (400 - 120 ps) in the temporal separation for a change in cavity length of only 25 mm. This cannot be explained in terms of the action of GVD and a shift in wavelength, as for the FRO, since the wavelength here is fixed by the grating, rather it corresponds to a change in the position in the fibre at which the pulses separate (360 - 108 m from the fibre end). One might expect that making the FROG1 cavity length different from the pump laser cavity, would cause the Raman pulses to loose synchronisation due to a different cavity round-trip time. This would then show up as a Raman pulse moving across the screen of the streak camera display since it was triggered from the pump laser. However, over the full operating range of the FROG1, a stationary Raman pulse was always observed, indicating that no matter what the cavity length (within the 5 cm operating range) the round-trip time of the Raman pulses was equal to that of the pump pulses and synchronous pumping was still being achieved. This then implies that some velocity modification of the Raman pulses must be occurring during the overlap with the pump pulses owing to a preferential pumping of the leading or trailing edge. A theoretical analysis of Raman-pump pulse walk-off has been undertaken by Schadt et al [56], in which such a velocity modification of the Stokes pulse is considered and it would be interesting to perform a similar model for the case here of a fixed wavelength system.

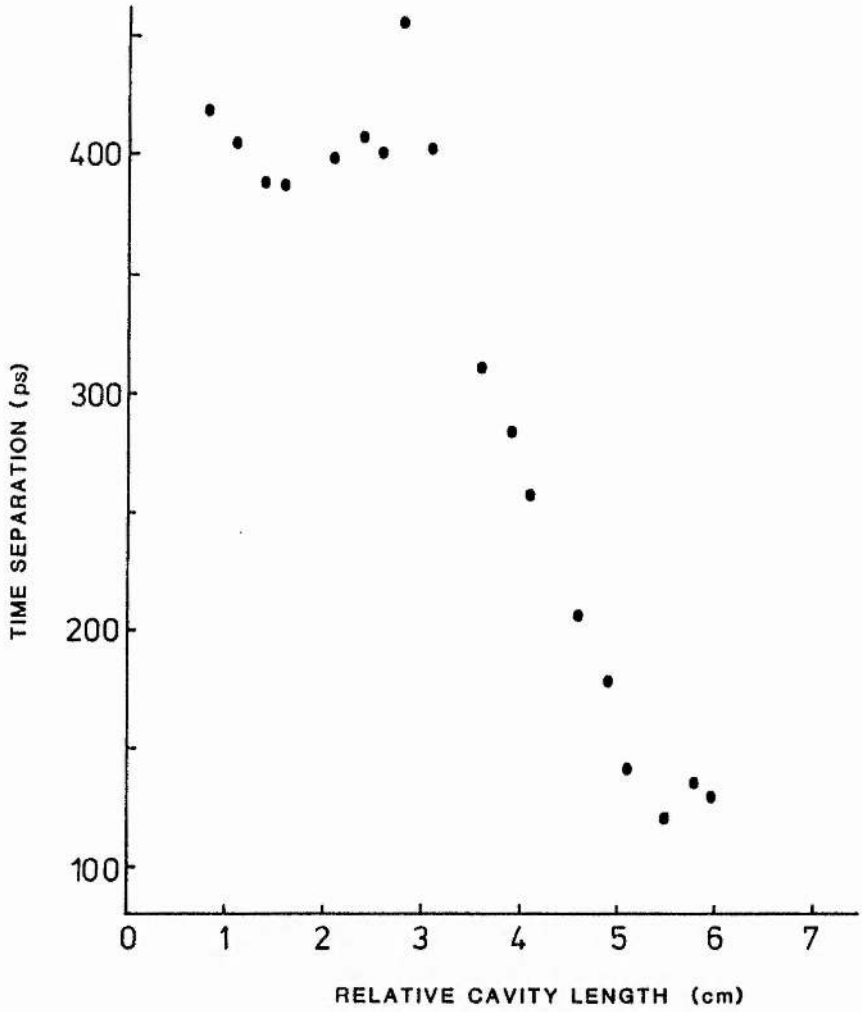

Figure 32.
Temporal separation of pump and oscillating first Stokes pulses as a function of relative cavity length for the FROG1.

The FROG2.

With the mirror M_2 positioned so as to give the best FROG1 operation, a measurement of the distance between the fibre end and M_2 was taken. From this it was possible to calculate the reduction in fibre length such that with the second grating (G_2) added, the optical path from G_1 to G_2 would still be an integral number of pump laser cavity lengths. Figure 33 is a schematic diagram of the all-fibre FROG (FROG2) where the output grating,G_2 , replaced the external prisms and mirror. By cleaving short (~ 10mm) lengths from the main fibre and then butt-coupling the pigtail of G_2 to this, we were able to gradually approach the correct length for synchronous pumping. The 'cut back' process was continued and the output monitored on the monochromator until a signal was seen at 1.089 μm, which indicated that the FROG2 was lasing. Clearly no alignment of the actual

fibre gratings was necessary. The threshold pump power measured at the output of the laser was 800 mW, corresponding to a peak power in the main fibre of 150 W (taking into account the grating transmission ~ 65% at 1.06 μm and the losses at the fibre butt). The maximum output from the FROG2 was 380 mW for maximum pump power coupled into the fibre.

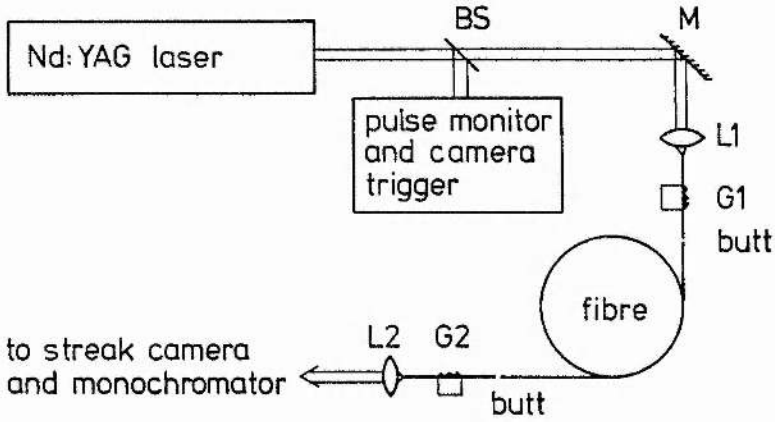

Figure 33.
The all-fibre FRO (FROG2) incorporating two fibre grating reflectors, G_1 and G_2.

Typical spectral and temporal characteristics of the FROG2 are presented in figure 34c,d, along with those for the single grating device (a,b) for comparison. The most striking feature of the FROG2, is the appearance of three sharp dips on an otherwise smooth profile in the output spectrum compared to that for the FROG1. Since they did not appear on the FROG1 spectrum, it was suspected that the dips were due to the transmission of the grating G_2. Figure 28c shows the presence of one minimum in the transmission curve due to coupling to lossy higher order modes as pointed out previously but this is only a low resolution trace supplied to us by the grating manufacturers. A higher resolution measurement of the grating transmission was performed by passing the output of a tunable FRO through the grating and monitoring the spectrum on a

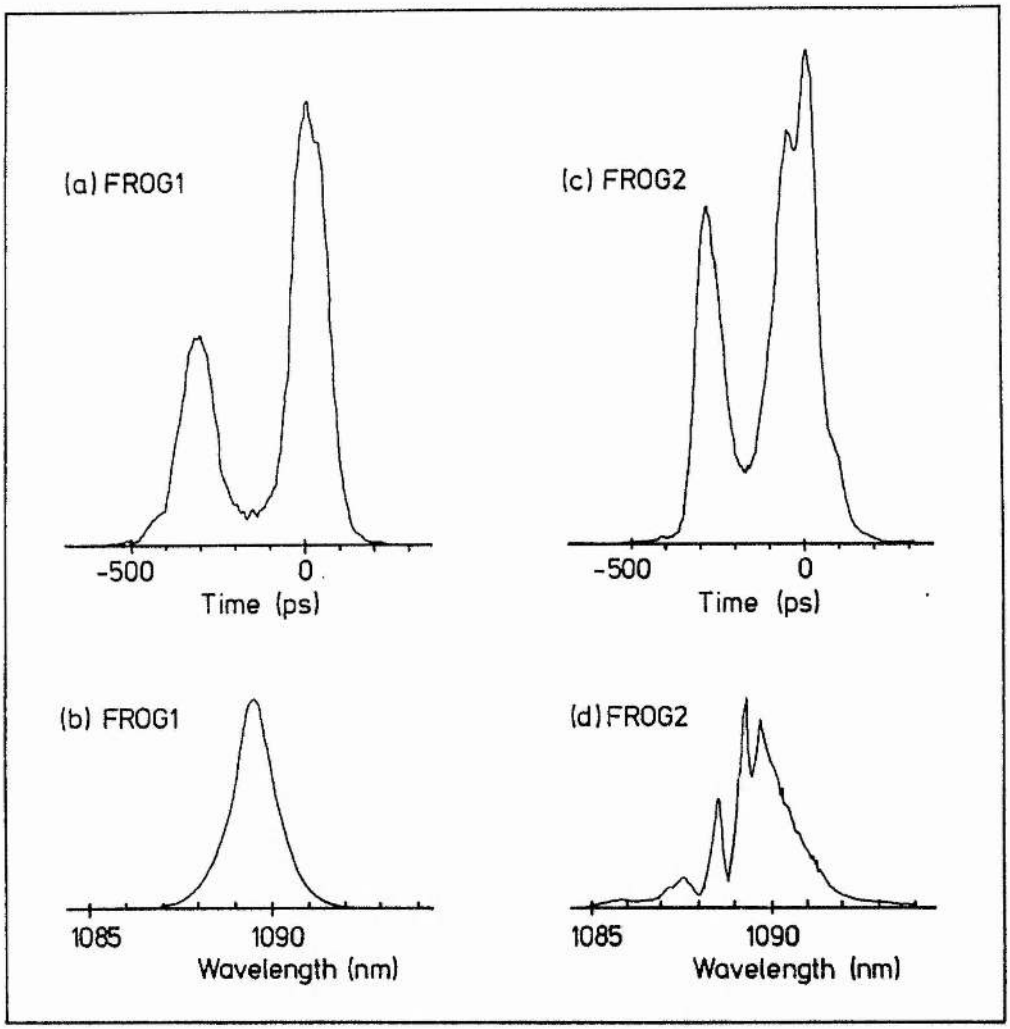

Figure 34.
Typical temporal and spectral outputs of the FROG1 (a,b) and the FROG2 (c,d).

monochromator (resolution ~ 0.5 Å). The trace shown in figure 35 was obtained and clearly reveals the presence of three minima in the transmission spectrum, the wavelength separation of these features corresponds exactly with the dips in the output spectrum from the FROG2. The output power from both the FROG1 and FROG2 was found to be dependent upon the stress applied to the fibre. This is perhaps not unexpected since as mentioned before, the Raman gain depends on the relative polarisations of the pump and Stokes electric fields.

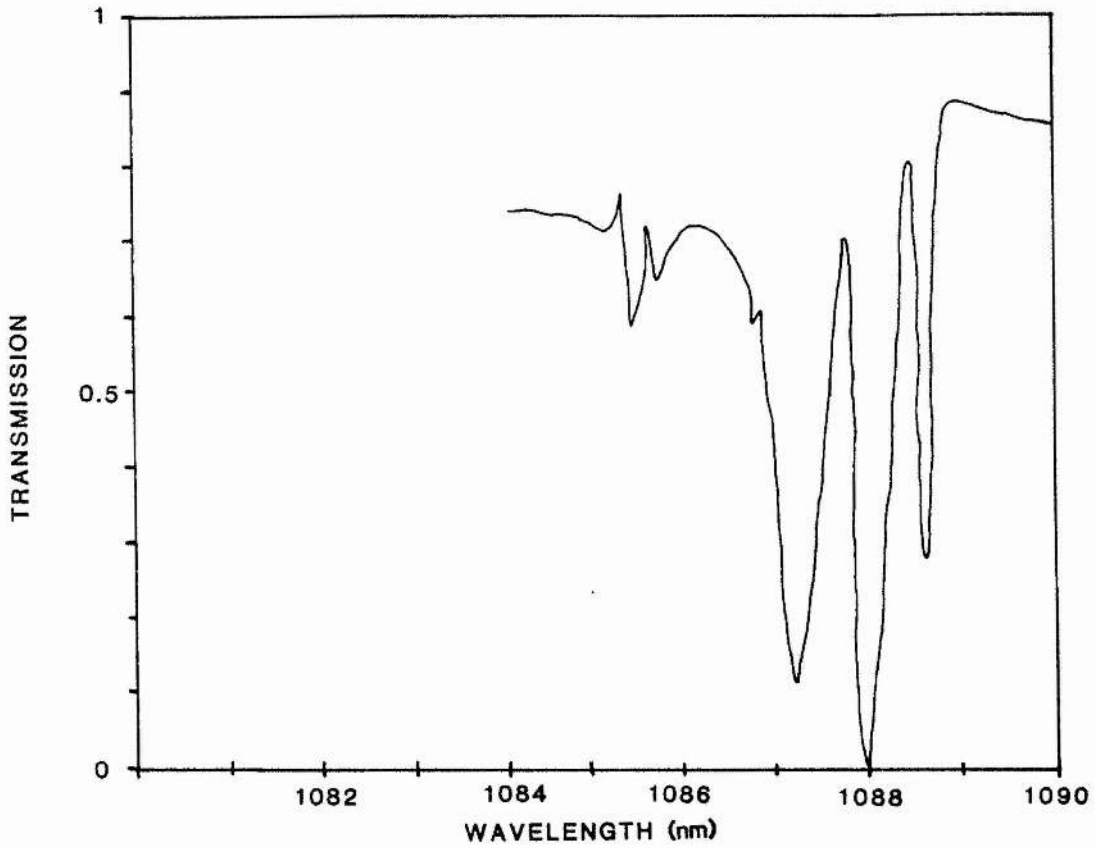

Figure 35.
High-resolution transmission curve for the output coupler grating. Note that the separation of the minima correspond to those in fig. 34d.

In non-polarisation maintaining fibre, as used in these experiments, changes in the birefringence along the fibre length cause the polarisation of the propagating radiation to change from linear through to elliptical over very short distances (effectively scrambling a well defined input polarisation). Any external stresses applied to the fibre, affect the birefringence with a consequent influence upon the relative polarisations of the pump and Raman pulses and hence the gain available. The use of polarisation preserving fibre would considerably stabilise the output and also increase the Raman gain.

3.5 Conclusions.

In this chapter a study of the two nonlinear processes of self-phase modulation and stimulated Raman scattering in optical fibres has been presented. The propagation of relatively long (~ 100 ps) optical pulses in short lengths of fibre is seen to obey a simple theory of SPM in the normal dispersion regime. Such self-phase modulated pulses were temporally compressed by a standard grating pair arrangement, providing a negatively

dispersive delay line, giving pulses of approximately 5 ps duration with peak powers ~ 600 W. Although the pulses generally had a broad pedestal, optimally compressed pulses could be obtained by using a longer fibre length as predicted by equations (3.20).Stimulated Raman generation has been shown to cause a deviation of the self-phase modulated pulse characteristics from the simple theory owing to a significant depletion of the pump pulse. Although it was thought that SRS would be the main power limitation for optical pulse compression, recent studies have shown that good quality compressed pulses may be obtained in the presence of significant SRS and that it can have a beneficial stabilising effect on the output pulses [33,46-49].

Following on from this, a synchronously pumped fibre Raman oscillator was constructed and examined in some detail. There are many advantages for all-fibre lasers, obviating the need for any external optical components and by incorporating two fibre-grating reflectors in the FRO, an all-fibre version of the FRO has been made. Although the use of the gratings restricted the tunability of the FRO, some limited tuning is possible by varying the index matching fluid on the grating [55]. It would also be possible to tune the laser by piezo-electrically stretching the grating (thereby changing the grating period). The stability and robustness of the FROG may be greatly improved by the use of polarisation preserving fibre and fusion splicing of the two butt-coupled joints. A solid superstrate on top of the gratings may also be used instead of the matching oil. Finally, the doping of the Raman fibre by gases would provide a greater Stokes shift and laser action at ~ 1.5 μm could be obtained [57]. Alternatively, the frequency-tunable KCl:Tl colour centre laser also provides ultrashort pulses in this spectral region and this is the subject of the next chapter.

References.

1. R Shen; "Nonlinear Optics", Hopf and Stegeman.
2. A Yariv; "Quantum Electronics" 2nd edition, Wiley (1975).
3. E Lichtman, A A Friesem, R G Waarts, H H Yaffe; J.Opt.Soc.Am.B **4**, 1397 (1987).
4. R H Stolen; Chapter 5 of "Optical Fibre Telecommunications", ed. S E Miller and A G Ghynoweth, Academic Press (1979).
5. D Cotter; Optical & Quant. Electron. **19**, 1 (1987).
6. R R Alfano, P P Ho; IEEE J. Quant. Electron. **QE-24**, 35 (1988).
7. U Osterberg, W Margulis; Opt. Lett. **12**, 57 (1988).
8. R Y Chiao, E Garmire, C H Townes; Phys. Rev. Lett. **13**, 479 (1964).
9. F Shimizu; Phys. Rev. Lett. **19**, 1097 (1967).
10. R R Alfano, L L Hope, S L Shapiro; Phys. Rev. A **6**, 433 (1972).
11. A Owyoung, R W Hellwarth, N George; Phys. Rev. B **5**, 628 (1972).
12. R H Stolen, C Lin; Phys. Rev. A **17**, 1448, (1978).
13. H Nakatsuka, D Grischkowsky, A C Balant; Phys. Rev. Lett. **47**, 910 (1981).
14. K J Blow, N J Doran; IEE Proc. **134**, pt J, 138 (1987).
15. L F Mollenauer R H Stolen J P Gordon; Phys. Rev. Lett. **45**, 1095 (1980).
16. R A Fisher, W K Bischel; J. Appl. Phys. **46**, 4921 (1975).
17. A Yariv; Chapter 6 of "Introduction to Optical Electronics" 3rd edition, Holt Rinehart Winston (1985).
18. J Noda, K Okamoto, Y Susak; J. Lightwave Tech. **LT-4**, 1071 (1986).
19. R H Stolen; Proc. IEEE **68**, 1232 (1980).
20. A S L Gomes, W Sibbett, J R Taylor; Appl. Phys. B **39**, 43 (1986).
21. W Koechner "Solid State Laser Engineering", Springer-Verlag (1976).
22. A Owyoung; IEEE J. Quant. Electron. **QE-9**, 1064 (1973).
23. J J Song, M D Levenson; J. Appl. Phys. **48**, 3496 (1977)
24. C V Shank, R L Fork, R Yen, R H Stolen; Appl. Phys. Lett. **40**, 761 (1982).
25. J G Fujimoto, A M Weiner, E P Ippen; Appl. Phys. Lett. **44**, 832 (1984).

26. W H Knox, R L Fork, M C Downer, R H Stolen, C V Shank; Appl. Phys. Lett. **46**, 1120 (1985).
27. F Gire, P Tournois; Compt. Rend. **258**, 6112 (1964).
28. E B Treacy; J. Quant. Electron. **5**, 454 (1969).
29. H Nakatsuka, D Grischkowsky; Opt. Lett. **6**, 13 (1981).
30. J D Kafka, T Baer; Opt. Lett. **12**, 401 (1987).
31. W J Tomlinson, R H Stolen, A M Johnson; Opt. Lett. **10**, 457 (1985).
32. D Grischkowsky, A C Balant; Appl. Phys. Lett. **41**, 1 (1982).
33. E A Golovchenko, E M Dianov, P V Mamyshev, A M Prokhorov; Optical & Quant. Electron. **20**, 343 (1988).
34. W J Tomlinson, R H Stolen, C V Shank; J. Opt. Soc. Am. B **1**, 139 (1984).
35. W J Tomlinson, W H Knox; J. Opt. Soc. Am. B **4**, 1404 (1987).
36. H C Lefevre; Electron. Lett. **16**, 778 (1980).
37. R L Fork, C H Britocruz, P C Becker, C V Shank; Opt.Lett. **12**, 483 (1987).
38. R H Stolen, E P Ippen, A R Tynes; Appl. Phys. Lett. **20**, 62 (1972).
39. R H Stolen, C Lee, R K Jain; J. Opt. Soc. Am. B **1**, 652 (1984).
40. B Stoltz, U Osterberg, A S L Gomes, W Sibbett, J R Taylor; IEEE J. Lightwave Tech. **LT-4**, 55 (1986).
41. C Lin; IEEE J. Lightwave Tech. **LT-4**, 1103 (1986).
42. A R Chraplyvy, J Stone, C A Burrus; Opt. Lett. **8**, 415 (1983).
43. R G Smith; Appl. Opt. **11**, 2489 (1972).
44. C Lin, R H Stolen, J K Jain; Opt. Lett. **1**, 205 (1977).
45. D Marcuse, C Lin; IEEE J. Quant. Electron. **QE-17**, 869 (1981).
46. T Nakashima, M Nakazawa, K Nishi, H K Ubota; Opt. Lett. **12**, 404 (1987).
47. A M Weiner, J P Heritage, R H Stolen; J. Opt. Soc. Am. B **5**, 364 (1988).
48. M Kuckartz, R Schultz, H Harde; J. Opt. Soc. Am. B **5**, 1353 (1988).
49. A S L Gomes, A S Gouveia-Neto, P M W French, H Avramopoulas, G H C New, J R Taylor; IEE Proc. **134**, pt.J, 171 (1987).
50. K O Hill, B S Kawasaki, D C Johnson; Appl. Phys. Lett. **29**, 181 (1976).

51. R K Jain, C lin, R H Stolen, A Ashkin; Appl. Phys. Lett. **31**, 89 (1977).

52. R H Stolen, C Lin, R K Jain; Appl. Phys. Lett. **30**, 340 (1977).

53. C G Cohen, C Lin; IEEE J. Quant. Electron. **QE-14**, 855 (1978).

54. I Bennion, D C J Reid, C J Rowe, W J Stewart; Electron. Lett. **22**, 341 (1986).

55. C J Rowe, I Bennion, D C J Reid; IEE Proc. **134**, pt.J, 197 (1987).

56. D Schadt, B Jaskorzynska, U Osterberg; J. Opt. Soc. Am. B **3**, 1257 (1986).

57. A R Chraplyvy, J Stone; Opt. Lett. **9**, 241 (1984).

Chapter 4.

The KCl:Tl and NaCl:OH^- colour centre lasers.

4.1 Introduction.

A colour centre is simply an electron trap at a point defect in a crystal structure, which gives rise to a characteristic colouration of the otherwise transparent medium. As will be discussed later, certain types of colour centre have very favourable properties for use as optical gain media in laser cavities. Most of the colour centre defects utilised in lasers are based upon an anion vacancy in an alkali halide crystal, they are relatively easy to create and the majority fluoresce in the infra-red end of the spectrum. By varying the host lattice, colour centre lasers have been able to cover the complete spectral range from 0.8 - 4 μm [1] hence covering a hitherto unobtainable region of the near infra-red. Dye lasers such as IR140, can operate out to ~ 980 nm [2], but the long chain molecules involved are easily broken down making the dye unstable and the laser performance soon degrades. Before the advent of the colour centre laser, no reliable, tunable sources were available for the 1 - 4 μm wavelength region and so colour centres have been able to extend the wavelength range accessible by laser sources and take over at the point where dye lasers fail. The first colour centre laser was reported in 1965 [3] and the first tuneable colour centre laser demonstrated by Mollenauer and Olsen in 1974 [4,5].

In certain respects colour centre lasers are closely analogous to dye lasers. A small crystal (typically ~ 2 mm thick) containing the active centres is positioned at a small beam waist in a laser cavity instead of a flowing dye jet. As with dyes, the fluorescence spectrum is homogeneously broadened enabling all centres to be pumped by a single frequency pump laser and all the centres are able to contribute energy into a particular laser mode. As well as being a four level system, which is an essential property for efficient laser operation, the transition from the upper laser level to the lower laser level is often almost fully allowed

and hence has a large oscillator strength. The quantum efficiency is thus close to unity and large single pass gains are available in crystals only 1 or 2 mm thick. This enables the laser mode and the pump beam to be focussed at the gain medium, so that laser threshold may be attained with only modest pump powers. The resulting operating efficiencies can be as high as 50% but with output powers limited to around 2.5 W due to problems associated with heat dissipation in the crystal.

The major drawback of colour centre lasers, is that continuous operation at room temperature results in a rapid fading of the output so the crystals need to be cooled to ~ 77 K using liquid nitrogen. The fading is caused by a photochemical destruction of the laser active centres and the creation of aggregate centres that absorb in the laser gain bandwidth. Even with cooling, certain centres still exhibit a fading property. This can often be countered by associating the centre with an impurity or other defect which has the effect of stabilising and localising the centres, producing a crystal that can have a very long life time. The prime examples being the thallium centre in potassium chloride (KCl:Tl) and a defect stabilised F_2^+ centre in sodium chloride ($NaCl:F_2^+:O^{2-}$), which may have useful lives exceeding a year.

Colour centre lasers operating in this near infrared region of the spectrum have found many applications in the fields of molecular spectroscopy, the physics of narrowband semiconductors and multiple quantum wells and as sources of optical pulses for research into fibre optic communications. The region of minimum loss in optical fibres is at around 1.5 μm while the zero chromatic dispersion occurs at ~ 1.3 μm. Thus mode-locked colour centre lasers tuneable over this wavelength range are extremely useful sources of ultrashort pulses for pulse propagation studies in optical fibres [6].

The laser active centres used in this project were the Tl^0 centre in KCl:Tl and a stabilised F_2^+ centre in NaCl:OH (NaCl doped with NaOH). Both of these crystals have a tuning range of roughly 1.4 - 1.6 μm. In this chapter a brief overview of colour centre laser physics will be given, dealing in more detail with these centres and a laser characterisation will then be presented.

4.2 Some basic physics of laser-active colour centres.

The building block of nearly all laser-active colour centres is the so called 'F' centre (the F originates from the German word Farbe, meaning colour). This is an electron trapped at an anion vacancy within the alkali-halide host lattice and is shown schematically in figure 1. The surrounding lattice provides an approximately square potential well in the vicinity of the vacancy and gives rise to the presence of energy levels within the band gap of the crystal. Electronic transitions between these levels produces optical absorptions (and emissions) which colour the crystal. Unfortunately, a laser based on this type of centre has never been demonstrated since a crystal containing F centres tends to show a net optical loss rather than gain. However, we may use this simplest of centres to gain an understanding of the general optical properties of more complex colour centres, which have been used successfully as laser gain media.

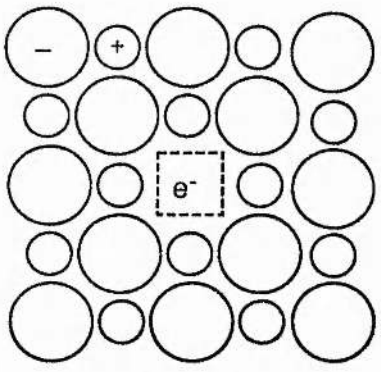

Figure 1.
Schematic representation of the simple F centre.

A simple model of the F centre can be obtained using the configurational coordinate model [7,8]. Although this gives only a qualitative understanding, it does show the origins of the major spectroscopic features that are observed for colour centres. The host lattice surrounding the defect supplies the potential experienced by the trapped electron and can be approximated to a three dimensional infinite square well. The energy difference between the ground and first excited state is then

$$\Delta E = E_2 - E_1 = \frac{3h^2}{8ma^2}$$

where h is Plancks constant, m the electron mass and a the well dimension. Lattice vibrations (phonons) vary the dimension of the well, so the energy of each electronic state is strongly dependent upon the lattice constant (inter-atomic spacing) and a strong coupling between lattice distortion and transition energy is expected. We now make use of the Born-Oppenheimer or adiabatic approximation where the electrons experience a potential that depends on the actual position of the surrounding ions, whereas the equilibrium position and vibrational states of the nuclei are assumed to depend only on the average position of the electron, and therefore on its energy state. The total wavefunction of the system can then be split into electronic and vibrational parts and written as

$$\Psi(r,R) = \Phi_j(r,R)\,\chi_{j,n}(R)$$

where Φ_j is the electronic wavefunction with j representing the electronic state (ground,g or k, excited), $\chi_{j,n}$ is the vibrational wavefunction (harmonic oscillator eigenfunction) and n the vibrational quantum number. R and r are the nuclear and electronic coordinates respectively. Rather than taking account of all possible vibrational modes, it is assumed that we may consider only one important lattice mode, which is usually taken to be the radial 'breathing mode' where the lattice expands and contracts about the F centre. For small vibrations this will be a harmonic oscillation (with a period ~10^{-13}s) and so each energy level of the centre will vary harmonically with the nuclear coordinate i.e. the distance between the centre and the neighbouring ions. This is termed the configuration coordinate. Figure 2a is the configurational coordinate diagram for a colour centre and shows the potential energy variation of the ground and first excited states as a function of the configurational coordinate. The ground state, g, energy varies as $1/2M\omega^2(R-R_0)^2$ where R_0 is the average value of the coordinate, M the effective ion mass and ω the vibrational frequency. A similar situation exists for the excited state, k, but since the electronic wavefunction will be more diffuse for this energy level, the parabolic curve becomes shallower and broader and the equilibrium separation increases (R_0'). For each electronic state there are certain allowed vibrational states which are represented by the horizontal lines on the configurational coordinate diagram, the

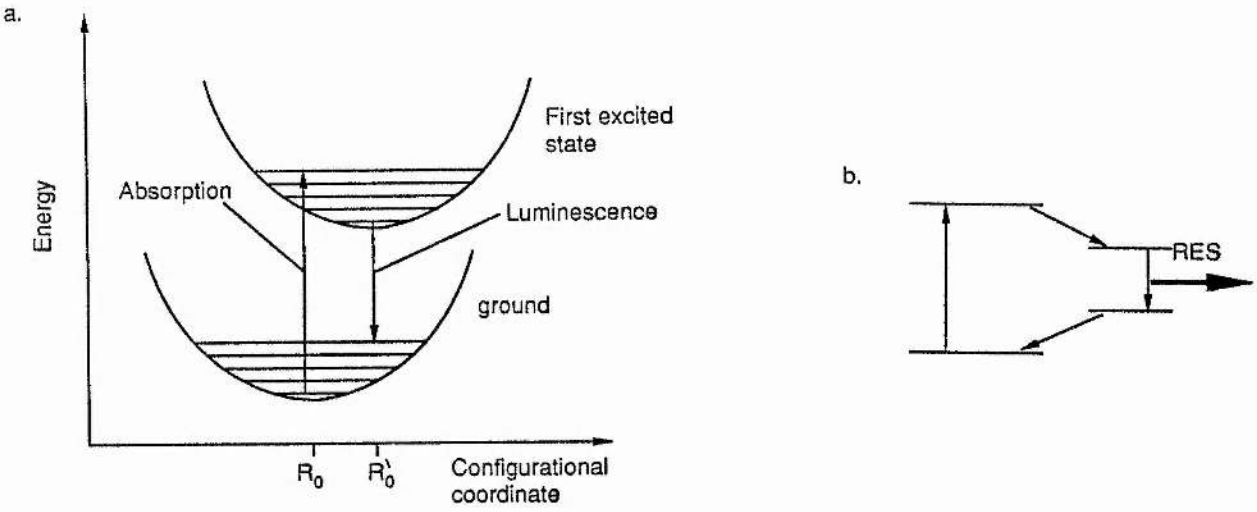

Figure 2.
(a) Configuration coordinate diagram for a colour centre (b) representation of the colour centre as a four level system.

wavefunctions for each of these being described by the harmonic oscillator eigenfunction $\chi_{j,n}$. There is one more approximation made use of in this model, which assumes that the lattice (or configurational) coordinate does not change during the transition from one electronic state to another (the Franck-Condon approximation). This enables the electronic transitions to be represented as vertical lines in figure 2a. The duration of an electronic transition (~10^{-16}s) is much faster than a period of vibration for the lattice nuclei (~10^{-13}s) and so this is a reasonable approximation [9].

We are now in a position to qualitatively understand the optical properties of a colour centre. There are essentially four steps involved in the absorption and emission processes. At low temperatures the most populated state will be the lowest vibrational state (n=0) in the ground electronic energy level, and absorption takes place from this level to some vibrational state in the first excited level, accompanied by the creation of phonons. The lattice will then quickly relax down to the lowest vibration level in the excited state (m=0) by a coupling of the phonon modes to the bulk lattice and this is then known as the relaxed excited state (RES). It is from this level that emission occurs back to a vibrational level in

the ground state (the relaxation process is fast, ~ 10^{-12} s [9], so significant luminescence occurs only from the RES) and then a final relaxation process takes the system back to the initial configuration. These four stages are indicated in figure 2b. Clearly the energy difference between the upper and lower radiational decay levels is less for emission than it is for absorption, due to the displacement of the equilibrium separation in the excited state relative to the ground level and the relaxation processes of the excited centre. This gives rise to a large Stokes shift between the absorption and emission bands. The transition probability for the radiative decay transitions is proportional to the square of $\langle\Psi_2|$ er $|\Psi_1\rangle$ which, when the wavefunctions are separated, becomes

$$[\langle\Phi_k|\ \text{er}\ |\Phi_j\rangle\langle\chi_{km}|\chi_{jn}\rangle]^2 \quad . \qquad [4.1]$$

The first term is the usual electric dipole matrix element and the second term gives the overlap of the vibrational wavefunctions. It is this term which is responsible for the general shape of the absorption and emission bands. As previously mentioned, for low temperatures absorption will mainly take place from the lowest vibrational state ($\chi_{j,0}$). The vibrational wavefunction for this state is of a Gaussian profile whereas the higher lying vibrational levels tend to have wavefunctions that are peaked near the boundary of the potential well (i.e. the limit of classical motion) and oscillatory elsewhere (see figure 2a). (This results generally from the solutions for χ to the Schrödinger equation for a harmonic oscillator potential). Thus the second term in equation (4.1) will tend to follow a Gaussian manner similar to the shape of the $\chi_{j,0}$ wavefunction. This then gives us the shape of the transition probability and hence the absorption profile. With the excitation of the centre, a number of phonons are created with a total average energy given by:

$$1/2M\omega^2(R_0-R_0')^2 = S\,\hbar\omega \qquad [4.2]$$

where S is known as the Huang-Rhys parameter and represents the mean number of phonons generated. A similar picture holds for the emission band and typical absorption and luminescence spectra are shown in figure 3. According to the model so far, the absorption and emission spectra should consist of discrete lines, each corresponding to the creation of a specific number of phonons of a

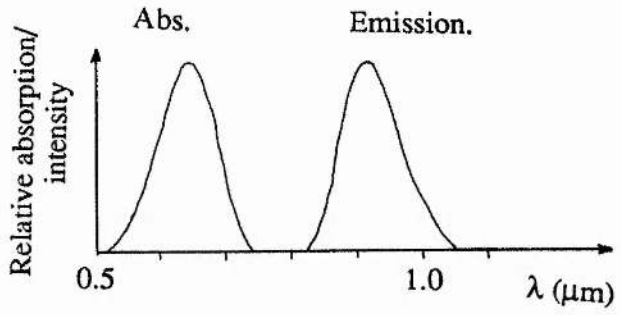

Figure 3.
Typical absorption and luminescence spectra for a F_2^+ colour centre. (After ref. [1])

single phonon mode. However, contrary to our initial assumption, there are of course many lattice vibrational modes causing the energy of each vibrational state to become less well defined. Hence the line spectra broaden and overlap, resulting in the continuous band spectra of figure 3. The displacement of the excited state relative to the ground level on the configurational coordinate diagram, ensures that the transition corresponding to the generation of no phonons ($\chi_{j,0} \rightarrow \chi_{k,0}$ or equally m=n), the zero-phonon line, is relatively weak for most colour centres.

The important features of colour centres for obtaining efficient laser operation can now be summarised. Since each centre interacts with the lattice vibrational modes, both the absorption and emission bands are homogeneously broadened. The radiative lifetime is long compared to the phonon lifetime [1,10] and so the RES is a metastable state and colour centres can be represented as four level systems (see figure 2b). This is very advantageous for laser operation since a population inversion may be obtained with any finite rate of pumping. The fast relaxation of the lower radiative emission level back to the ground state also ensures that there is no population build up in the lower laser level which would otherwise reduce the inversion. As only one electron is involved in the centre, there are no triplet states as in dyes and therefore singlet-triplet transitions are absent. Relatively large absorption and emission cross-sections ($\sim 10^{-16}$ cm^2 [1]) and large quantum

efficiencies (~ 100%) enable high single pass gains to be obtained with modest centre densities and low pump thresholds are achieved.

It was mentioned earlier that although the simple F-centre is the basis of more complex centres, it is not itself laser-active. The reason for this is that the F centre has an anomalously large degree of relaxation. The diffuse electronic wavefunction in the excited state (hence a lower charge density in the vacancy) causes the positive ions in the surrounding lattice to move apart due to mutual repulsion. This results in the potential well becoming shallower and the wavefunction of the electron becomes even more diffuse, with further repulsion of the ions. This continues until the restoring force of the rest of the lattice balances the repulsion. The relaxed-excited state then lies close to the continuum and the emission cross-section is small (i.e. low transition probability), there being only a small overlap of the wavefunctions. Combined with the fact that the centre is then easily ionized, F-centres tend to show a net optical loss. However, the centre is ionized near room temperature, leaving mobile anion vacancies that can form aggregate centres - an important process in the formation of colour centres that do provide optical gain.

4.3 The F_2^+ and $(F_2^+)_A$ Centres.

A description of the different types of colour centres can be found in several review papers [1,9,11,12 and refs. therein], along with their varying tuning ranges and other characteristics. A brief description of one of the most effective centres, the F_2^+, is relevant here however, since it is this defect which is present in the NaCl laser.

As its name implies, the F_2^+ centre consists of two adjacent F centres (lying along the <110> lattice direction) sharing a single electron. Figure 4a shows a schematic representation of the F_2^+ centre. Modelling the centre as a H_2^+ ion imbedded in a dielectric medium [13], where the two anion vacancies represent the hydrogen nuclei, has proved quite successful in predicting the absorption spectrum and the ground and excited states are designated $1s\sigma$ and $2p\sigma$ respectively as for the molecular ion. When the centre is optically excited to the first excited state, there is only a slight enlargement of the lattice and hence the change in configurational coordinate (R_0 - R_0') is small. This gives rise to only a small

Stokes shift and so only a small amount of energy is lost to the crystal as heat. Combined with a high oscillator strength for the radiative transitions, a high quantum efficiency (~100%) and the fact that there are no excited state absorptions, the F_2^+ centre is one of the most efficient colour centres known. Again, by varying the host lattice the peak wavelengths of absorption and emission can be altered so that F_2^+ lasers cover a wide spectral range [14-16].

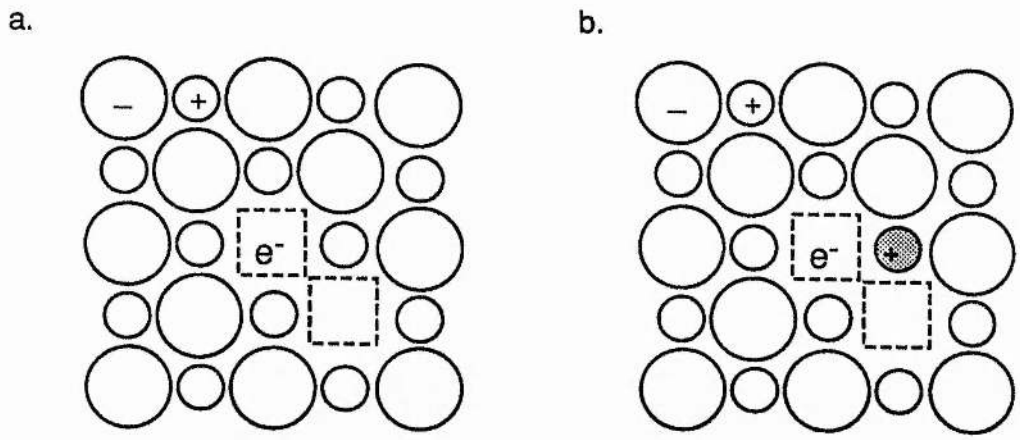

Figure 4.
(a) Schematic representation of a F_2^+ centre and (b) a stabilised $(F_2^+)_A$ centre.

Unfortunately the output of a laser based upon this centre experiences a slow fading (over a period ranging from a few seconds to several hours depending on the type of host), until laser action ceases due to a constant reorientation and random walk of the laser-active centres. This orientational bleaching effect occurs as follows. The electric dipole transition for the F_2^+ is polarised along a line joining the two vacancies and so the pump beam needs to be polarised likewise. Although pumping the centres into the first excited state does not cause a reorientation, multiphoton excitation of the centre into a higher state then enables a neighbouring anion to move into one of the vacancies and the centre has then 'flipped' into another orientation. Pumping of the centre is now less efficient, but still possible, and there still exists the possibility of another reorientation. This continues until the centre flips into an orientation which is orthogonal to the original state and is then unable to be optically excited by the pump beam. Alternately pumping the crystal with the pump polarisation

rotated by 90° can counter this somewhat, however the constant reorientation still causes the centres to make a random walk through the crystal. This eventually leads to aggregation or deionization of the centres and the output fades, putting a limit on the useful life of the crystal [16,17]. Another cause of fading in the output power is a local heating effect due to the focused pump light, which is probably caused by the centres reorientating and migrating. This may be reduced by chopping the pump beam, so reducing the average power incident on the crystal. In any case, virtually all colour centre lasers require the crystal to be cooled to liquid nitrogen temperatures (LNT) in order to prevent centre aggregation and deionization which would otherwise preclude laser operation. Deionization of the F_2^+ centres also limits the storage time or 'shelf life' of the crystals but by storing as F_2 centres and then ionizing by exposure to light just prior to use, a reasonable shelf life is obtained.

In order to prevent the random walk process caused by constant reorientation, the centres need to be stabilised by associating them with an impurity ion or other (radiation damaged) defect. If an alkali impurity ion is associated with the F_2^+ (figure 4b) the centre is termed an $(F_2^+)_A$ and this has the effect of localising the centre at a particular site, although reorientation around the impurity ion is still possible. This type of centre has a greatly increased shelf life and a prolonged operational lifetime over the F_2^+ [18]. Because the production of these stabilised centres is more complicated, involving the association of three entities instead of two, it is more difficult to produce high concentrations and tends to be an order of magnitude smaller than can be obtained for F_2^+ centres. Consequently the output powers of lasers based on the $(F_2^+)_A$ centre tend to be lower than those using F_2^+ centres. It should also be noted that in order to obtain a prolonged nonfading output, some sort of auxiliary illumination of the crystal is required to prevent orientational bleaching [19,20]. The presence of the impurity ion or defect also slightly perturbs the energy levels and generally shifts the luminescence band towards slightly longer wavelengths. An example is the F_2^+ centre in KCl. The luminescence peaks at approximately 1.7 μm for the unstabilised centre and shifts to 1.75 μm with Na ions incorporated into the lattice. With Li ions as the dopant the shift is accentuated, the emission peaking at 2.2 μm. The pump band

experiences a similar but usually small shift. A number of lasers based on defect stabilised F_2^+ centres in different hosts and their operational characteristics are described in references [1,18-20].

4.4 The Stabilised F_2^+ Centre in NaCl.

Furthering the research conducted by various groups on the stabilised $(F_2^+)_A$ centres in alkali-halide hosts [21], a group at Cornell University first reported a stabilised F_2^+ like centre in NaCl [22] in 1985. At that time the stabilising defect was thought to be a potassium ion but subsequent spectroscopic studies have shown that the perturbing ion is much more likely to be an O^{2-} ion [23]. Thus this centre is labeled $F_2^+:O^{2-}$ and a schematic representation of the centre is shown in figure 5.

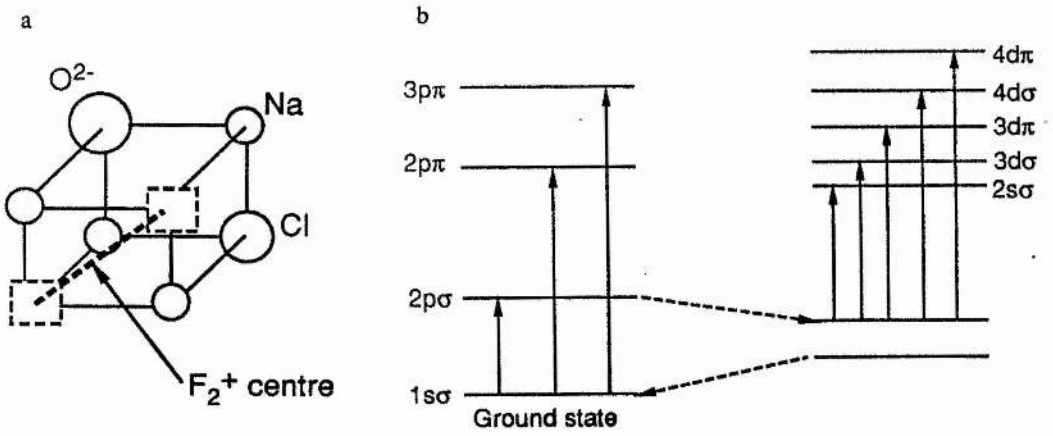

Figure 5.
(a) A schematic representation of the $F_2^+ :O^{2-}$ centre in NaCl (b) the energy levels of the centre in the relaxed and excited state.

Production of the centre is obtained by growing crystals of NaCl with small amounts of NaOH (~500×10^{-6} mol%) giving rise to an OH^- concentration ~50 ppm in the crystal. Additive colouration of the crystal in Na vapour [11,23] produces F, F_2, and F_3 centres, as well as dissociating the OH^- ions into H^-, O^{2-} and some O^- ions which occupy anion sites

in the lattice. When the crystal is to be used it is then exposed, at room temperature, to light corresponding to the fundamental absorption of the F centre (452 nm), from say a filtered mercury lamp, which causes the preferential formation of F_2 centres. A second photoaggregation process is then performed with the crystal cooled to 77K and exposed to the same blue\UV light for a few minutes. This causes a formation of the F_2^+ centres which then migrate until they become trapped at an O^{2-} ion. Electrons liberated by the ionization of F_2 centres are taken up by the O^- ions creating even more of the stabilising O^{2-} ions. A detailed description of the method of production of this centre can be found in references [23,24].

The identification of this centre as $F_2^+:O^{2-}$ was determined from a study of the visible and UV absorption and emission spectra in additively coloured NaCl containing OH^- [23,24]. Amongst other evidence, it was observed that before the second photoaggregation process, the absorption and emission bands in a treated crystal peaked at 1.05 and 1.47 μm respectively, corresponding to the F_2^+ absorption and emission bands in NaCl. After the illumination at 77K, the peaks shift to the longer wavelengths of 1.09 and 1.55 μm respectively which is very similar to the behaviour for the $(F_2^+)_A$ centres. A diagram showing the emission spectra of the F_2^+ and $F_2^+:O^{2-}$ centres at 77K (i.e. before and after UV illumination) is reproduced in figure 6. From the UV absorption spectra it is inferred that there is a strong presence of O^{2-} ions which are formed from the dissociation of OH^- ions. The centres may be effectively pumped by 1.06 μm radiation from the Nd:YAG laser, corresponding to the $1s\sigma \rightarrow 2p\sigma$ transition. The excited centre relaxes giving a fluorescence peaking at 1.55μm and a colour centre laser based on NaCl:OH^- should be tunable over approximately 1.45 - 1.7 μm (1333 cm^{-1}). The lifetime of this excited state is ≈ 150ns and corresponds to an oscillator strength $f \approx 0.29$. It has been found that this centre is very stable, with a shelf life at room temperature of at least a few months (in the dark). Laser operation is reported to show no fading what so ever under true CW conditions (with the crystal cooled to LNT) and output powers ~ 1 W for a pump power ~ 9 W have been reported [24]. The good stability of this centre is aided by the strong coloumb attraction between the positive F_2^+ centre and the negative O^{2-}

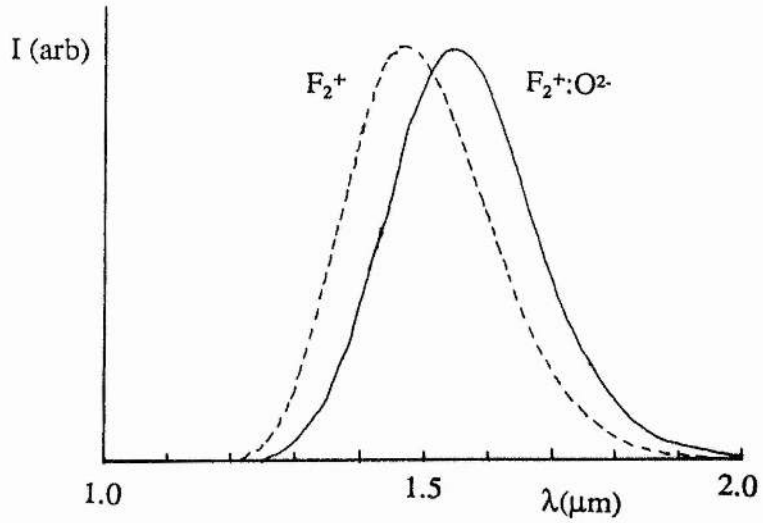

Figure 6.
Normalised emission spectra for the F_2^+ and stabilised $F_2^+ :O^{2-}$ centres at 77K in NaCl. Pump wavelength = 1.06 μm. (Ref [23])

Table 1.

Parameter	Value
n	1.53
λ	1.55 μm
τ_r	150 ns
δν	4×10^{13} Hz
η	~1
σ	8.5×10^{-17} cm^2

Important parameters for NaCl:O^{2-}: n refractive index, λ central emission wavelength, τ_r excited state lifetime, δν linewidth, η quantum efficiency and gain cross section σ [23].

ions but efficient operation still requires an auxiliary light source to provide a reorientation of the centres as for other stabilised F_2^+ lasers.

4.5 The Tl^0 (1) Centre in KCl.

The Thallium centre in KCl is unlike any of the other types of colour centre. It consists of a neutral Tl atom adjacent to either one, Tl(1) or (less commonly) two, Tl(2), anion vacancies (see figure 7a). The fact which makes this centre different is that the electronic transitions are derived from the perturbed energy levels of the Tl atom, rather than the anion vacancy.

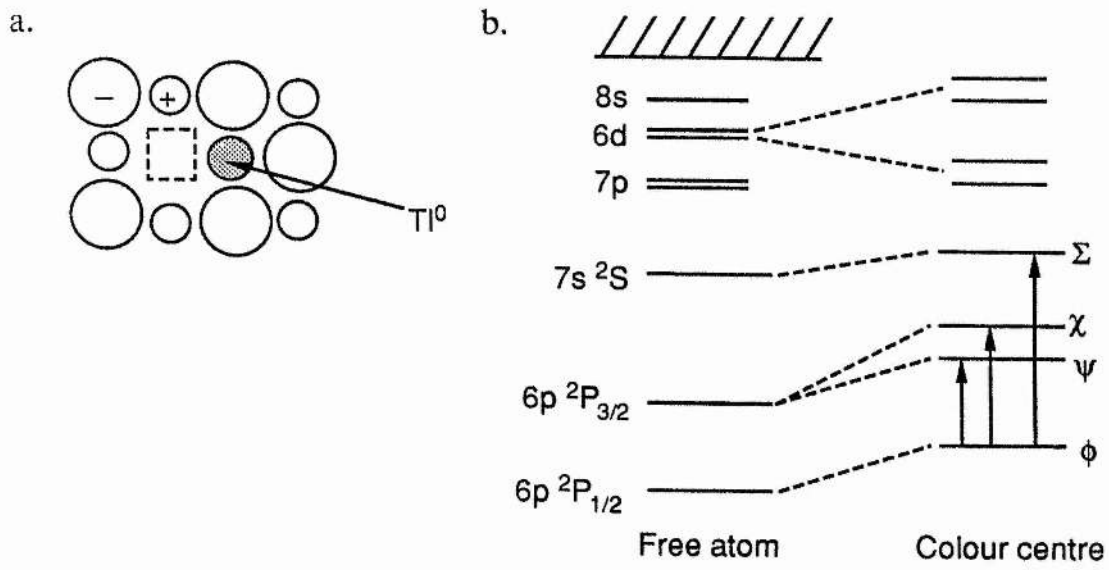

Figure 7.
(a) The Tl^0 centre in KCl (b) Energy levels of the free and perturbed Tl atom.

The free neutral Tl atom has one electron in the 6P orbital, the ground and first excited states being $6P_{1/2}$ and $6P_{3/2}$ respectively. No electric dipole transition is allowed between these states and they are separated by a spin-orbit splitting of approximately 0.97 eV. When combined with the anion vacancy these levels split, as do the higher lying states (see figure 7b), which then allows for (weak) electric dipole transitions. The anion vacancy effectively represents a positive charge which perturbs the energy levels of the Tl centre, splitting the 6P states into three levels - ϕ, ψ and χ. Laser operation is concerned with the ϕ - ψ transition and both the absorption and emission transitions are polarised along the axis of the centre, that is along the vacancy - Tl atom direction, parallel to a <100> crystallographic direction. In the ground state the electron is in a P orbital along the vacancy axis. When excited to the upper state it is largely in the orthogonal direction. The corresponding reduction of charge density in the vacancy, causes the surrounding ions to move apart due to mutual repulsion. The effective charge on the vacancy is thus reduced and this causes a decrease in the energy separation of the ϕ and ψ states, resulting in the stokes shift.

Production of the laser active centres is achieved by electron beam irradiation of KCl crystals doped with ≈ 0.2 mol% TlCl. Crystals are irradiated at about -100°C or lower,

which creates a high density of F centres. At ~ -30°C the crystals are exposed to light from a tungston lamp (e.g microscope lamp) which ionizes the F centres and the liberated electrons are captured by Tl^+ ions, forming $Tl^0(0)$ centres. This temperature is high enough that the F^+ centres can then migrate until they become bound to a neutral Tl atom, completing the formation of $Tl^0(1)$ centres. These centres may not be created by additive colouration which simply makes the crystals a brown colour.

The centre was first observed in 1980 [25] and independently a laser based on a Tl centre in KCl was first demonstrated in 1981 [26]. The luminescence decay time, τ, has been measured to be 1.6 μs [27]. The stimulated emission cross section at the band peak for a gaussian band is given by

$$\sigma_o = \frac{\lambda^2 \eta}{8\pi n^2 \tau} \frac{1}{1.07\ \delta\nu} \qquad (4.3)$$

where n is the refractive index, η the quantum efficiency and $\delta\nu$ the gain bandwidth. Combined with an emission bandwidth of 150 nm (670 cm^{-1}), equation 4.3 gives a gain cross section $\sigma_o \approx 10^{-17}$ cm^2. This value is smaller than that for other colour centres (by ~ 30

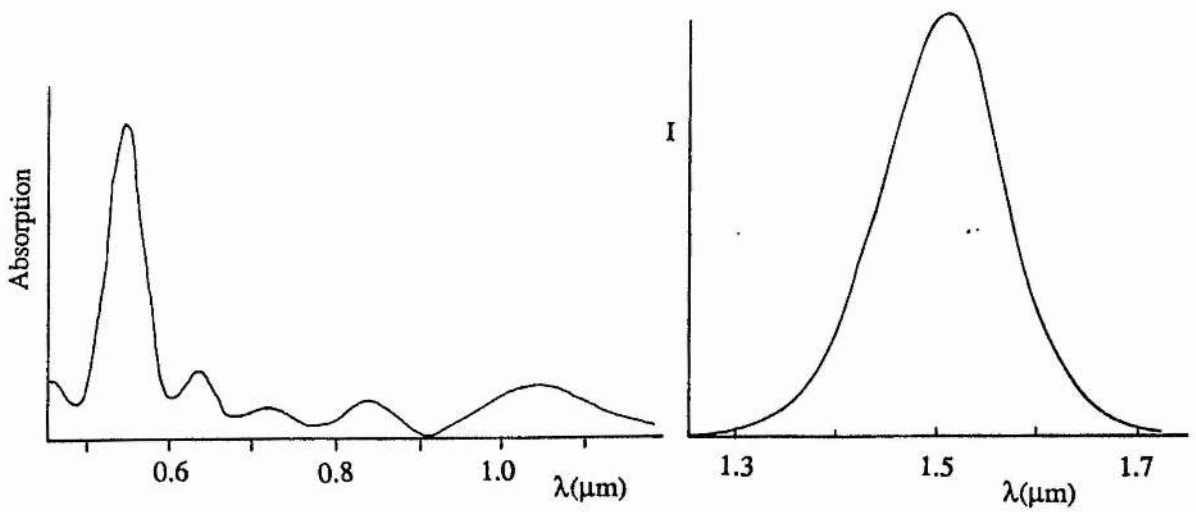

Figure 8.
The absorption and emission spectra for KCl:Tl. (Ref. [1])

times) such as F_2^+, but this is somewhat offset by the fact that higher centre densities may be created.

Table 2.

Parameter	value
n	1.48
λ	1.5 μm
τ	1.6 μs
σ	3×10^{-17} cm^2
$\delta\nu$	670 cm^{-1}
η	~ 1

Important optical parameters for KCl:Tl; n refractive index, τ fluorescence decay time, σ gain cross section, $\delta\nu$ emission bandwidth and η quantum efficiency.

The $Tl^0(1)$ centre is extremely stable under laser operation (orientational bleaching effects are absent) and may have an indefinite lifetime provided the crystals are kept at liquid nitrogen temperatures. Any long term fading effects are probably due to a migration of other defects present within the crystal. A storage lifetime of a few months is typical if the crystals are kept in the dark at just below normal freezing point (0°C). The enhanced stability of the centre seems to be due to a reluctance of the centres to reorientate and also because of a coloumb attraction between the thallium atom and the vacancy, as the electron is shared between the two entities.

4.6 Colour Centre Laser Resonators.

In this section a brief description is given of the astigmatically compensated laser resonator used in this work for the KCl:Tl and NaCl:OH colour centre crystals.

It has already been pointed out that the laser operation of colour centres is in many ways similar to that of dye lasers. Hence in the consideration of a resonator for colour centres it is not of great surprise to find that many systems use cavities very similar to those employed for dye lasers. The reasons for this are two fold. In the first place focusing of the pump beam into the crystal is necessary to obtain relatively low threshold powers, and this is usually accomplished by using two concave mirrors. Also, it is not practical to place anti-reflection coatings on the surface of colour centre crystals because of the hostile processes

which the crystal has to undergo, in order to create the laser active centres. Thus the crystal slab sits at Brewsters angle, preventing reflection losses from the surfaces, at a tight focus region within the cavity. Additionally, long cavity lengths may be required for mode-locking purposes. Meeting these requirements of a long cavity length containing a region of tight focus is attained in the resonator of figure 9. Rather than use lenses inside the cavity to provide focusing, a focusing mirror is preferred since the reflection losses are less than those due to Fresnel and bulk losses of an internal lens.

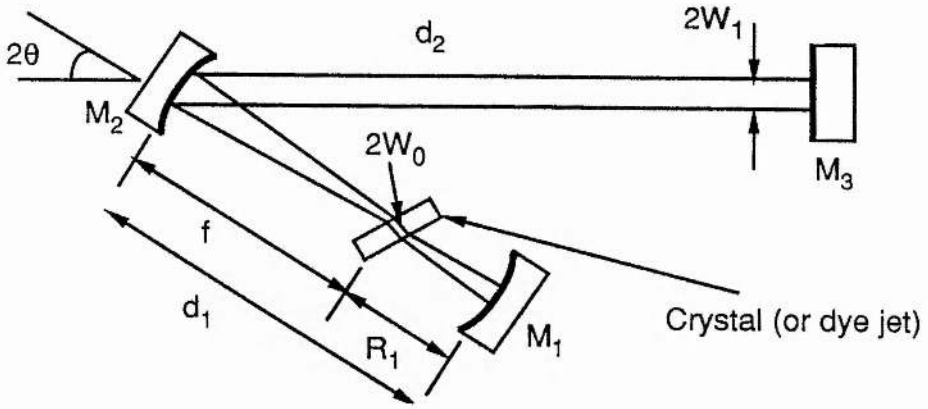

Figure 9.
Astigmatically compensated resonator for dye and colour centre lasers.

This type of resonator introduces a new set of problems - namely distortion of the beam due to astigmatism. The Brewster angled crystal introduces astigmatism in that the wave front radius of the gaussian beam is different for the xz and yz directions just inside the crystal [28]. Also a curved mirror operated at an oblique angle of incidence will focus the sagittal (xz) rays and tangential (yz) rays to different points. Kogelnik et al [29] have shown that the astigmatism introduced by these elements can in fact compensate each other under the appropriate circumstances and an undistorted circular beam results. If on the other hand an internal lens is used to focus the beam, only the astigmatism due to the Brewster angled crystal is present and no compensation is possible, resulting in an elliptical beam.

In the system of figure 9, the centre or focusing mirror (M_2) has a focal length f and the spacings between this and the two end mirrors are d_1 and d_2 with mirror radii of curvature R_1 and R_3 . Production of a small focal spot is achieved with $d_2 >> f$ and a short spacing d_1, with $d_1 \approx R_1 + f$. The beam waist is then produced close to the centre of curvature of M_1. The stability of the cavity is critically dependent on the magnitude of d_1, which may typically vary only over a few millimeters. To take account of this variation we can write:

$$d_1 = R_1 + f + \delta \tag{4.4}$$

where δ is an adjustment parameter which has limits δ_{min} and δ_{max} defining the stability range of the resonator. If (as in the work here) $R_3 = \infty$ and $d_2 >> f$, then the stability range is given by [29]

$$\delta_{max} - \delta_{min} = 2S \approx f^2/d_2 \tag{4.5}$$

The beam waist radius at the focal point is then given by

$$\left(\frac{\pi w_0^2}{\lambda}\right)^2 \approx (\delta_{max} - \delta)\,(\delta - \delta_{min}) \tag{4.6}$$

provided $R_1 >> S$. Thus w_0 becomes zero at the limits of stability. In the middle of the stability range we have

$$\delta = (\delta_{max} + \delta_{min})/2$$

hence

$$\left(\frac{\pi w_0^2}{\lambda}\right) \approx S\,. \tag{4.7}$$

For a gaussian mode, with beam waist radius w_0, the confocal parameter (see figure 12) is defined by

$$b = 2\pi w_0^2/\lambda \tag{4.8}$$

hence from equations (4.5), (4.7) and (4.8)

$$b \approx 2S \approx f^2/d_2 \tag{4.9}$$

Thus for a resonator of figure 9 adjusted to the centre of its stability range, the confocal parameter is equal to the stability range.

It is well known that for a curved mirror used at an angle, astigmatism causes the xz and yz rays to be focused at different points and this is reflected in two effective focal lengths of the mirror f_x and f_y given by [30]

$$f_x = f/\cos\theta$$
$$f_y = f\cos\theta \qquad (4.10)$$

where f is the actual focal length and θ is the angle of incidence - see figure 9. In the region of focus, a Brewster angled plate also causes astigmatism which results in a different distance of propagation through the plate for sagittal and tangential rays. For a plate of thickness t and refractive index n, at Brewsters angle, the effective distances are given by

$$d_x = t\sqrt{n^2 + 1}/n^2$$
$$d_y = t\sqrt{n^2 + 1}/n^4 . \qquad (4.11)$$

By considering the x and y planes of figure 9 separately, we can write two equations for (4.4):

$$d_{1x} = R_1 + f_x + \delta_x = d_{air} + d_x$$
$$d_{1y} = R_1 + f_y + \delta_y = d_{air} + d_y \qquad (4.12)$$

The right hand side of the above equations represents the path length between M_1 and M_2 for the xz and yz planes, the air path being the same for both cases. Note however, that the cavity will in general be at the middle of its stability range for *different* values of d_{air} for each of the two perpendicular planes. Compensation then, is achieved when $\delta_x - \delta_y = 0$ and from (4.12)

$$(d_x - d_y) - (f_x - f_y) = 0$$

which leads to

$$f\sin\theta\,\mathrm{Tan}\theta = t\sqrt{n^2 + 1}\,(n^2 - 1)/n^4 \qquad (4.13)$$

Astigmatic compensation is achieved by trading the plate thickness with the angle θ and when this condition is satisfied, the x and y stability ranges overlap. However, perfect

compensation is not required since failure to satisfy equation (4.13) exactly, will reduce the stability range but not necessarily take it to zero [29]. Also, compensation is only achieved after one round trip of the cavity. That is the astigmatism introduced by passage of the beam once through both faces of the crystal, is compensated by a single reflection from M_2. The asymmetric arrangement of M_1 and M_2 means that compensation is not obtained completely within the crystal, and the waist is slightly elliptical [29,31]. Thus the cavity may be astigmatically compensated with respect to stability but not focusing in the crystal.

4.6.1. The Burleigh Colour Centre Laser.

The laser used in this work was based upon a commercially available system (marketed as the 'F-centre laser' - FCl) manufactured by Burleigh Instruments. Figure 10 is a view of the crystal chamber and figure 11 shows a schematic representation of the resonator. Above the focusing section of the cavity, a liquid nitrogen dewar is supported within a chamber housing unit. The space around the nitrogen dewar is evacuated to provide thermal isolation and a small cryopump within the dewar enables a good vacuum to be kept once the external vacuum pump is removed. The crystal is clamped (at Brewsters angle) in a gold coated cassette (with facility for holding up to 3 crystals) which is in thermal contact with the liquid nitrogen dewar above, via the vertical metal bar (figure 10) known as the cold finger. The cold finger and crystal cassette could be moved up and down via a mechanical control system, enabling the cold finger to make contact with the nitrogen dewar as well as allowing for movement of the crystal position. The silver coated end mirror, M_1, had a radius of curvature $\approx$ 0.7 cm and could be mechanically adjusted along the beam axis by a control on the dewar exterior. The focusing mirror, M_2, (also silver coated to reflect both pump and laser radiation) had a focal length of 3 cm and its position was fixed, at 3 cm from the crystal. This system used a colinear pumping technique and as can be seen from figure 11, pump radiation is allowed into the nitrogen dewar and directed colinearly with the colour centre beam by a dielectrically coated

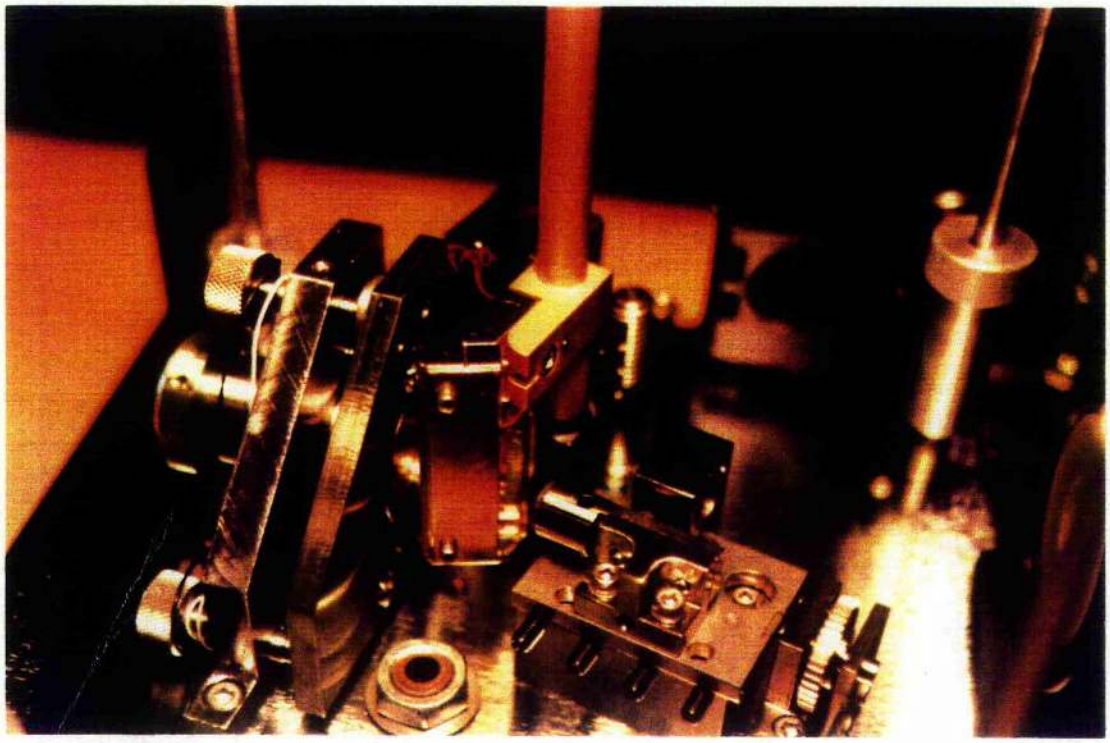

Figure 10.
Photograph of the crystal chamber; showing the crystal cassette, cold finger, end mirror and the focusing mirror. The liquid nitrogen dewar covers the chamber which is then evacuated, enabling the crystal to be cooled to LNT.

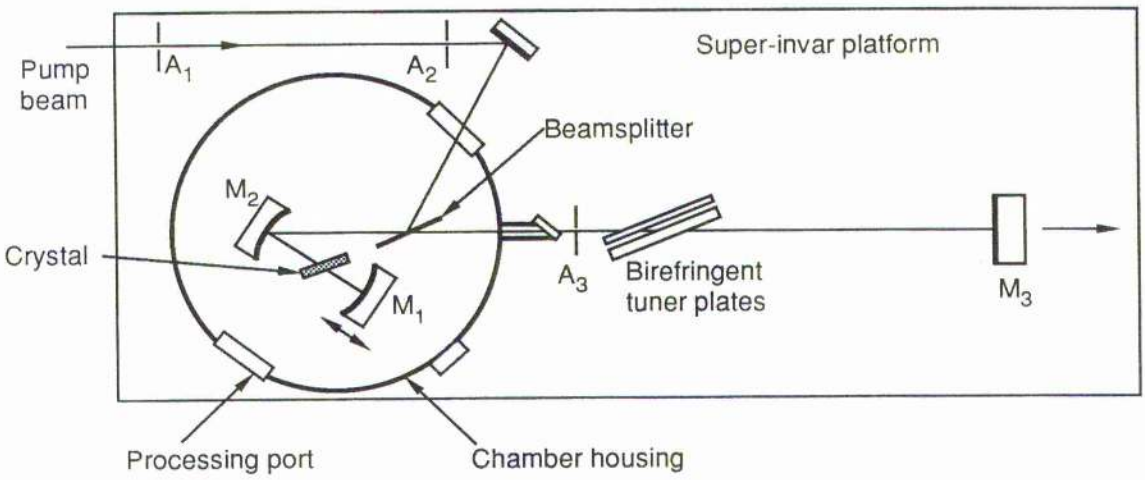

Figure 11.
A schematic diagram of the Burleigh resonator. M_3 is the output coupler.

beamsplitter. This was ≈ 95% reflecting at the pump wavelength of 1.06μm (for horizontally (p) polarised light) and highly transmissive (≈ 99%) at the laser wavelength of 1.5 μm. The folding mirror, M_2, then focused the pump beam into the crystal. A Brewster angled window in the dewar provided optical access to the rest of the cavity which, in the initial stages, simply comprised of an output mirror at the position M_3 - see figure 11. At this point all the optical components were mounted on the Burleigh platform.

Using equation (4.12) we can calculate the angle 2θ between the two arms of the cavity. The crystal of KCl:Tl was 2mm thick and had a refractive index of 1.48. Substituting these into (4.12) with f = 3cm, we obtain $2\theta = 20°$ which agrees with that of the Burleigh laser set by the manufacturers. In order to achieve optimum focusing in the crystal, and hence maximum gain, we should choose the confocal parameter of the focused mode to approximately equal the crystal thickness, b =t, at the centre of the stability range (as in figure 12). So

$$b \approx t \approx f^2/d_2$$

from equation (4.8).

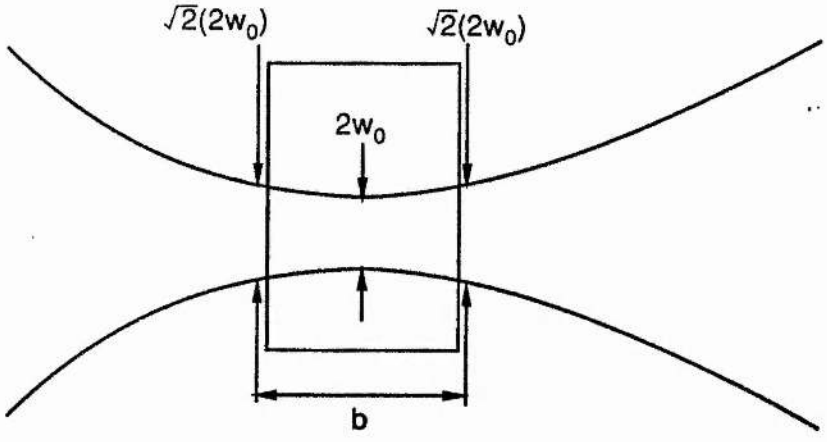

Figure 12.
Gaussian beam in the region of focus in a crystal. b confocal parameter; w_0 beam waist.

Thus the resonator has a stability range 2S ≈ 2mm and in the middle of its stability range we can calculate $d_2 \approx 45$ cm. A beam waist of ~ 40 μm diameter is calculated from equation (4.7). The beam waist at the output mirror can also be calculated from [29]

$$w_1 = (d_2 \lambda / \pi)^{1/2}$$

which gives a beam diameter of approximately 1mm. The physical cavity length is then $(R_1 + f + S) + d_2 \approx 48.8$ cm.

There are perhaps one or two practical details to note about the Burleigh laser. The crystal was a rectangle of approximate dimensions $10 \times 4 \times 2$ mm cut along a <100> axis. The laser transition is polarised along this axis, however, the crystal is mounted in the laser at 45° to the horizontal so that with horizontally polarised pump light, those centres aligned along both a <100> and <010> axes may be pumped. The colinear pumping scheme has two drawbacks in that (i) some pump radiation is present along with the laser output and (ii) a back reflection of pump radiation is present. The first of these disadvantages is not a serious problem since the intensity of the transmitted pump is only a small percentage of the laser radiation and the tracer beam does facilitate laser alignment. The back reflection is much more disadvantageous since it could cause a serious degradation of the mode-locked pump laser. This problem was over come in our case by positioning the Burleigh at such a distance from the Nd:YAG pump laser, that the reflected pulses had minimal effect on the mode-locking, in a similar way to that for optical fibre coupling - section 3.2.2. Another method would be to use an optical isolator situated between the pump and slave laser. A third window in the dewar is provided for any necessary processing of a crystal while at LNT, e.g auxiliary illumination. Finally it should be noted that prealignment of the laser, using a dummy crystal, with the nitrogen dewar in place but not evacuated or cooled, is recommended. This is necessary since once this is evacuated, there is no access to the focusing mirror and the end mirror M_1 may only be translated along the beam axis, severely restricting adjustment of the cavity.

Before the insertion of a laser crystal into the cavity, the alignment of the Burleigh laser was checked using a low power Nd:YAG beam. This was accomplished as follows. The pump beam was directed centrally through the two alignment apertures A_1 and A_2 mounted on the Burleigh platform (see figure 11). With a dummy crystal in position pump radiation was observed just behind the aperture A_3. Focusing this at a distance ~ 45 cm from M_2 by moving M_1, ensured that the cavity would be close to the centre of stability (an IR viewer

was used to see the 1.06 μm radiation). A KCl:Tl crystal was then loaded into the cassette under a low red light. A small amount of thermal grease was spread on the top of the cold finger to ensure good thermal contact between this and the liquid nitrogen dewar. The dewar housing was then placed onto the platform and evacuated to a pressure of approximately 10×10^{-3} torr (10 microns of mercury). Raising the cold finger brought it into contact with the dewar and liquid nitrogen could then be added to cool the system. A resistance thermometer attached to the cold finger enabled us to continually monitor the crystal temperature during cooling and throughout the lifetime of the crystal. The resistance thermometer had a logarithmic response and a resistance of approximately 30Ω at room temperature. With the crystal loaded and cooled, the resistance was typically 60-70KΩ, corresponding to a temperature of about -200°C (LNT). When pumped with ~ 2W pump power, the resistance normally dropped to around 45KΩ (-190°C) or lower as the vacuum in the chamber degraded. It was recommended that the resistance not fall below 20KΩ at any time.

In order to achieve laser action, a similar procedure is followed as for prealignment. In addition, the pump beam was chopped and an average power of about 5 W used. By observing the rear side of the chopper, the fed back spot could be seen and this was made coincident with the pump beam by adjusting one of the beam steering mirrors. The final step was to position the output coupler (at the M_3 position, approximately 45 cm from M_2) and feed the weak pump reflection back through the aperture A_3. A germanium diode (responding to wavelengths out to ≈1.61μm) was used to detect the 1.5μm fluorescence and the onset of laser action. Once lasing was established, the output could be peaked up and the power was monitored by a calorimeter type power meter. With a good crystal in place (crystals with an optical density ~ $1.5mm^{-1}$ at the pump wavelength are best - ours was obtained from Burleigh Instruments) an output power of ≈ 250 mW was obtained for 2 W pump under true continuous pumping conditions i.e. no chopping. At this stage the output was CW even though the pump beam consisted of mode-locked pulses, since the cavity length was incorrect for synchronous pumping. It is worth noting that contrary to say dye lasers, the KCl:Tl will lase at any reasonable cavity length when the pump is mode-

locked because of the long (1.6 μs) upper state lifetime which acts as a 'gain storage medium'. With their short (~ 1 ns) lifetimes, dye lasers, when pumped with a mode-locked pump will only lase when the cavity length is within a centimeter or so of some multiple of the pump laser cavity length.

4.7 The Mode-Locked KCl:Tl Colour Centre Laser.

Synchronous mode-locking of the KCl:Tl was obtained by increasing the resonator length to match that of the pump laser, which was ≈ 1.82 m, corresponding to a round trip time ≈ 12 ns. Extending the cavity required the use of a long focal length mirror to image the beam waist at the output coupler to a point approximately 45 cm from M_2. The ideal mirror would be one with a focal length equal to half of the required cavity extension. This would then leave the gaussian beam wavefront radii and beam waists unaltered. In particular, the beam waist in the crystal would remain the same and so the laser threshold and stability range would not be affected. In our case this would mean a mirror of radius 182 - 48.8 = 133.2 cm, i.e a focal length of about 66 cm. Unfortunately this is a non-standard focal length and the mirror available to us had a focal length of 50 cm (radius 1 m). To determine the correct position of this mirror in the extended cavity, a gaussian beam ray tracing program was used. This determined the ABCD matrix of a given resonator and computed the positions and spot sizes of beam waists within the cavity [32]. It was found that with the mirror positioned 110 cm from M_2 and approximately 68 cm from the output coupler, the beam waist W_1 remained at 45 cm from M_2 and was approximately the same size. Hence the folded cavity of figure 13 was constructed. A plane mirror, M_3, directed the beam onto the 1m curved mirror (M_4) and the cavity was terminated in the output coupler M_0. This was mounted on a precision translation stage for fine adjustment of the cavity length. All the mirrors external to the dewar were dielectric coated for ~100% reflectance over 1.4 - 1.6 μm, except M_0, which had a transmission of ≈ 20%. This mirror was also wedged in order to prevent any reflection from the uncoated side interfering with the mode-locked operation. In this extended configuration, and with a tuning element inserted, the

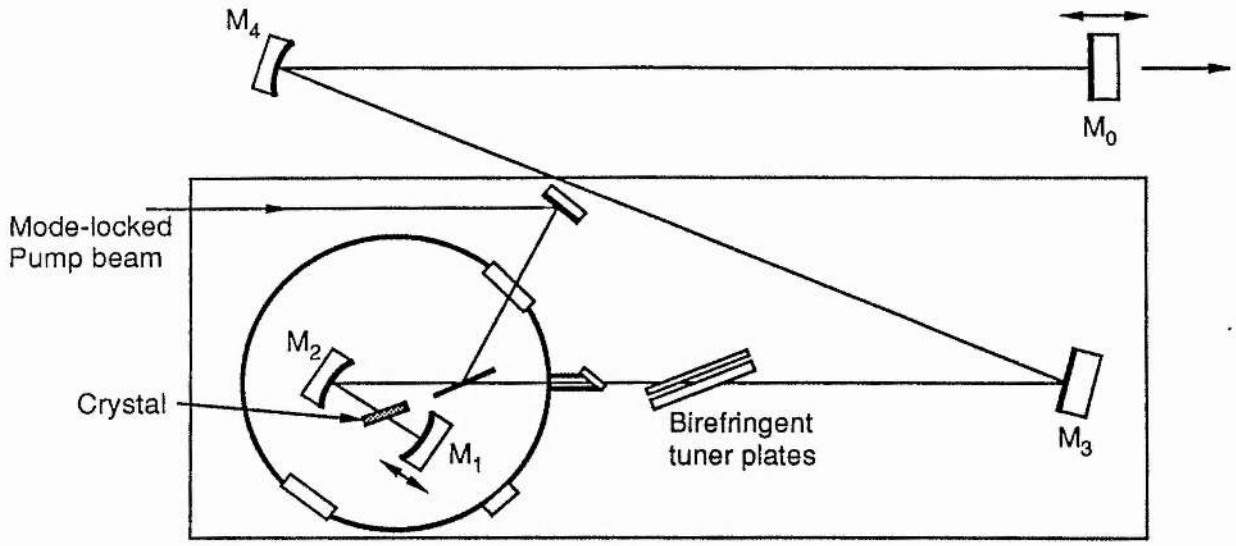

Figure 13.
The extended cavity for synchronous mode-locking. Cavity length ≈ 181cm, mirror radii: $M_3 = \infty$, $M_4 = 1m$, $M_0 = \infty$.

laser gave an output of ≈ 220 mW for a pump power of 2 W (the maximum recommended for unchopped operation).

Tuning of the laser was accomplished using a two plate birefringent filter (BRF) [33,34]. This element was also necessary in order to limit the laser bandwidth and ensure that the mode-locked pulses from the KCl:Tl laser were close to being bandwidth limited. A BRF was used for tuning since it is possible to tune the laser over its entire range without greatly changing the cavity length. The plates used here were of quartz and had thicknesses of approximately 2 mm and 0.3 mm. Each plate had its optic axis in the plane of the disc and were aligned parallel to each other. The plates were fixed together with a small air gap between them and mounted at Brewsters angle to the laser beam. Tuning was accomplished by rotation of the plates about the axis normal to the surface. A full description of the operation of a birefringent tuner can be found in references [33,34]. We note here, however, that the greatest wavelength selectivity of a BRF occurs when the optic axis is at 45° to the laser polarisation. Also the bandwidth of the laser is determined by the number of plates and their thickness, as well as the number of extra Brewster surfaces within the

cavity. Thinner plates enable a larger number of cavity modes to reach laser threshold and so are able to support shorter pulses.

A mode-locked tuning curve is shown in figure 14, for a pump power of 2W and it is seen that the laser operates over ~ 100nm. Note that tuning beyond the half power points could not be achieved since the laser then 'jumps' to the opposite side of the tuning curve.

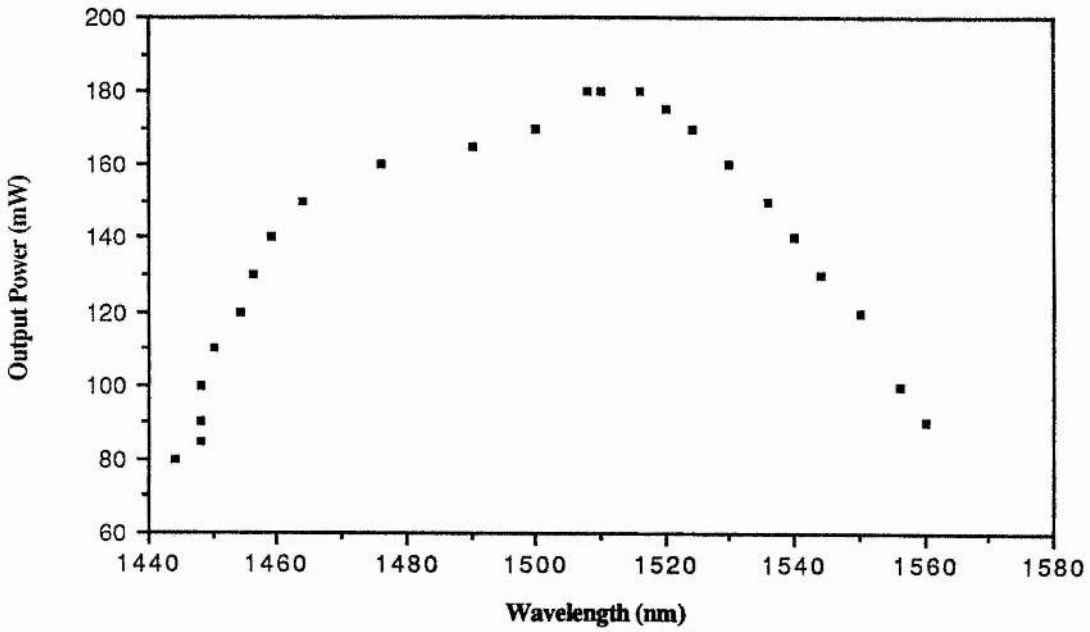

Figure 14.
A tuning curve for the mode-locked KCl:Tl colour centre laser.

The output power of the KCl:Tl laser as a function of input power is shown in figure 15. With a 20% output coupler the slope efficiency was ≈ 13% and the laser threshold was ≈ 135 mW. Higher outputs would be obtained with a 30% output mirror [35], but this would reduce the tuning range and also result in poorer mode-locking (the reasons for this will be discussed later). The long (1.6 μs) excited state lifetime and relatively low gain cross section (~10^{-17}) of KCl:Tl, give this laser an unusual mode-locked behaviour. Since the round trip time (τ_{rt}) of the pump laser is ≈ 12 ns, we have $\tau_r >> \tau_{rt}$ where τ_r is the excited state lifetime. Hence a different mode-locking regime is obtained compared with that of other synchronously

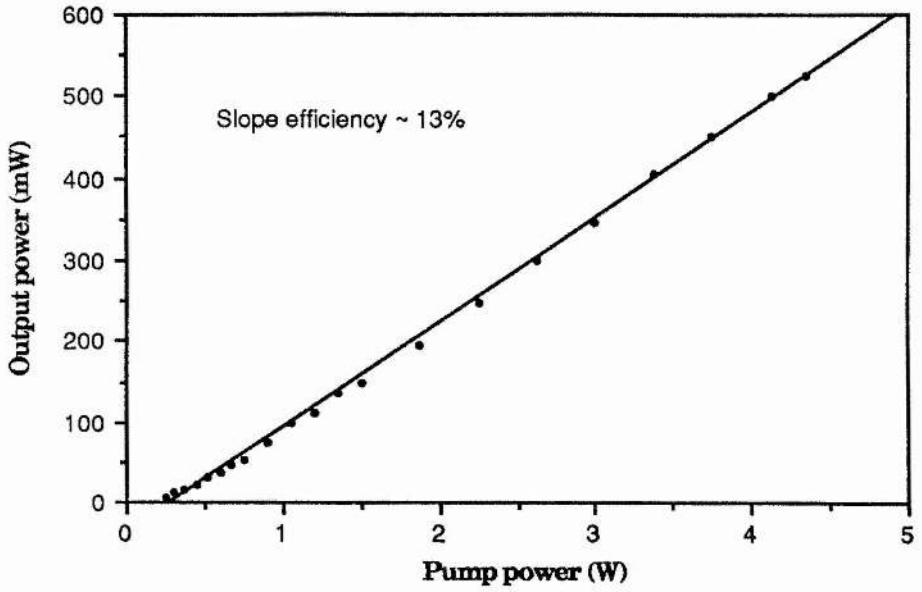

Figure 15.
Output power as a function of pump power. For input powers above 2W the pump laser was chopped to reduce heating of the crystal.

mode-locked systems (such as dye lasers) were $\tau_r << \tau_n$. Figure 16 is a plot of the mode-locked pulse width as a function of the (average) pump power, where the pump consisted of ~ 100ps pulses at 82 MHz repetition rate. The obvious point to note is the rapid decrease in duration of the laser pulses as the pump power is increased. When the pump power was below 1W, the output from the KCl:Tl laser (monitored on a second harmonic generation autocorrelator - chapter 1) consisted of poorly mode-locked pulses on top of a broad pedestal. Indeed, the laser could barely be said to be mode-locked at all in this region (see figure 17a). The transition between this regime and that for which good pulses were obtained was quite rapid, occurring over a change in pump power of only 400 mW. Figure 17b, shows an intensity autocorrelation of the pulses for a pump power of ≈ 3 W. (These and all the following results were obtained using a BRF consisting of a single plate, 2mm in thickness. With the combination of a 2 mm and 0.3 mm plate, the shortest pulses had durations of 20 ps and had a time-bandwidth product of ≈ 0.445, which is close to that for a bandwidth limited gaussian pulse).

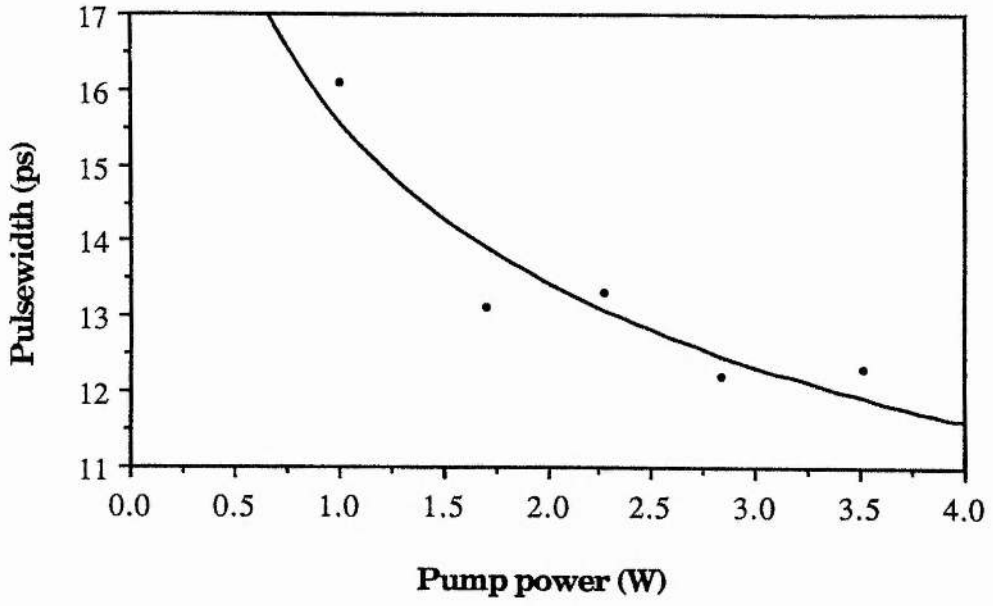

Figure 16.
Duration of the synchronously mode-locked colour centre pulses as a function of pump power. The laser was improperly mode-locked for powers less than 1W. Pump pulses were of ≈ 100ps duration.

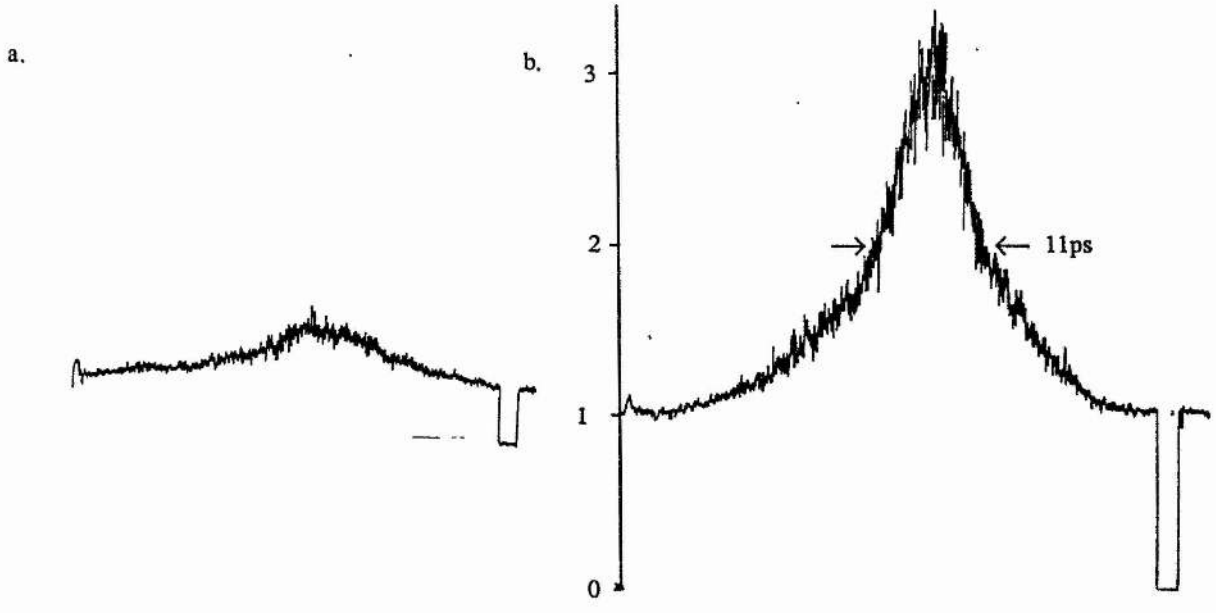

Figure 17.
Autocorrelation traces of the mode-locked pulses for pump powers of (a) 800 mW (b) 3 W.

This behaviour has been studied theoretically [36,37] and may be described in the following way. The mode-locked pulses formed by synchronous pumping arise due to the rapidly varying gain, whereby the laser pulse incident upon the amplifying medium causes the gain to rapidly fall below that required for laser oscillation. The change in gain, ΔG, induced by a pump pulse is given by $\Delta G = \exp(N\sigma/A)$, where N is the number of absorbed pump photons and A the beam area. For low pump powers (small N) the change in gain will be small compared to that required to overcome cavity losses. However, because of the long lifetime, an appreciable decrease in the gain over one round trip of the cavity does not occur and the level of gain after one pump pulse will be approximately equal to that just before the next. This equilibrium gain we call G_{eq} . Successive pump pulses cause G_{eq} to rise until the peak gain crosses the threshold value and a weak laser pulse then circulates in the cavity. Consequently, the stimulated emission is low and a small and slow gain saturation occurs resulting in the laser output being only poorly mode-locked. This situation is depicted in figure 18a. As the pump power is raised (figure 18b), the peak gain is increased and the intracavity pulse grows in intensity. G_{eq} between pulses, is pushed lower for higher intracavity powers due to stronger stimulated emission and so better gain saturation, which attenuates the trailing edge, is obtained leading to a reduction of the pulse duration. Thus for a gain medium whose excited state lifetime is long compared to the cavity round trip time, good mode-locking will only occur when the pump power is many times greater than the laser threshold value. For the case of $\tau_r << \tau_n$, well formed pulses are produced even for powers just greater than threshold. In a similar way, higher losses within the cavity (e.g. due to a higher output coupler) would lower the intracavity pulse energy and so reduce the gain saturation, resulting in broader pulses for a given pump power. It is also expected [37] that higher pump powers cause the laser pulse to be formed earlier with respect to the pump pulse due to amplification of the leading edge. Secondary pumping from the long pump pulse, may then cause the laser pulse to develop a long tail which could form into a distinct satellite pulse for even higher pump powers. In reference

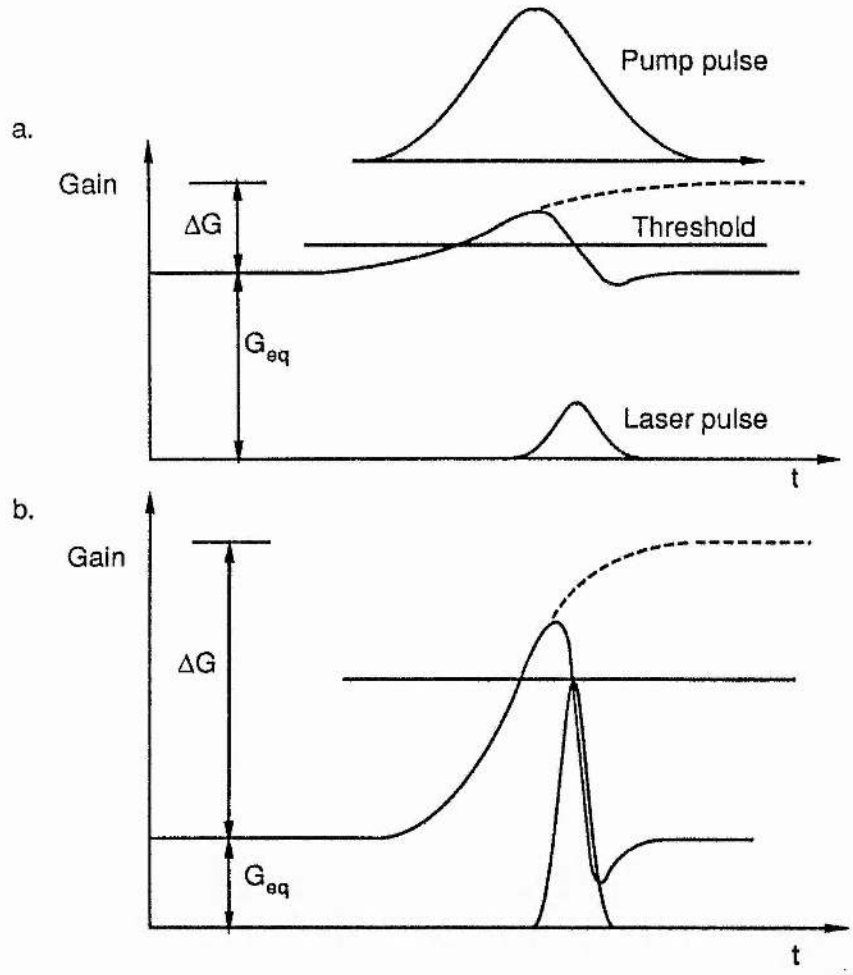

Figure 18.
Steady state gain and intracavity pulse for a gain medium with $\tau_r >> \tau_{rt}$. (a) Pump power just above threshold and (b) far above threshold.

[37] it seems that a satellite pulse would be expected to form only for pump powers about 300 times higher than the threshold value. In our experiments no satellites were observed, where the highest pump power corresponded to only ~ 30 times above threshold.

This regime ($\tau_r >> \tau_{rt}$) of mode-locking is more efficient than that for which $\tau_r << \tau_{rt}$, since the amount of energy lost as spontaneous fluorescence is negligible. Another discrepancy between the KCl:Tl and other synchronously mode-locked lasers, is seen by considering a mismatch parameter, Δ, defined as the delay of the laser pulse relative to the pump pulse after each round trip (caused by a cavity length mismatch). Dye lasers (for which $\tau_r << \tau_{rt}$) have an initial gain G_0 which is sensitively dependent on Δ, the shortest pulses being obtained for Δ slightly smaller than that for which maximum second harmonic

signal (maximum gain) is obtained [38,39]. Also the pulse shapes are critically dependent on Δ and laser action ceases if Δ is made too small or too large [39]. In contrast to this, with the Tl laser, G_0 is relatively insensitive to Δ. The result is that the shortest pulses can be obtained without loss of energy and that the output power increases with pump-pulse energy.

In our experiments, proper mode-locking occurred for a pump power $\approx$ 7 times greater than threshold with the shortest pulses occurring for a cavity length that also produced the maximum second harmonic signal. Detuning the cavity length, simply caused the pulses to broaden until mode-locked operation was lost. Although output mirrors of higher transmission were not available to us, these would be expected to decrease the mode-locking quality and raise the pump power required to obtain well mode-locked pulses, as previously reported [35]. The ultimate duration of the laser pulses is limited by the broadening effect of various dispersion elements within the cavity. Theoretically if all the bandwidth of the KCl:Tl laser could be utilised, pulse durations ~ 30 fs could be supported. By employing active (acousto-optic) mode-locking, pulses of 6ps in duration have been obtained from the KCl:Tl [40] with only modest pump powers.

4.8 The NaCl:OH^- Colour Centre Laser.

Although the KCl:Tl and NaCl:OH laser active centres tune over approximately the same wavelength region, the latter is reported to have the advantages of a slightly wider tuning range (1.4 - 1.7 μm) and higher output powers [24]. It should also be possible to pump the crystal much harder without having to resort to the use of an optical chopper. For these reasons it was decided to try a suitable crystal of NaCl. Using the laser resonator already described, a sodium chloride crystal containing the F_2^+:O^{2-} centres was inserted into the crystal cassette in place of the KCl:Tl. The crystal thickness was 3 mm and so a slight (horizontal) adjustment had to be made of the focusing mirror (M_2) such that a tracer beam was seen emerging through the aperture A_3 (figure 13). (A small change in the position of M_1 was also required to focus the beam but otherwise the cavity was unchanged). With a CW Nd:YAG pump, a series of experiments were performed in order to establish the best

operating conditions. Various combinations of pump polarisation (circular or horizontal) and auxiliary illumination were tried, the results being summarised in table 3.

Table 3.

Pump polarisation	Auxiliary illumination	Result
Horizontal	None	Initially high output but faded until laser action ceased.
Circular	None	Nonfading output ≈ 60mW for 5W pump.
Horizontal	UV from mercury lamp	Constant but low output ≈10mW.
Circular	UV from mercury lamp	Nonfading output ≈ 80mW.

Output of the NaCl:OH laser for different combinations of pump polarisation and auxiliary illumination. For explanation see text.

The results described above may be explained in terms of the reorientation of the $F_2^+:O^{2-}$ laser active centres which was mentioned in section 4.4. The crystal was mounted in the cassette such that a <110> axis was lying in a horizontal plane. The dipole moment corresponding to the absorption at 1.09 μm is polarised along this direction. Although it is not completely understood, pumping of this transition with an intense beam can cause the centres to reorientate, eventually leading to all of the centres being in a state orthogonal to the laser polarisation. This causes the laser output to fade, until laser action ceases within a matter of minutes, as in the first case shown in table 3. (A two photon excitation of the centres in the 2pσ state to the 3dπ, may occur, which could then cause reorientation on decaying back to the 2pσ level, see figure 5). With a circularly polarised pump beam, there is obviously a horizontal and vertical component, each tending to align the centres in the opposite direction. This enables a dynamic equilibrium to be set up and a constant output is obtained. It is thought [23] that reorientation occurs during the radiationless transition 2pπ → 2pσ. So if the misaligned centres are pumped to the 2pπ level (or higher, in which case a nonradiative decay to the 2pπ occurs) we can bring the centres back into a useful orientation. There are in fact three ways to do this. The first is a single step excitation using

UV light at ≈ 436 nm or 365 nm (obtained from a filtered mercury arc lamp) which induces the transitions $1s\sigma \rightarrow 2p\pi$ (460nm) or $1s\sigma \rightarrow 3p\pi$ (318nm). In our experiments illumination was provided by an (unpolarised) Hg lamp, weakly focused onto the crystal through the crystal processing window. Combined with a horizontal pump beam, it did prevent the laser fading altogether but the lamp intensity was insufficient to provide a high power output. Slightly better results were obtained with a circularly polarized pump beam.

The second is a two step orientation achieved by pumping the centres to the $2p\sigma$ level with (polarised) 1.06 μm and then a further excitation using either similarly polarised 650nm (causing the transition $2p\sigma \rightarrow 3d\sigma$) or orthogonaly polarised 518nm ($2p\sigma \rightarrow 3d\pi$) [23]. These transitions are broad enough to allow excitation with a He-Ne laser (633nm) or an Argon ion laser (514nm) [23a] respectively. Another method is to use frequency doubled YAG (532nm) for the $2p\sigma \rightarrow 3d\pi$ transition, avoiding the use of a second laser [41]. It is necessary to point out that the polarisation of the auxiliary light is crucial to the successful operation of the laser. If the polarisations are incorrect, laser oscillation can actually be inhibited. Along with a circularly polarised pump beam and UV illumination, the polarised beam of a 10mW He-Ne laser was directed into the laser cavity through the output coupler. (This was achieved by using a coated silicon filter which had a 90% transmission at 1.5 μm but reflected visible light). When the polarisation of the He-Ne was vertical, a slight enhancement in the NaCl laser output was observed. However, if the polarisation was orientated in the horizontal plane, laser action was totally quenched. The vertical component of the pump beam and the vertical He-Ne beam cause reorientation of the misaligned centres, enabling them to contribute to the laser field again. Horizontally polarised 633 nm light, acts in conjunction with the horizontal component of the pump beam to actually misalign those centres which are correctly orientated, thus destroying the laser gain. A similar picture holds for pumping colinearly with 1.06 μm and doubled 532nm radiation. This time the dipole moments are such that vertical Nd:YAG radiation and *horizontally* polarised frequency doubled light enable a reorientation of the misaligned centres. Thus for this scheme to work, the crystal should be excited with a circularly polarised pump beam and a horizontally polarised frequency doubled (532 nm) beam [41].

Unfortunately, none of the above reorientation schemes proved singularly successful in providing a high, unfading output from our crystal of NaCl. This was probably due to a low optical density of the crystal at 1.06 μm and the fact that our mercury lamp was unfiltered and of insufficient intensity. Due to these reasons, further investigations of this centre were postponed until a crystal of higher quality could be obtained.

4.9 Conclusions.

This chapter has provided a description of the KCl:Tl and NaCl:OH colour centre lasers. Colour centre lasers in general have been widely used, enabling access to the wavelength region of 0.8 - 4 μm. Such lasers configured in both linear [42,43] and ring [43,44] cavities have enabled the production of subpicosecond pulses via passive and synchronous mode-locking techniques. The high output power provided by the KCl:Tl and its tremendous stability, have, until most recently, given this laser a unique status in the production of ultrashort pulses around the 1.5 μm region. Even greater powers should be available from the NaCl:OH laser and it is hoped that production of good quality laser crystals at St.Andrews will enable further studies of this laser.

The following chapters describe nonlinear pulse propagation experiments in optical fibres utilising the KCl:Tl laser and a scheme whereby subpicosecond pulses may be produced from the laser, realising the full potential of this broad bandwidth gain medium.

References.

1. L F Mollenauer; "Colour Centre Lasers" Laser Handbook vol.4 (1985)
2. "Dye Lasers" Topics in Applied Physics, vol.1, ed. F P Schafer, Springer Verlag (1973)

2a. H J Polland, T Elsaisser, A Selmeier, W Kaiser, M Kussler, M J Marx, B Sens, K H Drexhage; Appl. Phys. B, **32**, 53 (1983)

3. B Fritz, E Menke; Solid State Comm.; **3**, 61 (1965)
4. L F Mollenauer, D H Olsen; Appl. Phys. Lett. **24**, 386 (1974)
5. L F Mollenauer, D H Olsen; J. Appl. Phys. **46**, 3109 (1975)
6. L F Mollenauer, R H Stolen, J P Gordon; Phys. Rev. Lett. **45**, 1095 (1980)
7. G F Imbush, R Kopelmann; in "Laser Spectroscopy of Solids" Topics in Appl. Phys. **49** Ed. W M Yen, P M Selzer (1986)
8. W B Fowler in "Physics of Colour Centres" ed. W B Fowler, Academic press (1968)
9. C R Pollock; J. Luminescence **35**, 65 (1986)
10. J M Wiesenfold, L F Mollenauer, E P Ippen; Phys. Rev. Lett. **47**, 1668 (1981)
11. L F Mollenauer in "Tunable Lasers" Topics in Appl. Phys. **59**, ed.L F Mollenauer, J C White; Springer Verlag (1987)
12. W Gellermann, K P Koch, F Luty; Laser Focus p.71 April 1982
13. M A Aegerter, F Luty; Phys. Stat. Sol. B **43**, 227f and 245f (1971)
14. L F Mollenauer; Opt. Lett. **1**, 164 (1977)
15. L F Mollenauer, D L Bloom, A M DeGaudio; Opt. Lett. **3**, 49 (1978)
16. L F Mollenauer, D L Bloom; Opt. Lett. **4**, 247 (1979)
17. G Trénec, P J Nacher, M Leduc; Opt.Comm. **43**, 37 (1982)
18. I Schneider, M J Marrone; Opt. Lett. **4**, 390 (1979)
19. D R foster, I Schneider; Opt. Lett. **13**, 207 (1988)
20. I Schneider, S C Moss; Opt. Lett. **8**, 7 (1983)
21. W Gellermann, F Luty, K P Koch, H Welling; Opt. comm. **35**, 430 (1980)

22. J F Pinto, L W Stratton, C R Pollock; Opt. Lett. **10**, 384 (1985)

23. E Georgiou, J F Pinto, C R Pollock; Phys. Rev. B **35**, 7636 (1987)

23a R Beigang, K Klameth, B Becker, Z Yoon, H Welling; Opt. Comm. **65**, 383 (1988)

24. J F Pinto, E Georgiou, C R Pollock; Opt. Lett. **11**, 519 (1986)

25. P G Baranov, V A Khramtsov; Phys. Stat. Sol. B **101**, 153 (1980)

26. W Gellermann, F Luty, C R Pollock; Opt. Comm. **39**, 391 (1981)

27. L F Mollenauer, N D Vieira, L Szeto; Phys. Rev. B **27**, 5332 (1983)

28. D C Hanna; IEEE J. Quant. Electronics **QE-5**, 483 (1969)

29. H W Kogelnik, E P Ippen, A Dienes, C V Shank; IEEE J. Quant. Electron. **QE-8**, 373 (1972)

30. F A Jenkins, H E White; "Fundamentals of Optics" p.95 McGraw-Hill (1957)

31. M H Dunn, A I Ferguson; Opt. Comm. **20**, 214 (1977)

32. A Finch; MSc Thesis St. Andrews University (1985)

33. A L Bloom; J. Opt. Soc. Am. **64**, 447 (1974)

34. D R Preuss, J L Gole; Appl. Optics **19**, 702 (1980)

35. L F Mollenauer, N D Vieira, L Szeto; Opt. Lett. **7**, 414 (1982)

36. Z A Yasa; Opt. Lett. **8**, 277 (1983)

37. S Kelly, G H C New, D Wood; Appl. Phys. B **47**, 349 (1988)

38. K Smith; PhD Thesis Imperial College of Science and Technology (1985)

39. C P Ausschnitt, R K Jain, J P Heritage; IEEE J. Quant. Electron. **QE-15**, 912 (1979)

40. J F Pinto, C P Yakymyshyn, C R Pollock; Opt. Lett. **13**, 383 (1988)

41. K R German, C R Pollock; Opt. Lett. **12**, 474 (1987)

42. N Langford, K Smith, W Sibbett; Opt. Lett. **12**, 817 (1987)

43. N Langford; PhD Thesis Imperial College of Science and Technology (1988)

44. N Langford, K Smith, W Sibbett; Opt. Lett. **12**, 903 (1987)

Chapter 5.

Optical Solitons and the Soliton Laser.

5.1 Introduction.

In chapter 3, a simple theory of self-phase modulation (SPM) was developed for a broad pulse propagating in a length of fibre, where the effect of dispersion was negligible. We now come to examine the case for which both SPM and GVD play a role in the nonlinear propagation of pulses in optical fibres. It will be seen that the compensation of SPM by negative, or anomalous, group velocity dispersion, enables the formation of optical solitons - pulses that propagate without a change in shape or else change shape in a *periodic* manner. The existence of such pulses in optical fibres was first proposed by Hasegawa and Tappert [1] and subsequently many theoretical and experimental studies have been undertaken.

It is well known that the variation of refractive index with wavelength in fused silica, causes the material dispersion ($dn/d\lambda$) to pass through a minimum at approximately 1.3 μm [2]. Thus the group velocity dispersion (represented by $d^2n/d\lambda^2$, $dv_g/d\lambda$) will pass from positive, through zero at ≈ 1.3 μm, to negative for longer wavelengths. It also happens that the minimum loss in silica-based optical fibres occurs at ≈ 1.55 μm. Any long distance fibre-optic communications system would preferably operate in the wavelength region of minimum attenuation, since this would enable the largest spacing between repeaters along the transmission line, which are necessary for signal amplification. Such a system would therefore involve the propagation of optical pulses in the negative, or anomalous, group velocity dispersion (GVD) regime (see figure 1). In the consideration of dispersion, one would naturally choose to operate at the point where GVD becomes zero, thus minimising simple pulse broadening in the time domain. However, in this case higher order dispersive terms ($d^3\omega/dk^3$ etc.) become important, again causing broadening and also pulse break-up

[3,4]. Although the exact wavelength of zero (group velocity) dispersion may be altered by suitable dopants, it is practically impossible to exactly match the wavelength of suitable sources to that of the zero dispersion in fibres. Given these factors, it is possible that future optical communications systems will operate around the 1.5 μm wavelength region. Much theoretical and experimental work has been done therefore, on the propagation of pulses in optical fibres under the influence of anomalous GVD and, because only modest powers are necessary for its observation, the nonlinear process of self-phase modulation.

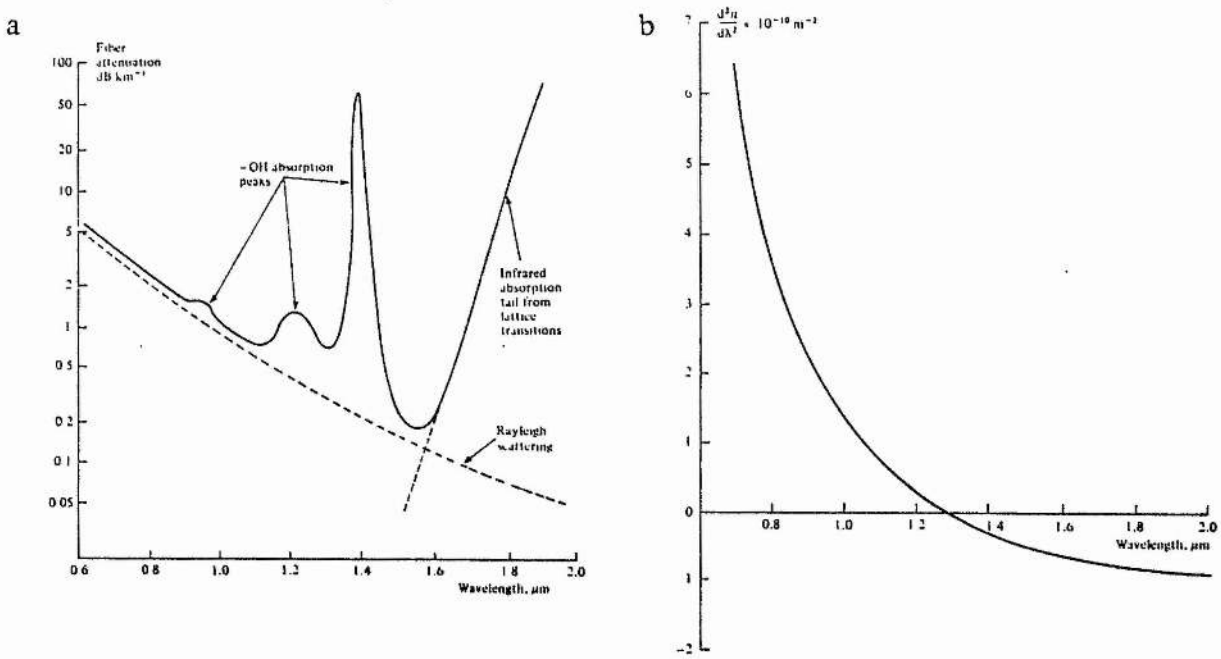

Figure 1.
(a) Attenuation and (b) group velocity dispersion ($d^2n/d\lambda^2$) as a function of wavelength for a typical SiO_2 optical fibre.

It may be helpful in the first instance, to form an intuitive picture of the processes involved. A low intensity pulse, where no SPM takes place, will always temporally broaden regardless of the sign of dispersion. In the case of significant SPM and positive GVD, accentuated pulse broadening occurs with the leading and trailing edges of the pulse experiencing a red and blue shift respectively due to SPM, as described in chapter 3. Note

that the extreme (low intensity) tails of the pulse do not experience any frequency shift. Consequently the red-shifted light in the leading part of the pulse, travels faster than and eventually overtakes, the unshifted light in the front tail. The reverse is true for the trailing edge of the pulse. This leads to the development of a square shaped pulse and then to a shock-wave process, which has been described as 'optical wave-breaking' [5,6]. Now consider a similar case but where the GVD is negative, $dv_g/d\lambda<0$, that is the group velocity increases for decreasing λ. SPM will act in the usual way causing the pulse to have, initially, a positive frequency chirp i.e. red and blue shifted leading and trailing edges. Now however, it can be seen that the pulse will collapse in upon itself, progressively narrowing as it propagates along the fibre. The two frequency chirping effects of GVD and SPM are now opposing each other and in general a pulse in the negative GVD region will alternately broaden and narrow in some complicated fashion as it propagates down the fibre. It is possible to imagine a case whereby the opposing frequency chirps produced by SPM and GVD balance each other, producing a pulse that neither broadens or narrows but retains its shape indefinitely (assuming the absence of attenuation). Such a pulse is known as a soliton or solitary wave. (The formal definition of a soliton involves the way in which two such pulses collide - they actually pass right through each other, even though there is no simple superposition principle for solitons. Any pulse in a medium where there is no dispersion or nonlinearity could be called a soliton according to the above).

Solitons occur in many areas of physics - fluid mechanics, waves in plasma physics, solid state physics and a classic example being water waves. The first reported observation of a soliton was in fact, a large solitary water wave in a canal by John Scott Russell in 1834 [7]. Solitary waves may be expressed as solutions to a wave equation containing both dispersive and nonlinear terms. Many types of such an equation exist, the nonlinear propagation of gravity waves in shallow water being described by the Korteweg-de Vires equation. The one applicable to nonlinear optics is known as the nonlinear Schrödinger equation (the NLS). A brief review of solitons can be found in reference [7] and a more mathematical approach is given in references [8,9]. We will now go on to give a brief

derivation of the NLS and to look at some solutions and the physical phenomena of optical solitons.

5.2 A Derivation of the NLS for Nonlinear Pulse Propagation.

In presenting a derivation of the NLS to describe the propagation of optical pulses along a fibre, we shall limit ourselves to the case of a one dimensional wave propagating along the z axis. In order to make the problem tractable, several standard simplifying assumptions are made: (i) we treat the optical pulse as having a slowly varying envelope compared to the carrier frequency, (ii) the nonlinearity is assumed to be small $n_{2E}\,|E|^2 << 1$ and to have an instantaneous response time, (iii) we neglect dispersive effects associated with the nonlinearity and (iv) the medium is assumed to be lossless.

The formal method of derivation involves starting from Maxwell's equations for electromagnetic waves in a dielectric medium. These give the wave equation

$$\frac{\partial^2 E}{\partial z^2} - \mu_0 \frac{\partial^2 D}{\partial t^2} = 0 \qquad (5.1)$$

for the one dimensional case assuming the medium is nonmagnetic i.e. $\mu_r = 1$. Using the relations given in chapter 3 (section 3.2.1) the nonlinear term may be expressly given and the following equation results:

$$\frac{\partial^2 E}{\partial z^2} - \frac{1}{c^2}\frac{\partial^2 D_L}{\partial t^2} = \frac{2 n_0 n_{2E}}{c^2}\frac{\partial^2}{\partial t^2}|E|^2 E \qquad (5.2)$$

where D_L is the linear electric displacement. This is the nonlinear wave equation and material dispersion is taken into account by remembering that $D_L = D_L(\omega)$. The derivation of the NLS from here is somewhat involved and we may obtain the same result directly from the dispersion relation for electromagnetic waves in a dispersive and nonlinear medium. The refractive index is assumed to have the form

$$n = n(\omega) + n_{2E}\,|E|^2 \ .$$

This is expanded as a Taylor series about $\omega = \omega_0$ to give

$$n = n_0 + \frac{dn}{d\omega}(\omega-\omega_0) + 1/2\,\frac{d^2 n}{d\omega^2}(\omega-\omega_0)^2 + n_{2E}\,|E|^2$$

where higher order dispersion terms have been neglected. Since the propagation constant in the fibre is given by $\beta(\omega) = n\omega/c$, we have

$$\beta(\omega) = \beta_0 + \beta`(\omega-\omega_0) + 1/2\ \beta``(\omega-\omega_0)^2 + \beta_{2E}\,|E|^2 \qquad (5.3)$$

where $\beta` = d\beta/d\omega$ and $\beta`` = d^2\beta/d\omega^2$ and are evaluated at $\omega=\omega_0$. Also $\beta_0 = \beta(\omega_0)$ and $\beta_{2E} = \beta_0 n_{2E}/n_0$. The electric field is assumed to be of the form

$$E(z,t) = \phi(z,t)\ \exp\ \{i(\omega_0 t - \beta_0 z)\}$$

with $\phi(z,t)$ being the slowly varying amplitude. To find the field at the plane z+dz, we take the Fourier transform of E, giving $E(z,\omega)$, propagate each frequency component forward by dz using the dispersive and nonlinear propagation constant and then transform back to the time domain. Hence

$$E(z,\omega) = 1/2\pi \int_{-\infty}^{\infty} \phi(z,t')\ \exp\ \{i(\omega_0 t'-\beta_0 z)\}\ \exp\{-i\omega t'\}\ dt' \qquad (5.4)$$

where t' has been used as a dummy variable. After propagating by dz, each frequency component will acquire a phase shift $-\beta dz$. so

$$E(z+dz,\omega) = 1/2\pi \int_{-\infty}^{\infty} \phi(z,t')\ \exp\{-i(\omega-\omega_0)t'\}\ \exp\{-i\beta_0 z\}\ \exp\{-i\beta dz\}\ dt'$$

Then transforming back to the time domain

$$E(z+dz,t) = 1/2\pi \int_{-\infty}^{\infty}\int \phi(z,t')\ \exp\{-i\Delta\omega t'\}\ \exp\{-i\beta_0 z\}\ \exp\{-i\beta dz\}\ \exp\{i\omega t\}\ dt'd\omega$$

where $\Delta\omega = \omega - \omega_0$. Substituting for E(z,t)

$$E(z+dz,t) = \phi(z+dz,t)\ \exp\{i[\omega_0 t-\beta_0(z+dz)]\}$$

$$\therefore \qquad \phi(z+dz,t) = 1/2\pi \int_{-\infty}^{\infty}\int \phi(z,t')\ \exp\{i\Delta\omega(t-t')\}\ \exp\{-i\Delta\beta dz\}\ dt'd\omega \qquad (5.5)$$

where $\Delta\beta = \beta - \beta_0$. We now find $\partial\phi/\partial z$ by using the definition:

$$\frac{\partial\phi}{\partial z} = \lim\ dz\to 0\ \frac{\phi(z+dz,t) - \phi(z,t)}{dz}$$

and expanding to second order the term $\exp\{-i\Delta\beta dz\}$ $(= 1 - i\Delta\beta dz - 1/2\Delta\beta^2 dz^2 + ...)$. Also $\partial\phi/\partial t$ and $\partial^2\phi/\partial t^2$ are found by letting $dz \rightarrow 0$ and differentiating (5.5) with respect to t. Having done this, it is seen that the following equation is satisfied:

$$\frac{\partial\phi}{\partial z} = -\beta` \frac{\partial\phi}{\partial t} + 1/2 i\beta`` \frac{\partial^2\phi}{\partial t^2} - i\beta_{2E} |\phi|^2 \phi \ . \qquad (5.6)$$

For the last term of (5.6) the two following relations were used

$$1/2\pi \int_{-\infty}^{\infty} \exp i(\omega-\omega_0)(t-t') \, d\omega = \delta(t-t') = \delta(t'-t)$$

and

$$\int_{-\infty}^{\infty} f(t') \, \delta(t'-t) \, dt' = f(t)$$

where $\delta(t-t')$ is the Dirac delta function. Now a change to a coordinate system that moves with the pulse is made, using the following transformations:

$$s = (t - z/v_g)/\tau \ \text{ and } \xi = z\,|\beta``|/\tau^2 \qquad (5.7)$$

since the group velocity $v_g = d\omega/d\beta$, then $s = (t - \beta` z)/\tau$. The scalar constants in (5.7) simply enable the final equation to be written in dimensionless form but we assign s the meaning of time and ξ that of distance. So we have

$$\frac{\partial\phi}{\partial t} = \frac{\partial\phi}{\partial s}\frac{\partial s}{\partial t} + \frac{\partial\phi}{\partial\xi}\frac{\partial\xi}{\partial t} = \frac{1}{\tau}\frac{\partial\phi}{\partial s}$$

also

$$\frac{\partial\phi}{\partial z} = \frac{\partial\phi}{\partial\xi}\frac{\partial\xi}{\partial z} + \frac{\partial\phi}{\partial s}\frac{\partial s}{\partial z} = \frac{|\beta``|}{\tau^2}\frac{\partial\phi}{\partial\xi} - \frac{\beta`}{\tau}\frac{\partial\phi}{\partial s}$$

Hence equation (5.6) becomes:

$$i\frac{\partial\phi}{\partial\xi}\frac{|\beta``|}{\tau^2} = -\frac{1}{2}\frac{\beta``}{\tau^2}\frac{\partial^2\phi}{\partial s^2} + \beta_{2E}|\phi|^2\phi \qquad (5.8)$$

Finally, the equation may be normalised by making the substitution

$$U = \tau\left(\frac{\beta_{2E}}{|\beta``|}\right)^{1/2}\phi$$

and since we are interested in the anomalous dispersion regime where $\beta``<0$, we include the sign of $\beta``$ explicitly, replacing with $\pm|\beta``|$ and obtain

$$i\frac{\partial U}{\partial \xi} = \pm\frac{1}{2}\frac{\partial^2 U}{\partial s^2} + |U|^2 U \qquad (5.9)$$

The positive sign is for the case of anomalous GVD ($\beta``<0$) and the negative sign for normal GVD. It is seen that this equation is similar in form to the Schrödinger equation of quantum mechanics, with a potential $|U|^2$ and so (5.9) is referred to as the dimensionless nonlinear Schrödinger equation, or NLS for short. It should be explained that the equation does not have any physical relation to Schrödingers equation in QM.

This method of derivation does not make obviously apparent some of the approximations involved in arriving at the NLS. It is seen that we neglect dispersion terms higher than $d^2n/d\omega^2$ in the expansion of the refractive index. While this will be valid for most of the results reported here, it should be remembered that if one is operating close to the dispersion minimum in a particular fibre, then higher order dispersion terms may well prove important. The validity of the slowly varying envelope approximation is thought to hold for pulses of a few picoseconds in duration but for much shorter pulses, a less severe approximation should be used [10,11]. Also in the derivation, the radial dependence of the field has been neglected. This is taken account of by including a factor, α, in the nonlinear term, defined as the average of the field over the fibre mode [1,12]. Ultimately this is included by using the effective area rather than the actual core area of the fibre (see below).

5.3 Soliton Solutions to the NLS.

In general, the NLS has to be solved by numerical methods, such as the inverse scattering technique of Zakharov and Shabat [13] (see also Satsuma and Yajima [14]). However, if a pulse of the form

$$U(\xi=0,s) = N\,\mathrm{sech}(s)$$

is launched into the fibre, it has been shown that this will propagate as a soliton for integer N. Analytical expressions have been derived for solutions of U for N = 1,2 [14] and are:

$$U_1(\xi,s) = e^{-i\xi/2}\,\mathrm{Sech}(s)$$

$$U_2(\xi,s) = 4\,e^{-i\xi/2}\,\frac{[\cosh(3s) + 3e^{-i4\xi}\cosh(s)]}{[\cosh(4s) + 4\cosh(2s) + 3\cosh(4\xi)]}$$

U_1 (N=1) is known as the fundamental soliton and N=2 etc. are higher order solitons. We see that $|U_1|^2$, which will represent the intensity envelope of the pulse, is independent of ξ and therefore propagates without a change in shape. This is not true for $|U_2|^2$ which will change shape in a periodic manner. The period is in fact $\xi=\pi/2$ and after traveling such a distance, the initial pulse shape, duration and amplitude are reconstructed. Note that $U_2(\xi,s)$ reduces to 2sech(s) when $\xi=0$. No analytical formulae exist for N>2 but all higher order solutions have the same $\xi=\pi/2$ period. Also the pulse shape evolution becomes increasingly more complex for higher N. Solitons with N≥2 represent a bound state of N superimposed solitons and form an infinite set of solutions. It has been shown by the inverse scattering method, that finding soliton solutions, corresponds to finding poles in the complex plane. A soliton of order N has N poles, with only imaginary parts, giving N solitons forming a bound state. The fundamental soliton has one pole and is therefore uniquely defined, but for an N=2 soliton, two poles exist with $\eta_1 + \eta_2 = 2$ where η_1 and η_2 are the imaginary parts of the poles and represent the amplitudes of the component solitons. The ratio η_1/η_2 may take on any real value (giving the infinite set of solutions) and for the particular U_2 given above i.e. sech² input pulse, it is 1/3 [15].

For the fundamental soliton, the intensity envelope will be

$$|U_1(0,s)|^2 = N^2\,\mathrm{sech}^2(s)\,.$$

Using the transformations (5.7) and the fact that the intensity FWHM duration of the input pulse is given by $\tau_p = 1.762\tau$, we may obtain expressions for the soliton period (Z_0) and peak power (P_N) in 'real world' dimensions:

$$\xi = \pi/2 = \frac{Z_0\,|\beta``|}{\tau^2} \qquad |\beta``| = \frac{\lambda^2 D}{2\pi c}$$

$$\Rightarrow \qquad Z_0 = 0.322\frac{\pi^2\,c\,\tau_p^2}{\lambda^2\,D} \qquad (5.10a)$$

Since intensity I, is given by $n_0 c\varepsilon_0/2 |E|^2$, we have

$$n_{2E} = n_2 n_0 c\varepsilon_0/2$$

also
$$|E|^2 = |\phi|^2 = \frac{1}{\tau^2}\frac{|\beta``|}{\beta_{2E}}|U|^2$$

$$\therefore \quad P_1 = 0.776\frac{\lambda^3 D}{\pi^2 c n_2 \tau_p^2} A \qquad (5.10b)$$

and $P_N = N^2 P_1$ for the N^{th} order soliton. The dispersion is in the units of s/m/m and typically has the value 15 ps/nm/km at 1.5 μm. In the above, c and λ are the velocity of light and wavelength respectively in a vacuum and n_2 is the nonlinear index coefficient, as defined in chapter 3. Typically $n_2 = 3.2\times10^{-20}$ m²/W in fused silica but for randomly polarised light this value is reduced by 5/6 (see chapter 3). The area A, is the effective core area also as defined in chapter 3.

To get an idea of the numbers involved, we see that a pulse of 7ps duration (FWHM) at 1.5 μm launched into a non-polarisation maintaining fibre, will have a soliton period of $Z_0 \approx 1.38$km and a fundamental soliton peak power (assuming a core area ~10^{-10} m) of $P_1 \approx$ 1W. Thus a pulse launched with this value of peak power will travel down a length of fibre undistorted - provided the losses are negligible. A pulse of peak power $P = N^2 P_1$ will experience a more complicated behaviour but we may note three important properties: (i) the input pulse always returns to its initial duration and amplitude at integral multiples of the soliton period Z_0 , (ii) for N≥2, the pulse always experiences, at first, a simple narrowing followed in general by splitting, the point of optimal narrowing moving closer to Z = 0 for higher N and (iii) the behaviour of these exact solitons is symmetrical about Z = $Z_0/2$ (ξ=π/4). These properties are readily seen in the perspective plots of figure 2a,b,c where the first three solitons are shown. The plots were obtained from a computer package which numerically solved the NLS and was developed by a summer student at the University [16].

Corresponding to the temporal compression of the soliton pulses shown in figure 2, a broadening occurs in the frequency spectrum - caused by SPM. This would obviously be expected since an initially transform limited pulse must broaden in frequency if it is to

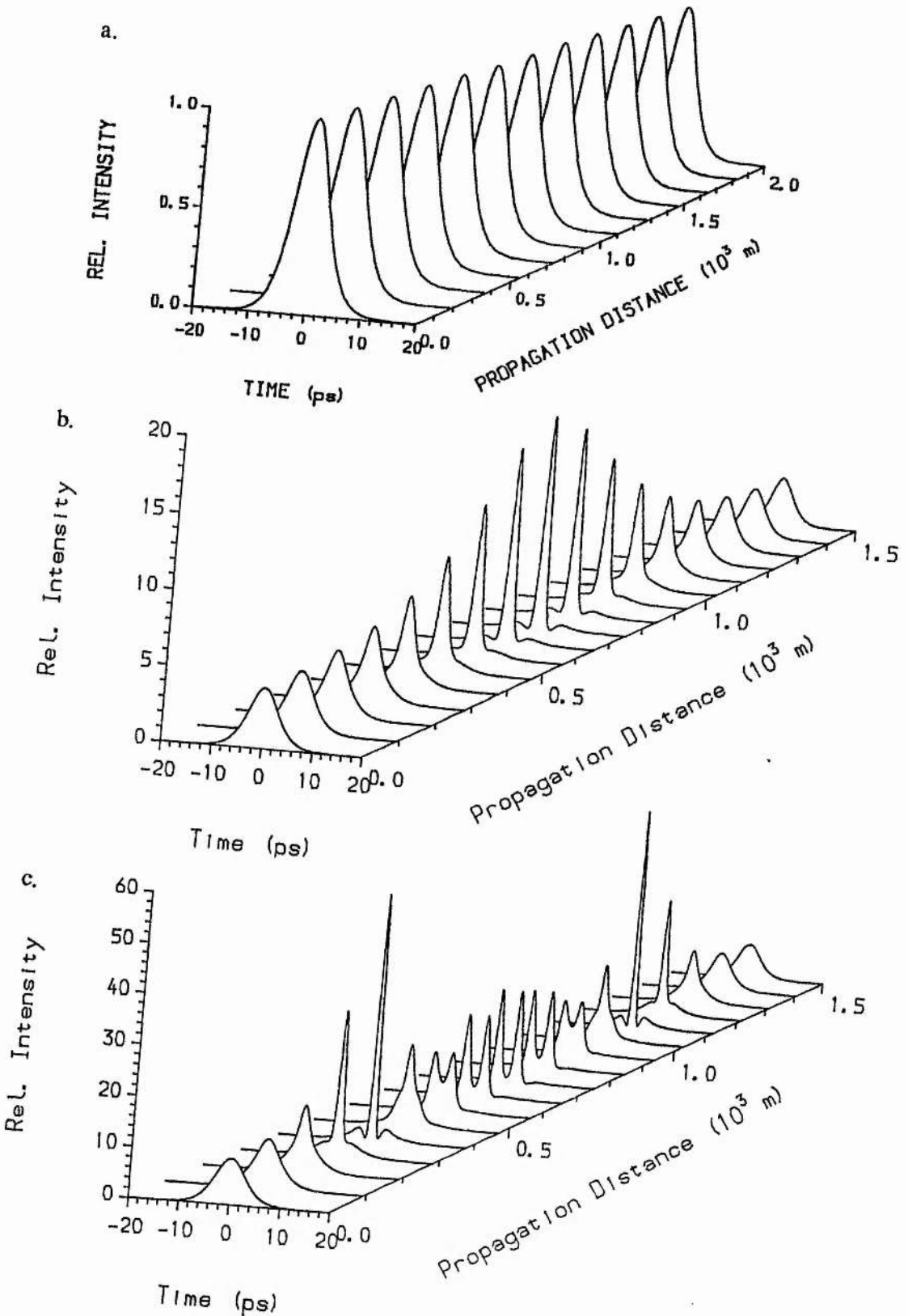

Figure 2.

Perspective plots for the first three order solitons (a) N=1 (b) N=2 (c) N=3; initial pulse duration 7ps.

narrow in the time domain. However, a perhaps surprising result occurs as the soliton broadens back to its original duration at Z_0, namely a corresponding *decrease* in the frequency spectrum. This frequency condensation occurs quite generally in soliton propagation and is known as the Fermi-Pasta-Ulam occurrence. We can think of the effect arising due to frequency-shifted light being compensated or reverse-shifted under the action of SPM

In a practical sense, it is unlikely that *exactly* the correct power level could be launched into a fibre to create a soliton. So what happens if a pulse of intermediate amplitude is launched? Consider the pulse to be of the form

$$U(0,s) = A\ \mathrm{sech}(s)$$

where A is a real number. It turns out that a soliton will still evolve from this input pulse, the soliton number being determined by $N \leq A+1/2$. Thus considering the 7ps sech^2 pulse as above, an N=1 soliton will form for $1/2 \leq A \leq 3/2$ i.e. for peak powers between $(1/2)^2 \times 1$=250mW and $(3/2)^2 \times 1$=2.25W. However, in general the emergent soliton will not have the same width or amplitude as for the exact A=N=1 case. This 'soliton forming' property results from the fact that for solitons, the area under the pulse is a constant of motion, that is

$$\int_{-\infty}^{\infty} |U|\, ds = \text{constant} \qquad (5.11)$$

and is in fact another definition of a soliton. An input pulse of incorrect amplitude will initially undergo both pulse width and amplitude oscillations [14], which decay as the shape of the pulse adjusts to satisfy (5.11) and the pulse approaches a true soliton [17,18]. Note that the emergent soliton will not in general be a sech^2 profile but some other similar function. Excess energy becomes dispersed and produces a low intensity background. Again for U=A sech(s) and for input power levels greater than P_1, the pulse will always initially narrow. Note also that the region where no soliton-type effects occur is defined by $A<1/2$ or $P< 1/4\ P_1$.

Although we do not consider it here, the effects of higher order dispersion terms, loss and the result of a break down in the slowly varying envelope approximation, have all been examined in the literature [17,19-22].

5.4 Observation of Optical Solitons.

The synchronously mode-locked KCl:Tl and NaCl colour centre lasers are able to provide relatively high power ultrashort optical pulses in the 1.5 μm wavelength region and so are ideally suited as sources for the study of solitons in optical fibres. The first such observations of pulse narrowing and soliton propagation by Mollenauer et al are described in references [23] and [24]. As a complement to the work done on pulse compression in chapter 3, a simple experiment was carried out to observe such soliton like narrowing utilising our KCl:Tl colour centre laser (CCL).

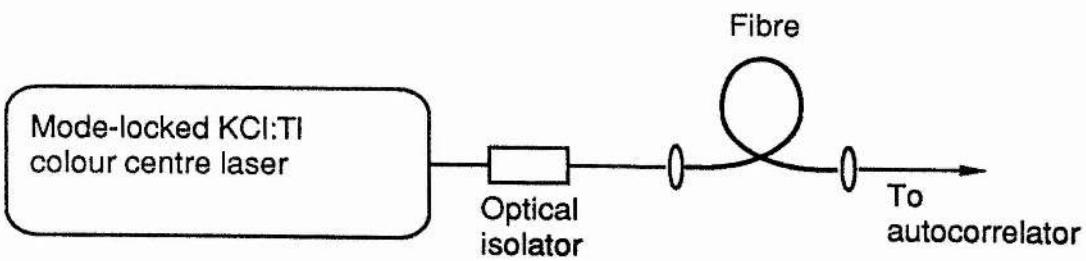

Figure 3.
Experimental arrangement for the observation of solitons in an optical fibre.

The experimental arrangement for this is shown in figure 3. The colour centre laser provided pulses of typically 18ps duration which were coupled into a length of monomode optical fibre via a ×20 microscope objective and both the input and output pulse trains could be monitored on the real time autocorrelator. From equation (5.10a) the soliton period for these pulses was estimated to be $Z_0 \approx 9.1$km. In order to clearly observe soliton effects, it is advantageous to use a length of fibre $\approx Z_0/2$ since it is at this point that the maximum change in pulse shape occurs. The length available to us was approximately 3km

- slightly under half the soliton period and had the following properties: core diameter = 9.2μm, core/cladding index difference $\Delta = 0.0034$, $n_{core} = 1.45$ and was non-polarisation maintaining (hence $n_2 \approx 2.67\times10^{-20}$ m²/W). From these values the normalised frequency, V, can be calculated for $\lambda = 1.5\mu m$ and then from table 1 in chapter 3, we have $A = 1.2A_{core} \approx 8\times10^{-11}m^2$. The peak power for the fundamental soliton is calculated to be (from 5.10b) $P_1 \approx 123mW$ and for the next two higher order solitons: $P_2 \approx 490mW$, $P_3 \approx 1.1W$. For a sech² intensity profile, the corresponding average powers are calculated to be

$p_1 \approx 0.21mW$ $p_5 \approx 5.2mW$

$p_2 \approx 0.8mW$ $p_6 \approx 7.5mW$ $\tau_p = 18ps$, 82MHz rep. rate.

$p_3 \approx 1.9mw$ $p_7 \approx 10mW$

$p_4 \approx 3.3mW$ $p_{10} \approx 21mw$

The maximum power we were able to couple into the fibre was 22mW and so it was expected that soliton orders up to N=10 should be observable. A series of observed SHG autocorrelations for different average powers in the fibre are shown in figure 4. Even for the lowest power used (limited by signal detection in the autocorrelator) pulse narrowing and splitting were clearly observed. The triple peaked autocorrelation for p = 2mW (figure 4b) corresponds to a two fold splitting in the pulse, indicating an N=3 soliton which is substantiated by the agreement with the power p_3 calculated above. Quantitative comparisons were difficult since the fibre is not exactly half a soliton period and also because the input pulse from the colour centre laser, was more Gaussian in shape rather than sech². As the average power level was increased, a 3-fold pulse splitting was seen to occur (fig.4c) indicating an N=4 soliton and again the power approximately corresponds to that expected. The maximum compression of the input pulse occurred for the highest power ≈ 22mW, and gave a pulse of approximately 810fs (assuming a sech² pulse shape). As can be seen in figure 4e, this pulse sat on top of a broad pedestal. This may be due to dispersed excess energy in the pulse and also Blow and Wood [25], have shown that if the input pulse is not transform limited, then a soliton will still form but again on top of a broad pedestal (see also ref. 26). These results are in general agreement with those reported in the literature [24,27].

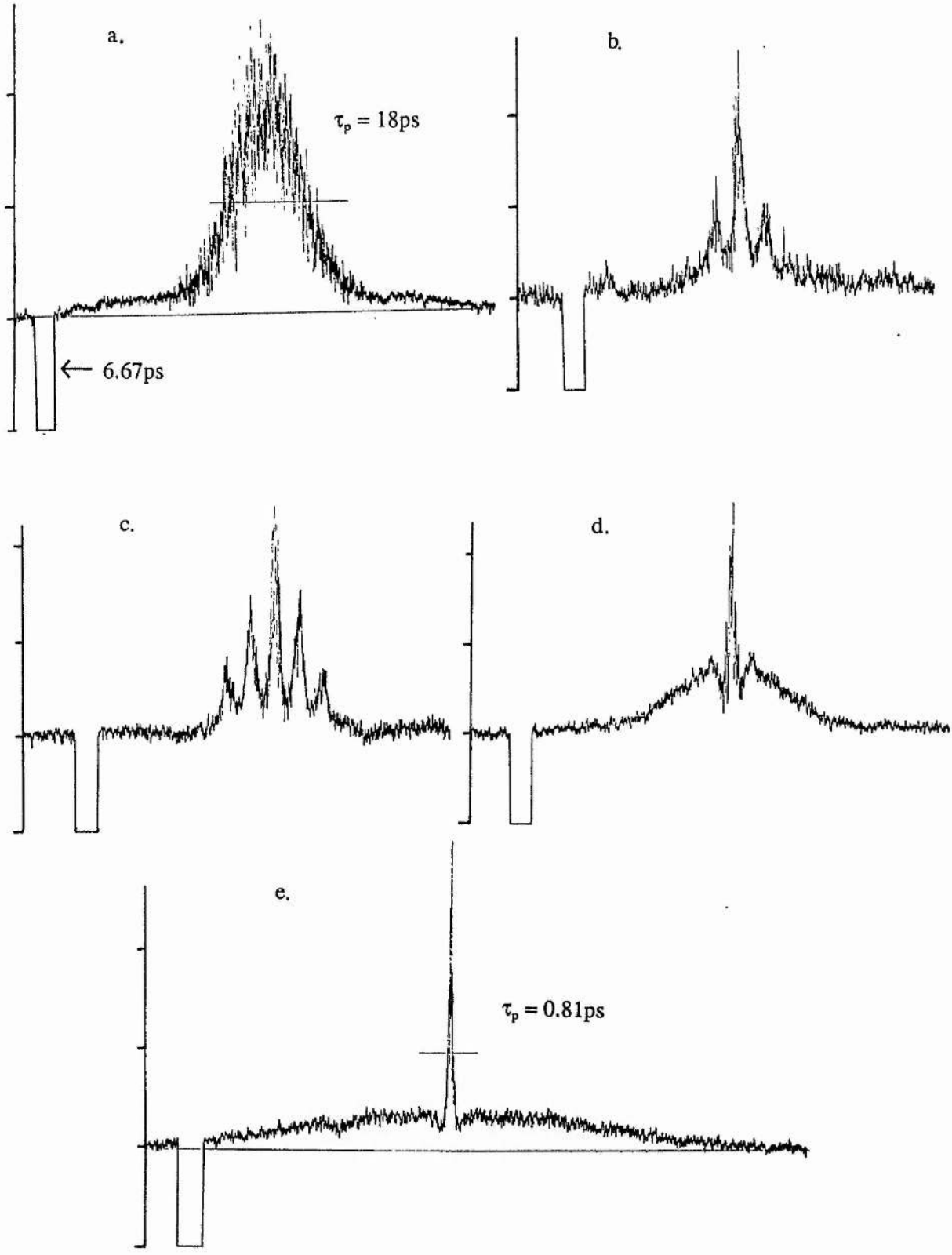

Figure 4.
Autocorrelation traces of the input pulse, (a), and output pulses from 3km of optical fibre; (b) p = 2mW (c) p = 3mW (d) p = 6.5 mW (e) p = 22mW average powers.

5.5 The Soliton Laser.

In 1984 Mollenauer and Stolen [28], reported the production of mode-locked pulses from a KCl:Tl CCL which were not only much shorter in duration (substantially less than 1ps) than any previously reported from such a colour centre laser, but also were very close to transform limited $sech^2$ profiles and the duration of these pulses could be easily controlled. This was achieved by the use of a length of optical fibre incorporated into an external cavity, providing a type of optical feedback for the colour centre laser. With reference to the schematic diagram in figure 5, the device was thought to operate in the following way. The synchronously mode-locked laser would by itself, produce pulses of around 10ps duration at 1.5μm. A given fraction of the output is fed into the external cavity via a beamsplitter and the initially broad pulses are coupled into a length of optical fibre. Here, the combined effects of anomalous GVD and SPM cause the pulse to narrow. The round trip time of the external, or control cavity as it is called, is made equal to or a multiple of, the main colour centre cavity.

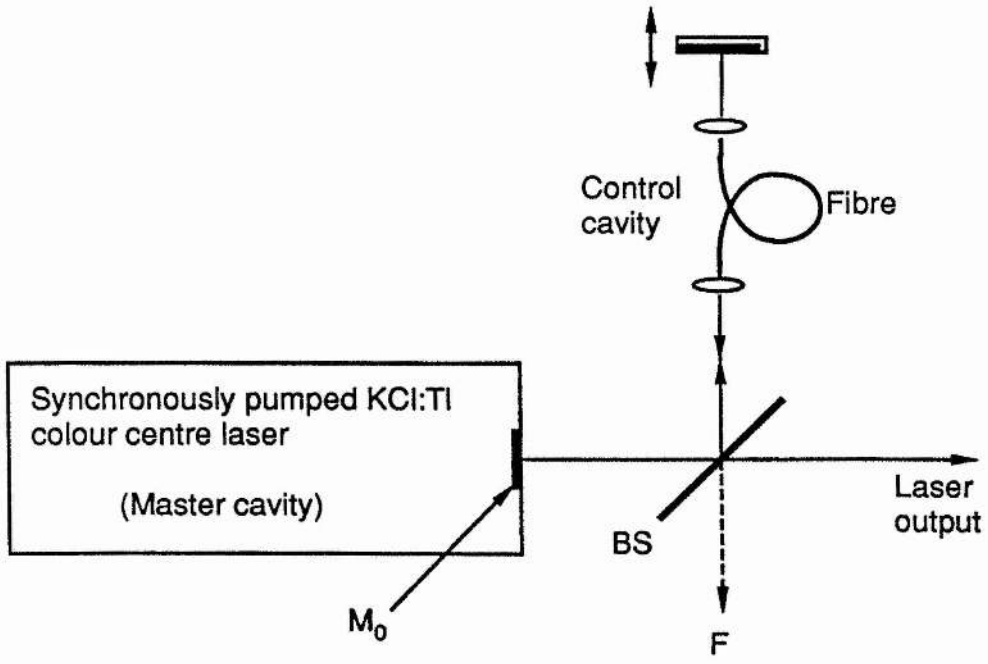

Figure 5.
A Schematic diagram of the Soliton Laser. BS: Beamsplitter.

The temporally compressed pulse is then fed back into the master cavity where interference with the pulse circulating there, stimulates the production of narrower pulses from the colour centre laser. This process continues with the control cavity returning even shorter pulses, until an equilibrium is reached when the pulses have essentially the same shape on both entering and leaving the fibre, i.e. they become optical solitons. In reference [28] it was reported that the laser was found to operate on an N=2 soliton which was inferred from three observations. In the first place it was found that the pulse duration exiting the laser was consistent with that expected if the fibre length in the control cavity was half the soliton period, that is $2L = Z_0$. This means that in the steady state, the pulse reaches a minimum duration after one pass through the fibre and then returns to its original width after the second pass. Also the pulse duration was found to be proportional to the square root of the fibre length - as would be predicted by equation 5.10a. Finally the average power in the fibre corresponded, to within experimental error, to that predicted for an N=2 soliton from equation 5.10b.

The operation of the soliton laser is critically dependent on the length of the control cavity, and in fact it is required that the feedback pulses have a constant phase relative to those in the master cavity. Consequently the coupled cavity arrangement is very sensitive to mirror vibrations, air currents or other effects which alter the optical path length of either cavity. This causes soliton laser action to flick on and off as the correct phase match condition is swept through and an electronic stabilisation system is employed to keep the two cavities phase-matched. This is described in reference [29] and our stabilisation scheme will be detailed in the next chapter. Needless to say, without this electronic stabilisation, the accurate temporal measurement of the pulses emitted by the soliton laser is made somewhat difficult and since the addition of the stabilisation loop, it has been found that the operation of the soliton laser is not quite as straight forward as at first thought. Indeed as will be described in the following chapter, it is not even necessary for the pulses in the control cavity to narrow in order to see a dramatic shortening in the duration of the laser output pulses.

Although my initial experiments on such a coupled-cavity arrangement were performed with a dispersion-shifted fibre, some of the results obtained by including a fibre identical to that used by Mollenauer in the control cavity will be described here, as it follows on from the discussion of nonlinear pulse propagation in an anomalous GVD fibre. The detailed experimental system and operation will be described in the next chapter.

The fibre was obtained from Dr L Mollenauer and had a core diameter of 8.6μm and an elliptical shaped cladding providing polarisation maintaining propagation [30]. The outer protective coating was also elliptically shaped making the polarisation axis easy to locate. At a wavelength of 1.5 μm the fibre dispersion was D≈15 ps/nm/km (anomalous) and $n_2 \approx 3.2\times10^{-20}$ m²/W. The effective core area for this fibre is $A = 1.11A_{core}$ [28]. With the control cavity blocked, the KCl:Tl CCL produced pulses ≈ 15ps in duration as described in chapter 4. In contrast, when optical access to the control cavity was allowed, and adjusted to the correct length, the output pulses narrowed to durations of less than 1ps depending upon the fibre length used. Also, with the stabilisation loop in operation the output pulse train was very stable with less than ~ 4% noise fluctuations. Normally a 0.8mm birefringent plate was used in the master cavity as a tuning and bandwidth limiting element.

Table 1.

	Calculated for N=2 (Z_0=2L)		
Fibre Length (m)	τ_p (ps)	Peak power required (W)	Av.power (mW)
0.56	0.20	2654	50
0.92	0.255	1632	40
1.7	0.35	866	29
2.8	0.445	536	23

Calculated values for pulse durations from the soliton laser and powers required.

In table 1, the calculated values of the pulse duration expected from the soliton laser for the fibre lengths used are shown, assuming N=2 operation. Also tabulated are the calculated peak and average power values for an N=2 soliton in the fibre. Setting the power in each fibre close to that calculated for the N=2 soliton, the laser output pulse durations were measured and were in reasonable agreement with the expected values. Figure 6 is a

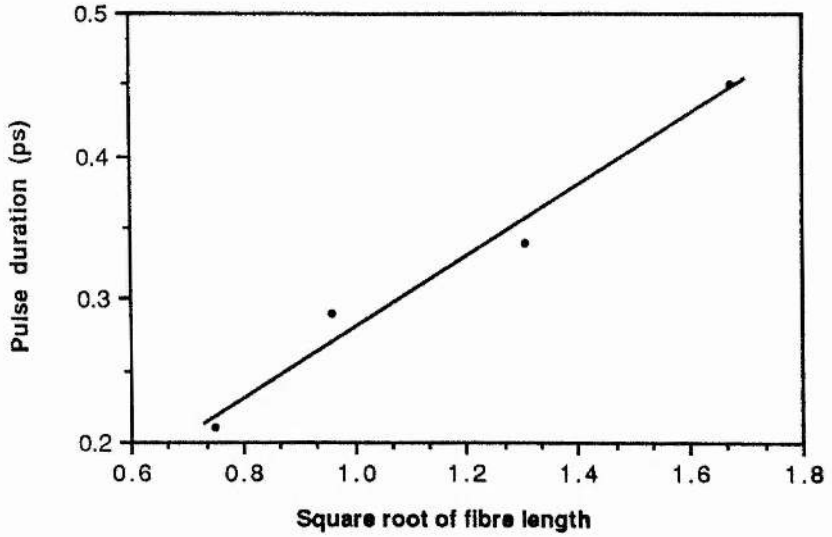

Figure 6.
Pulse duration from the soliton laser against the square root of fibre length. For each data point, the power in the fibre was set equal to that calculated for the N=2 soliton using $Z_0 = 2L$ (see table 1).

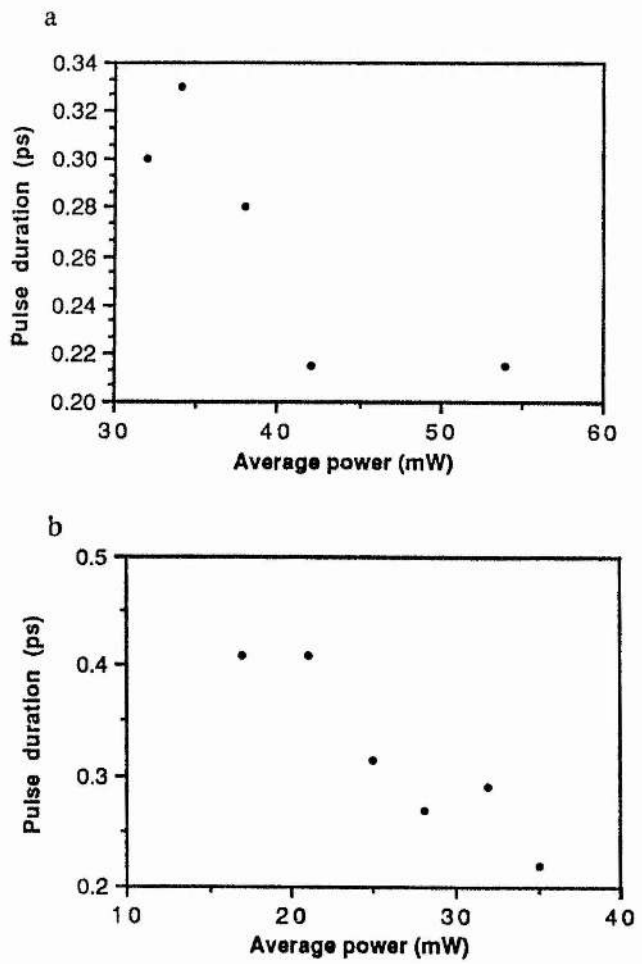

Figure 7.
Laser pulse duration vs average power in the fibre for two lengths (a) 92cm (b) 56cm.

plot of the pulse durations against the square root of the fibre length and is approximately linear as predicted from equation (5.10a) and in agreement with reference [28]. However, these data are selected points and it was found that in general the duration of the pulses did not match with those expected for N=2 soliton operation. It was found possible to produce a range of pulse widths for a given length by altering the average power coupled into the fibre. Figures 7a,b show the laser pulse duration as a function of average power for two of the fibre lengths used. In figures 8a,b a typical laser pulse SHG autocorrelation and spectrum are shown for a fibre length of 92cm. Note the flat and noiseless background on the autocorrelation indicating good pulse to pulse stability. The time bandwidth product is approximately 0.35 indicating that the pulses are close to a $sech^2$ shape. By monitoring the signal at point F in figure 5 (see also the following chapter), the pulses fed back from the fibre and reinjected into the laser could be monitored. It was found that in all cases and in agreement with reference [29], these pulses had durations less than those exiting the laser.

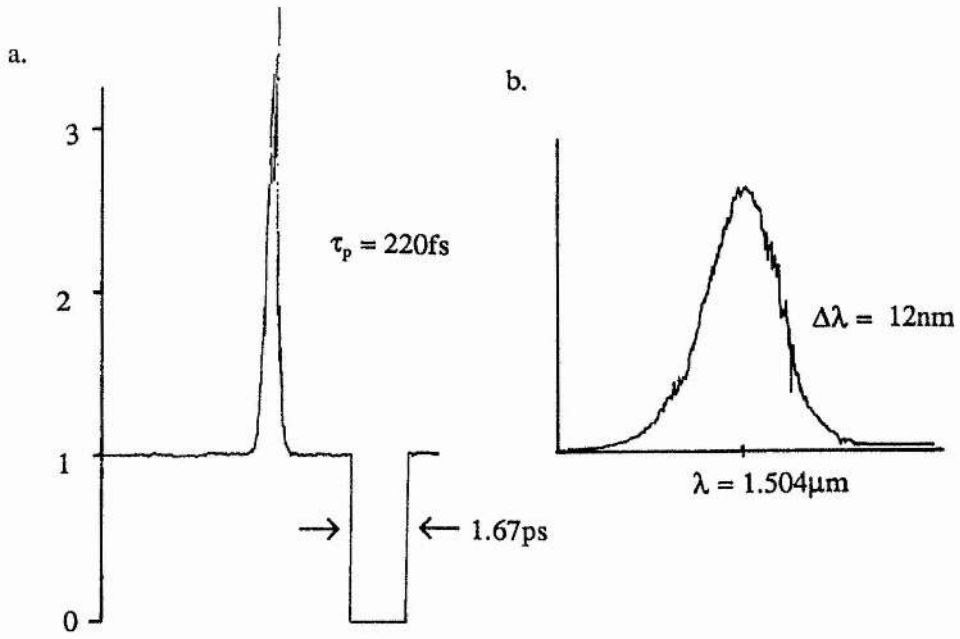

Figure 8.
(a) Autocorrelation and (b) spectrum of the pulses from the soliton laser with a fibre length of 92cm in the control cavity.

Figure 9 shows SHG autocorrelation traces of the laser and fed back pulses for a fibre length of 2.8m. Figure 9b indicates the existence of a sub-pulse or possibly, a pulse shape similar to that for the N=2 soliton at the half period, since it is just possible to make out five peaks in the autocorrelation.

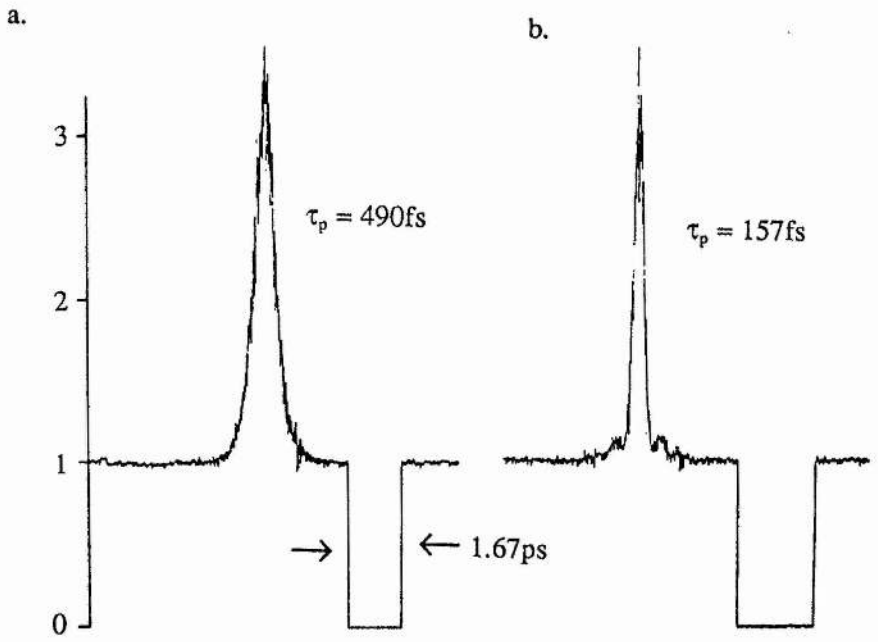

Figure 9.
Autocorrelation traces of (a) the laser and (b) fed back pulse for a fibre length of 2.8m.

These results then, imply that in fact a certain degree of pulse narrowing of the feedback pulse is required and that the fibre length is not in general, exactly half a soliton period. Even for the results of figure 6, the pulses returned from the fibre were found to be narrower than the laser output, again indicating that the fibre length is not exactly equal to $Z_0/2$. Furthermore, as already alluded to, it was found that actual temporal compression of the pulses in the control cavity was not required, as long as the pulse frequency spectrum

was broadened in some nonlinear manner. These experiments will be described in detail and a discussion of the proposed mechanism presented, in the following chapter.

5.6 Conclusions.

The propagation of optical solitons in an optical fibre has been described and a simple experiment performed to demonstrate this. By launching pulses of ~18ps at 1.5μm into a length of anomalously dispersive fibre, a compression factor of ≈ ×22 was obtained. It is interesting to compare this method of pulse compression within the fibre, to that described in chapter 3 where the anomalously dispersive delay is provided by diffraction gratings. The arrangement is obviously simpler since only a length of fibre is required. Unfortunately, in both methods the compressed pulse is generally produced on top of a broad pedestal, but in the case of soliton type compression this may be removed since the pedestal tends to be orthoganally polarised to the compressed pulse [27].

It is perhaps worth noting the stability of solitons with regard to small perturbations. Many theoretical and numerical studies have shown that solitons are quite insensitive to minor fluctuations in fibre parameters [31] and will be formed even from non-transform limited pulses and non-sech^2 shaped pulses [25,32], although the duration of the soliton will generally be different to the input pulse. It has also been shown that solitons can form from an initially unmodulated CW beam - due to the process of modulation instability. Small perturbations (either induced or spontaneous) on a CW beam become amplified in the presence of SPM and anomalous dispersion, the modulation deepens and eventually forms soliton pulses [33,34]. Experiments have also been performed to study the interaction of solitons and have demonstrated the stability of such pulses to collisions [35].

Soliton propagation studies have also shown that, for narrow pulses, a continual transfer in energy occurs from the shorter to longer wavelengths within the pulse spectrum due to Raman scattering [36,37]. This process is known as the soliton self frequency shift (SSFS) and results from the fact that the Raman gain curve in fused silica extends right down to zero frequency shift. The effect is inversely proportional to the fourth power of the pulse duration and so is negligible for pulses with durations >10ps. This self frequency

shifting process actually causes higher order solitons in a real fibre to become progressively more unstable with increasing N. The many peaks frequency shift by different amounts and then collide with each other due to the action of GVD and eventually a single soliton emerges. Recently the energy loss due to fibre attenuation has been overcome by using Raman amplification and distortionless propagation of solitons has been demonstrated over ~4000km [38,39].

The soliton laser, formed by incorporating a length of fibre into a control cavity, is able to produce pulses a fraction of the duration obtainable by synchronous pumping alone, the shortest reported to date being 60fs [40]. By compression of these pulses in an external fibre, pulses of 19fs at 1.5μm were produced, representing only 4 optical cycles. It has also been reported that soliton laser action can be obtained when the KCl:Tl laser is acousto-optically mode-locked [41]. In the light of the results presented above, it is questioned whether the coupled-cavity laser is really a 'soliton' laser in the true sense and in the following chapter, experiments will be described which show that in fact soliton formation or even pulse narrowing, are not required for an enhancement in the mode-locking of a KCl:Tl colour centre laser.

References.

1. A Hasegawa, F Tappert; Appl. Phys. Lett. **23**, 142 (1973)
2. I H Malitson; J Opt. Soc. Am. **55**, 1205 (1965)
3. K J Blow, N J Doran, E Cummins; Opt. Comm. **48**, 181 (1983)
4. M Miyagi, S Nishida; Appl. Optics **18**, 678 (1979)
5. W J Tomlinson, R H Stolen, A M Johnston; Opt. Lett. **10**, 457 (1985)
6. J E Rothenberg, D Grischkowski; Phys. Rev. Lett. **62**, 531 (1989)
7. R K Bullough; Physics Bulletin February 1978
8. A C Newell; 'Solitons in Mathematics and Physics' (1985)
9. G B Witham; 'Linear and Nonlinear Waves' Wiley (1974)
10. D N Christodoulides, R I Joseph; Appl. Phys. Lett. **47**, 76 (1985)
11. G Yang, Y R Shen; Opt. Lett. **9**, 510 (1984)
12. M Jain, N Tzoar; Opt. Lett. **3**, 202 (1978)
13. V E Zakharov, A B Shabat; Sov. Phys. JETP **34**, 62 (1972)
14. J Satsuma, N Yajima; Supplement Prog. Theoretical Phys. **55**, 281 (1974)
15. H A Haus, M N Islam; IEEE J Quant. Electron. **QE-21**, 1172 (1985)
16. S G Wenden; Summer vacation report, University of St.Andrews 1988
17. N J Doran, K J Blow; IEEE J. Quant. Electron. **QE-19**, 1883 (1983)
18. A Hasegawa, Y Kodama; Proc. IEEE **69**, 1145 (1981)
19. N Tzoar, M Jain; Phys. Rev. A **23**, 1266 (1981)
20. P K A Wai, C R Menyuk, Y C Lee, H H Chen; Opt. Lett. **11**, 464 (1986)
21. K J Blow, N J Doran; Opt. Comm. **52**, 367 (1985)
22. W Zhao, E Bourkoff; IEEE J Quant. Electron. **QE-24**, 365 (1988)
23. D M Bloom, L F Mollenauer, C Lin, D W Taylor, A M Del Gaudio; Opt. Lett. **4**, 279 (1979)
24. L F Mollenauer, R H Stolen, J P Gordon; Phys. Rev. Lett. **45**, 1095 (1980)
25. K J Blow, D Wood; Opt. Comm. **58**, 349 (1986)
26. A S Gouveia-Neto, A S L Gomes, J R Taylor; Opt. Comm. **64**, 383 (1987)
27. L F Mollenauer, R H Stolen, J P Gordon, W J Tomlinson; Opt. Lett. **8**, 289 (1983)

28. L F Mollenauer, R H Stolen; Opt. Lett. **9**, 13 (1984)

29. F M Mitschke, L F Mollenauer; IEEE J Quant. Electron. **QE-22**, 2242 (1986)

30. J R Simpson, R H Stolen, F M Sears, W Pleibel, J B MacChesney, R E Howard; J Lightwave Tech. **LT-1**, 370 (1983)

31. G R Lamb; 'Elements of Soliton Theory' Wiley (1980)

32. C Desem, P L chu; Opt. Lett. **11**, 248 (1986)

33. A Hasegawa; Opt. Lett. **9**, 288 (1984)

34. K Tai, A Tomita, J L Jewell, A Hasegawa; Appl. Phys. Lett. **49**, 236 (1986)

35. F M Mitschke, L F Mollenauer; Opt. Lett. **12**, 355 (1987)

36. F M Mitschke, L F Mollenauer; Opt. Lett. **11**, 659 (1986)

37. J P Gordon; Opt. Lett. **11**, 662 (1986)

38. L F Mollenauer, J P Gordon, M N Islam; IEEE J Quant. Electron. **QE-22**, 157 (1986)

39. L F Mollenauer, K Smith; Opt. Lett. **13**, 675 (1988)

40. F M Mitschke, L F Mollenauer; Opt. Lett. **12**, 407 (1987)

41. J F Pinto, C P Yakymyshyn, C R Pollock; Opt. Lett. **13**, 383 (1988)

Chapter 6.

Coupled-Cavity Mode-Locking.

6.1 Introduction.

The idea of including a length of fibre in the optical feedback loop of a KCl:Tl colour centre laser was discussed towards the end of the chapter 5. Such a dual-cavity system enables the production of sub-picosecond pulses at 1.5 μm, greatly enhancing the mode-locking characteristics of the KCl:Tl laser. The initial explanation of this effect was that the laser output stabilised when the pulse propagating in the external cavity constituted a second order soliton [1]. However, subsequent experimental (see chapter 5) and theoretical [2,3] studies have shown that the operating point is in fact significantly more complicated. In this chapter, experiments will be described which for the first time demonstrate that soliton formation, or even temporal narrowing of the pulse in the control cavity, is not required in order to see a dramatic enhancement in the mode-locking of the colour centre laser (similar results were also observed by other authors at about the same time [4,5]). Since the enhanced mode-locking process was found not to depend on the formation of optical solitons and as will be described below, soliton formation is actually precluded, the system cannot really be called a 'soliton' laser. Rather the process is referred to here as coupled-cavity mode-locking (CCM).

6.2 The Experimental System.

A schematic diagram of the coupled-cavity laser is shown in figure 1. The colour centre laser alone, bounded by mirrors M_1 and M_0, typically produced pulses of ≈ 15 ps duration and was tunable from 1.45 to 1.55 μm as described in chapter 4. The laser was pumped continuously (no chopping) with ≈ 2 W time average power from the Nd:YAG laser. The control cavity was formed by the output coupler, M_0, of the colour centre laser, the beamsplitter, S_1, and a small dielectric mirror M_3 mounted on a piezoelectric translator

(PZT). For all the experiments described here, S_1 had a reflectivity of 50%. Two ×20 microscope objectives were used to couple into and out of the fibre in the control cavity. It is vital to the success of coupled-cavity operation that any reflections other than that from M_3 be eliminated. To this end, both microscope objectives were AR coated over the tuning range of the laser and both ends of the optical fibre were immersed in index matching fluid contacted to the front surface of each objective, preventing the ~4% reflections from the cleaved ends. A variable neutral density filter enabled the average power in the fibre to be varied without altering the coupling efficiency. Beamsplitter S_2 enabled the pulses exiting the fibre and reinjected back into the laser to be monitored, as well as allowing for the operation of a stabilisation loop which will be described below.

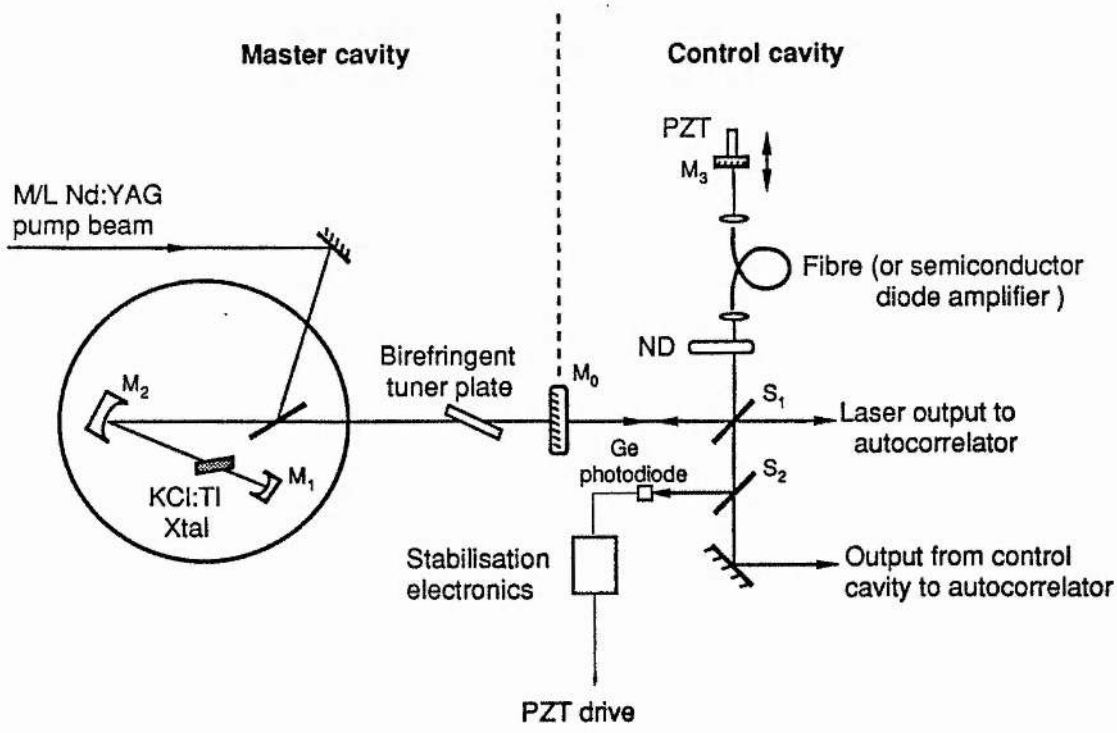

Figure 1.
The experimental arrangement of the coupled-cavity laser. Mirror reflectivities: M_1, M_2, $M_3 \approx$ 100%; $M_0 \approx$ 80%. The beamsplitters had reflectivities $S_1 \approx$ 50%, $S_2 \approx$ 30%. ND - variable neutral density filter.

With the colour centre laser properly adjusted for synchronous pumping, the control cavity length is made roughly equal to (or a multiple of) that of the master cavity. A detector is then placed just in front of M_3 and coupling through the fibre optimised. If a high birefringent fibre is used, it is then necessary to adjust the rotation angle of the input end so that radiation is launched along one of the polarisation axes, enabling linear polarisation to be maintained. In order to achieve efficient feedback, it was found easiest to focus the beam emerging from the fibre onto M_3 which is then adjusted to retroreflect the light back into the fibre. The fed-back light may either be detected using a germanium photodiode just before S_2 or by monitoring the second harmonic signal generated by the laser pulses. In general, when the control cavity length is incorrect, any feedback will seriously degrade the mode-locked pulses from the CCL, reducing (to almost zero) the amount of signal from the autocorrelator. The final step is to adjust the length of the control cavity until it is matched with the master cavity. This was achieved by having the input fibre end and objective mounted as one unit on a precision translation stage but it was often found easier to move mirror M_3, which was mounted on an optical rail, and then peak up the feedback signal once the matching point was obtained.

The onset of coupled-cavity operation was easily seen as a dramatic enhancement in the second harmonic signal from the autocorrelator (by as much as ~200 times!) due to the coupled-cavity laser producing much shorter pulses but with approximately the same time average power. At this stage, with no stabilisation loop, vibrations or other effects altering the optical path of either cavity, caused the laser to jump randomly between producing CCM pulses and the much broader ones produced by the colour centre laser alone. This was accompanied by power fluctuations (typically 10% peak to peak) in both the control and master cavities. As described in reference [2], it was noticed that CCM operation was correlated to some well defined time average power level in the control cavity, presumably corresponding to a particular value of phase mismatch between the pulses interfering at M_0. Figure 2 shows a trace of the real-time autocorrelation and simultaneous time average power in the control cavity (measured on a Ge diode) for the unstabilised laser over a time period of approximately 20 ms. The CCM level is easily seen.

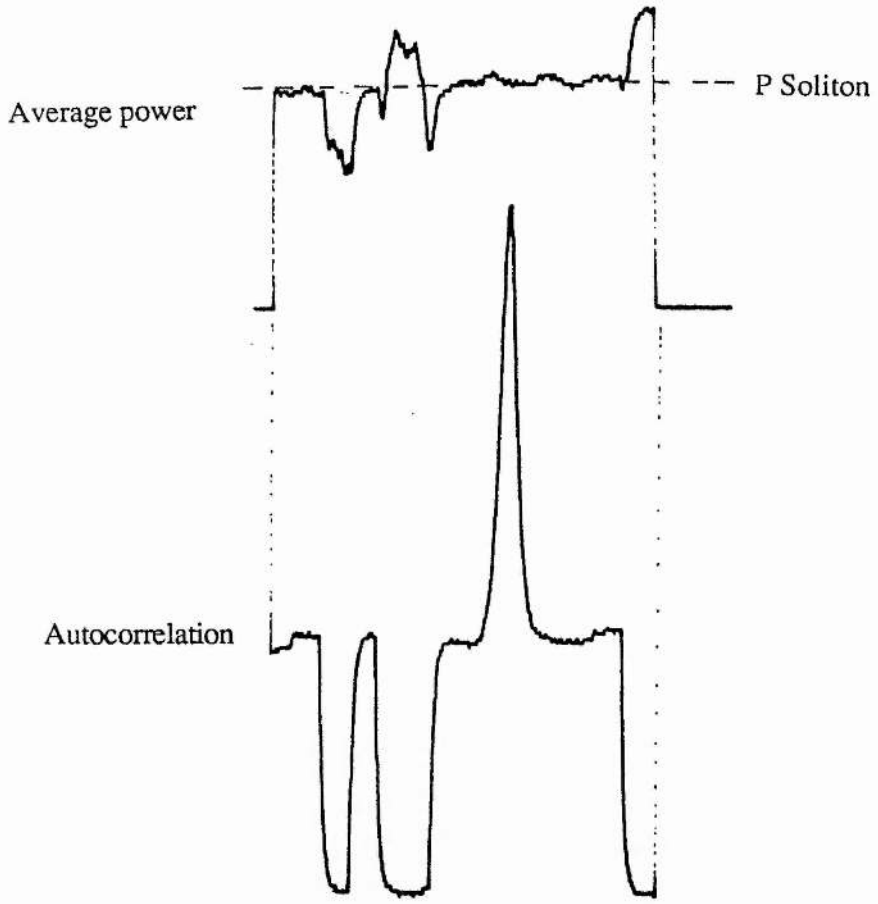

Figure 2.
Autocorrelation trace and corresponding power in the control cavity for the unstabilised CCM laser.

Thus as described in [2], a stabilisation loop was implemented whereby an amplified error signal derived from the difference between the voltage produced from the Ge diode and an empirically set reference voltage, drove a piezoelectric translator. Given the correct polarity of error signal, any deviation in the cavity length caused a corrective movement of the PZT. Figure 3 shows a more detailed diagram of the feedback loop. Switching in one of five capacitors across the integrating op-amp enabled the frequency response of the loop to be determined, the one producing the fastest, stable operation was used. A low voltage PZT with an excursion of 15 μm for 150 V was used, and biased to its mid-position.

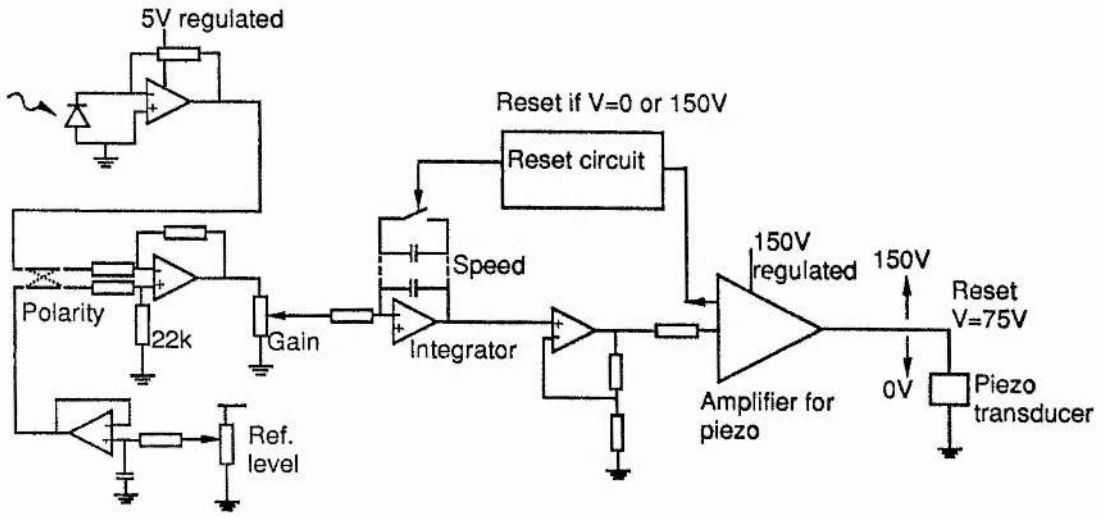

Figure 3.
Circuit diagram of the electronic feedback loop.

If the PZT reached one end of its range, the circuit reset, positioning the PZT at its mid-point and began searching for a new stable operating point. This action interrupted the pulse train occasionally but once the loop was in operation, the coupled-cavity laser produced a train of sub-picosecond pulses which were very stable with ≤ 3% noise fluctuations. A photograph of the pulse train is shown in figure 4b and figure 5 is a time exposure typical of the real-time autocorrelation trace of the pulses from the stabilised coupled-cavity laser. For pulse durations greater than ~ 0.5 ps a 2 mm BRF was generally used in the main cavity for bandwidth restriction and a ≈ 0.3 mm plate was used when shorter pulses were to be generated. It was found that a certain adjustment in the length of the control cavity could be tolerated for CCM operation. This was approximately 400 μm for the longest fibre length and decreased as the fibre length was reduced. Also, it was found that stable CCM

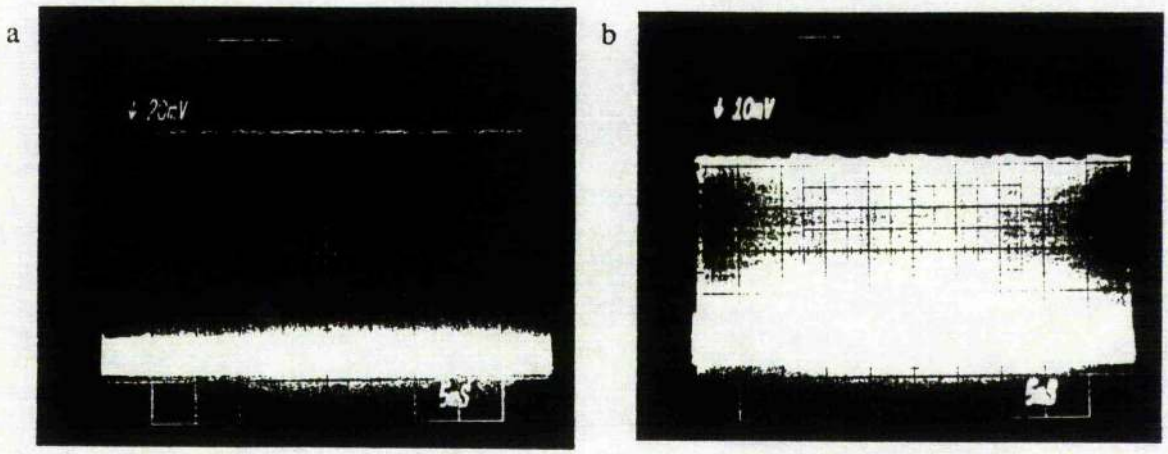

Figure 4.
(a) Pulse train exiting the synchronously pumped colour centre laser and (b) pulse train of the CCM laser, taken from a stray beam exiting the laser cavity (with stabilisation). (5ms/div)

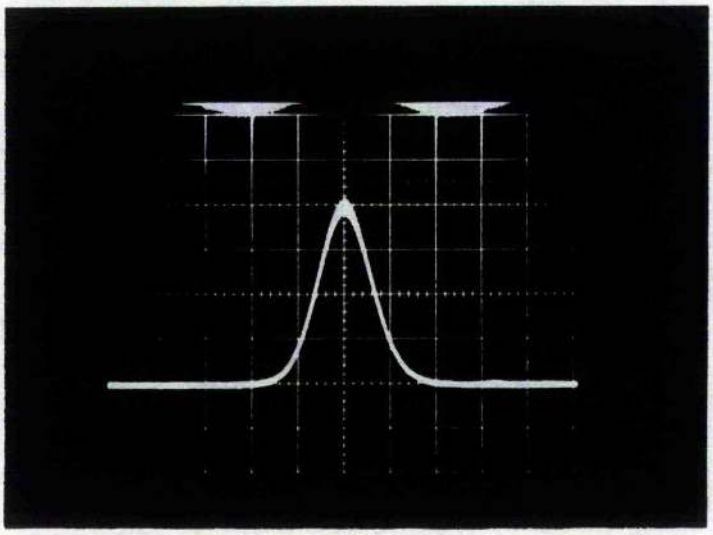

Figure 5.
Time exposure of a real-time autocorrelation trace for the stabilised CCM laser pulses.

operation was obtained over a small range of reference level voltages (small range of phase mismatch) and a slight variation in the pulse duration (and power) were observed as the reference level was altered over this stable range.

6.3 The CCM Laser with Normally Dispersive Fibre.

The initial experiments were conducted with a fibre obtained from STL and manufactured by the Andrew Corporation Inc. [6]. It had an elliptical core (2.8 μm × 1.6

μm) providing single-mode and polarisation maintaining propagation at 1.5 μm. Polarisation maintaining fibre was thought necessary since otherwise the signal fed back into the (polarisation sensitive) laser would fluctuate randomly resulting in an unstable output. However, we have found recently that non-polarisation preserving fibre (low birefringence) works just as well. The small core size necessitated a relatively large Δn (≈ 0.046) provided by a high germania content, in order to obtain propagation in a single mode. Also because of the small core, the fibre had a large waveguide dispersion which actually exceeded the material dispersion, giving a net positive (normal) GVD at 1.5 μm. An experimental measurement of the dispersion on a fibre similar to ours is shown in figure 6 and indicates a value of ≈ 40 ps/nm/km. (Unfortunately an insufficient length of fibre was available to enable a dispersion measurement of the actual fibre used here.)

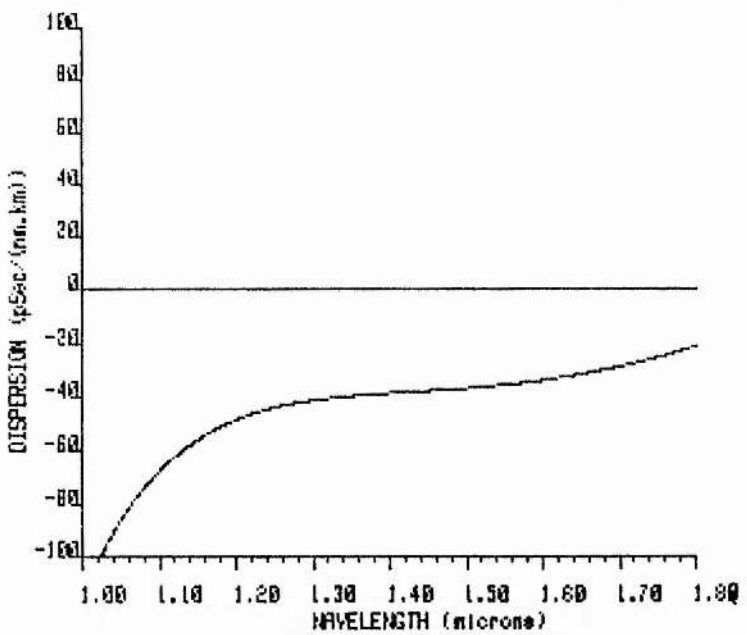

Figure 6.
Experimental measurement of dispersion on a fibre similar to that used here. (Provided by Dr K Byron of STL Technology Ltd.)

Because of the positive GVD, the fibre is unable to support (bright) solitons and pulses propagating along such a fibre are dispersively broadened.

Initially a 2.2 m length of this fibre was inserted into the control cavity and with the laser set up as described above, a significant shortening of the laser pulses to ≈ 1.1 ps occurred (see figure 7a) assuming a $sech^2$ pulse shape. In figure 7b a $sech^2$ fit to the

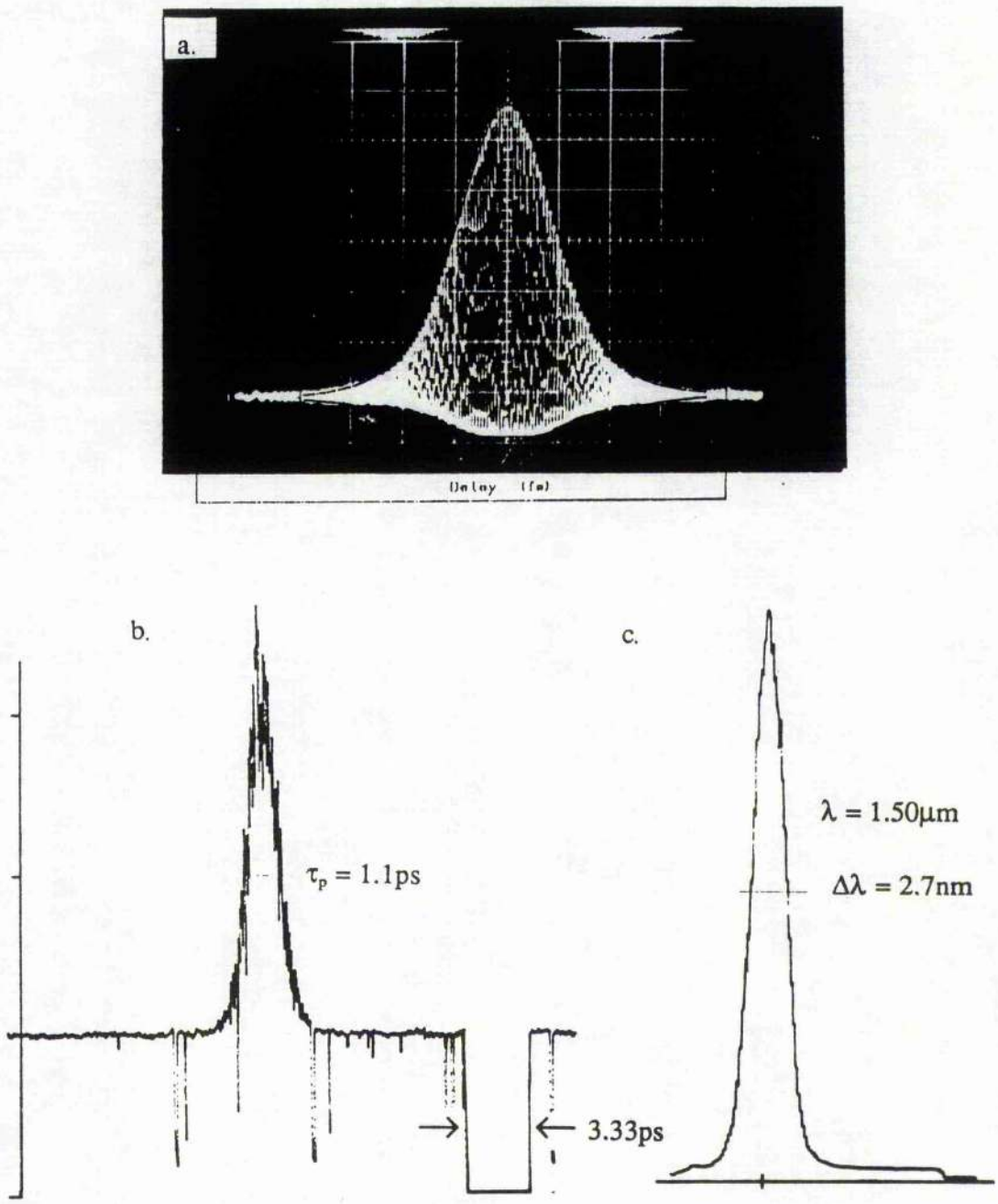

Figure 7.
Interferometric, (a), and intensity, (b), autocorrelations for the CCM laser pulses with a fibre length = 2.2 m. (c) Corresponding spectrum.

interferometric autocorrelation is shown for comparison. There is a slight departure in the wings of the pulse which may imply some excess frequency chirp, but it should be remembered that since the pulses are not solitons, there is no particular reason why they should have $sech^2$ intensity profiles. Because of the reasonably good overall fit, all the pulse durations quoted here are deconvolved assuming a $sech^2$ pulse shape. The measured

spectral width from fig.7c gives a time-bandwidth product of approximately 0.4 (slightly greater than that for a $sech^2$ pulse - 0.315) which was typical for all the CCM pulses measured with this fibre. Stable pulses of approximately constant duration were obtained over an average power range of 10 - 25 mW in the fibre (measured just before M_3). The shortest pulses of 260 fs were obtained with a fibre length of 24 cm representing a shortening of the colour centre laser pulses by ~ 60× without feedback. For this shortest length, the minimum power required in the fibre to obtain CCM operation was ≈ 30mW. Figure 8 shows the intensity autocorrelation trace obtained from the laser with this fibre length and the plot in figure 9 displays the duration of the pulses exiting the coupled-cavity laser as a function of fibre length.

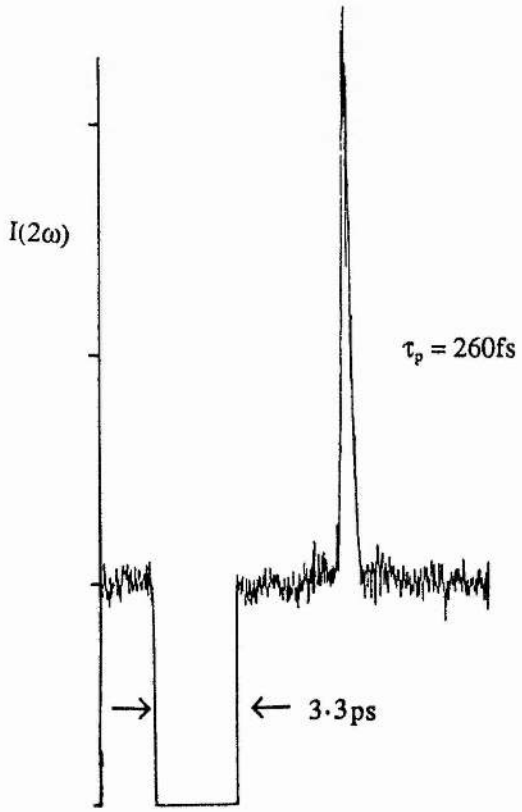

Figure 8.
Intensity autocorrelation trace of the shortest pulse obtained from the CCM laser. Fibre length = 24 cm.

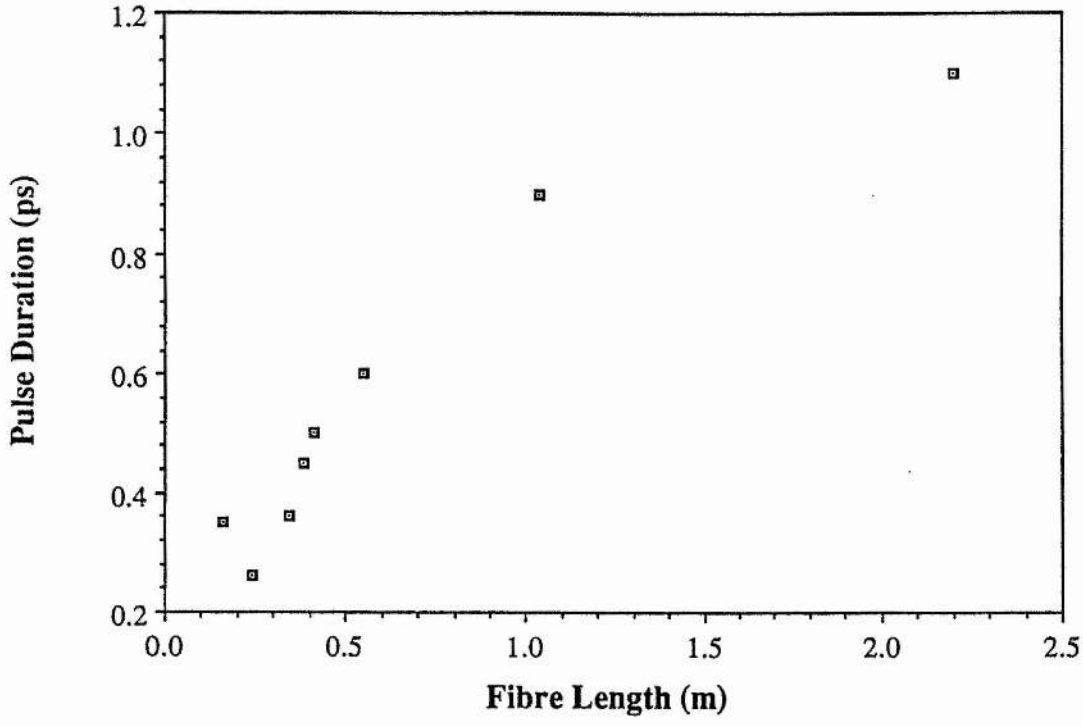

Figure 9.
Variation of the pulse duration from the coupled-cavity laser as a function of fibre length.

Although a decrease in pulse duration with fibre length was observed, in contrast to the soliton laser (chapter 5) where the output pulse duration is proportional to the square root of the fibre length, no such simple relationship is seen here. It may also be inferred from this graph that an optimum fibre length exists for the production of the shortest output pulses. Owing to physical constraints in our experimental system (16 cm was the shortest fibre length possible), further data around this apparent minimum were not taken but this would be required in order to establish the true existence of an optimum fibre length.

The best indication that our coupled-cavity laser was not operating as a 'soliton' laser came from the observation of pulses returned from the control cavity (see figure 1). In all cases these were longer in duration than the laser pulses and normally by a factor of approximately two. Figure 10 is the corresponding plot to figure 9 for the pulses returned from the fibre and injected back into the laser. Typical intensity and interferometric autocorrelation traces of both pulses are shown in figure 11 for a 55cm fibre length. Temporal broadening is clearly seen for the return pulses. The interferometric

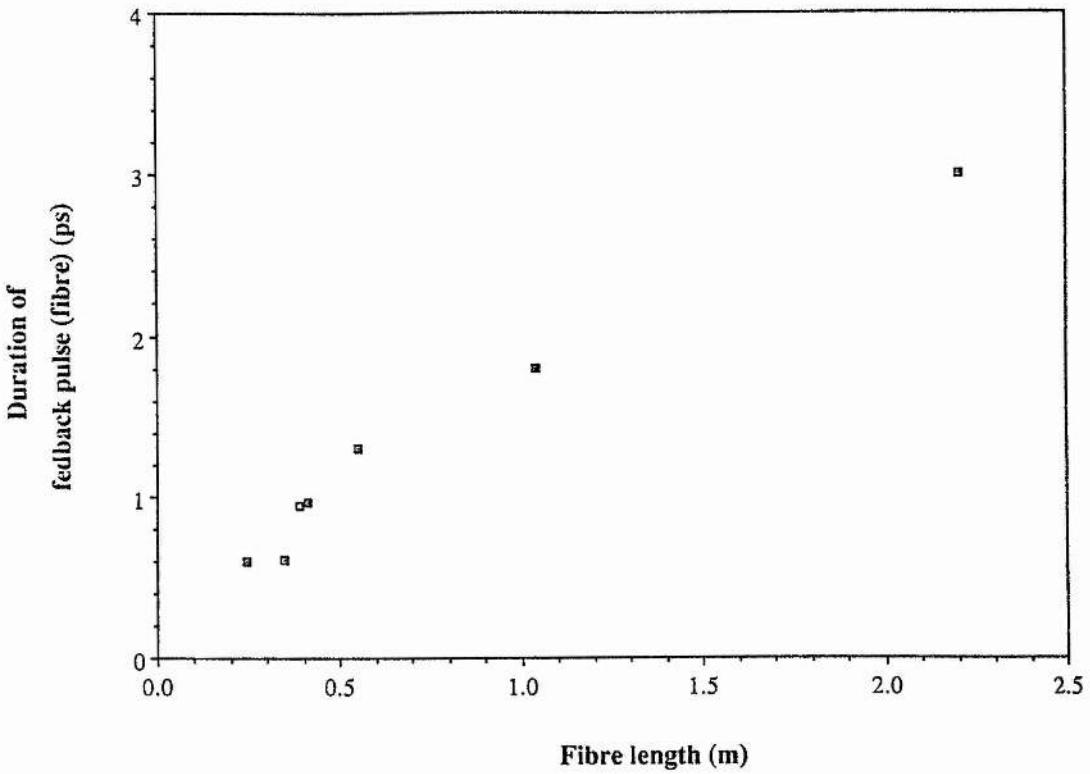

Figure 10.
Pulse duration of the pulses returned from the control cavity as a function of fibre length.

autocorrelation traces show a substantial difference between the two pulse trains. For the laser output (fig. 11b) the pulses are well phase locked (as shown by the 8:1 contrast ratio) and again for comparison a $sech^2$ fit to the envelope is also shown. The pulses returning from the control cavity (figure 11d) however, show a substantial linear frequency chirp due to the positive GVD of the fibre (indicated by the rising wings of the autocorrelation trace [7]) and a similar structure was seen in all cases for these pulses. It was also found that, as would be expected, the spectrum of the pulses returned from the control cavity was broadened by the action of SPM in the fibre. Confirmation that the Andrew Corporation fibre was indeed positively dispersive at 1.5 μm was obtained by performing a 'single-pass' experiment with an external length of fibre. Pulses of ~ 0.6 ps duration obtained from the CCM laser (actually using a length of negatively dispersive fibre in the control cavity as described in the last chapter) were passed

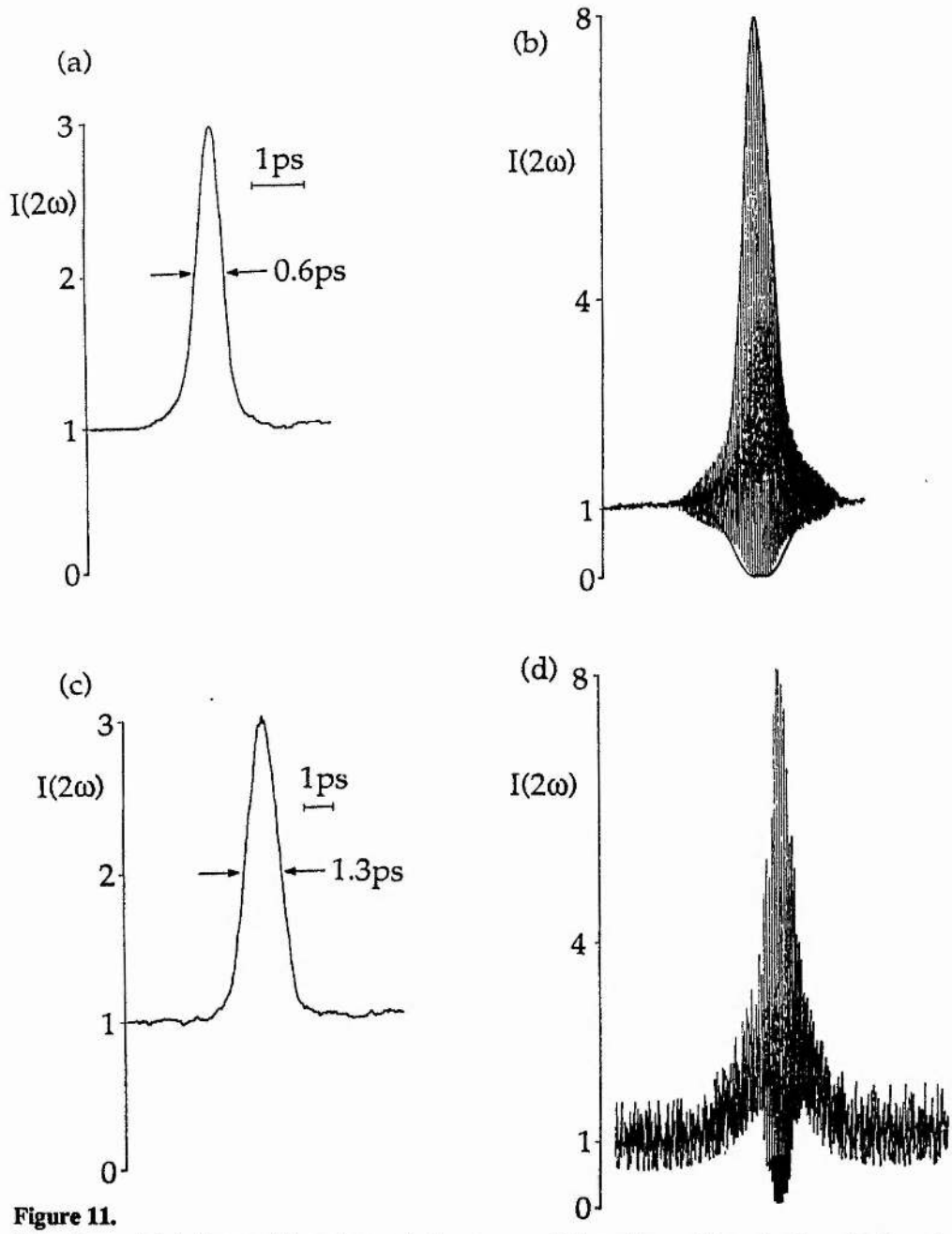

Figure 11.
Intensity and interferometric autocorrelation traces of the pulses exiting the laser (a,b) and returning from the control cavity (c,d) for a fibre length of 55cm. The fringes seen on the interferometric autocorrelations are not actual interference fringes but are due to a sampling limitation on the digital oscilloscope used.

through a 2 m length of the Andrew fibre and the output pulses monitored. It was necessary to insert an optical isolator between the test fibre and the laser output, preventing any feedback from the fibre end destroying CCM operation. The results are reproduced in figure 12 for two different power levels. As can be seen, for both high and low power levels, the output pulses are broadened in both duration and frequency, the spectra displaying typical SPM broadening.

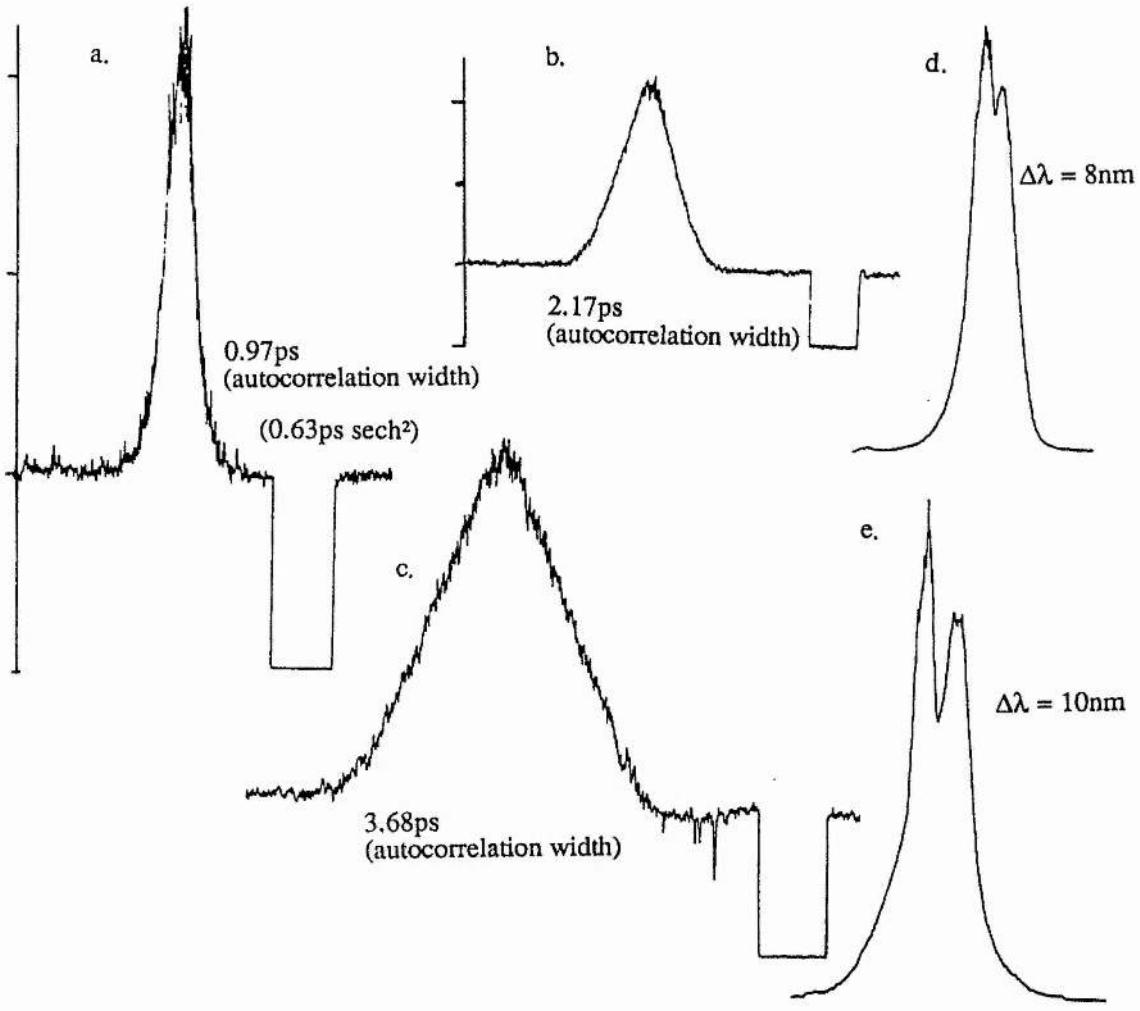

Figure 12.
(a) Input pulse to 2 m of Andrew Corporation fibre and output pulses for (b) 4 mW (c) 12 mW average power. (d) and (e) corresponding spectra.

In reference [2], it was discovered that in some sense the coupled cavity laser is passively mode-locked. This remarkable feature was observed in our laser also in the following way. The pulse train from the laser was monitored on a fast Ge photodiode and a Tektronix sampling oscilloscope, externally triggered by a signal derived from the Nd:YAG pulse train. The colour centre pulse train (blocked control cavity) was stationary, indicating synchronism with the pump pulses, as would be expected. However, with the control cavity unblocked and the laser operating in a CCM manner, the pulse train no longer appeared stationary but swept across the screen at a variable rate (in both directions)

depending on the control cavity length (the pulse as monitored on the autocorrelator, always remained steady). Thus the CCM laser seemed to be operating in a mode independent of the pump laser since this sweeping of the CCM pulses, meant that they were out of synchronism with the pump pulses and hence synchronous pumping was no longer effective. Although it was not tried here, it was expected that CCM operation would continue for a short time with the AO modulator in the pump laser switched off, pumping continuously, as described in reference [2].

Finally, a curious double pulsing regime was sometimes observed for the longer fibre lengths when a high average power was coupled into the fibre. An example is shown in figure 13 and it was found that this state could be as stable as the single pulse operation.

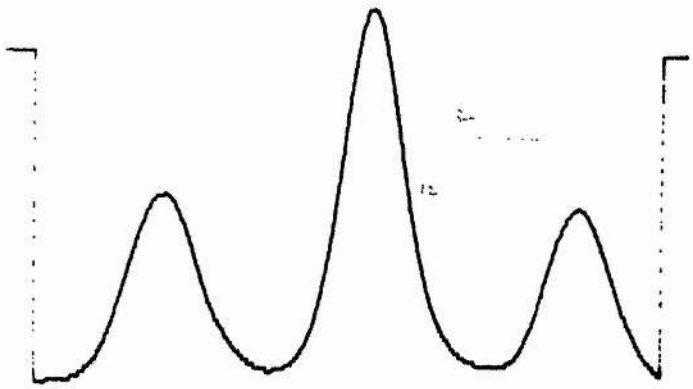

Figure 13.
Autocorrelation of the stable double pulsing operation of the CCM for a fibre length of 2.2 m and an average power ≈ 25 mW.

In chapter 5 where negative (anomalous) GVD fibre was used, qualitatively similar results (in terms of actual CCM operation) to those described above were observed. In this case the reinjected pulses were shorter in duration than those exiting the laser and for a given fibre length, the laser pulses were shorter in duration for this negative GVD fibre than with the positive GVD fibre. It was also noticed that (for the negative GVD fibre of the last chapter) a slight shift in wavelength sometimes occurred between the

synchronously pumped colour centre laser and the CCM laser, depending on the length of the control cavity.

6.3.1 The LiF:F_2^+ Coupled-Cavity Laser.

Although in the experimental configuration of figure 1, the fibre itself provided positive GVD, any glass within the master cavity (e.g. Brewster-angled plates, output coupler) would have negative GVD and therefore possibly lead to temporal compression of the frequency-chirped pulses. In order to verify that this was not responsible for the enhanced mode-locking, a similar experiment was performed using a synchronously mode-locked LiF:F_2^+ colour centre laser [8]. This produced pulses of typically 4 ps duration at a wavelength near 900 nm where the material dispersion for glass is positive and so nowhere in the system would pulse compression occur due to negative GVD. A coupled-cavity arrangement was set up with a 2 m length of monomode, polarisation preserving fibre similar to that previously described. With feedback from the control cavity an observable pulse reshaping and narrowing occurred, the laser pulses being shortened to ≈ 1.3 ps - see figure 14.

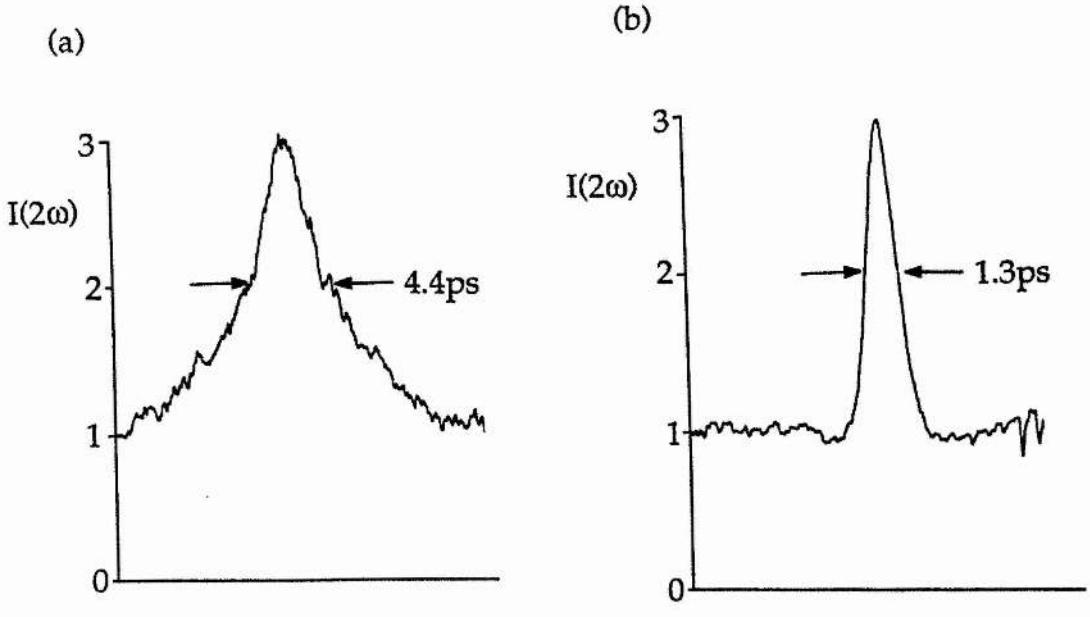

Figure 14.
Autocorrelation traces of (a) the synchronously mode-locked LiF:F_2^+ colour centre laser and (b) in coupled-cavity operation.

In this case the CCM laser was operated without a stabilisation loop but it was found that the output was more unstable than that for the KCl:Tl CCM laser also without stabilisation.

6.4 The CCM Laser with a Semiconductor Diode Amplifier.

Blow and Wood [9] have studied theoretically the effect of both a saturable absorber and a saturable amplifier within the control cavity of a CCM laser. While the former returns, to the master cavity, pulses shorter in duration, the latter may return broader pulses. Interestingly it was predicted that both nonlinear elements should enhance the mode-locking of a colour centre laser. Stimulated by this, it was decided to try a semiconductor diode in place of the fibre in the control cavity to act as a saturable amplifier. Also, a recent report [23], has demonstrated the compression of pulses enabled by the gain saturation-induced temporal variations in the refractive index, leading directly to a frequency chirp being imposed upon the pulse through SPM. The experimental arrangement was identical to that in figure 1 but with an InGaAsP diode [10] replacing the fibre. Operated in a DC mode with injection currents in the range 10 - 35 mA (higher currents were not used to prevent laser action occurring between one facet of the diode and mirror M_3), our initial results showed a pulse shortening to ~ 1.5 ps. Figure 15 is a plot of the pulse duration obtained against diode current where the inset is a typical autocorrelation of the output pulse for I = 35mA. The average power measured just before the diode (and just after the ND attenuator) was approximately 10 mW, thus the actual power fed back into the laser was much less than in the fibre case. By optimisation of the cavity (specifically by insertion of a thinner birefringent filter plate) pulse durations of approximately 250 fs were obtained which is comparable performance to that of the fibre based control cavity. In this (diode amplifier) case, the CCM laser was observed to suffer regular dropouts, i.e. switching to the much broader colour centre laser pulses.

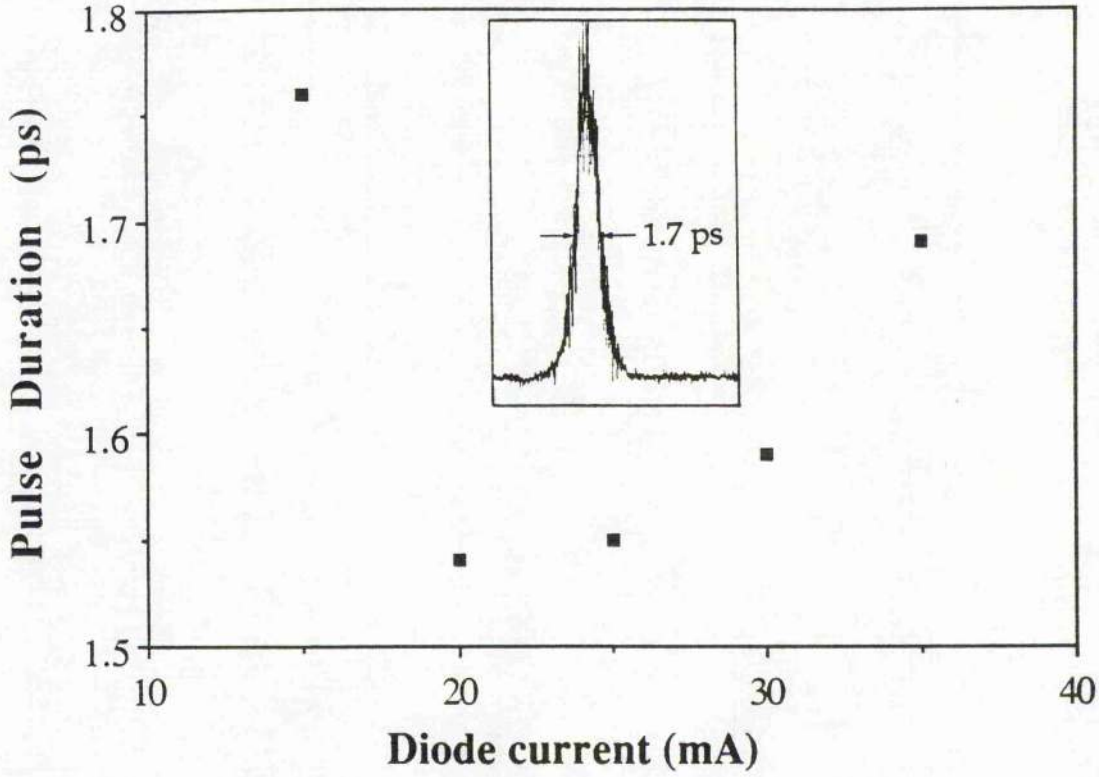

Figure 15.
The CCM laser output pulse duration as a function of diode current. Inset: typical autocorrelation for a current of 35 mA.

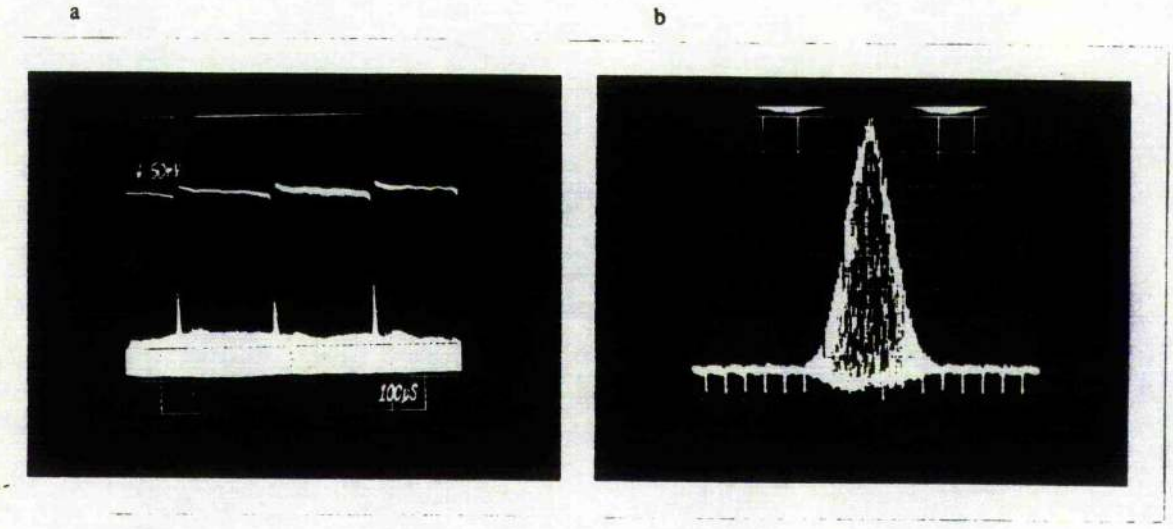

Figure 16.
(a) Exposure of the diode CCM pulse train (b) pulse autocorrelation; both show the regular dropouts seen in this case.

The stabilisation loop, although compensating for relatively slow cavity length changes, was not able to eliminate these sudden and periodic dropouts. Figure 16a shows

the pulse train and fig.16b is an exposure of the autocorrelation trace, both indicate the regular dropouts. It was also found that the period of the dropouts could be varied over ~ 20 - 0.5 ms (50 Hz - 2 kHz) by adjusting the cavity length of the colour centre laser but could never quite be eliminated altogether. The average power fed back into the master cavity in this case was estimated to be less than 0.2 mW, that is ~ 0.05% of the intracavity power, and yet this was still sufficient to produce the dramatic narrowing of the laser pulses described here. Because of this extremely small feedback power, we were unable in this case to monitor the return pulses.

6.5 A Discussion of the CCM Process.

Primarily six observations about the operation of the coupled-cavity colour centre laser may be made from the above results:

(i) temporal compression of the pulses in the control cavity is not required, provided the pulse frequency spectrum is broadened by some nonlinear process;

(ii) the enhanced mode-locking process is not due to pulse compression resulting from negative GVD elements within the main cavity;

(iii) for stable operation, the feedback pulses need to have a particular, constant phase relative to those circulating in the main cavity;

(iv) the CCM laser appears to run on its own frequency - independent of the pump pulse repetition rate;

(v) with the fibre based control cavity, some self adjustment seems possible due to the dispersion of the fibre, enabling a small tolerance on the precise length of the control cavity. To some extent this also produces a shift in wavelength of the CCM laser from the colour centre alone (only observed in the negative GVD fibre case);

(vi) the CCM pulse width generally decreases with fibre length.

An explanation of the CCM process would need to encompass all of these observations as well as those pertaining to the 'soliton' laser (i.e. negative GVD in the control cavity) described in chapter 5. It would also be desirable for the model to reproduce the stable double pulsing operation which has been observed here and elsewhere [11].

Several theoretical papers attempting to model the soliton laser have been published [3,12-14] but most of these demand that the control cavity returns a narrower pulse than incident. Blow and Wood [3] have predicted the actual operating point to be more complex than a straight forward N=2 soliton and also obtained a prediction about the double pulsing case for high powers in the control cavity, as observed here for both positive and negative GVD fibres. Over the last year several papers [4,5,9,15] have appeared dealing with the more general case of coupled-cavity mode-locking.

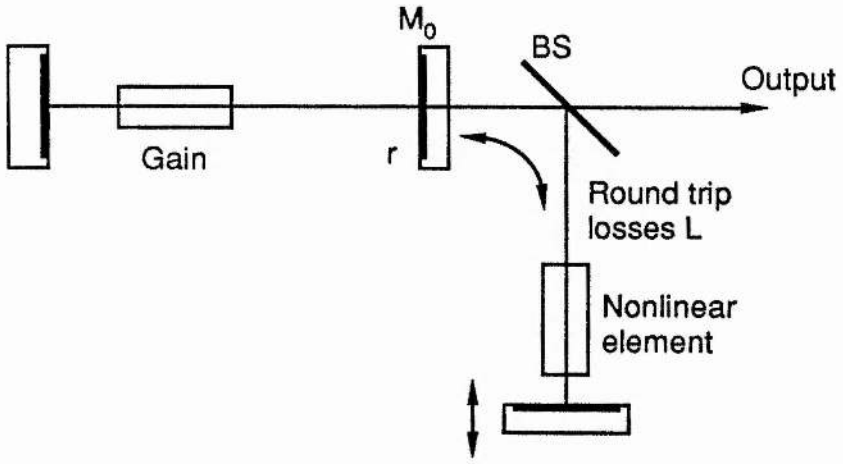

Figure 17.
A schematic diagram of a coupled-cavity laser. Mirror M_0 has an amplitude reflectivity r and the round trip amplitude attenuation factor of the control cavity is L.

A simple model of the process by Mark et al [5], considers the pulses interfering at the mirror M_0. If a pulse is returned from the matched control cavity unchanged in any way (e.g an empty external cavity), then the pulses will either constructively or destructively interfere if there is a phase shift of 0 or π respectively, between the peaks. In this case the external cavity acts to effectively change the reflectivity of the output coupler M_0. This gives rise to the observed power fluctuations as vibrations etc. change the relative phase of the interfering pulses. Note that the same degree of constructive or destructive interference

occurs across the full temporal extent of the pulse. If the control cavity pulse acquires an intensity dependent phase shift due to SPM, the maximum shift occurs at the peak of the pulse and decreases in the wings. If also the control cavity length is arranged so that there is zero phase shift between the peaks of the return and main cavity pulses, less than complete constructive interference will occur everywhere except at the peak and the net result is that a shorter pulse is returned to the gain medium from M_0. With reference to figure 17, the fields reflected from the output mirror, M_0, can be expressed as

$$b_1 = r\, a_1 + (1- r^2)^{1/2}\, a_2$$
$$b_2 = - r\, a_2 + (1- r^2)^{1/2}\, a_1 \qquad (6.1)$$

where a_1, b_1 and a_2, b_2 are the fields incident and reflected from M_0 in the main and control cavities respectively. If we assume that the two cavity lengths are matched apart from a phase mis-match, ϕ, then

$$a_2(t) = b_2(t)\, L \exp -j\, \phi \qquad (6.2)$$

where L is the round trip attenuation factor of the control cavity, ϕ is the phase mis-match and will be composed of two parts. That due to a length mis-match ϕ_L, for a low intensity pulse, and a time dependent part $\Phi(t)$, due to SPM. This nonlinear part may be written as:

$$\Phi(t) = \kappa[\, |b_2(t)|^2 - |b_2(0)|^2\,] \qquad (6.3)$$

and so $$\phi = \phi_L + \Phi(t)$$

κ is a constant proportional to the nonlinear index, the peak intensity of the pulse and (for a fibre based control cavity) the fibre length. The phase shift at the peak of the pulse (t=0), $\kappa|b(0)|^2$, is subtracted from Φ, so that ϕ contains a bias due to the nonlinear phase shift at the pulse peak. Thus $\Phi = 0$ at the peak of the pulse and becomes negative in the wings. The amplitude reflection coefficient of M_0, b_1/a_1, may be obtained by combining equations (6.1) and (6.2) to give:

$$\Gamma = \frac{b_1}{a_1} = \frac{1 + r/L \exp j\, \phi}{r + 1/L \exp j\, \phi} \qquad (6.4)$$

Figure 18 shows a plot of $|\Gamma|$ ($=\sqrt{\Gamma\,\Gamma^*}$) as a function of the phase angle ϕ (upper curve) and its derivative (lower curve), for r = 0.9 (i.e mirror reflectivity ≈80%) and L = 0.3 (compounded of approximately 50% beamsplitter reflectivity and 70% coupling efficiency through the fibre). For $\phi = 0$ (or 2π etc.) then the effective reflectivity of M_0 is seen to be a maximum, but only at the peak of the pulse since in the wings $\phi < 0$ and the reflectivity decreases. Hence, as described above, the peak of the pulse experiences a higher reflectance and effectively a shorter pulse is returned to the gain medium. In the region were the reflectivity gradient is negative, $|\Gamma|$ *decreases* at the pulse peak and so no stable CCM operating point would be expected. Actually, $\phi = 0$ is also not a preferred operating phase value and there are two reasons why this is so. In the first place, we see that if $\phi \sim -\pi/2$ (or $3\pi/2$ in figure 18) say, then the magnitude of the change in $|\Gamma|$ is greater for a given $\Phi(t)$ - as indicated by the larger value of $d|\Gamma|/d\phi$.

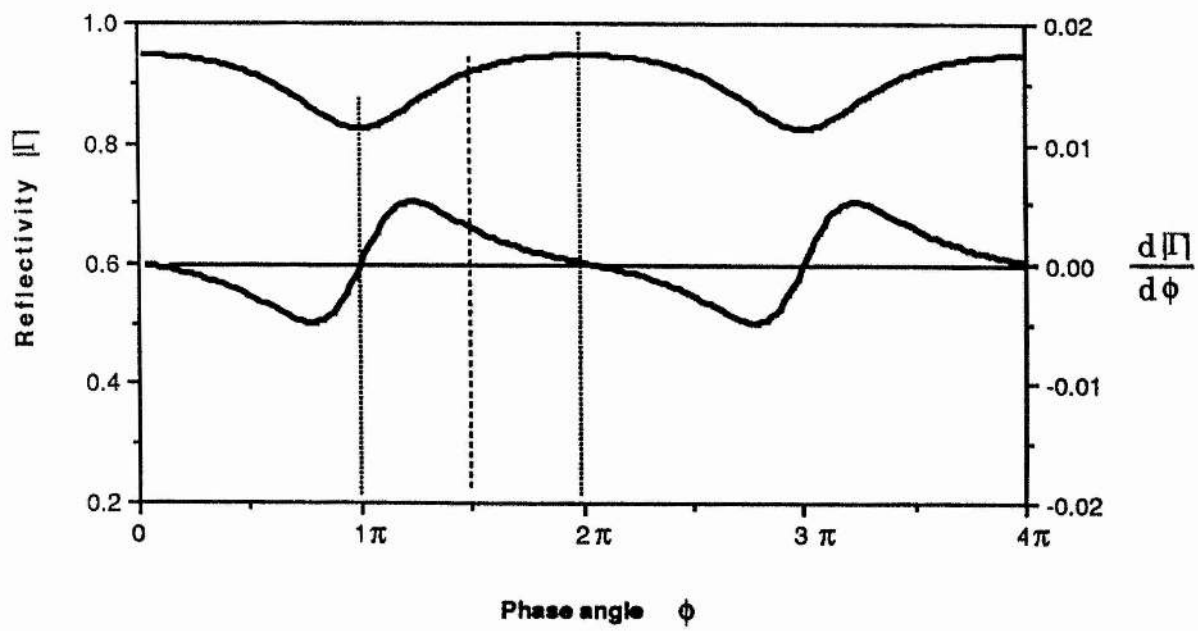

Figure 18.
A plot of the effective mirror reflectivity ($|\Gamma|$) of M_0 (upper curve) and its derivative with respect to ϕ (lower curve).

That is, the pulse shortening per round trip is greater for $\phi = -\pi/2$ than for $\phi = 0$. A second restriction on ϕ for stable operation may be seen if we consider the build up of the coupled-cavity mode-locking process. Consider the case of ϕ slightly less than or equal to 2π. As soon as the control cavity is unblocked the intracavity pulse begins to shorten, increasing the peak intensity and therefore pushing up the peak value of ϕ. This causes greater pulse shortening, a higher intensity and even more SPM, so increasing further ϕ_{max}. It is then quite likely that this peak value of ϕ will be pushed over to $\phi > 2\pi$, which is the unstable region and then no stable operating point will be found. So it would seem that a small range of phase values, around $\phi = -\pi/2$ (i.e. some intermediate power level), are preferred and this was in fact observed experimentally. Generally in the experiments, it was found that the laser would stabilise for only one sign of feedback polarity as expected from the above. Occasionally however, stable operating points could be found for both polarities (also observed by Mollenauer [2]) and it is not yet clear why this should be so. The avalanche effect described above whereby shorter pulses cause more SPM and so on, explains the rapid turn-on of CCM action and Mark et al [5a], have shown that this turn-on point corresponds to the region where $d|\Gamma|/d\phi$ is a maximum, i.e. where $|\Gamma|$ is most sensitive to phase variations.

It is important to note that this process does not rely upon any reshaping of the pulse envelope and is therefore not dependent on any dispersion within the control cavity. The laser pulse shortening per round trip, may be described as a pulse shortening velocity and in this regard any GVD (positive or negative) within the fibre (or nonlinear element) serves to decrease this velocity and limit the steady state duration of the laser pulses. This would imply that for a given length, fibres with a lower dispersion value, D, should enable the production of shorter pulses. Comparing various results reported in the literature, this would seem to be the case - see Table 1. This also explains the decrease in pulse duration with fibre length since shorter fibre lengths mean a smaller total dispersion value in the control cavity but it is not clear to date, as to the exact relation between the ultimate steady state pulse duration and dispersion.

Table 1.

Reference	Fibre dispersion	Fibre length	τ_p from CCM	Shortening factor
This work	+40 ps/nm/km	40 cm	500 fs	~ 30
[1]	-15 ps/nm/km	≈ 40 cm	≈200 fs	~ 50
[5]	+2 ps/nm/km	40 cm	130 fs	~ 170
[16]	-2.2 ps/nm/km	40 cm	60 fs	~ 170

Table displaying the pulse durations from a KCl:Tl CCM laser reported by various groups for a fibre length of 40 cm. Positive dispersion values imply normal GVD and visa versa.

Developing their theory, Blow and Wood [9] have studied the effect of including a nonlinear element in the control cavity which may either return narrower or broader pulses to the main cavity and the observations presented in this chapter are qualitatively in agreement with their predictions. The synchronously pumped laser alone has a mode-locked bandwidth determined by the pump pulse intensity. Modulating the pump beam causes the excitation of cavity sidebands from the central frequency, ω_0, of the gain medium. These sidebands will tend to be phase locked to the central frequency by stimulated emission. Away from ω_0 the amplitude of these sidebands decreases until they are eventually lost in the spontaneous noise level, so ceasing to be phased locked. Greater gain modulation causes sidebands further from ω_0 to be phase-locked, enabling a larger mode-locked bandwidth and the generation of shorter pulses. Generally a bandwidth limiting element is included to restrict laser oscillation to only those modes which are phase-locked. The central question is then, how does the nonlinear element in the control cavity increase the mode-locked bandwidth?

Blow and Wood suggest that the nonlinear element provides induced coupling between the longitudinal modes of the laser cavity, enabling more efficient communication of phase information to the extreme edges of the lasing bandwidth, thereby increasing the mode-locked bandwidth. This could perhaps be described as a type of induced FM mode-locking involving an external cavity where the nonlinear element acts as a kind of passive (self) phase modulator. Although these are quite general descriptions of mode-locking, in this case the injection locking of more cavity modes occurs through the presence of the nonlinear external control cavity. Since it is only the communication of

phase information (in order to phase lock more cavity modes) that is important, this would explain why only a very small fraction of the intracavity power need be injected back into the main cavity for the external cavity to completely dominate the mode-locking of the laser. The results of [9], show that even if the injected pulse has a narrower bandwidth than the initial *lasing* bandwidth of the laser, an enhancement in the mode-locked pulses can still occur as the *mode-locked* bandwidth is increased by the above mechanism. Our results so far indicate that in all cases where we observe enhanced mode-locking, the bandwidth of the return pulse is greater than that exiting the laser. A slightly different explanation of the CCM process to that above, is that the increased mode-locked bandwidth occurs due to the injection of energy into modes far from the gain peak. Although the signal fed back into the main cavity is very small, the increased spectral width means that there is proportionally more energy in the edges of the pulse spectrum.

It was noted earlier that the CCM laser exhibited a kind of passive mode-locking in that the pulse round trip time did not synchronise to the pump laser pulses. Thus it seems that although synchronous pumping serves to initiate the process, CCM operation does not generally depend upon a modulated gain. In this regard it is important to note that the long excited state lifetime (1.6 μs) of KCl:Tl is advantageous for the CCM process. A gain medium with a short lifetime (~ just a few round trips) would loose a significant amount of energy by spontaneous emission when the pump and laser pulses were not coincident in the gain medium. This would probably cause the CCM output to be unstable if not preclude its initiation. In contrast, the KCl:Tl acts as gain storage medium ensuring that a net gain is available even when the pump and laser pulses are in anti-phase. Any perturbations (eg in the pump laser) become more critical when the slave laser upper state lifetime is relatively short and will thus more strongly influence CCM operation. For the coupled cavity LiF:F_2^+ experiment, the enhanced mode-locking was observed to be more unstable and this may be attributed to the shorter lifetime (~ 29 ns) of the excited state.

The observation that small adjustments in the length of the control cavity could be tolerated may be due to the dispersion of the fibre. A slight mismatch in cavity lengths could be corrected for by a slight shift in wavelength, thus altering the optical path length

of the control cavity. Although a definite shift was observed in some cases for the soliton laser, as described in the last chapter, no significant shift was seen in the normal GVD fibre case. This may be due to the fact that the dispersion of this fibre was much larger and so only an extremely small wavelength shift was required for compensation. This effect may also have some relevance to the fact that in the diode amplifier case, the CCM laser was observed to suffer regular dropouts. Since no dispersion compensation was available, cavity length mismatches would cause the pulses to be improperly overlapped and CCM operation would falter. This is also supported by the fact that the period of the dropouts could be adjusted by altering the master cavity length, but it still is not clear why they could not be eliminated. The luminescence decay time of the gain medium may also be important for CCM operation in terms of gain saturation effects. In a gain medium with a long luminescence decay time, gain saturation plays a reduced role in pulse shortening in a mode-locked laser - hence the need for high intracavity powers in synchronously pumped KCl:Tl lasers, than in a laser with a short excited state lifetime, say dye lasers. Thus it may be that the external cavity will have a smaller effect on the mode-locking of lasers containing gain media with short upper state lifetimes, since these will already be effectively mode-locked by synchronous pumping. In order to increase the influence of the control cavity, an increased coupling between the cavities may be necessary.

It is worth commenting on some earlier experiments performed with coupled-cavities were an active element, namely an AO modulator, was inserted in the control cavity. This seems to have been first suggested as a method of mode-locking a laser in 1965 [17]. An AO modulator is placed in a matched external cavity and driven at a frequency corresponding to half the intermodal frequency spacing of the CW pumped laser. This will induce a Doppler shift onto the first order diffracted beam equal to the cavity mode spacing (after two passes) in a manner similar to that described in chapter 2. Thus a fraction of laser energy is injected into the laser at an adjacent cavity mode and this Doppler shifted mode locks to the fundamental by injection locking [18,19]. This continues, the laser bandwidth widening and the output becomes a train of mode-locked pulses. A similar experiment has been performed with the AO modulator acting as a modulated loss element in the control

cavity [20]. Surprisingly in these experiments, no mention was made of any necessary interferometric stabilisation between the two cavities.

6.6 Conclusions.

The results presented in this chapter have shown that the existence of negative GVD in the control cavity of a KCl:Tl colour centre laser is not necessary to provide an enhancement in the mode-locking. The effect has also been observed in a LiF:F_2^+ laser, indicating beyond doubt that anomalous GVD is not required anywhere in the system. A semiconductor diode amplifier in the control cavity has also been demonstrated to give similar results, in agreement with previous theoretical considerations by Blow and Wood [9]. The control cavity seems to completely dominate the mode-locking characteristics of the laser even when the injected power is only a fraction of that in the master cavity.

One may ask the question why not include the nonlinear element within the main cavity itself, thereby eliminating the problem of coupled cavities and stabilisation? In the first place, by using an external cavity, losses involved in coupling into the nonlinear element (fibre etc.) become much less important and the main laser cavity may remain unaltered, having the same threshold value and able to produce high output powers. Also, as for the diode amplifier case, the power required within the nonlinear element may be much less than that in the main cavity, where it would be clearly disadvantageous to reduce the power.

Finally we may address the question as to whether the technique may be applied to other broad bandwidth lasers. It seems that synchronously pumped lasers will work well in a coupled-cavity mode especially where the gain medium has a long (~ microsecond) upper state lifetime. Most recently several groups have observed similar mode-locking enhancement in other lasers [21]. Perhaps one of the more exciting results has come from CCM operation of a Ti:Sapphire laser (tunable over 650 nm - 1.1 μm) which has been reported to produce pulses ~ 1ps duration [21,22], compared to ~ 50 ps without the control cavity. (This gain medium has an excited state lifetime ≈3.2 μs, which is very close to that of KCl:Tl.) A Nd:YAG laser has recently been mode-locked in a coupled cavity

arrangement using a nonlinear mirror [21], although the extremely long lifetime of this gain medium (250μs) causes the laser to readily break into relaxation oscillations. One way around this problem of needing long excited state lifetimes, may be to pump the laser CW and either actively (acousto-optically) mode-lock or include an AO modulator in the control cavity as in ref. [18], to provide initiation of the CCM process, together with a length of optical fibre. Several interesting avenues of investigation remain therefore, in order to fully examine and to exploit, the full potential of the coupled-cavity mode-locking process.

References.

1. L F Mollenauer, R H Stolen; Opt. Lett. **9**, 13 (1984)
2. F M Mitschke, L F Mollenauer; IEEE J. Quant. Electron. **QE-22**, 2242 (1986)
3. K J Blow, D Wood; IEEE J. Quant. Electron. **QE-22**, 1109 (1986)
4. K J Blow, B P Nelson; Opt. Lett. **13**, 1026 (1988)
5. J Mark, L Y Liu, K L Hall, H A Haus, E P Ippen; Opt. Lett. **14**, 48 (1989)

5a. J Mark, L Y Liu, K L Hall, H A Haus, E P Ippen; IEE Colloquium May 1989

6. K C Byron; Electronics Lett. **23**, 1324 (1987)
7. J C Diels, J J Fontaine, I C McMichael, F Simoni; Appl. Opt. **24**, 1270 (1985)
8. N Langford, K Smith, W Sibbett; Opt. Comm. **64**, 247 (1987)
9. K J Blow, D Wood; J. Opt. Soc. Am. B **5**, 629 (1988)
10. P Besomi, R B Wilson, R L Brown, N K Dutta, P D Wright, R J Nelson; Electron. Lett **20**, 417 (1984)
11. L F Mollenauer; Phil. Trans. R. Soc. London A **315**, 437 (1985)
12. H A Haus, M N Islam; IEEE J. Quant. Electron. **QE-21**, 1172 (1985)
13. F If, P L Christiansen, J N Elgin, J D Gibbon, O Skovgaard; Opt. Comm. **57**, 350 (1986)
14. P A Belanger; J Opt. Soc. Am. B **5**, 793 (1988)
15. S M J Kelly; Opt. Comm. **70**, 495 (1989)
16. F M Mitschke, L F Mollenauer; Opt. Lett. **12**, 407 (1987)
17. L C Foster, M D Ewy, C B Crumly; Appl. Phys. Lett. **6**, 6 (1965)
18. R W Dunn, S T Hendow, J G Small, E Stijns; Appl. Opt. **21**, 3984 (1982)
19. C Buczek, R Freiberg, M Skolnick; Proc. IEEE **61**, 1411 (1973)
20. M. DiDomenico, V Czarniewski; Appl. Phys. Lett. **6**, 150 (1965)
21. See papers in session FQ; Conference on Lasers and Electro-Optics, CLEO '89 Technical Digest vol.11 (1989)
22. J Williams, P French, J R Taylor; Laser Focus p.9 January 1989.
23. G P Agrawal, N A Olsson; Paper THI5, CLEO'89 Technical Digest (1989)

Chapter 7.

General Conclusions.

The work presented in this thesis has been concerned with the generation of ultrashort near infrared laser pulses and the nonlinear propagation of such pulses in optical fibres. Using the Nd:YAG laser as a pump source, which produced pulses of duration ~ 100ps at 1.06 μm, an investigation of self-phase modulation (SPM) and stimulated Raman scattering (SRS) in single-mode optical fibres was conducted. Over sufficiently short lengths of fibre that the effect of group velocity dispersion may be neglected, these pulses were seen to obey a simple theory giving a frequency broadening linear with the launched optical power. A deviation from this relationship occurred due to the onset of stimulated Raman scattering, causing an attenuation of the leading edge of the pulse and a consequent increased spectral broadening towards longer wavelengths. The use of SPM for optical pulse compression has been demonstrated and the ≈120ps Nd:YAG laser pulses were compressed to ≈ 5ps by a pair of diffraction gratings. This pulse compression technique has been extensively used in many laboratories and has become a standard method for the production of picosecond and subpicosecond optical pulses [1,2]. Recent experiments [3,4] have shown that contrary to initial assumptions, the nonlinear process of stimulated Raman scattering actually aids the stability of the compressed pulse train by reducing peak power fluctuations (which cause fluctuations in the degree of spectral broadening) within the fibre.

Utilising SRS in a length of fibre, the construction of a synchronously pumped fibre Raman oscillator (FRO) has been demonstrated. This enabled the production of frequency tunable, ultrashort pulses over the range 1.07 - 1.12 μm, by the technique of time dispersion tuning. Incorporating a pair of fibre optic reflection gratings into the FRO, transforms the device into an all fibre laser, which has the potential to be very compact and stable once all the fibre joints are fusion spliced. Simply by launching mode-locked pulses

into the fibre, frequency shifted mode-locked pulses can be obtained and no alignment is necessary. Although the addition of gratings to the FRO restricts the operation to a fixed wavelength, tuning could be accomplished by varying some parameter of the grating (the grating period, surface index) and by stretching the fibre in some way, causing the laser to favour a different wavelength because of time dispersion tuning. The fibre Raman oscillator and its counter part in the anomalous GVD regime, the fibre Raman soliton laser [5,6], have received substantial interest over the last few years as simple but effective sources of near infrared ultrashort pulses.

A more direct approach to the generation of ultrashort pulses in the near infrared, is with the use of colour centres. Chapter 4 has described the operation of two colour centre lasers, using KCl:Tl and NaCl:OH^- crystals as the gain media. Although they require operation at cryogenic temperatures, these crystals are able to produce ultrashort pulses in the important 1.5 μm wavelength region, with average powers in excess of 1W [7,8]. These two centres, the thallium centre in KCl and the defect stabilised F_2^+:O_2^- centre in NaCl, are unparalleled in terms of stability and crystal lifetime. The KCl:Tl crystal has a useful lifetime >1 year, tunable over approximately 1.45 - 1.55 μm and pumped by 2W from the Nd:YAG laser, has successfully produced ≈ 100 - 200mW for that time. The relatively recent discovery of NaCl:OH^- provides another source tunable over 1.4 - 1.6 μm and has so far been reported to show no fading properties at all, provided it is illuminated with auxiliary radiation preventing orientational bleaching [8-10]. Synchronous mode-locking of these lasers enables the production of pulses ~ 1 - 10 ps in duration [7,8].

In chapter 5 the nonlinear propagation of pulses at 1.5 μm in an optical fibre was examined. It is in this wavelength region that the fibre dispersion is anomalous and, combined with SPM, leads to the formation of optical solitons. Since a pulse in this wavelength region (with a power greater than that required for the fundamental soliton) always experiences an initial narrowing, pulse compression is obtained without the use of external components such as diffraction gratings. Simple soliton-like pulse splitting was observed for a pulse of ≈ 18 ps launched into a length of fibre, roughly in agreement with predictions for the pulse shapes expected at half the soliton period. Modern optical fibres

have a minimum attenuation at 1.55 μm and so this is a very possible operating wavelength for future optical telecommunications systems. Many calculations have been performed on estimating the maximum transmission data rates using solitons in a digital communications system [11-13]. In a fibre with zero attenuation, solitons would propagate indefinitely without any temporal broadening (pulse shape evolution occurs but the maximum duration of the intensity envelope at any point along this ideal fibre, never exceeds the input pulse duration [12]). Note that due to the existence of the soliton self-frequency shift [14,15], pulses of duration not less than 10ps would be preferred so that over long distance fibre cables, self frequency shifting becomes negligible. For such pulses the power required to obtain the fundamental soliton is extremely low and would be easily obtained from present day semiconductor diode lasers. However a real fibre does not have zero attenuation and so over a long distance fibre optic cable, the solitons would eventually loose energy and be dispersively broadened with a probable loss of information. In order to compensate for this loss, theoretical [16] and experimental [17] studies have been conducted on the amplification of solitons by Raman gain. The idea is to use wavelength dependent couplers to inject CW light (at ≈1.4 μm) into the main fibre cable, where the solitons experience gain through the process of SRS. In fact a recent experiment has shown distortionless soliton propagation over a remarkable 4000 km [18]. Present day optical communications systems have a transmission data rate of around 200 - 500 Mbit/sec and the first transatlantic optical fibre cable system, TAT8, installed in 1988, has a rate of 280 Mbit/sec. Electronic repeaters (spaced between 20 and 100 km apart), limit the data rate to ~ 1Gbit/sec but with a Raman amplification system and wavelength division multiplexing, rates of up to 100 Gbit/sec could be feasible [19].

By itself, the KCl:Tl colour centre laser produces pulses of typically 10 ps duration tunable around 1.5 μm with an average power of the order of hundreds of milliwatts. The large gain bandwidth, ≈ 100 nm, gives this laser the potential to produce mode-locked pulses of only a few tens of femtoseconds. Incorporating a length of optical fibre into an external control cavity of the laser (chapter 5), has enabled a dramatic enhancement in the mode-locking, with the shortest pulses reported to-date being ≈ 60 fs in duration [20].

Although initially, the explanation of this effect was that of soliton formation in the fibre, the experiments presented in chapters 5 and 6 of this thesis, and also elsewhere [21,22], have now shown that in fact actual soliton formation is a specific case of a more general phenomena, whereby frequency broadened pulses reinjected into the master cavity can cause a great enhancement in the mode-locked characteristics of the laser. It has been seen that pulse narrowing within the control cavity, caused by the existence of anomalous group velocity dispersion, is not required and that provided the frequency spectrum is broadened in a nonlinear way, the mode-locked bandwidth of the laser may be increased. Most experiments so far have been performed with a length of fibre as the nonlinear element. In chapter 6, it was described how similar results were also obtained with a semiconductor diode amplifier in the control cavity. To date this experiment is unique and it is hoped that further studies on this and other nonlinear elements (e.g saturable absorbers, combined active and fibre elements) will be carried out in the near future. There also remains much detailed work to be done on fully characterising and understanding the factors influencing the coupled-cavity mode-locking process.

In this work all the experiments were performed on a KCl:Tl laser but other lasers have also been shown to benefit from the coupled-cavity scheme. One of the most notable being the relatively new solid state titanium sapphire laser [23]. This has a tunability over approximately 700 nm - 1 μm and may well find wide spread applications, replacing many dye laser systems. With its excited state lifetime of 3.2 μs, close to that of KCl:Tl, one would expect a very similar coupled-cavity mode-locked (CCM) behaviour. It is hoped that in the near future, detailed experiments will be conducted on this laser at St. Andrews. The $NaCl:OH^-$ colour centre laser has also been demonstrated to show an enhanced mode-locking due to CCM [24]. This crystal has a greater centre stability, larger tuning range and is also able to produce higher output powers than the KCl:Tl laser, so if it proves to be as successful in a coupled-cavity mode, it should largely replace the KCl:Tl as a gain medium. The applicability of the CCM process to other broad bandwidth lasers has yet to be fully examined, but it does seem that certain pertinent factors, described in chapter 6, may influence the effectiveness of the technique, limiting the ultimate steady state pulse duration

or causing insurmountable instabilities. Despite these misgivings, it is hoped that coupled-cavity mode-locking will be used to enhance the mode-locking characteristics of certain broad bandwidth lasers. The production of ultrashort (picosecond and femtosecond) near infrared optical pulses will continue to be useful in many fields of physics and chemistry, as well having a major technological importance in both the further development of mode-locked lasers and more generally in the field of optical telecommunications.

References.

1. J D Kafka, B H Kolner, T Baer, D M Bloom; Opt. Lett. **9**, 505 (1984)
2. C V Shank, R L Fork, R Yen, R H Stolen; Appl. Phys. Lett. **40**, 761 (1982)
3. A M Weiner, J P Heritage, R H Stolen; J Opt. Soc. Am. B **5**, 364 (1988)
4. M Kuckartz, R Schulz, H Harde; J Opt. Soc. Am. B **5**, 1353 (1988)
5. J D Kafka, T Baer; Opt. Lett. **12**, 181 (1987)

6a. A S Gouveia-Neto, A S L Gomes, J R Taylor; IEEE J Quant. Electron. **QE-24**, 332 (1988)

6b. H A Haus, M Nakazawa; J Opt. Soc. Am. B **4**, 652 (1987)

7. L F Mollenauer, N D Vieira, L Szeto; Opt. Lett. **7**, 414 (1982)
8. J F Pinto, E Georgiou, C R Pollock; Opt. Lett. **11**, 519 (1986)
9. K R German, C R Pollock; Opt. Lett. **12**, 474 (1987)
10. R Beigang, K Klameth, B Becker, Z Yoon, H Welling; Opt. Comm. **65**, 383 (1988)
11. A Hasegawa, Y Kodama; IEEE Proc. **69**, 1145 (1981)
12. N J Doran, K J Blow; IEEE J Quant. Electron. **QE-19**, 1883 (1983)
13. D Anderson, M Lisak; Opt. Lett. **11**, 659 (1986)
14. F M Mitschke, L F Mollenauer; Opt. Lett. **11**, 659 (1986)
15. J P Gordon; Opt. Lett. **11**, 662 (1986)
16. A Hasegawa; Opt. Lett. **8**, 650 (1983)
17. L F Mollenauer, R H Stolen, M N Islam; Opt. Lett. **10**, 229 (1985)
18. L F Mollenauer, K Smith; Opt. Lett. **13**, 675 (1988)
19. L F Mollenauer; Optics News p42 May 1986
20. F M Mitschke, L F Mollenauer; Opt. Lett. **12**, 407 (1987)
21. K J Blow, B P Nelson; Opt. Lett. **13**, 1026 (1988)
22. J Mark, L Y Liu, K L Hall, H A Haus, E P Ippen; Opt. Lett. **14**, 48 (1989)
23. J Goobert, J Wang, J G Fujimoto, P A Schulz, S Henion; Conference on Lasers and Electro-Optics, paper FQ4 CLEO'89 Technical Digest (1989)
24. C P Yakymyshyn, J F Pinto, C R Pollock; CLEO'89 Technical Digest, paper FQ3 (1989)

Appendix.

A derivation of the expression (equation 3.14) for simple dispersive broadening of a gaussian pulse along a length of optical fibre.

The input pulse (with no frequency chirp) is assumed to be of the form

$$\varepsilon(t) = \exp(-at^2)\exp j(\omega_0 - \beta z) \qquad \{\tau_p = \sqrt{2\ln 2/a}\}$$

We then Fourier transform this to give:

$$E(\omega,z) = \sqrt{\frac{\pi}{a}}\exp\left(\frac{-(\omega-\omega_0)^2}{4a}\right)\exp\{-j\beta z\}$$

In a dispersive fibre $\beta = \beta(\omega)$ and expanding this about ω_0

$$\beta(\omega) = \beta(\omega_0) + \beta'(\omega-\omega_0) + 1/2\,\beta''(\omega-\omega_0)^2 + \ldots$$

after a length L, the pulse will have aquired a phase shift $\exp -j\beta L$, hence

$$E(\omega,L) = \sqrt{\frac{\pi}{a}}\exp\{-j\beta_0 L - j\beta'(\omega-\omega_0)L - (1/4a + j\,1/2\beta''L)(\omega-\omega_0)^2\}.$$

We then take the inverse Fourier transform of this :

$$\varepsilon(t,L) = \sqrt{\frac{\pi}{a}}\frac{\exp j(\omega_0 t - \beta_0 L)}{2\pi}\int_{-\infty}^{\infty}\exp -\{Pu^2 + j(\beta' L - t)u\}\,du$$

where $P = 1/4a + j1/2\beta''L$ and $u = \omega - \omega_0$. Performing this integral and after some algebra, the following expression for ε is obtained

$$\varepsilon = \frac{1}{2(1/4 + j1/2\beta''La)}\exp\frac{(\beta' L - t)^2\,(1/a - 2j\beta''L)}{1/a^2 + 4\beta''^2L^2}\exp\{j(\omega_0 t - \beta_0 L)\}$$

The intensity envelope of the pulse is $\varepsilon.\varepsilon^*$ and the FWHM pulse duration is found by setting the exponential part to 1/2. Once this has been done we get

$$\tau = [\,\ln 2/2a + 2a\ln 2\,\beta''^2L^2\,]^{1/2}$$

The FWHM is 2τ and remembering that $\tau_{in} = \sqrt{(2\ln 2/a)}$, the final equation is obtained:

$$T_{out} = \left(T_{in}^2 + \left[\frac{4\ln 2\,\beta``\,L}{T_{in}}\right]^2\right)^{1/2} \qquad (3.14)$$

Acknowledgements.

I would like to express many thanks to my supervisor, Professor Wilson Sibbett, for his continued support and guidance throughout the duration of this project. I would also like to thank Dr Kevin Smith and Dr Nigel Langford for their help, especially during the early stages and Dr Bill Sleat for his invaluable help with electronics. I am grateful to the technical workshop staff who have constructed several pieces of equipment and to Bob Mitchel for his help with the various vacuum and cryogenic aspects of the work.

I feel that I must mention the 'guys' who have formed the WS group, for the many, varied and fruitful (?!) discussions that have been had. Also thanks to David Crust for much help with the computing side of things.

Finally, I am indebted to the Science and Engineering Research Council for financial support.

Publications.

1. P N Kean, K Smith, W Sibbett; *Opt Comm.* **61**, 129 (1987) 'Modulator Detuning Effects in a CW Mode-locked Nd:YAG Laser with Active Stabilisation'.
2. K Smith, P N Kean, D W Crust, W Sibbett; *J. Mod. Optics* **34**, 1227 (1987) 'An Experimental Study of a Synchronously Pumped Fibre Raman Oscillator'.
3. P N Kean, K Smith, W Sibbett; *IEE Proc. pt J* **34**, 163 (1987) 'Spectral and Temporal Investigation of Self-Phase Modulation and Stimulated Raman Scattering in a Single Mode Optical Fibre'.
4. P N Kean, K Smith, B D Sinclair, W Sibbett, C J Rowe, D C J Reid; *Elecron. Lett.* **23**, 1241 (1987) also: *J. Mod. Optics* **35**, 397 (1988) 'Characterisation of a Fibre Raman Oscillator Using Fibre Grating Reflectors'.
5. P N Kean, X Zhu, D W Crust, R S Grant, N Langford, W Sibbett; *Opt. Lett.* **14**, 39 (1989) 'Enhanced Mode-locking of Colour Centre Lasers'.

MODULATOR FREQUENCY DETUNING EFFECTS IN A CW MODE-LOCKED Nd:YAG LASER WITH ACTIVE STABILISATION

P. KEAN, K. SMITH and W. SIBBETT
Physics Department, University of St. Andrews, North Haugh, St. Andrews, Fife KY16 9SS, Scotland

Received 30 July 1986; revised manuscript received 10 September 1986

The effect of modulator frequency detuning in a cw mode-locked Nd:YAG laser has been studied. For small negative detunings (~150 Hz) from the frequency which produces the shortest pulses, amplitude fluctuations due to relaxation oscillations were drastically reduced but at the expense of pulse broadening. Further negative frequency detuning (in the region ~ 2–4 kHz) led to the formation of undamped relaxation oscillations or stable Q-switched operation.

1. Introduction

The cw mode-locked Nd:YAG laser is now well established as a pump source (employing both the fundamental (1.064 μm) and second harmonic emissions) for dye [1–3] and colour centre [4] lasers. The most recent advance in the latter system type has been the development of a soliton laser [5] capable of generating optical pulses <100 fs duration at ~1.55 μm. The high sensitivity of the cw mode-locked Nd:YAG laser output characteristics to modulator frequency or cavity length detuning is well known. In this paper, we investigate modulator frequency detuning effects in such a laser with active modulator stabilisation and observe that significant enhancement in pulse amplitude stability on a timescale ~10 μs can be achieved by slight detuning from the shortest pulse modulator frequency. We also investigate experimentally in some detail the phenomenon of Q-switching by drive frequency detuning. It is worth noting that the effects described in this paper were also observed to result from variations in cavity length detuning. The magnitude of such length detuning was in agreement with the corresponding frequency detuning measurements.

2. The experimental arrangement

The experimental arrangement, shown in fig. 1, consisted of a Spectra Physics Series 3000 cw mode-locked Nd:YAG laser in conjunction with a synchronously operating ("Synchroscan") streak camera system. The cw Nd:YAG laser was mode-locked with a high-Q acousto-optic modulator incorporating an active stabilisation feedback loop similar to that developed by Klann and coworkers [6]. This system, which ensured that the acousto-optic resonance and the electrical drive frequency (~41 MHz) remain locked even for high ($\gtrsim$1.2 W) rf powers, provided typical time averaged powers ~8–9 W ~80 ps duration pulses separated by ~12.4 ns at 1.064 μm for a lamp current ~17 A. The Synchroscan pulse width measurement system which has been described elsewhere [7] has a photodiode/tunnel diode electronic arrangement to generate a sinusoidal voltage synchronised to the output pulse repetition frequency. This was then amplified to a power ~2 W to

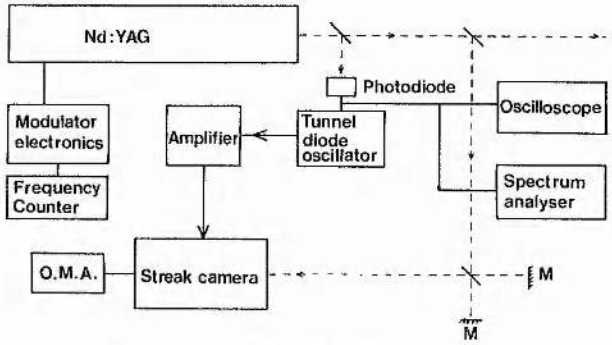

Fig. 1. The experimental arrangement.

0 030-401/87/$03.50

provide the deflection signal to the Photochron II [8] streak camera. The streak camera used in this work was equipped with a near infra-red wavelength response S-1 type photocathode. The streak images formed on the camera phosphor were then lens coupled to an optical multichannel analyser (OMA) which displayed directly the intensity profiles of the mode-locked pulses. A Michelson delay line (comprising two mirrors (M)) provided a time calibration for the pulses. The laser output characteristics were also monitored using an AEG Telefunken BPW 28 photodiode in conjunction with a Tektronix 7834 storage oscilloscope and Hewlett-Packard 8558B spectrum analyser. The rf drive frequency was monitored using a Philips PM6664 frequency counter.

3. Results and discussion

For a particular laser alignment and cavity length, which remained unaltered throughout the experiment, the shortest pulses (79 ps duration (fwhm)) were obtained at a modulator frequency of 40.800272 MHz (fig. 2(a)). An average output power of 8.4 W was recorded for these pulses. It is worth noting that these shortest pulses were usually observed to have a small "foot" to the rear of the pulse. In some cases this "foot" possessed sufficient intensity so as to constitute a second pulse. By correct alignment of the laser cavity, however, short pulses such as those in fig. 2(a) could be maintained with only slight pulse asymmetry. Pulse amplitude fluctuations for the "optimally" mode-locked Nd:YAG were found to have two major components. ("Optimal" mode-locking is taken here to mean minimum pulse duration at operating average power levels in excess of 7.5 W). First of these components was a regular ~ms timescale ripple attributed to the krypton arc lamp power supply. The second component, attributed to damped relaxation oscillations in the gain medium as in ref. [9], was manifested both as a pair of sidebands (separated from the central ~82 MHz peak by ~60 MHz) on the spectrum analyser and as a ~4% peak to ripple with a period ~15 μs (fig. 2(a)) on the 7834 oscilloscope. From a simple theoretical treatment of these relaxation oscillations [10] periods ~20 μs are predicted for the parameters that apply to our laser cavity, which is in good agreement with these observations. Whilst maintaining the laser cavity alignment and length, an investigation of the output pulse characteristics as a function of the frequency detuning, Δf, from the modulator frequency associated with the shortest duration pulses was performed. (The relative frequency difference between

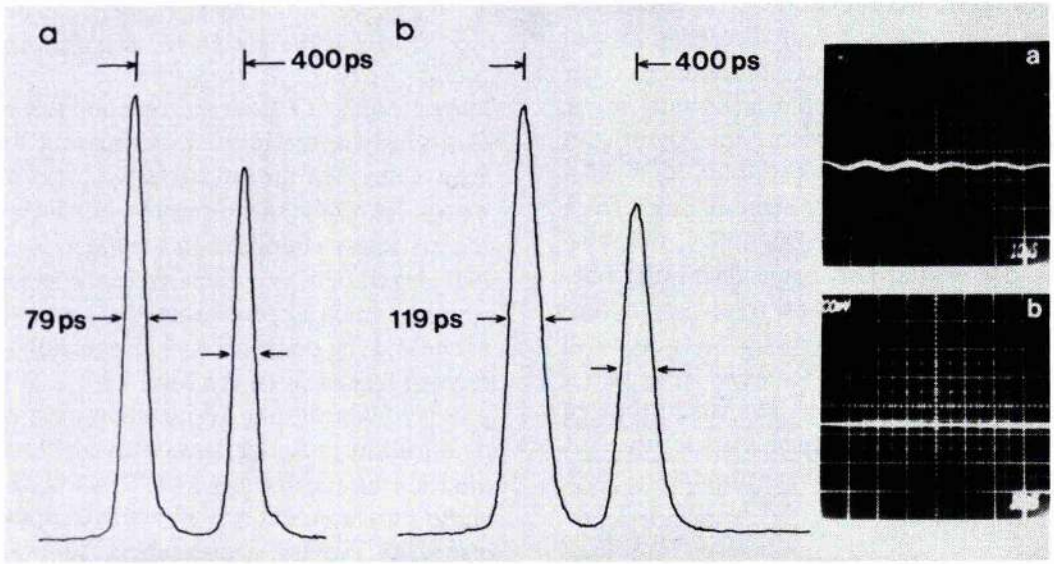

Fig. 2. Synchroscan streak camera intensity profiles of (a) shortest pulses (f=40.800272 MHz) and (b) pulses corresponding to minimum 60 kHz modulation (Δf= −181 Hz). Photographs show pulse amplitude fluctuations due to relaxation oscillations corresponding to Synchroscan traces (a) and (b). (200 mV/large div., 10μs/large div.).

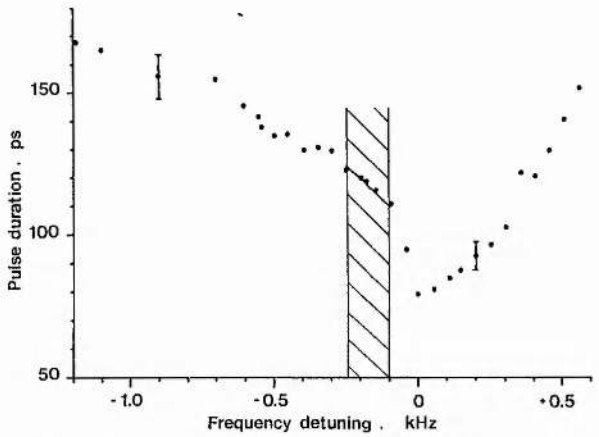

Fig. 3. The dependence of mode-locked pulse duration on frequency detuning from shortest pulse modulator frequency (f=40.800272 MHz).

modulator and free cavity was unknown). As expected from theory [11,12], small frequency detunings led to increased mode-locked pulsewidths. A plot of the pulsewidth, as determined by the Synchroscan streak camera, versus drive frequency detuning is presented in fig. 3. It can be seen that for frequency detunings of $\sim +600$ Hz and ~ -1000 Hz the pulse durations are approximately doubled. For positive detunings $\gtrsim 50$ Hz there was a marked increase in amplitude modulations and instabilities due to relaxation oscillations. Modulation depths approaching 100% were observed for detunings $\sim +500$ Hz). Of particular interest was the laser behaviour for slightly negative detuning frequencies. For a small frequency range ($\Delta f \sim -100$ Hz to -250 Hz), which is shown shaded in fig. 3, significant reduction in relaxation oscillation amplitude modulation and corresponding sideband intensity was observed.

The Synchroscan streak camera record of the pulse intensity profiles included as fig. 2(b) was obtained for a detuning frequency of -181 Hz where the 60 kHz sidebands were no longer apparent. Symmetrical pulses having durations of 119 ps were observed and the output power showed no reduction from that measured for the shortest pulses. This same behaviour was observed for a range of lamp current around the typical operating value. At further negative frequency detunings increased pulse durations with an increased presence of 60 kHz modulation were observed. However even at the largest negative detunings ($\gtrsim 1$ kHz) shown in fig. 3, the 60 kHz modulation depth did not approach the magnitudes experienced at only ~ 500 Hz positive detuning where similar pulse durations were recorded.

In ref. [13] it was reported that by correct experimental choice of the frequency detuning (both positive and negative values), undamped oscillations were obtained so that the laser emitted a regular series of spikes as the envelope of the mode-locked pulse train. This "Q-switching" was also observed in our laser for detuning frequencies in the approximate range -2 kHz to -4 kHz and $+1$ kHz to $+3$ kHz. The typical Q-switched oscillation period was ~ 25 μs and ~ 15 μs for the positive and negative frequency detuning ranges respectively. Operation in the positive detuning range, however, was undesirable since the stability of the pulse train in terms of pulse amplitude fluctuation, Q-switched oscillation period and envelope duration were poor. The stability of the Q-switched output train arising from a negative detuning (fig. 4 shows such a train recorded for $\Delta f \simeq -2.1$ kHz) was found to be excellent and peak-to-peak pulse amplitude fluctuations were as low as $\sim 5\%$ on an $\sim$ms timescale. During Q-switched operation the spectrum analyser revealed a series of very stable sidebands (typically 5–10 pairs) separated by 50–100 kHz. Time averaged output powers of 7.5 W were typical for the laser operating in the frequency regions giving rise to these stable, undamped Q-switched envelopes. Fig. 5 shows how both the oscillation period and envelope duration vary as a function of the frequency detuning. It can be seen that as the detuning increased, the oscillation period decreased and the pulse envelope broadened. In addition, it was noted that the peak intensity of the Q-switched envelope increased with decreased frequency detuning in accordance with the observation that the average power emitted from the laser remained essentially constant over the Q-switching frequency range. This overall behaviour was also repeated for Q-switching at positive detuning frequencies. Investigation of the background radiation between the Q-switched oscillations in fig. 4, using the 7834 oscilloscope, revealed mode-locked pulses whose energy content was about 1000 times smaller than those at the peak of the Q-switched train. This was evidence that the picosecond nature of the pulses did not decay completely between the Q-switched

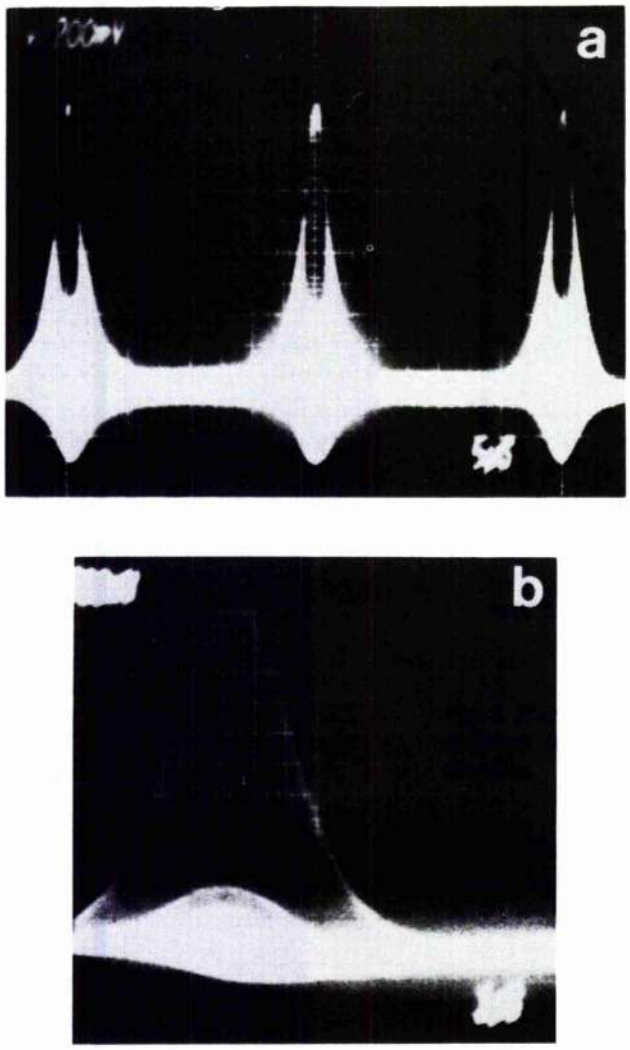

Fig. 4. (a) Output train of Q-switched pulse envelopes (5μs/large div.). (b) Single Q-switched envelope (1μs/large div.) ($\Delta f \simeq -2.1$ kHz).

spikes. In order to obtain an estimate of the Q-switched mode-locked pulse duration the Synchroscan streak camera was employed. In this case the driving signal for the deflection plates was derived from a synchronised output from the modulator electronics. Typical pulse intensity profiles of the Q-switched mode-locked pulses are displayed in fig. 6 for a frequency detuning of approximately -2.1 kHz. The pulse measurement of 237 ps duration (fwhm) is in good agreement with the photodetector and sampling oscilloscope measurement (~ 200 ps) reported in ref. [13]. At detuning frequencies in the

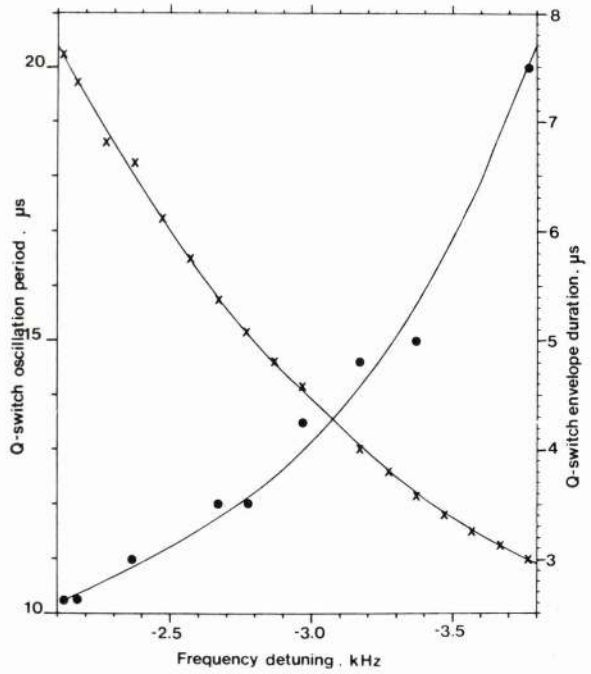

Fig. 5. Plot of Q-switched oscillation period (crosses) and Q-switched envelope width (fwhm) (dots) versus frequency detuning.

neighbourhood of 2 kHz the Q-switched mode-locked pulse energy was typically increased by a factor of 4–5 compared to cw mode-locking at $\Delta f = 0$.

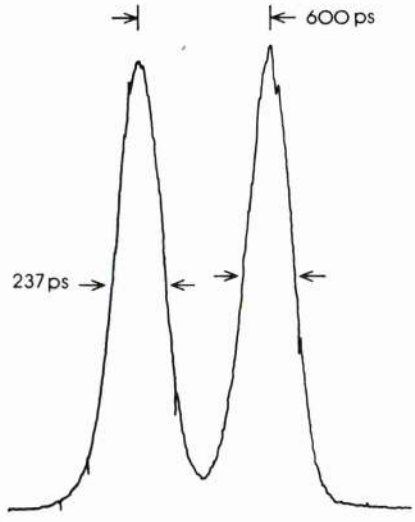

Fig. 6. Synchroscan streak camera intensity profiles of Q-switched mode-locked pulses. ($\Delta f \simeq -2.1$ kHz).

4. Conclusions

Operation of the acousto-optic modulator for the cw mode-locked Nd:YAG laser at a slightly negative detuning frequency ($\sim$150 Hz from the shortest pulse frequency) has been observed to severely reduce pulse amplitude fluctuations due to relaxation oscillations. This effect is likely to be important, in terms of overall system stability, when the laser is used to synchronously pump dye and colour centre lasers. (In particular the stability of the soliton laser [14] is reported to be strongly dependent on the behaviour of the pump source.) Although the detuning leads to an increased pulse duration ($\sim$110–120 ps) emitted by the laser, by employing standard pulse compression techniques [15], short pulses ($\sim$ps) are still available at 1.064 μm. In addition, at larger detuning frequencies ($\sim$kHz) we have studied the self Q-switching behaviour of the laser and found that for negative detuning frequencies in the range $\sim$2–4 kHz, stable, Q-switched mode-locked pulses with durations $\sim$200 ps can be readily achieved. To our knowledge a detailed theoretical treatment for these operating conditions has not yet been developed. The data presented here may vary in exact detail for different lasers and alignments but should form a useful parameter basis for this laser type.

References

[1] G.A. Mourou and T. Sizer II, Optics Comm. 41 (1982) 47.
[2] A. Seilmeier, W. Kaiser, B. Sens and K.H. Drexhage, Optics Lett. 8 (1983) 205.
[3] P. Beaud, B. Zysset, A.P. Schwartzenbach and H.P. Weber, Optics Lett. 11 (1986) 24.
[4] L.F. Mollenauer, N.D. Vieira and L. Szeto, Optics Lett. 7 (1982) 414.
[5] L.F. Mollenauer and R.H. Stolen, Optics Lett. 9 (1984) 13.
[6] H. Klann, J. Kuhl and D. von der Linde, Optics Comm. 38 (1981) 390.
[7] W. Sibbett, Proc. 15th Congress on High speed photography and photonics, (San Diego, 1982), SPIE 343 (1982) 15.
[8] D.J. Bradley and W. Sibbett, Appl. Phys. Lett. 27 (1975) 382.
[9] T.M. Baer and D.D. Smith, Proc. Fourth Intern. Conf. on Ultrafast phenomena (Monterey, 1984).
[10] A. Yariv, Introduction to optical electronics, 2nd Edition, (Holt, Rinehart and Winston) Chapter VI, Section 9.
[11] D.T. Kuizenga and A.E. Siegmann, IEEE J. QE-6 (1970) 694, 709.
[12] G.H.C. New, L.A. Zenteno and P.M. Radmore, Optics Comm. 48 (1983) 149.
[13] H.J. Eichler, Optics Comm. 56 (1986) 351.
[14] F.M. Mitschke and L.F. Mollenauer, Stabilising the soliton laser, to be published.
[15] J.K. Kafka, B.H. Kolner, T. Baer and D.M. Bloom, Optics Lett. 9 (1984) 505.

JOURNAL OF MODERN OPTICS, 1987, VOL. 34, NO. 9, 1227–1233

An experimental study of a synchronously pumped fibre Raman oscillator

K. SMITH, P. N. KEAN, D. W. CRUST and W. SIBBETT
University of St. Andrews, Department of Physics, North Haugh, St. Andrews, Fife KY16 9SS, Scotland

(*Received 18 February 1987*)

Abstract. A synchronously pumped fibre Raman oscillator has been constructed employing a mode-locked c.w. Nd:YAG laser as a pump source and 150 m of single-mode optical fibre as the Raman-active medium. A detailed spectral and temporal study of the laser has been undertaken. Time-dispersion tuning offered an operating spectral range of 1·0725–1·1220 μm for the first Stokes oscillation and 1·149–1·179 μm for the associated second Stokes component. Pulse durations $\sim$100 ps were generated with average output powers of about 40 and 9 mW for the first and second Stokes Raman pulses respectively.

1. Introduction

The fibre Raman oscillator [1] offers a very attractive, efficient source of broadly tunable coherent light over visible [2] and near-infrared spectral [3, 4] regions. The large potential laser bandwidths available make possible the generation of ultrashort light pulses via the mode-locking technique of synchronous pumping. The work presented here is a detailed spectral and temporal study of a simple fibre Raman oscillator (FRO) and is considered timely since recent work [5], involving a more sophisticated dispersion-compensated ring FRO, has led to the generation of sub-picosecond optical pulses at 1·1 μm.

2. Experimental arrangement

The experimental arrangement is shown in figure 1 and is similar to that described in [3]. The pump source was a Spectra Physics Series 3000 mode-locked c.w. Nd:YAG laser which, at the time of this work, produced 120–140 ps duration pulses at a repetition rate of about 82 MHz at a typical average power of 7 W. The laser output was coupled (via mirror M_1) into the single-mode optical fibre using a $\times 10$ antireflection (AR) coated microscope objective (L_1) with a typical coupling efficiency of 40 per cent (an average pump power of almost 3 W was coupled into the fibre). The optical fibre was single mode at the pump wavelength of 1·064 μm and typical parameters for this fibre type are 3·5 μm for the core radius, 0·004 for the average core/cladding refractive index difference and losses of 0·9 dB km^{-1}. Output coupling from the fibre was achieved with a $\times 20$ AR-coated microscope objective (L_2) which collimated the fibre output and directed the beam onto the first of the two fused-silica Brewster-angled prisms (P_1 and P_2) within the FRO cavity. The prisms were incorporated in order to provide spatial separation of the pump (P) and the

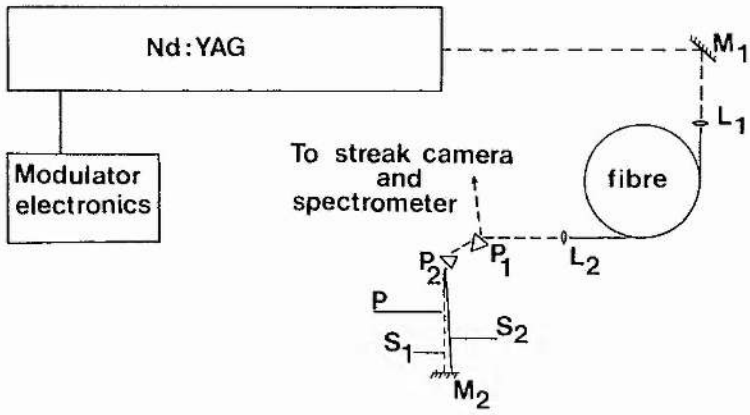

Figure 1. The experimental arrangement (see text).

Raman wavelengths (S_1 and S_2) and thereby prevent mode-locking degradation of the pump laser arising from strong feedback of the 1·064 μm radiation. Mirror M_2 ($\sim$100 per cent reflecting gold mirror) constituted one reflector for the FRO and was suitably adjusted to direct the first Stokes Raman pulse back into the optical fibre via L_2. In addition, the position of end-mirror M_2 was adjustable on an optical rail in order to meet the synchronous pumping requirement that the FRO cavity length be matched to a large integral multiple (roughly 120 in this case) of the pump laser cavity length. The output mirror of the Nd:YAG laser also served as the second reflector for the FRO cavity [3]. A reflection from the first prism allowed the FRO output to be monitored both spectrally and temporally. Spectral measurements were taken using a 1 m scanning spectrograph (with a resolution of $\sim$0·05 nm) and an S1 response photomultiplier. Temporal measurements were taken using a synchronously operating ('Synchroscan') streak camera system which has been described in detail elsewhere [6]. In this work, the trigger signal for the Synchroscan sweep electronics was derived from the r.f. modulator drive electronics of the mode-locked pump laser.

3. Results and discussion

One of the most important features of the FRO is the time-dispersion tuning property [1–4] which is a consequence of the time-synchronization requirement of synchronous pumping and the effect of group-velocity dispersion in the optical fibre. This is demonstrated in figure 2 where the peak wavelength of the first Stokes oscillation is plotted as a function of the relative position, ΔL ($\Delta L = 0$ at $\lambda = 1{\cdot}0725\ \mu$m), of mirror M_2 also depicted in terms of a relative time delay ($\Delta T = \Delta L/c$). It can be seen that a tuning range of almost 50 nm (1·0725–1·1220 μm) was achieved by translating the mirror by 10 cm (equivalent to 330 ps relative time delay) with the longer-wavelength Stokes oscillation occurring at extended cavity lengths. A curve of the type shown in figure 2 can be employed in the determination of the dispersion characteristics of single-mode optical fibres. In order to evaluate the group-velocity dispersion, $D(\lambda)$ (in ps nm^{-1} km^{-1}), over the wavelength region in figure 2, we first consider the time delay, ΔT, between two Stokes pulses, separated in wavelength by $\Delta\lambda$, in a single pass through the fibre. This is given by

$$\Delta T = LD(\lambda)\,\Delta\lambda,$$

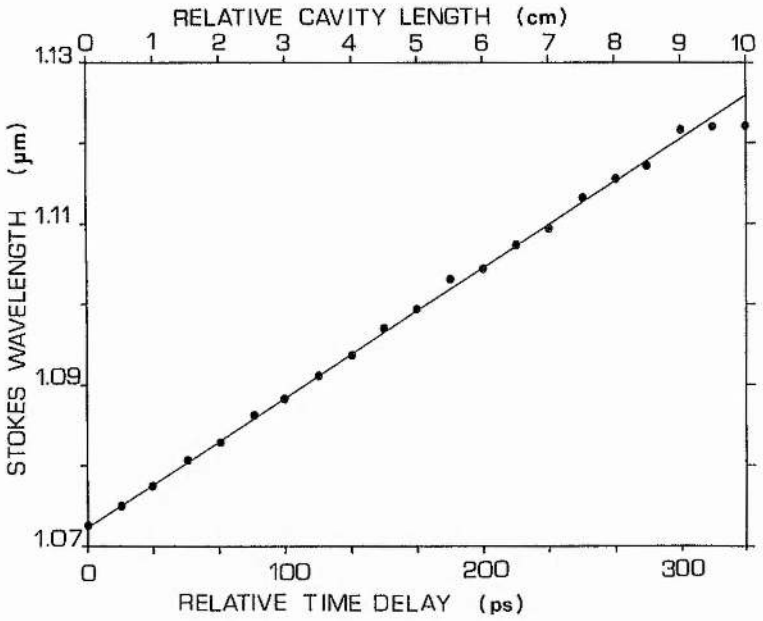

Figure 2. The dependance of the wavelength peak of first Stokes oscillation on the relative cavity length, ΔL (also depicted in terms of the relative time delay, $\Delta T = \Delta L/c$).

where L is the fibre length (in km). The slope of the tuning curve in figure 2 ($\Delta\lambda/\Delta T = 0{\cdot}1613$ nm ps^{-1}), which to a very good approximation is constant over the 50 nm range shown, gives a value of $D(\lambda) = 41$ ps nm km near 1·1 μm.

The spectral characteristics of the FRO output are presented in figures 3 and 4. Figure 3 shows the intensities (in arbitrary units) of the various spectral components of the FRO output plotted as a function of the cavity length and figure 4 shows the spectral nature of the output for the three relative cavity lengths of (*a*) +10 cm, (*b*) +3·5 cm and (*c*) +1 cm. (In all cases the sharp peak on the right of the trace (at 1·064 μm) corresponds to the pump pulses exiting the optical fibre.) For the long cavity (figure 4 (*a*)) the peak oscillation wavelength was 1·122 μm and the intensity of the resonant first Stokes pulse was sufficiently intense so as to generate a weak non-resonant second Stokes–Raman pulse at 1·179 μm (corresponding to a frequency shift of about 490 cm^{-1} from the resonant first Stokes component). The shorter cavity length (figure 4 (*b*)) leads to a peak oscillation wavelength of 1·0910 μm, and owing to its higher intensity, a larger non-resonant second Stokes–Raman component at 1·149 μm. Also of note is the appearance of a band with a peak at ~1·12 μm which coincides with that observed for a non-resonant first Stokes–Raman pulse. This peak is further enhanced, apparently at the expense of the second Stokes intensity, as the cavity length is further shortened (figure 3). In some cases (shown in figure 4 (*c*) where the resonant first Stokes wavelength is 1·0770 μm) a clearly visible double-humped spectral feature was recorded at 1·12 μm.

To understand, in qualitative terms at least, the behaviour depicted in figures 3 and 4 one must consider the wavelength-dependent factors that influence the FRO operation. These are firstly, the magnitude of the Raman gain cross-section (shown in figure 1 of [7]). Secondly, the effective gain or interaction length of the laser (this wavelength dependence is a consequence of the effect of group velocity dispersion on the pump and Raman wavelengths). Thirdly, there is the reflectivity characteristic of the output mirror of the ND:Yag laser. This is a maximum at 1·064 μm and falls

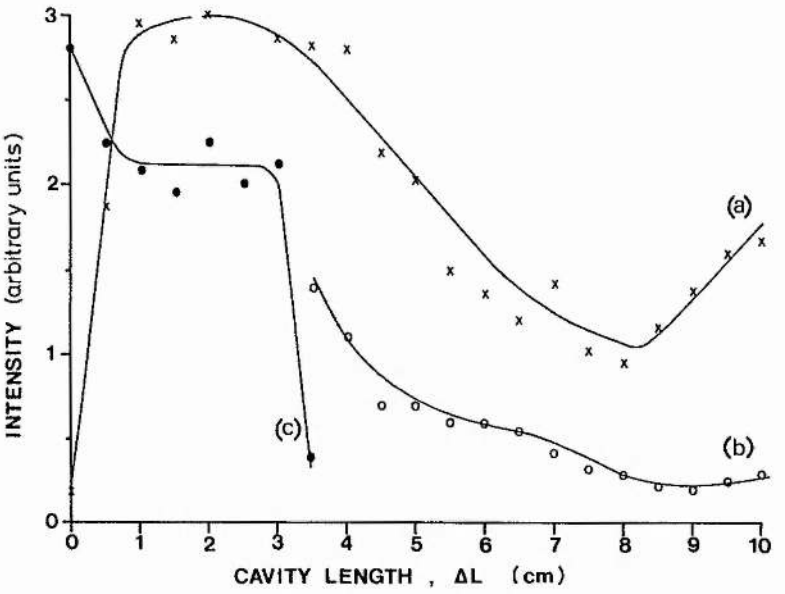

Figure 3. The intensity (arbitrary units) of (*a*) the resonant first Stokes, (*b*) the non-resonant second Stokes and (*c*) the non-resonant first Stokes–Raman pulses as a function of ΔL.

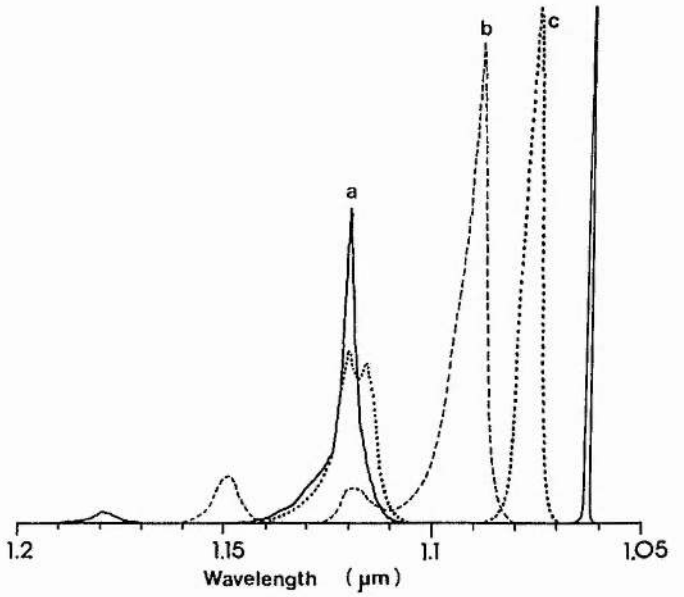

Figure 4. The spectral output of the FRO for a ΔL of (*a*) +10, (*b*) +3·5 and (*c*) +1 cm.

slightly over the operational range of the FRO. Although this third factor will contribute to the overall wavelength dependence of the FRO efficiency it is the product of the first two factors that predominantly determines the output characteristics of the FRO. Although long cavities (and therefore long oscillation wavelengths) offer a short interaction length (owing to the large difference in Raman and pump pulse propagation velocities) the Raman gain coefficient is high, and efficient laser operation is maintained with an associated non-resonant second Stokes–Raman component. For the shorter FRO cavity length depicted in figure 4 (*c*), however, the regime is one of long interaction length (owing to the close proximity of

the pump and resonant Raman wavelengths) and low Raman gain cross-section. While the overall resonant Raman laser efficiency is ensured in this region (owing to a large-gain cross-section–interaction length product) a strong non-resonant first Stokes–Raman component (at $\sim 1{\cdot}12\,\mu$m) is obvious with no second Stokes component being present. The appearance of the non-resonant first Stokes–Raman pulse is attributed to the associated low Raman gain cross-section at the resonant Stokes wavelength which implies a low instantaneous energy depletion of the pump pulse by the resonant Raman pulse. Consequently, sufficiently high gain is available close to the peak of the Raman gain curve to permit the growth of a non-resonant Raman component. The double-humped feature at $\sim 1{\cdot}12\,\mu$m (peak separation $\sim 4{\cdot}5$ nm) depicted in figure 4 (*c*) results from the twin peaks in the Raman gain curve at ~ 450 and $490\,\text{cm}^{-1}$. Figure 4 (*b*) shows the onset of a non-resonant first Stokes–Raman pulse formation together with a large non-resonant second Stokes–Raman component. For cavity lengths shorter than that for figure 4 (*b*) the latter component was completely frustrated by the presence of the non-resonant first Stokes pulse (see figure 3). An additional feature of figure 3 is the dip in the intensity profile of the first Stokes–Raman oscillation at a relative cavity length of approximately +8 cm. This is attributed to the dip in the Raman gain curve at a frequency separation $\sim 470\,\text{cm}^{-1}$ from the pump wavelength at $1{\cdot}064\,\mu$m.

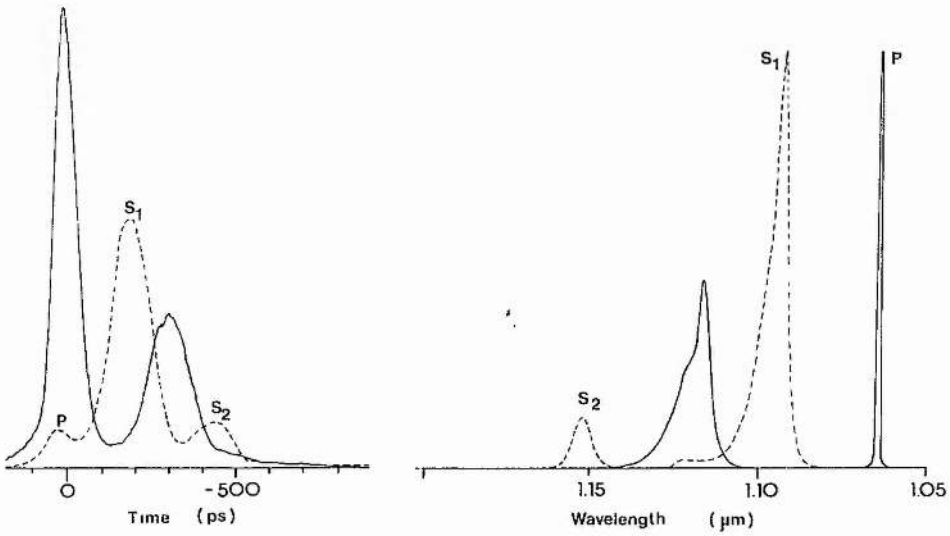

Figure 5. The temporal output (*a*) and spectral output (*b*) of the FRO ($\Delta L = +4{\cdot}0$ cm) for the cases of resonant (dashed curve) and non-resonant (full curve) operation. The zero time point in (*a*) corresponds to the peak of the pump pulse in the full curve.

The temporal behaviour of the FRO for a cavity length of +4·0 cm is shown in figure 5 (*a*). This cavity length gave wavelengths of 1·093 and $1{\cdot}053\,\mu$m for the resonant first and non-resonant second Stokes–Raman pulse peaks respectively, and with no significant presence of the non-resonant first Stokes component. The full curve (taken with the resonator blocked between P_2 and M_2) shows the single-pass Raman pulse leading the $1{\cdot}064\,\mu$m pump pulse by approximately 300 ps. The dashed curve (plotted on the same intensity scale as the full curve but with the resonator unblocked) shows the resonant output of the FRO with clear evidence of the resonant first Stokes–Raman, non-resonant second Stokes–Raman, and severely depleted pump pulses. Of particular note is the time retardation by 120 ps of the

resonant First Stokes–Raman pulse relative to the non-resonant first Stokes–Raman pulse. This is predominantly due to the large wavelength shift (from 1·12 μm to that defined by the FRO cavity length) shown in figure 5 (*b*). An additional effect is due to the finite length of fibre required to generate a non-resonant Raman pulse. From figure 5 (*a*) the time advancement of the non-resonant second Stokes relative to the resonant first Stokes can be measured to be $\sim$260 ps. From the dispersion data (assuming the value of 41 ps nm^{-1} km^{-1} to apply at the second Stokes wavelength) we would expect a temporal separation of 370 ps for the 150 m-long fibre. This discrepancy is taken to indicate that the non-resonant second Stokes pulse is generated only when a considerable length ($\sim$50 m) of optical fibre has been traversed.

Further temporal information is presented in figure 6 where the intensity profiles of the pump, first and second Stokes Raman pulses are reproduced on a normalized scale ($\Delta L = +4{\cdot}0$ cm). By using the laser output reflected from the second prism (P_2) these three components were spatially distinct and could be studied independently by suitable alignment onto the input slit of the streak camera. The slight humps (especially noticeable on the second Stokes–Raman and pump pulses) were due to incomplete isolation of these components from the more intense resonant first Stokes–Raman pulse. From figure 6, pulse durations of 91, 111 and 116 ps are measured for the depleted pump, resonant first Stokes and non-resonant second Stokes components respectively. In addition, output powers $\sim$40 and 9 mW were measured for the first and second Raman bands respectively.

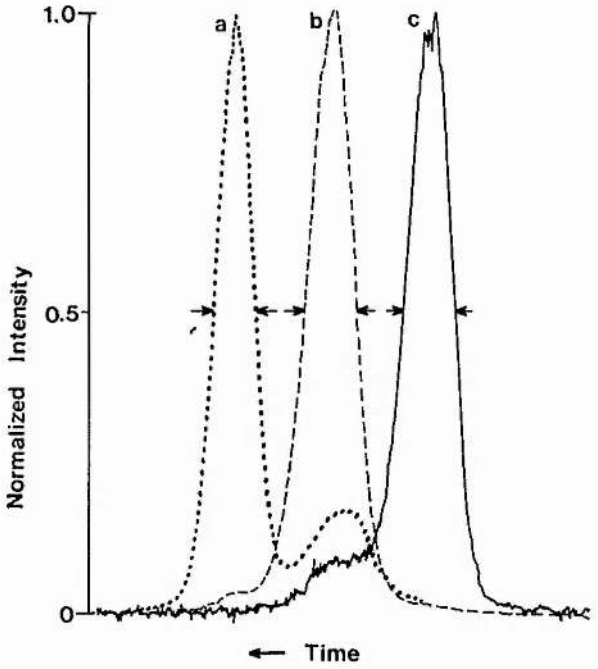

Figure 6. The depleted pump (*a*), resonant first Stokes (*b*) and non-resonant second Stokes (*c*) Raman pulses plotted on a normalized scale ($\Delta L = +4{\cdot}0$ cm).

4. Conclusions

A synchronously pumped fibre Raman oscillator (FRO) has been constructed and its spectral and temporal characteristics studied in some detail. Time-dispersion tuning has allowed a value for the group-velocity dispersion of 41 ps nm^{-1} km^{-1} near 1·1 μm to be determined. A tuning range of almost 50 nm from 1·0725–1·1220 μm was obtained for the first Stokes oscillation but the appearance of a non-resonant first Stokes band (for $\Delta L < +3{\cdot}5$ cm) limited the tuning range of the associated second Stokes–Raman component to 30 nm from 1·149–1·179 μm. The pulse durations for both the first and second Stokes–Raman bands were typically 100 ps with peak powers of 5 W (40 mW average) and 1 W (9 mW average) respectively. This study has been useful as a first stage of FRO development and future work will involve more sophisticated cavity designs incorporating both dispersion-compensating and integrated optical elements. In conjunction with various fibre Raman media (for example gas in glass [8]) this type of laser should permit the convenient generation of ultrashort pulses ($\sim$ps) over much of the wavelength range of interest for pulse-propagation studies in optical fibres and for other time-domain spectroscopic investigations in the near-infrared region.

Acknowledgments

The financial support of British Telecommunications plc (K.S.) and the SERC–JOERS is gratefully acknowledged.

References

[1] Stolen, R. H., 1979, *Fibre and Integrated Optics*, edited by D. B. Ostrowsky (New York: Plenum), p. 157.
[2] Stolen, R. H., Lin, C., and Jain, R. K., 1977, *Appl. Phys. Lett.*, **30**, 340.
[3] Lin, C., Stolen, R. H., and Cohen, L. G., 1977, *Appl. Phys. Lett.*, **31**, 97.
[4] Lin, C., and French, W. G., 1979, *Appl. Phys. Lett.*, **34**, 666.
[5] Kafka, J. D., Head, D. F., and Baer, T., 1986, *Ultrafast Phenomena V*, edited by G. R. Fleming and A. E. Siegman, Springer Series in Chemical Physics 46 (Berlin: Springer Verlag), p.34.
[6] Sibbett, W., 1982, *Proc. SPIE*, Vol. 348 (Bellingham: Society of Photo-optical Instrumentation Engineers), p. 15.
[7] Stolen, R. H., 1980, *Proc. IEEE*, **68**, 1232.
[8] Chraplyvy, A. R., and Stone, J., 1984, *Optics Lett.*, **9**, 241.

Spectral and temporal investigation of self-phase modulation and stimulated Raman scattering in a single-mode optical fibre

P.N. Kean
K. Smith
W. Sibbett

Indexing terms: Optical fibres, Nonlinear optics

Abstract: An investigation of the spectral and temporal characteristics of the self-phase modulated pulses exiting from a germania-doped fused-silica-core single-mode optical fibre has been undertaken at 1.064 μm. For peak powers below the stimulated Raman scattering threshold the spectral data were in excellent agreement with a simple theory developed for negligible fibre group-velocity dispersion and symmetrical chirp-free input pulses. For elevated peak-power levels a complementary study of the temporal and spectral features of the first-order Stokes Raman and pump pulses has been carried out. It was observed that the onset of stimulated Raman scattering leads to both spectral and temporal pump-pulse asymmetry and hence to deviation from the theoretical spectral predictions. In addition, a simple fibre Raman oscillator was constructed and its characteristics are described in some detail.

1 Introduction

The utilisation of laser-induced nonlinearities in optical fibres for optical pulse compression has received much attention in recent years. Pulse compression is a consequence of the interaction of a linear frequency-chirped optical pulse (owing to the nonlinear process of self-phase modulation (SPM)) and an appropriate group-velocity dispersion which may be provided by a grating pair [1, 2] or suitable optical fibre [3–5]. The nonlinear process of stimulated Raman scattering not only limits the maximum achievable power in a fibre-grating compression system but can also lead to a marked increase in the noise associated with the compressed pulses [6, 7]. We therefore consider that a detailed investigation of these two nonlinear effects is of primary importance and we present experimental data relating to their relevant temporal and spectral features. In addition, we have included preliminary results of the exploitation of stimulated Raman scattering in the construction of a simple fibre Raman oscillator.

Paper 5367J (E13), received 16th January 1987

The authors are with the Department of Physics, University of St. Andrews, North Haugh, St. Andrews, Fife KY16 9SS, Scotland, United Kingdom

2 Experimental

The optical fibre, obtained from British Telecom Research Laboratories, was single mode at the Nd : YAG laser wavelength of 1.064 μm. Quoted fibre parameters for this sample were 3.5 μm for the core radius a, 0.004 for the average core/cladding refractive-index difference Δ, 0.9 dB/km attenuation and a germania doping level of 3–5 mol %. The experimental arrangement for the spectral and temporal investigation of induced self-phase modulation and Raman generation is shown in Fig. 1.

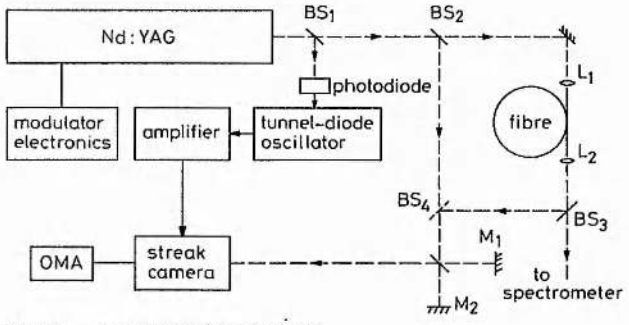

Fig. 1 *Experimental arrangement*

The acousto-optically mode-locked CW Nd : YAG laser (Spectra Physics Series 3000) typically generated 120–140 ps duration pulses at a repetition frequency of ~82 MHz with a time-averaged power of 7 W. A small fraction of the laser output was taken via beamsplitter BS_1, to trigger the sweep electronics of the synchronously operating Photochron II streak camera [8]. Beamsplitter BS_2 allowed the input pulses to the fibre to be monitored continuously throughout the series of experiments. Time calibration of the pulses was achieved using the now-conventional optical delay line comprising a beamsplitter and mirrors M_1 and M_2. The pulses were displayed in real time using an optical multichannel analyser (OMA). The remainder of the laser output was then coupled into the optical fibre via an antireflection (AR) coated $\times 10$ microscope objective (L_1). Coupling efficiencies of ~50% were typical, and under these operating conditions the effect of optical feedback of the 1.064 μm radiation was essentially negligible. Output coupling from the fibre was achieved with a $\times 20$ AR-coated microscope objective (L_2) which allowed the laser and Raman pulses to be directed both to the input slit of the streak camera (via BS_3 and BS_4) and to a 1 m scanning grating monochromator (resolution ~0.05 nm). (Spectral measurements of

the Raman pulses were taken using an S1 response photomultiplier tube.) The spectral width of the fundamental pulses exiting the fibre, however, was displayed in real time by employing a charge-coupled device (CCD) linear array mounted in the plane of the output slit of the spectrograph. Although pulse durations of less than 100 ps could be generated from the laser source, significant enhancement in the SPM spectral stability (in terms of both width and spectral fringe visibility) was achieved by the use of somewhat longer pulses occurring at an RF modulator frequency slightly detuned (~ -200 Hz) from the shortest pulse frequency. This increase in spectral stability is attributed to the enhanced Nd : YAG laser stability reported previously [9].

3 Self-phase modulation

By altering the focus position of the microscope objective L_1 it was possible to alter the coupling efficiency and thereby to alter the average (peak) power in the fibre. Fig. 2 shows the spectral character of the pulses from a 150 m length of optical fibre as a function of the peak power in the fibre (pump-pulse duration $t_p = 140$ ps). For the lowest power (3 W, Fig. 2*a*) no SPM was recorded which is consistent with the theoretical SPM power threshold P_c of 3.5 W calculated from [10]

$$P_c = 1.2 \times 10^{-2} \frac{\lambda A}{L} \text{ Watts} \quad (1)$$

where A is the effective core area (taken as πa^2) and L is the effective fibre length (140 m [11]). As the peak power in the fibre was increased the spectra broadened significantly and the classical SPM spectra (Fig. 2*b–e*) were clearly in evidence. For average powers in excess of 1.2 W (100 W peak power) first-order Stokes Raman light (at ~ 1.12 μm) was detectable by the streak camera and spectrograph. In addition, a depletion of the downshifted frequency components of the SPM spectra was noted. Fig. 2*f* ($P = 106$ W), taken just above Raman threshold, shows a slight spectral asymmetry, whereas Fig. 2*g* taken at higher powers ($P = 148$ W) shows fairly severe low-frequency-component depletion. This effect has been the subject of previous studies [6, 12] and is attributed to the depletion of the leading edge of the 1.064 μm pump pulse in the stimulated Raman scattering process.

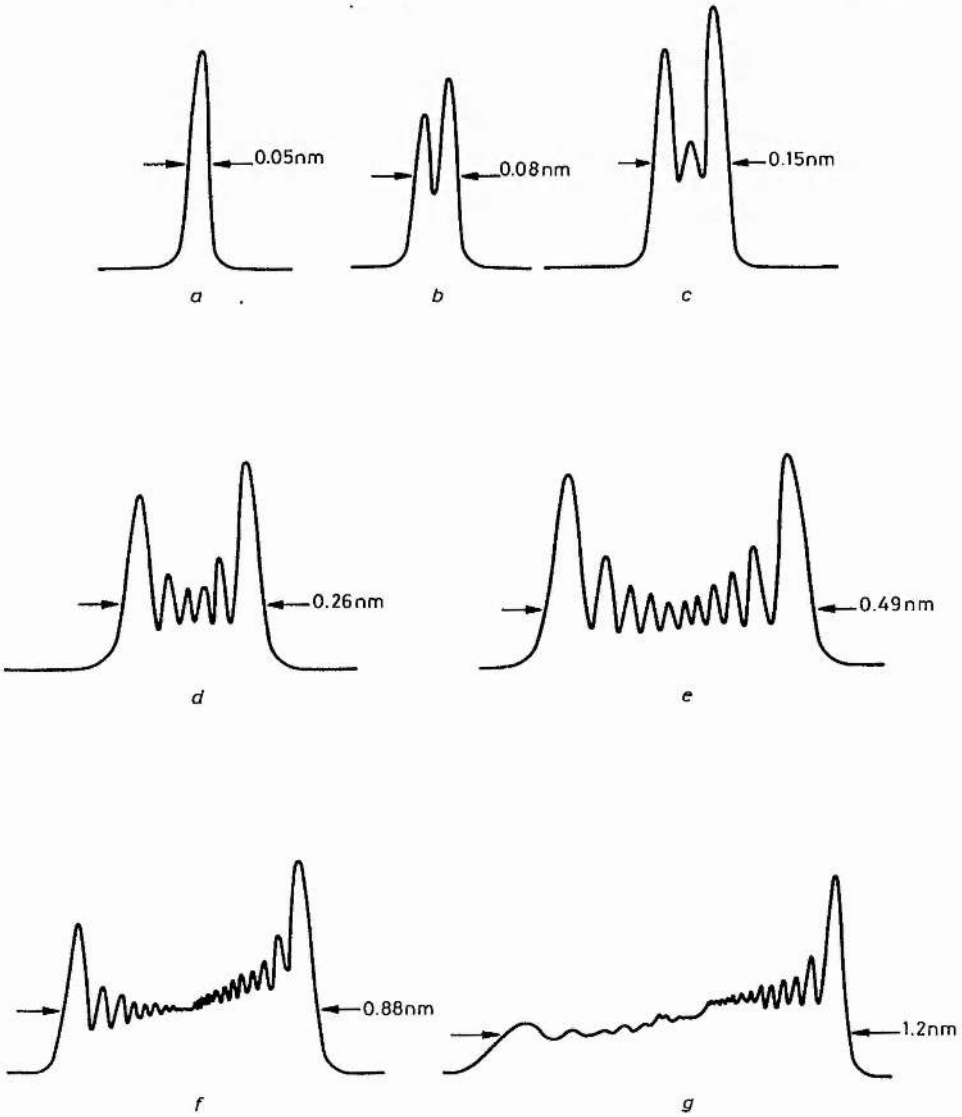

Fig. 2 *Self-phase modulated spectra of output pulses from 150 m fibre sample*
For peak powers of *a* 3 W; *b* 8 W; *c* 12 W; *d* 25 W; *e* 53 W; *f* 106 W; *g* 148 W
Wavelength increases from right to left

In Fig. 3 the total spectral width $\Delta\lambda$ of the SPM pulse has been plotted against the peak power in the fibre. The ordinate at 100 W peak power represents the experimentally determined value of the stimulated Raman threshold. For peak powers up to ~130 W (only slightly in

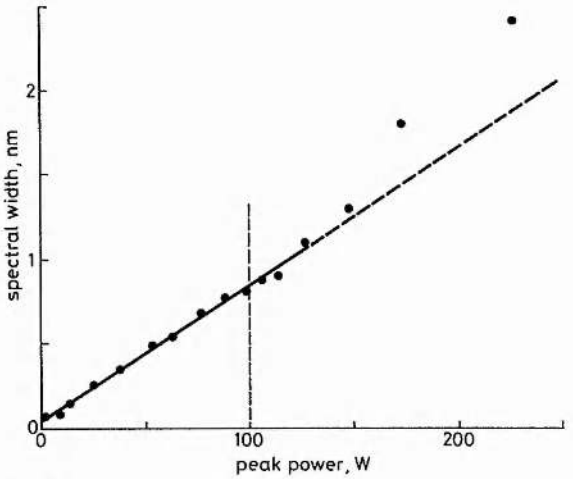

Fig. 3 *SPM spectral bandwidth as a function of peak power in the fibre*
For input pulses of 140 ps and 150 m of optical fibre

excess of Raman threshold) a linear relationship between spectral width and peak power was observed to hold. At higher peak powers, however, severe pump-pulse shape modification due to the onset of Raman generation (discussed in the next Section) can lead to acute SPM spectral asymmetry and deviation from linearity. A simple theory can be employed to successfully explain the linear relationship observed (for $P \lesssim 130$ W). The theory was developed for negligible influence of fibre group-velocity dispersion (i.e. there was no change in pulse duration during propagation) and symmetrical (Gaussian) frequency chirp-free input pulses and is now briefly outlined. The instantaneous angular-frequency shift $\delta\omega$ associated with the time-dependent phase change (a consequence of the intensity-dependent refractive index) is given by

$$\delta\omega = \frac{-2\pi}{\lambda} \cdot n_2 \cdot L \cdot \frac{dI(t)}{dt} \tag{2}$$

where n_2 is the self-focusing coefficient, L is the effective fibre length and $I(t)$ is the temporal pulse intensity profile. For a Gaussian input pulse it is easy to derive the expression for the maximum wavelength shift and thereby derive the total spectral width $\Delta\lambda$ of the SPM pulse. The expression is

$$\Delta\lambda = \Delta\lambda_i + 4\sqrt{\frac{2\ln 2}{e}} \cdot \frac{\lambda n_2 L}{cA} \cdot \frac{P}{t_p} \tag{3}$$

where $\Delta\lambda_i$ is the bandwidth of the input laser pulse, P is the peak pulse power and t_p is the pulsewidth (full width at half maximum (FWHM)). The equation can also be expressed in terms of the maximum phase change, $\Delta\phi$ max $= 2\pi n_2 LP/\lambda A$, experienced by the pulse.

The full line in Fig. 3 is a least-squares fit to the data points taken below 100 W peak power and has a gradient and intercept of $8.1 \pm 0.3 \times 10^{-12}$ m/W and 0.04 ± 0.01 nm, respectively. The latter value, according to this theoretical treatment, represents the Nd : YAG laser pulse bandwidth and is in good agreement with accepted values [6, 13]. The linear relationship is also verified in Fig. 4 which shows a plot of the SPM spectral width versus peak power for a shorter fibre length of

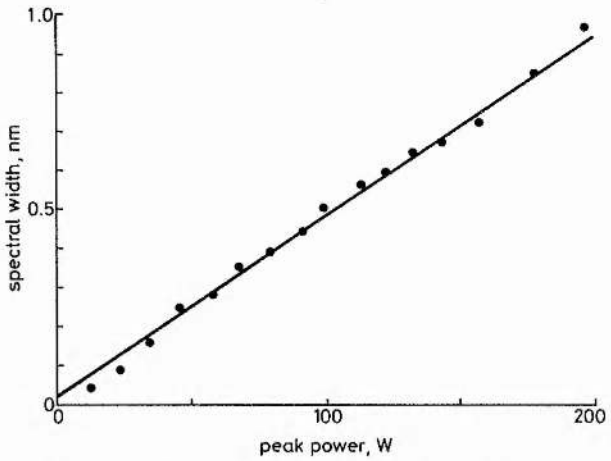

Fig. 4 *SPM spectral bandwidth versus peak power in the fibre*
For $t_p = 127$ ps and 70 m of optical fibre

70 m (for this fibre length stimulated Raman scattering threshold occurs at a peak power of approximately 200 W). Again the full line represents a least-squares fit to the data and has a gradient value of $4.6 \pm 0.2 \times 10^{-12}$ m/W. From the gradients deduced from the data in Figs. 3 and 4 it is possible to obtain values for the self-focusing coefficient. Values of 3.7×10^{-20} m^2/W and 3.8×10^{-20} m^2/W for n_2 have thus been deduced from the data in Figs. 3 and 4, respectively, with an estimated error of approximately 10%. Since the polarisation of the light in the fibre is completely scrambled, the intensity-induced refractive-index change is effectively reduced. A suitable correction factor is obtained by averaging the values of the refractive-index change for linear and circular polarisation [11]. This correction factor has been used in the above calculations. Both values agree well with the value of 3.3×10^{-20} m^2/W (1.14×10^{-13} electrostatic units with a 15% error) calculated by Stolen and Lin [11] for a silica-core borosilicate-clad optical fibre. Such good agreement with the simple theory applied is perhaps surprising since two factors have been ignored. These are first, group-velocity dispersion in the fibre, and secondly, any frequency chirp on the input pulses. Both these factors can lead to pulse shape and duration changes on propagation through the fibre. Interaction of frequency broadening due to SPM and positive group-velocity dispersion has been studied theoretically in some detail and has been shown to give rise to broader self-steepened output pulses [1, 14] (Fig. 6*a*). For the peak powers and fibre lengths used here, however, we were well within the region where this effect could be ignored in our considerations. (In Reference 14 a critical length Z_c is defined. For fibre lengths significantly less than Z_c one is justified in neglecting the effects of pulse broadening due to group-velocity dispersion. In our case we obtain $Z_c = 1.7$ km for the quoted fibre parameters and maximum peak powers (~100 W) employed). Group-velocity dispersion in the fibre may, however, interact with an initial frequency chirp to affect the duration of the pulse as it propagates in the fibre [6]. Nevertheless, the analytical solution provided by the theory is quite adequate in predicting SPM bandwidths for the peak powers and fibre lengths used in this work providing that pulse shape deformation due to stimulated

Raman scattering is not severe. Further SPM spectra are shown in Fig. 5 for input pulse durations of 127, 143 and

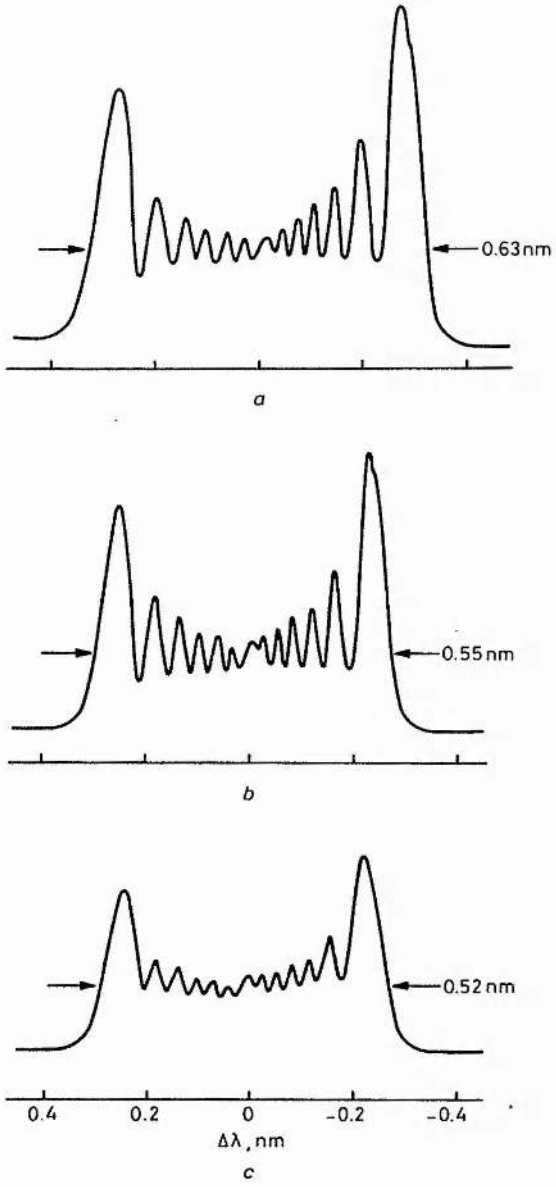

Fig. 5 *SPM spectra*
For input pulse durations of *a* 127 ps; *b* 143 ps; *c* 172 ps
Peak power in fibre $P = 70$ W

172 ps at a constant peak power of ~70 W maintained in the fibre by suitable adjustment of the L_1 focus position. Since the peak power is kept constant, the maximum phase shift experienced by the pulse ($\Delta\phi$ max) should also be constant. It is the latter factor that determines the number of oscillation peaks within the SPM spectrum and we would therefore expect that the number of such oscillations should remain fixed throughout the set of readings in Fig. 5. We also see that the SPM bandwidth decreased with increased input pulse duration which is as expected from eqn. 3.

4 Raman pulse generation

As noted in the previous Section, for the 150 m long fibre, average powers in excess of 1.2 W (100 W peak power) produced detectable first-order Stokes Raman light at ~1.12 μm. This threshold for stimulated Raman generation is in close agreement with theory [15]. Theoretical considerations predict a peak-power threshold P_{th} given by

$$P_{th} = 32A/GL \tag{4}$$

where A is the effective core area (taken as πa^2), G is the Raman gain coefficient and L is the effective optical-fibre length. For the fibre used here the respective values taken were 39×10^{-8} cm^2, 0.9×10^{-11} cm/W and 140 m. A value of 99 W can then be calculated for stimulated Raman generation.

The sequence of Fig. 6 *a–e* shows the recorded streak-camera pulse intensity profiles of the laser and first-order Raman pulses. (Time is increasing from right to left in all traces.) The effect of positive group-velocity dispersion can clearly be seen on the arrival time of the Raman pulse relative to the output fundamental pulse. Fig. 6*a* was taken just above stimulated Raman threshold and reveals a broadened pump pulse (compared to the 140 ps duration input pulses) together with a weak stimulated Raman pulse just ahead of the leading edge of the pump pulse. The broadened pump pulse is explained in terms of the combined action of group-velocity dispersion and SPM [1, 2, 14]. As the power in the fibre was increased the pump pulse was observed to narrow significantly (to an asymmetric ~85 ps duration pulse at a peak power of 226 W (Fig. 6*e*)) and the time delay between the Raman and pump-pulse peaks grows. The peak wavelength (1.116 μm) of the Raman pulse (the spectrum of which is shown in Fig. 6*f*) was not observed to change throughout the set of results. The behaviour depicted in Figs 6*a–e* is attributed to the combination of two factors. First, there is the finite length of fibre (which may be considerable for lower pump powers) within which a stimulated Raman pulse is generated and this gives rise to the shorter time delay between the Raman and pump pulses for low peak powers in the fibre. For high peak powers, however, the Raman pulse will be generated at an early stage in the fibre and thus it will propagate independently of the pump pulse for most of the fibre length. An estimate of the time delay can be made from the known fibre dispersion of 41 ps/nm.km (Fig. 11). Assuming that the pulses propagate independently very close to the beginning of the fibre (i.e. $L = 150$ m) a time delay of approximately 320 ps is expected. This is close to that observed experimentally for the highest pump powers. The second factor is the depletion of the pump-pulse leading edge [6, 12] by the Raman signal and gives rise to both a shortening and reshaping of the pump pulse. To be more specific, it has been shown theoretically [16] that the stimulated Raman scattering process steepens the leading edge of the propagating laser pulse. This is evident in the temporal pulse intensity profile asymmetry recorded for the higher peak powers (Figs. 6*d* and *e*) where pump depletion is most dominant.

In addition to monitoring both the spectral (Fig. 6*f*) and temporal (Figs. 6*a–e*) features of the Raman pulse, an associated depletion of the downshifted frequency components (arising from the pump-pulse rising edge) of the SPM spectra was recorded after the onset of stimulated Raman scattering. This was evident in Figs. 2*f* and *g* and is displayed more clearly in Fig. 7. Fig 7*a* represents the SPM spectrum for a low peak power (53 W) in the fibre (well below stimulated Raman scattering threshold) and shows a spectrum which is symmetrical about the centre 1.064 μm wavelength ($\Delta\lambda = 0$). Figs. 7*b* and *c*, however, correspond to higher peak powers (above stimulated

Raman scattering threshold) and, in addition to low-frequency-component depletion, reveal the asymmetric nature of the wavelength spectrum. In particular Fig. 7*c* shows the severe erosion of the low-frequency components ($\Delta\lambda > 0$) associated with the SPM spectrum for the highest peak power (226 W) coupled into the optical fibre. These spectral distortions were especially evident at peak powers above 150 W and led to a marked deviation from the linear relationship between the SPM bandwidth and peak power (Fig. 3). Such observations are consistent with the inference of significant depletion and steepening of the pump-pulse leading edge by the Raman pulse generation as depicted in Fig. 6. A direct consequence of this steepening of the pulse-pulse profile is the extended low-frequency range in the SPM spectra presented in Figs. 7*b* and *c*. From the spectral measurements shown, the trailing edge of the pump pulse appears to be essentially unaffected by the presence of the Raman pulse. It is worth noting that the linear relationship in Fig. 3 is found to hold for peak pump powers well into the Raman region (up to ~230 W) if the SPM bandwidth measurements are taken from the undepleted upshifted frequency components.

An investigation of the pulse intensity temporal profile dependence on fibre length was undertaken for the highest power coupled into the fibre (~230 W). Fig. 8 shows a plot of the time delay between the Raman- and pump-pulse peaks for fibre lengths from 150 to 70 m (below this length the two peaks were not sufficiently resolved for accurate measurements to be taken). The full line drawn through the data points is a least-squares fit and has a gradient of 2.2 ps/m giving a dispersion of approximately 42 ps/nm.km which is in good agreement with the value (41 ps/nm.km) calculated from Fig. 11 for the fibre Raman oscillator described in the next Section. It is clear that during propagation over the fibre length examined in Fig. 8, the Raman pulse is seen to travel with a group velocity associated with the Stokes wavelength shift (~52 nm). This is not surprising since over this region Raman- and pump-pulse interaction is essentially nonexistent owing to their large temporal separation. For fibre lengths significantly less than 70 m

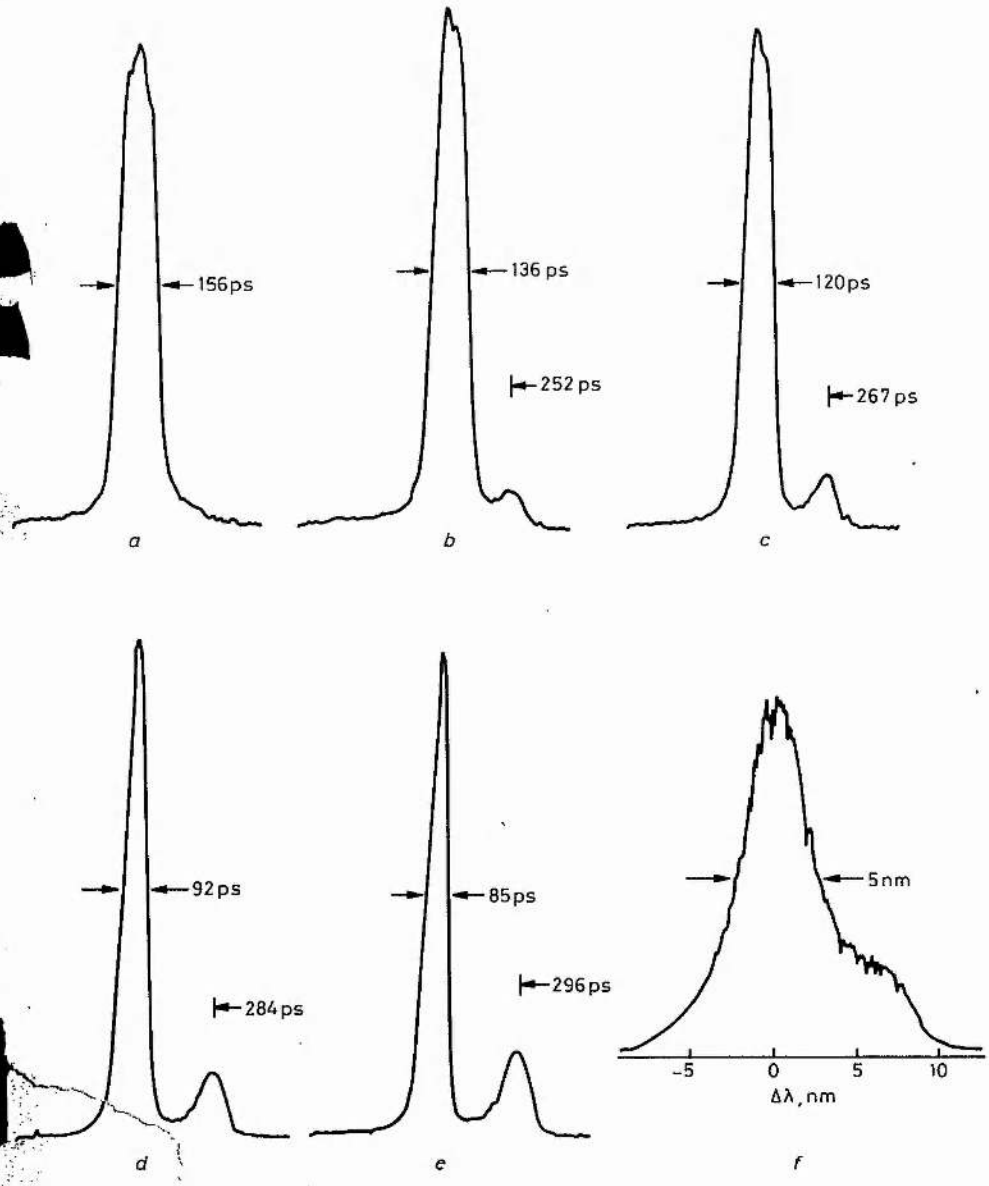

Fig. 6 *Synchroscan streak-camera intensity profiles of pump and Raman pulses*
For peak pump powers of *a* 113 W; *b* 126 W; *c* 148 W; *d* 174 W; *e* 226 W
f first Stokes Raman pulse spectrum for a peak pump power of 148 W

however, the group velocity may be significantly modified owing to the way in which pump-pulse energy is transferred into the Stokes component [16]. The modified Raman-pulse group velocity (which tends to extend the interaction region) is indicated by the positive, nonzero length-axis intercept (~20 m) for the extrapolation given in Fig. 8. Fig. 9 shows a pulse intensity temporal profile of the pump and Raman pulses for a peak power of ~230 W (as in Fig. 8) and a fibre length of 85 m. A Raman pulse of ~80 ps in duration is followed by a highly asymmetric (~75 ps) pump pulse. If these pulses were then to propagate along a further 65 m of optical fibre (i.e. 150 m in total), we would observe a temporal intensity profile (further influenced by group-velocity dispersion effects) similar to that depicted in Fig. 6*e*.

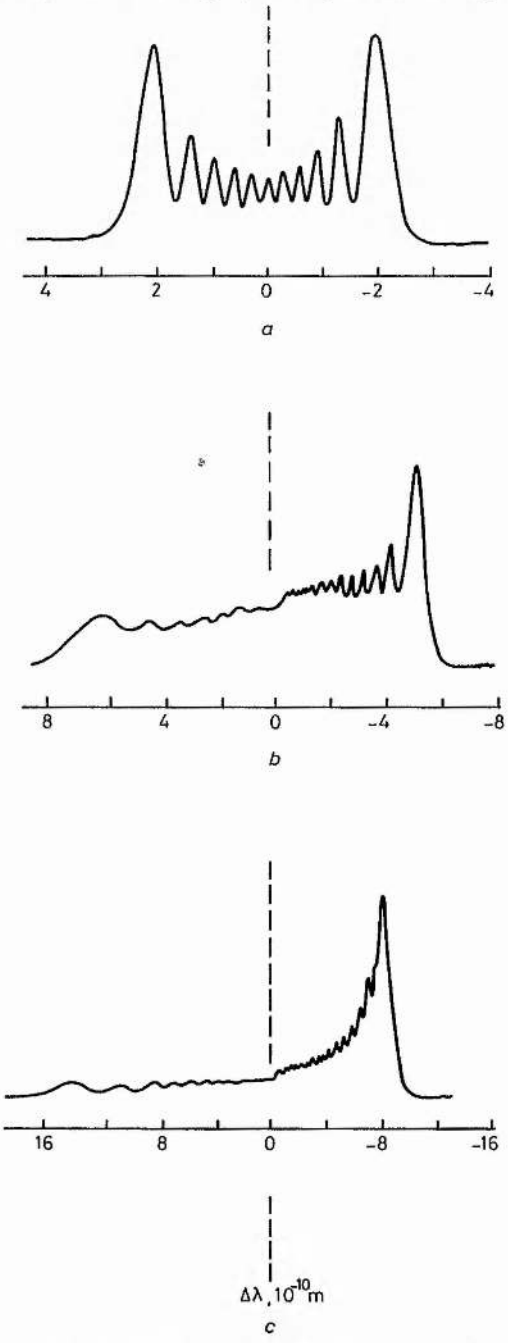

Fig. 7 *Spectra of SPM pump pulses*
For peak powers of *a* 53 W; *b* 148 W; *c* 226 W
Wavelength increases from right to left; t_p = 140 ps

Another interesting feature of the temporal data presented in Fig. 6 and Fig. 9 is the slightly asymmetric nature of the Raman pulse (i.e. a sharp rising edge and prolonged trailing edge). This is another consequence of simultaneous group-velocity dispersion and pump depletion and is predicted theoretically [16].

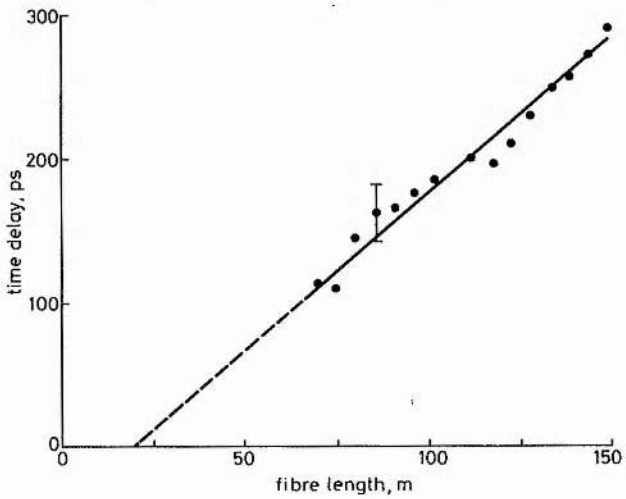

Fig. 8 *Plot of time delay between the Raman- and pump-pulse peaks versus optical-fibre length for P = 230 W*

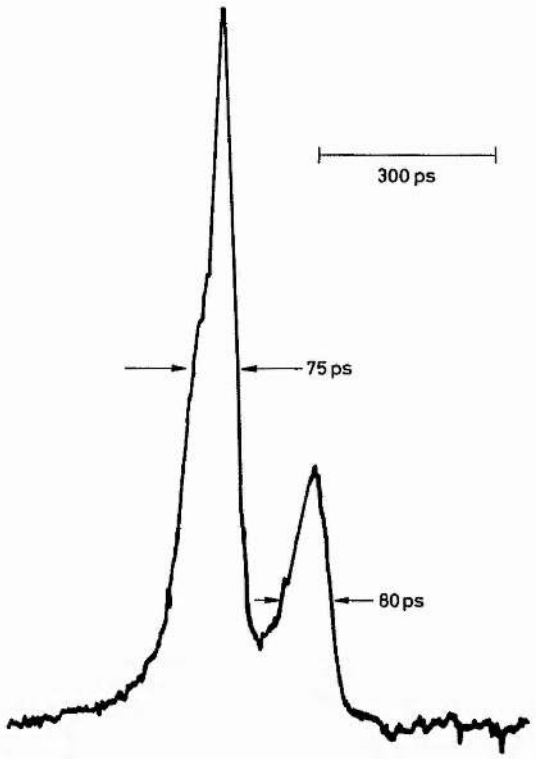

Fig. 9 *Synchroscan streak-camera intensity profile of pump and Raman pulses*
For P = 230 W and a fibre length of 85 m
Time increases from right to left

5 Fibre-Raman oscillator

In the preceding Section the initial results relate to generation and propagation of the first-order Raman pulse at ~1.12 μm in 150 m of single-optical fibre. An extension of this work, described be involved the construction of an optical resonator inc porating the length of fibre as the Raman-active medi [17].

The experimental arrangement for the fibre Raman oscillator (FRO) is shown in Fig. 10 and is similar to that described in Reference 18. The output from the mode-

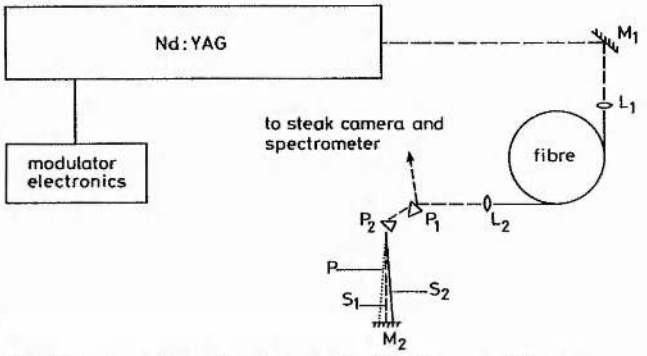

Fig. 10 *Experimental arrangement for fibre Raman oscillator*

locked CW Nd : YAG laser was coupled via mirror M_1 into the fibre using a $\times 10$ AR-coated microscope objective L_1. Output coupling from the fibre was achieved with a $\times 20$ AR-coated microscope objective L_2 which collimated the fibre output and directed the beam onto the first of the two fused-silica Brewster-angled prisms (P_1 and P_2) within the FRO cavity. The prisms were incorporated to provide spatial separation of the pump (P) and Raman wavelengths (S_1 and S_2) and thereby prevent mode-locking degradation of the pump laser due to feedback of the 1.064 μm radiation. Mirror M_2 ($\sim 100\%$ reflecting gold mirror) constituted one reflector of the FRO and was suitably adjusted to direct the first Stokes Raman pulse back into the optical fibre via L_2. In addition, the end mirror M_2 was mounted on an optical mount to meet the synchronous pumping requirement that the FRO cavity period be matched to a large integral multiple (~ 120 in this case) of the pump laser cavity period. The output mirror of the Nd : YAG laser also served as the second reflector. A reflection from the first prism allowed the FRO output to be monitored both spectrally and temporally. Spectral measurements were taken using a 1 m scanning spectrograph (with a resolution of ~ 0.05 nm) and an S1 response photomultiplier. Temporal measurements were taken using the synchronously operating streak-camera system which, in this

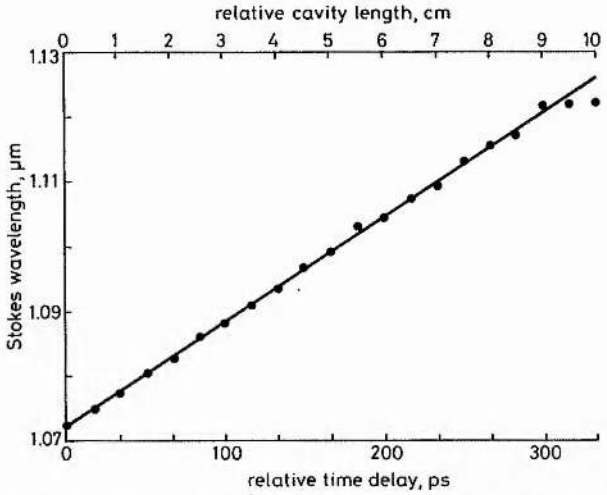

Fig. 11 *Dependence of wavelength peak of first Stokes oscillation on relative cavity length ΔL*

Also depicted in terms of relative time delay $\Delta T = \Delta L/c$

work, was triggered from the RF modulator drive electronics of the mode-locked pump laser.

One of the most important features of the FRO is the time dispersion tuning property which is a consequence of the time synchronisation requirement of synchronous pumping and the effect of group-velocity dispersion in the optical fibre. This is demonstrated in Fig. 11 where the peak wavelength of the first Stokes oscillation is plotted as a function of the relative position ΔL ($\Delta L = 0$ at $\lambda = 1.0725$ μm) of mirror M_2 (also depicted in terms of a relative time delay $\Delta T = \Delta L/c$). It can be seen that a tuning range of almost 50 nm (1.0725–1.220 μm) was achieved by translating the mirror by 10 cm (equivalent to 330 ps relative time delay) with longer-wavelength Stokes oscillation occurring at extended cavity lengths.

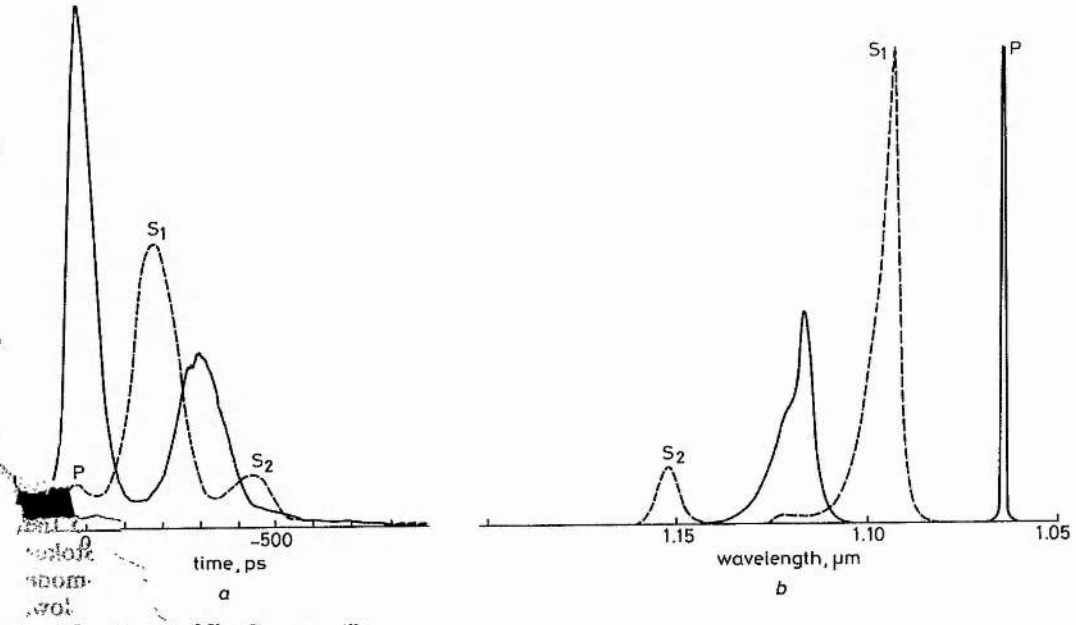

52 *Output of fibre Raman oscillator*

4 cm

temporal output; zero time point corresponds to peak of pump pulse in solid curve — resonant operation —— nonresonant operation

b Spectral output

To evaluate the group-velocity dispersion $D(\lambda)$ (in ps/nm.km) over the wavelength region in Fig. 11 we consider the time delay ΔT between two Stokes pulses, separated in wavelength by $\Delta\lambda$, in a single pass through the fibre. This is given by

$$\Delta T = L \cdot D(\lambda) \cdot \Delta\lambda \quad (5)$$

where L is the fibre length (in km). The slope of the tuning curve in Fig. 11 ($\Delta\lambda/\Delta T = 0.1613$ nm/ps), which to a very good approximation is constant over the 50 nm range shown, gives a value for $D(\lambda)$ of 41 ps/nm.km near 1.1 μm. This value is in excellent agreement with the value obtained from the temporal data plotted in Fig. 8. Of further interest is the appearance of a second Stokes Raman component associated with the intense resonant first Stokes Raman pulse which provides additional tunability over the 1.149–1.179 μm spectral region.

The temporal behaviour of the FRO for $\Delta L = +4$ cm is shown in Fig. 12*a*. This cavity length gave wavelengths of 1.093 and 1.153 μm for the first and second Stokes Raman pulse peaks, respectively. The full-line profile (taken with the resonator blocked between P_2 and M_2) corresponds to the single-pass Raman pulse ahead of the 1.064 μm pump pulse by approximately 300 ps which is in good agreement with the results shown in Fig. 6*e*. The broken-line profile (plotted on the same intensity scale as the full curve but with the resonator unblocked) shows the resonant output of the FRO with clear evidence of the first (S_1) and second (S_2) Stokes Raman pulses together with the severely depleted pump pulse P. Fig. 12*b* shows the corresponding spectral changes in the FRO output for the blocked and unblocked resonator cases depicted in Fig. 12*a*.

Pulse durations for both the first and second Stokes Raman bands were typically 100 ps with peak powers of 5 W (40 mW average) and 1 W (9 mW average), respectively. Although the pulse durations recorded here were relatively long, the large potential Raman laser bandwidths available make possible the generation of ultrashort (~ps) light pulses by the employment of appropriately designed dispersion-compensated cavities [19].

6 Conclusion

We have made a detailed experimental investigation of self-phase modulation, stimulated Raman scattering and pulse propagation in a single-mode fibre where a mode-locked CW Nd : YAG laser has been the pump source. A simple theory of SPM has been applied successfully to explain the experimental dependence of the spectral width on peak power. The theory was developed for negligible influence of fibre group-velocity dispersion and symmetrical (Gaussian) frequency chirp-free input pulses. The onset of stimulated Raman scattering, however, led to a marked deviation from the predictions of the simple theory. The process of stimulated Raman scattering in removing energy from the leading edge of the pump pulse gives rise to substantial reshaping of the intensity profile of the pump laser pulse. This leads to a steepened rising edge which consequently extends the low-frequency side of the SPM spectra.

An extension of this work was the construction of an optical resonator incorporating a length of fibre as the Raman-active medium. A tuning range of almost 50 nm from 1.0725 to 1.1220 μm was obtained for the first Stokes oscillation. Additional tunability from 1.149 to 1.179 μm was available through the second Stokes Raman band. Recent work [19], involving a more sophisticated dispersion-compensated ring fibre Raman oscillator, has led to the generation of subpicosecond optical pulses in the first Stokes band. In conjunction with various fibre Raman media (e.g. gas in glass) this laser type should permit the convenient generation of ultrashort pulses (~ps) over much of the wavelength range of interest for pulse propagation studies in optical fibres and for other time-domain spectroscopic investigations in the near infra-red region.

7 Acknowledgments

The financial support of the British Telecommunications plc (KS) and the UK Science and Engineering Research Council (SERC) and Joint Optoelectronics Research Scheme (JOERS) is gratefully acknowledged.

8 References

1 GRICHKOWSKY, D., and BALANT, A.C.: 'Optical pulse compression based on enhanced frequency chirping', *Appl. Phys. Lett.*, 1982, **41**, pp. 1–3
2 TOMLINSON, W.J., STOLEN, R.H., and SHANK, C.V.: 'Compression of optical pulses chirped by self-phase modulation in fibres', *J. Opt. Soc. Am. B*, 1984, **1**, pp. 139–149
3 MOLLENAUER, L.F., STOLEN, R.H., and GORDON, J.P.: 'Experimental observation of picosecond pulse narrowing and solitons in optical fibres', *Phys. Rev. Lett.*, 1980, **45**, pp. 1095–1098
4 BLOW, K.J., DORAN, N.J., and NELSON, B.P.: 'All-fibre pulse compression at 1.32 μm', *Opt. Lett.*, 1985, **10**, pp. 393–395
5 TAI, K., and TOMITA, A.: '1100X optical fibre pulse compression using grating pair and soliton effect at 1.319 μm', *Appl. Phys. Lett.*, 1986, **48**, pp. 1033–1035
6 GOMES, A.S.L., SIBBETT, W., and TAYLOR, J.R.: 'Spectral and temporal study of picosecond-pulse propagation in a single-mode optical fibre', *Appl. Phys. B*, 1986, **39**, pp. 43–46
7 STOLEN, R.H., and JOHNSON, A.M.: 'The effect of pulse walkoff on stimulated Raman scattering in fibres', *IEEE J. Quantum. Electron.*, 1986, **22**, pp. 2154–2160
8 SIBBETT, W.: 'Synchroscan streak camera systems'. Proceedings 15th International Congress on High speed photography and photonics, San Diego, USA, 1982, Society of Photo-Optical Instrumentation Engineers, 1982, **348**, pp. 15–26
9 KEAN, P., SMITH, K., and SIBBETT, W.: 'Modulator frequency detuning effects in a CW mode-locked Nd : YAG laser with active stabilisation', *Opt. Commun.*, 1987, **61**, pp. 129–133
10 STOLEN, R.H.: 'Nonlinearity in fibre transmission', *Proc. IEEE*, 1980, **68**, pp. 1232–1236
11 STOLEN, R.H., and LIN, C.: 'Self-phase modulation in silica optical fibres', *Phys. Rev. A*, 1978, **17**, pp. 1448–1453
12 HERITAGE, J.P., WEINER, A.M., and THURSTON, R.N.: 'Fourier transform picosecond pulse shaping and spectral phase measurement in a grating pulse-compressor', *in* FLEMING, G.R., and SIEGMAN, A.E. (Eds.): 'Ultrafast phenomena V' Series in Chemical Physics (Springer, 1986) Vol. 46, pp. 34–37
13 COHEN, M.G.: 'Continuous-wave mode-locked Nd : YAG laser: A picosecond pump source for the future', *Proc. SPIE Int. Soc. Opt. Eng.*, 1982, **322**, pp. 44–51
14 FISHER, R.A., and BISCHEL, W.K.: 'Numerical studies of the interplay between self-phase modulation and dispersion for the intense plane-wave laser pulses', *J. Appl. Phys.*, 1975, **46**, pp. 4921–4934
15 SMITH, R.G.: 'Optical power handling capacity of low loss optical fibres as determined by stimulated Raman and Brillouin scattering', *Appl. Opt.*, 1972, **11**, pp. 2489–2494
16 SCHADT, D., JASKORZYNSKA, B., and ÖSTERBERG, U.: 'Numerical study on combined stimulated Raman scattering and self-phase modulation in optical fibres influenced by walk-off between pump and Stokes pulses', *J. Opt. Soc. Am. B*, 1986, **3**, pp. 1257–1262
17 STOLEN, R.H.: 'Fibre Raman laser', *in* OSTROWSKY, D.B. [redacted] 'Fibre and integrated optics' (Plenum, New York, 1979)
18 LIN, C., and FRENCH, W.G.: 'A near-infrared fibre Raman oscillator tunable from 1.07 to 1.32 μm', *Appl. Phys. Lett.*, 1979, **34**, pp. 666–668
19 KAFKA, J.D., HEAD, D.F., and BAER, T.: 'Dispersion compensated Raman Oscillator', *in* FLEMING, G.R., and SIEGMAN, A.E. (Eds.): 'Ultrafast phenomena V' (Series in Chemical Physics, Springer, 1986), Vol. 46, pp. 51–54

CHARACTERISATION OF A FIBRE RAMAN OSCILLATOR USING FIBRE GRATING REFLECTORS

Indexing terms: Optics, Optical fibres, Oscillators, Integrated optics

We have constructed a completely integrated fibre Raman oscillator using two fibre grating reflectors. This was synchronously mode-locked using a CW mode-locked Nd : YAG laser operating at 1·06 μm. Spectral and temporal characteristics of the Raman oscillator are presented.

Introduction: The fibe Raman oscillator[1] offers a very attractive source of broadly tunable coherent light in the visible and near-infra-red spectral regions. The large laser bandwidths which are available make possible the generation of ultrashort light pulses via the standard mode-locking technique of synchronous pumping. This femtosecond potential has recently been realised in such systems by utilising the soliton compression effects[2,3] or dispersion compensation via a grating pair.[4] Generally, the fibre Raman oscillator (FRO) consists of a length of optical fibre with associated external optical components.[1–4] In this letter we report on the preliminary results from a completely integrated fibre Raman oscillator using fibre gratings (FROGs), which has the advantages of alignment simplicity, compactness and mechanical stability.

Experiment: The experimental arrangement is shown in Fig. 1. A Spectra-Physics series 3000 CW mode-locked Nd : YAG laser was used as a pump source; it typically produced pulses of 140 ps duration at a repetition rate of 82 MHz, with an average power of 6·5 W. The Raman medium was a 500 m length of single-mode optical fibre, which had a 3·5 μm core radius, 0·004 average difference in core/cladding refractive index, 40 ps nm^{-1} km^{-1} dispersion and losses of 0·9 dB km^{-1}. Two fibre grating reflectors, which were similar to those described in Reference 5, were used to terminate the Raman resonator. The input and output gratings used in this work had peak reflectivities of approximately 97% and 70%, respectively, at 1089·5 nm when oil of a refractive index of 1·454 was used to cover the grating. The input grating was measured to be 80% transmitting at 1064 nm. The short fibres containing the gratings were butted to the main fibre, using index-matching fluid to eliminate etalon effects (fusion splicing of the fibres was not attempted, but would greatly simplify the system). The pump beam was coupled into the input grating fibre with typically 50% efficiency (measured with no oil overlay) using a ×20 antireflection-coated microscope objective. A similar type of objective was used to collimate the output from the fibre. The laser beam was usually chopped to extend the lifetime of the coatings of the objectives, although the powers quoted here are those present during the open period of the chop. The temporal and spectral characteristics of the FROG were measured using a synchronously operating ('Synchroscan') streak camera[6] and a 0·05 nm resolution grating monochromator, respectively.

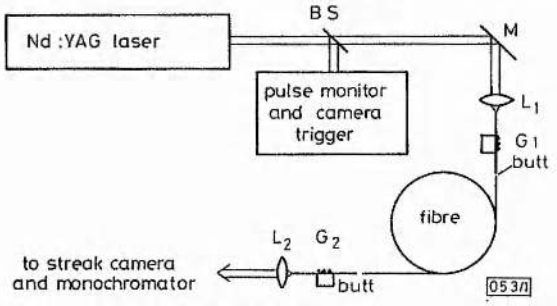

Fig. 1 *Experimental arrangement*

BS = beamsplitter, M = mirror, L_1 and L_2 = input and output objectives, G_1 and G_2 = input and output gratings

Results and discussion: The Raman oscillator was initially configured without the output grating, but using two prisms and an external mirror to select and reflect the Raman pulse back into the fibre. Depending on the distance of the mirror from the end of the fibre, the system behaved as a wavelength-tunable FRO[7] (with the Nd : YAG output coupler acting as one of the FRO mirrors) or as a single-grating FROG, in which case the input grating defined the FROG wavelength of 1·089 μm. Figs. 2*a* and *b* show the temporal and spectral characteristics, respectively, of the single-grating FROG output. Synchronous pumping of the FROG was achieved by adjusting the cavity length for optimum performance. Raman oscillation was maintained for a tolerance of ±25 mm about this optimum position. The appropriate fibre length for the two grating FROG was calculated from these measurements. It was found that synchronous pumping was somewhat more critical on cavity length selection, with a tolerance of ±10 mm in the length of fibre between the gratings. The average pump power measured at the output of the two-grating FROG (FROG2) at threshold was 800 mW, corresponding to a peak power in the 500 m fibre of 150 W. The total power out of the fibre at maximum pump power was 952 mW, of which 60% was at the pump wavelength and 40% at the FROG2 wavelength. No other significant first or second Stokes components were observed.

Typical results of the temporal and spectral measurements are shown in Figs. 2*c* and *d*. The FROG2 pulse leads the Nd : YAG pulse by ~280 ps, which is a consequence of the group velocity dispersion within the fibre.[7,8] The FROG2 pulsewidth was measured to be 92 ps, compared with 131 ps for the pump pulse, which had been depleted and deformed by the combined effects of self-phase modulation, group velocity dispersion and stimulated Raman scattering.[7] The FROG2 wavelength was centred on the reflectivity peaks of the fibre gratings. The overall width of the FROG2 spectrum varied with stress applied to the fibre; it is thought likely that this effect was due to the non-polarisation-preserving nature of the fibre.

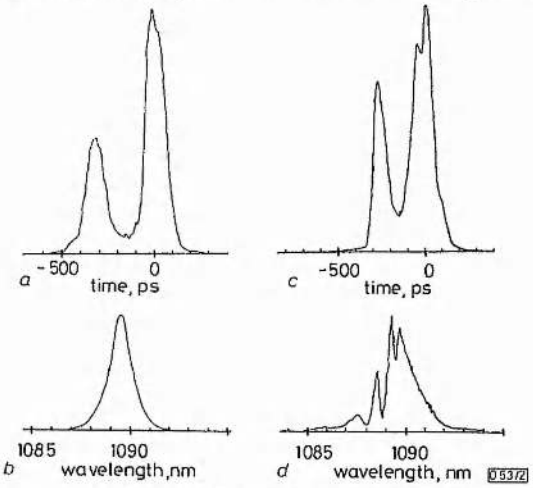

Fig. 2 *Typical temporal (a and c) and spectral (b and d) traces of fibre Raman oscillators with one grating (a and b) and two gratings (c and d)*

The shape of the spectrum is attributed to the shapes of the reflectivity curves of the two gratings and the transmission curve of the output coupler. The transmission curve of the output grating showed sharp dips, similar to those shown in Reference 5. The separation of these coincided with the dips in the spectrum of the FROG2 output. The results shown in Fig. 2 were taken with an oil of 1·454 refractive index on both gratings; changing the refractive index of the oil overlay altered the FROG2 output power and the detailed shape of the spectra, but the general behaviour of the FROG2 was the same in all these cases.

Conclusions: We have constructed a synchronously mode-locked integrated fibre Raman oscillator by employing two fibre-grating reflectors and 500 m of single-mode optical fibre. This system has the advantages of simplicity, compactness and mechanical stability. The temporal and spectral characteristics of the oscillator have been presented. A more detailed investigation of the single-grating FROG is in progress. Future

extensions to our FRO/FROG work include the demonstration of their femtosecond capability via dispersion compensation (using soliton effects at wavelengths greater than 1·3 μm) and ring FROGs employing optical fibre directional couplers.

Acknowledgment: We thank Plessey Research Ltd. for the fibre gratings. The financial support of British Telecom plc (KS) and SERC JOERS is gratefully acknowledged.

P. N. KEAN
K. SMITH*
B. D. SINCLAIR
W. SIBBETT

Department of Physics
University of St. Andrews
North Haugh, St. Andrews, Fife KY16 9SS, United Kingdom

C. J. ROWE
D. C. J. REID

Plessey Research (Caswell) Ltd.
Caswell
Towcester, Northants, NN12 8EQ, United Kingdom

* Current address: AT&T Bell Laboratories, Crawford Corner Road, Holmdel, NJ 07733, USA

14th September 1987

References

1 STOLEN, R. H.: 'Fibre Raman lasers', *in* OSTROWSKY, D. B. (Ed.): 'Fibre and integrated optics' (Plenum, New York, 1979), pp. 157–171
2 ISLAM, M. N., MOLLENAUER, L. F., and STOLEN, R. H.: 'Fiber Raman amplification soliton laser (FRASL)'. Ultrafast Phenomena V, Springer Verlag Series, 1986, **46**, pp. 46–50
3 KAFKA, J. D., and BAER, T.: 'Fiber Raman soliton laser pumped by a Nd : YAG laser', *Opt. Lett.*, 1987, **12**, pp. 181–183
4 KAFKA, J. D., HEAD, D. F., and BAER, T.: 'Dispersion compensated fibre Raman oscillator'. Ultrafast Phenomena V, Springer Verlag Series, 1986, **46**, pp. 51–54
5 BENNION, I., REID, D. C. J., ROWE, C. J., and STEWART, W. J.: 'High-reflectivity monomode-fibre grating filters', *Electron. Lett.*, 1986, **22**, pp. 341–343
6 SIBBETT, W.: 'Synchroscan streak camera systems'. *Proc. SPIE*, 1982, **343**, pp. 15–26 (Proc. 15 int. congress on high-speed photography and photonics, San Diego, 1982)
7 SMITH, K., KEAN, P. N., CRUST, D. W., and SIBBETT, W.: 'An experimental study of a synchronously pumped fibre Raman oscillator', *J. Modern Opt.*, 1987, to be published
8 KEAN, P. N., SMITH, K., and SIBBETT, W.: 'Spectral and temporal investigation of self-phase modulation and stimulated Raman scattering in a single-mode optical fibre', *IEE Proc. J, Optoelectron.*, 1987, **134**, pp. 163–170

Reprinted from Optics Letters, Vol. 14, page 39, January 1, 1989.

Enhanced mode locking of color-center lasers

P. N. Kean, X. Zhu, D. W. Crust, R. S. Grant, N. Langford, and W. Sibbett

Department of Physics and Astronomy, University of St. Andrews, St. Andrews, Fife KY16 9SS, Scotland

Received July 18, 1988; accepted October 14, 1988

A significant enhancement in the mode locking of a KCl:Tl color-center laser has been observed when a length of optical fiber having positive group-velocity dispersion was incorporated within an external control cavity. Pulse durations of ~260 fsec were obtained by this method, representing a compression factor ~60× that with the color-center laser alone. Similar results have also been observed with an InGaAsP semiconductor diode amplifier as the nonlinear element within the control cavity.

The synchronously mode-locked KCl:Tl color-center laser can typically produce pulses of ~8–20-psec duration at a wavelength of approximately 1.5 μm. In the research by Mollenauer and Stolen,[1] the mode-locked characteristics of such a laser were dramatically improved by incorporating a length of optical fiber into an optical feedback loop, or control cavity. A small fraction of the output from the color-center laser was fed into the fiber, where the combined effects of self-phase modulation and negative group-velocity dispersion (GVD) caused the pulses to be temporally compressed. These compressed pulses are then reinjected into the master cavity, stimulating the production of narrower pulses from the laser itself. This process continues until the pulses have essentially the same shape on entering and returning from the fiber, i.e., they become optical solitons. Although it was observed that for a single length of fiber a variety of pulse durations could be obtained,[2] the pulses returning from the control cavity and injected back into the laser were always observed to be as short or shorter than those exiting the composite cavity laser. In this Letter we describe experiments whereby an optical fiber having positive GVD was inserted into a control cavity (similar results have also recently been observed by other authors[3]). Pulses propagating along such a fiber are dispersively broadened, and the fiber is unable to support (bright) solitons. Nevertheless, we have found that even these temporally broadened pulses reinjected back into the master cavity can significantly improve the mode locking of the color-center laser in a dramatic way.

A schematic diagram of the coupled-cavity laser is shown in Fig. 1. The color-center laser alone, bounded by mirrors M_1 and M_0, typically produced pulses of ~15-psec duration and was tunable from 1.45 to 1.55 μm. The control cavity containing the fiber was formed by the output coupler M_0 of the color-center laser, beam splitter S_1, and a small dielectric mirror M_3 mounted on a piezoelectric translator (PZT). An elliptical-core fiber[4] (produced by the Andrew Corporation) was used to provide polarization-preserving and single-mode propagation at 1.5 μm. The relatively large germania content of the fiber (giving a Δn ~0.046) necessitates a small core (2.8 μm × 1.6 μm) in order to obtain propagation in a single mode, and this in turn produces a large waveguide dispersion, giving the fiber a net positive GVD. The average power coupled into the fiber was adjusted by a variable neutral-density (ND) filter.

With the control cavity unblocked and its length made equal to (or a multiple of) the master cavity, a significant shortening of the laser output pulses was seen to occur. An electronic stabilization scheme similar to that described in Ref. 2 was employed in order to provide for the correct relative optical phase matching between the pulses fed back from the fiber and those circulating in the master cavity. Once this stabilization loop was in operation, the output pulses from the composite cavity laser were very stable, with ~1% noise fluctuations. For a fiber length of 2.2 m the composite cavity laser produced pulses of ~1.1-psec duration, and the shortest pulses of 260 fsec (see inset of Fig. 3) were obtained with a fiber length of 24 cm. For the 2.2-m fiber, the laser produced stable pulses of constant duration for a power range of 10–25 mW within the fiber (measured just before M_3), and for shorter fiber lengths, the stability range shifted to

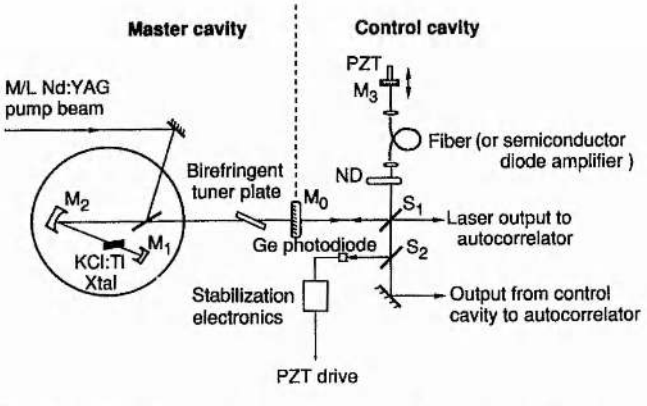

Fig. 1. Experimental arrangement of the coupled-cavity color-center laser. M/L, mode locked. Mirror reflectivities: M_1, M_2, M_3, ~100%; M_0, ~80%. Beam-splitter reflectivities: S_1, ~50%; S_2, ~30%.

0146-9592/89/010039-03$2.00/0

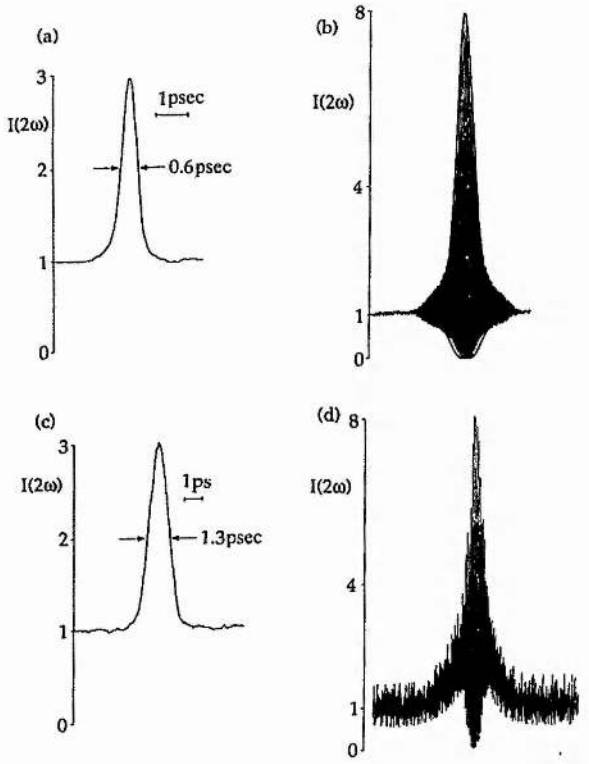

Fig. 2. Intensity and interferometric autocorrelation traces for pulses exiting the laser [(a) and (b)] and for pulses returning from the control fiber [(c) and (d)] with a fiber length of 55 cm. The fringes seen on the interferometric autocorrelations are not actual interference fringes but are due to sampling limitations on the digital oscilloscope.

slightly higher powers, approximately 30 mW for 24 cm. As can be seen from Fig. 1, we were also to monitor the pulses returning from the control cavity, and it was found that the duration of these pulses exceeded the duration of those exiting the laser for all the fiber lengths used. For the 2.2-m and 24-cm lengths, the fed-back pulse durations were 3.0 and 0.6 psec, respectively. Typical second-harmonic intensity and interferometric autocorrelation traces of the pulses are shown in Fig. 2 for a control fiber length of 55 cm. The laser output pulses had durations of 0.6 psec, whereas those fed back into the master cavity had durations of ~1.3 psec. The interferometric autocorrelation traces show a substantial difference between the two pulse trains. For the laser output [Fig. 2(b)] the pulses are well phase locked (as shown by the 8:1 contrast ratio); for comparison, a sech^2 fit to the envelope is also shown. There is a slight departure in the wings of the pulse, which may imply some excess frequency chirp, but it should be remembered that since the pulses are not solitons, there is no particular reason why the pulses should have sech^2 intensity profiles. The pulses returning from the control cavity [Fig. 2(d)] show a substantial linear frequency chirp due to the positive GVD of the fiber (indicated by the rising wings of the autocorrelation[5]), with only the central portion of the pulse being coherent. A similar structure was seen in all cases for these pulses. A plot of the pulse durations obtained from the coupled-cavity laser as a function of fiber length is shown as Fig. 3. In contrast to the soliton laser, where the output-pulse duration is proportional to the square root of the fiber length, no such simple relationship is observed here. It may also be inferred from this graph that an optimum fiber length exists for the production of the shortest output pulses. Owing to physical constraints of our experimental arrangement, further data around this minimum were not taken, but this would be required in order to establish the true existence of an optimum fiber length.

In our experimental configuration (Fig. 1), although the fiber itself provided positive GVD, any glass within the master cavity (e.g., Brewster-angled plates, an output coupler) may provide negative GVD and thereby lead to temporal compression of the frequency-chirped pulses. To verify that this was not the case and that negative GVD is not necessary for enhanced mode locking, a similar experiment was performed using a synchronously mode-locked LiF:F_2^+ color-center laser.[6] This laser produced pulses of typically 4-psec duration at a wavelength near 900 nm, where the material dispersion for glass is positive. A coupled-cavity arrangement was set up with a 2-m length of fiber, which was polarization preserving and monomode in the lasing wavelength region (Andrew Corporation fiber) similar to that previously described. With feedback from the control cavity, preliminary results have shown an observable pulse reshaping and narrowing, with the laser output pulses shortened to ~1 psec (Fig. 4).

The results described here seem to be in general agreement with the theoretical modeling characteristics reported recently by Blow and Wood.[7] They showed that pulses broadened by passage through a nonlinear element in the control cavity could still enhance the mode locking of a homogeneously broadened laser. The mechanism may be described as being due to the enhanced phase coupling involving additional longitudinal modes of the laser cavity (induced by the processes occurring within the nonlin-

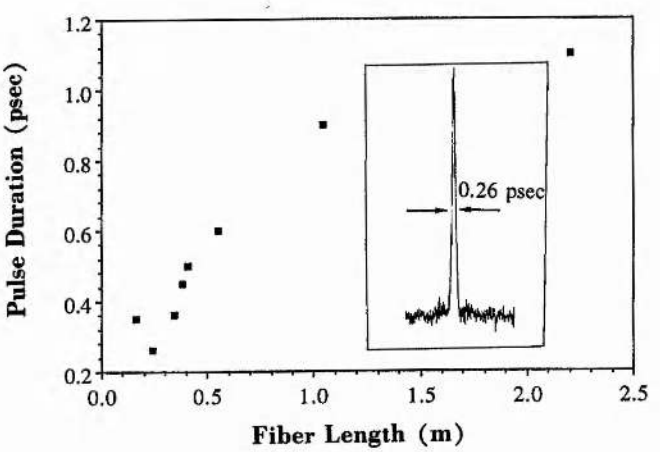

Fig. 3. Variation of the pulse duration from the coupled-cavity laser as a function of fiber length. The inset shows an autocorrelation trace of the 0.26-psec pulse with $L = 24$ cm.

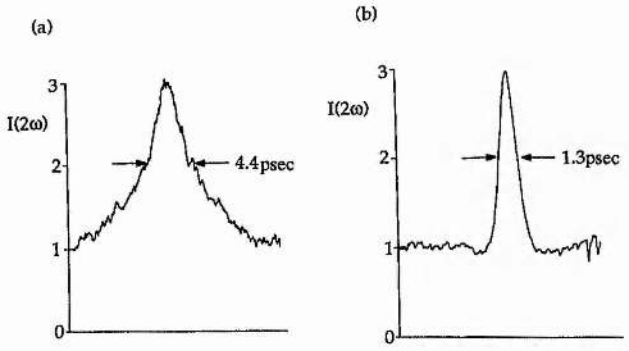

Fig. 4. Autocorrelation traces of the pulses obtained (a) from the LiF:F_2^+ laser alone and (b) with feedback from the control cavity for a fiber length of 2 m.

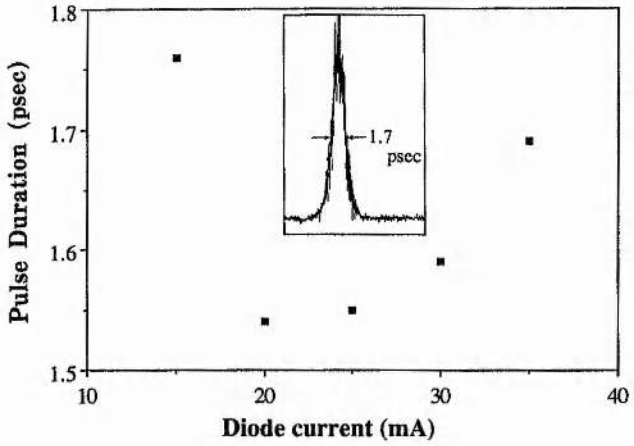

Fig. 5. Pulse duration versus drive current to the InGaAsP diode amplifier in the control cavity of the KCl:Tl color-center laser. The inset shows typical intensity autocorrelation of the output pulses for a 35-mA diode injection current.

ear element), thereby increasing the mode-locked bandwidth. Our experimental data are qualitatively consistent with this, but we did observe that the pulses reinjected into the master cavity had a broader bandwidth (owing to self-phase modulation) than the pulses exiting the laser. The role of saturable amplification in the control cavity has also been studied theoretically,[7] and we have evaluated this experimentally by using an InGaAsP semiconductor diode amplifier as the nonlinear element within a control cavity. The diode was operated at injection currents in the 10–35-mA range, and higher currents were not used in order to prevent lasing between one facet of the diode and mirror M_3 (Fig. 1). Our initial results showed pulse shortening to ~1.4 psec for a current of 20 mA. A plot of the pulse durations from the coupled-cavity laser as a function of diode current is shown in Fig. 5, where the inset is a typical autocorrelation trace of the output pulses for a current of 35 mA. Most recently, by optimization of the laser we have obtained pulses as short as 250 fsec, which is comparable with that of the fiber-based control cavity. In the diode-amplifier case, however, the laser has been observed to suffer regular dropouts, i.e., switching to the much broader color-center-laser pulses. The stabilization loop, although compensating for relatively slow cavity-length changes, was not able to eliminate these higher-frequency (~1-kHz) dropouts. It was also noted that the period of these could be varied by altering the length of the master cavity, and further study of these features is ongoing. The average power fed back into the master cavity was estimated to be less than 1 mW, yet, interestingly, this is still sufficient to produce the dramatic narrowing of the laser pulses reported here.

In summary, we have found that the existence of negative GVD in the control cavity of a color-center laser is not necessary to provide an enhanced mode locking of the laser. A semiconductor diode amplifier has also been demonstrated to produce a similar effect, in agreement with previous theoretical considerations.[7] Finally, it would seem from the results described here that actual soliton formation in the control cavity is a specific case of a more general phenomenon, whereby pulses reinjected into the master cavity from a control cavity containing a nonlinear element can completely dominate the mode-locking characteristics (i.e., coupled-cavity mode locking) of color-center lasers and will perhaps be applicable to other broad-bandwidth laser systems.

We wish to thank K. C. Byron (STC Technology Ltd.) and I. White (Cambridge University) for the loan of the samples of the Andrew Corporation fiber and K. J. Blow and B. P. Nelson (British Telecom Research Laboratories) for communicating their results to us before publication. The overall funding of this research by the UK Science and Engineering Research Council is gratefully acknowledged. Part of this funding was provided through the Joint Opto-Electronics Research Scheme initiative.

References

1. L. F. Mollenauer and R. H. Stolen, Opt. Lett. **9,** 13 (1984).
2. F. M. Mitschke and L. F. Mollenauer, IEEE J. Quantum Electron. **QE-22,** 2242 (1986).
3. K. J. Blow and B. P. Nelson, Opt. Lett. **13,** 1026 (1988).
4. K. C. Byron, Electron. Lett. **23,** 1324 (1987).
5. J. C. Diels, J. J. Fontaine, I. C. McMichael, and F. Simoni, Appl. Opt. **24,** 1270 (1985).
6. N. Langford, K. Smith, and W. Sibbett, Opt. Commun. **64,** 247 (1987).
7. K. J. Blow and D. Wood, J. Opt. Soc. Am. B **5,** 629 (1988).